AN EQUILIBRIUM AND KINETIC STUDY OF CRYPTAND, LARIAT ETHER AND FLUORESCENT ZINC(II) COMPLEXES

by
Theo Rodopoulos B.Sc.(Hons.) (Adelaide)

This thesis is presented for the degree of
Doctor of Philosophy

Department of Chemistry
University of Adelaide
September, 1993

Contents

Abstract

In the first part of this work the complexation of M^+ = Li^+, Na^+, Ag^+ and Tl^+ by the cryptands 4,7,13,18-tetraoxa-1,10-diazabicyclo[8.5.5]eicosane (C211) and 4,7,13-trioxa-1,10-diazabicyclo[8.5.5]eicosane ($C21C_5$) to form the cryptates $[M.C211]^+$ and $[M.C21C_5]^+$ was studied in a variety of trialkyl phosphate solvents by potentiometric titration and ^7Li and ^{23}Na NMR spectroscopy. This study enabled the effect of variation in donor atoms and the influence of solvent molecular size on cryptate stability and lability to be investigated. The decomplexation kinetic parameters for $[Na.C211]^+$ in trimethyl phosphate, triethyl phosphate and tri-*n*-butyl phosphate, and for $[Li.C21C_5]^+$ in trimethyl phosphate and triethyl phosphate were derived by complete two-site lineshape analysis of the coalescing ^{23}Na or ^7Li resonances. The dominant mechanism for metal ion exchange in these systems involved a monomolecular decomplexation of the metal ion. Metal ion exchange on $[Li.C211]^+$ and $[Na.C21C_5]^+$ was in the very slow and very fast extreme of the NMR time scale, respectively, in trimethyl phosphate and triethyl phosphate. The equilibrium and kinetic data are compared with data obtained in other solvents and discussed in terms of the metal ion and cryptand intramolecular cavity size, metal ion-cryptand bonding interactions, solvent interactions and the solid state crystal structures of the cryptates.

Furthermore, the complexation characteristics of the pendant armed bibracchial lariat ethers 1,7-bis(2-hydroxyethyl)-4,10,13-trioxa-1,7-diazacyclopentadecane (BHE-C21) and 1,10-bis(2-hydroxyethyl)-4,7,13,16-tetraoxa-1,10-diazacyclooctadecane (BHE-C22) with alkali, alkaline-earth, transition and heavy metal cations in aqueous solution and several non-aqueous solvents was investigated by potentiometric and pH-metric titration. The results are discussed in conjunction with data from related structures, such as the bibracchial lariat ethers BME-C21 and BME-C22, the diaza crown ethers C21 and C22, and the cryptands C221, C222, $C22C_5$ and $C22C_8$. The kinetics of decomplexation of $[Na.BHE-C21]^+$ in acetonitrile, $[Na.BHE-C22]^+$ in methanol and $[Li.BHE-C21]^+$ in methanol and N,N-dimethylformamide were measured by ^{23}Na and ^7Li variable temperature NMR. A monomolecular exchange mechanism was found to be in operation in each of the systems lineshaped. The kinetic data are compared with data from related systems.

In the second part of this work the viability of the fluorophore 2-methyl-8-*p*-toluenesulfonamido-6-quinolyloxyacetic acid (MTS-QAA) to behave as a Zn^{2+} specific probe and quantify intracellular Zn^{2+} levels was investigated. The spectral and kinetic properties of MTS-QAA with Zn^{2+} were studied as well as its complexation properties with Zn^{2+}, Co^{2+}, Ni^{2+}, Cu^{2+}, Cd^{2+} and Mg^{2+} in a 50% ethanol/50% water solvent mixture. MTS-QAA formed two stable Zn^{2+} complexes, namely [Zn.MTS-QAA] and $[Zn.MTS\text{-}QAA_2]^{2-}$, which would complicate the quantification of Zn^{2+} levels in biological systems. The Zn^{2+}-free and Zn^{2+}-bound forms of MTS-QAA were seen to fluoresce at the same wavelength. In addition, a MTS-QAA molecule in the [Zn.MTS-QAA] complex form was found to fluoresce much more strongly than a MTS-QAA molecule in the uncomplexed form and more strongly than a MTS-QAA molecule in the $[Zn.MTS\text{-}QAA_2]^{2-}$ complex form. The kinetic study of the Zn^{2+}-MTS-QAA complexes in 50% ethanol/50% water provided an insight into their complexation and decomplexation mechanisms. Results from the study of the formation of [Zn.MTS-QAA] suggested that ring closure or formation of the second coordinate bond was the rate determining step.

Statement

This work contains no material which has been accepted for the award of any other degree or diploma in any university or other tertiary institution and, to the best of my knowledge and belief, contains no material previously published or written by another person, except where due reference has been made in the text.

I give consent to this copy of my thesis, when deposited in the University Library, being available for loan and photocopying.

SIGNED: DATE: 20/9/93

Theo Rodopoulos

Acknowledgements

I wish to extend my thanks to my supervisor, Prof. S.F. Lincoln for his help, guidance and encouragement throughout the course of this work. I would like to thank Dr. P.-A. Pittet for his invaluable help with the fluorescence work and Dr. I. Mahadevan for supplying the sulfonamidoquinoline ligand. I would also like to thank my fellow research students for their helpful discussions and suggestions, their frienship and the many good time shared, especially my fiancee Mary Manikas and Rob Jones.

I gratefully acknowledge the financial support of an Australian Postgraduate Research Award for the period of my candidature.

Finally, I would like to express my gratitude to my family for their encouragement, support, patience and understanding.

Abbreviations

The following abbreviations have been used in this study:

18-crown-6	1,4,7,10,13,16-hexaoctadecane
C21	4,7,13-trioxa-1,10-diazacyclopentadecane
C22	4,7,13,16-tetraoxa-1,10-diazacyclooctadecane
C211	4,7,13,18-tetraoxa-1,10-diazabicyclo[8.5.5]eicosane
$C21C_5$	4,7,13-trioxa-1,10-diazabicyclo[8.5.5]eicosane
C221	4,7,13,16,21-pentaoxa-1,10-diazabicyclo[8.8.5]tricosane
C222	4,7,13,16,21,24-hexaoxa-1,10-diazabicyclo[8.8.8]-hexacosane
$C22C_5$	4,7,13,16-tetraoxa-1,10-diazabicyclo[8.8.5]tricosane
$C22C_8$	4,7,13,16-tetraoxa-1,10-diazabicyclo[8.8.8]hexacosane
BHE-C21	1,7-bis(2-hydroxyethyl)-4,10,13-trioxa-1,7-diazacyclo-pentadecane
BHE-C22	1,10-bis(2-hydroxyethyl)-4,7,13,16-tetraoxa-1,10-diaza-cyclooctadecane
BME-C21	1,7-bis(2-methoxyethyl)-4,10,13-trioxa-1,7-diazacyclo-pentadecane
BME-C22	1,10-bis(2-methoxyethyl)-4,7,13,16-tetraoxa-1,10-diaza-cyclooctadecane
BHDME-C22	1,10-bis(2-hydroxy-1,1-dimethylethyl)-4,7,13,16-tetraoxa-1,10-diazacyclooctadecane
BHEE-C22	1,10-bis(2-*o*-hydroxyethyl-2-oxyethyl)-4,7,13,16-tetraoxa-1,10-diazacyclooctadecane
BMNM-C22	1,10-bis(2-methoxy-1-naphthylmethyl)-4,7,13,16-tetraoxa-1,10-diazacyclooctadecane
BiBLE	bibracchial lariat ether
TriBLE	tribracchial lariat ether
MTS-QAA	2-methyl-8-*p*-toluenesulfonamido-6-quinolyloxyacetic acid
MTS-Q	6-methoxy-8-(*p*-toluenesulfonamido)quinoline
BS-Q	8-(benzenesulfonamido)quinoline
TS-Q	8-(*p*-toluenesulfonamido)quinoline
MMTS-Q	2-methyl-6-methoxy-8-(*p*-toluenesulfonamido)quinoline
MMS-Q	2-methyl-8-(methanesulfonamido)quinoline
MMsS-Q	2-methyl-8-(mesitylenesulfonamido)quinoline
MHTS-Q	2-methyl-6-hydroxy-8-(*p*-toluenesulfonamido)quinoline

AN	acetonitrile
n-BuOH	*n*-butanol
DMF	N,N-dimethylformamide
MeOH	methanol
TMP	trimethyl phosphate
TEP	triethyl phosphate
TBP	tri-*n*-butyl phosphate
$CDCl_3$	deuterated chloroform, the D represents deuterium (^2H); also in the case of D_2O
d_n-	n-deuterated
NEt_4ClO_4	tetraethylammonium perchlorate
NBu_4ClO_4	tetrabutylammonium perchlorate
NEt_4OH	tetraethylammonium hydroxide
NaPIPES	sodium piperazine-N,N'-bis(2-ethane-sulfonate)
EDTA	ethylenediamine tetraacetic acid
Å	angström (10^{-10} metres)
r	radius
D_N	Gutmann donor number
V_s	molar volume
E	observed potential (volts)
E_0	standard electrode potential (volts)
e.m.f.	electromotive force
mV	millivolts (10^{-3} volts)
pK_w	ion product constant for water
expt	experimental
calc	calculated
obs	observed
pH	$-\log_{10}[H^+]$
pOH	$-\log_{10}[OH^-]$
NMR	nuclear magnetic resonance
ppm	parts per million
δ	chemical shift (in ppm)
Hz	hertz (s^{-1})
MHz	megahertz (10^6 s^{-1})
$\Delta H_d^{\ddagger}$	decomplexation enthalpy of activation (kJ mol^{-1})
$\Delta S_d^{\ddagger}$	decomplexation entropy of activation (J K^{-1} mol^{-1})
$\Delta G_d^{\ddagger}$	decomplexation free energy of activation (kJ mol^{-1})

$W_{1/2}$	resonance linewidth at half-height (s^{-1} or Hz)
FID	free induction decay
ν	resonant frequency (in s^{-1})
ω	angular frequency (in rad s^{-1})
T_1	longitudinal or spin-lattice relaxation time (s)
T_2	transverse or spin-spin relaxation time (s)
λ_{max}	absorption maximum wavelength
ε	molar extinction coefficient
I_a	associative interchange mechanism
I_d	dissociative interchange mechanism
r.d.s.	rate determining step
ϵ	solvent dielectric constant

Chapter 1 : Cryptands, Lariat Ethers and their Complexes

1.1 : General Introduction

Charles J. Pedersen was the first to recognise the complexing ability of macrocyclic polyethers with alkali and alkaline earth metal cations.[1-4] Whilst studying the effects of bi- and multidentate phenolic ligands on the catalytic properties of the vanadyl (VO) group he unexpectedly synthesized 2,3,11,12-dibenzo-1,4,7,10,13,16-hexaoxacyclooctadeca-2,11-diene, more commonly known as dibenzo-18-crown-6. Upon reacting partially protected catechol (contaminated with about 10% unreacted catechol) with bis(2-chloroethyl)ether in the presence of sodium hydroxide in the solvent *n*-butanol, Pedersen obtained the desired quinquedentate ligand bis[2-(*o*-hydroxyphenoxy)ethyl]ether as well as a small amount of white, fibrous crystals (Figure 1.1). The mysterious by-product which proved to be dibenzo-18-crown-6, had the unusual property of not being very soluble in methanol but becoming freely soluble upon the addition of any sodium salt.

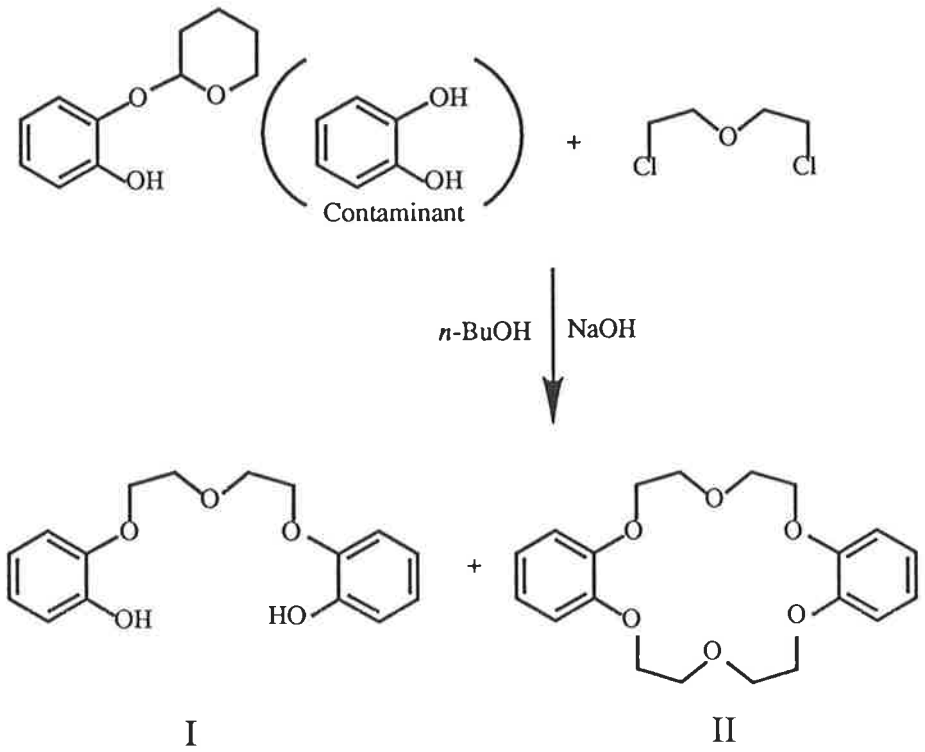

Figure 1.1 *Formation of bis[2-(o-hydroxyphenoxy)ethyl]ether (I) and the crown ether dibenzo-18-crown-6 (II).*

In 1967, Pedersen reported the syntheses and cation complex formation for a wide variety of macrocyclic polyethers.[1-2] This class of compounds were trivially named crown ethers,[2] because of the appearence of their molecular models and also because of their ability to crown and uncrown cations without physical damage to the ligand. Some simple crown ethers and their trivial nomenclatures are illustrated in Figure 1.2.

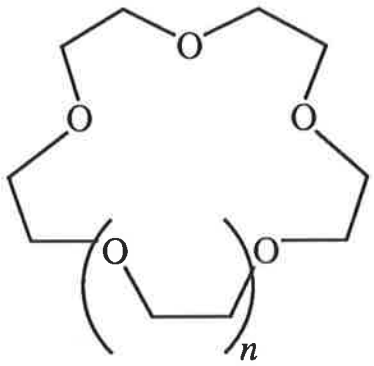

n =0	12-crown-4
n =1	15-crown-5
n =2	18-crown-6
n =3	21-crown-7
	etc.

Figure 1.2 *General structure and trivial nomenclatures of some simple crown ethers.*

Crown ethers are identified by (i) the number and type of substituent groups on the ring, (ii) the total number of atoms in the polyether ring, (iii) the class name ie. crown, and (iv) the number of oxygen atoms in the polyether ring.

The discovery that the crown ethers selectively complex biologically relevant alkali and alkaline earth metal cations was the catalyst for the enormous and rapid evolution in the field of host-guest chemistry (ie. the host being the ligand and the guest being a metal ion). In the meantime, it had also been demonstrated that various naturally occuring macrocyclic antibiotics, enniatins, monactin, nonactin and valinomycin (Figure 1.3), selectively complex alkali metal cations and also displayed the ability to transport these ions across membranes.[5-11]

Valinomycin exhibits ionophoric behaviour, as it facilitates the transport of K^+ ions into mitochondria.[8] The K^+ ion is too large to be accomodated by valinomycin's 36-membered ring, therefore the valinomycin molecule folds over to form a three dimensional cavity which is quite selective for K^+.[9] Coordination is by six octahedrally arranged ester carbonyl oxygen atoms which line the cavity. Nonactin completely encapsulates the K^+ ion in the K^+-nonactin complex.[10,11] The 32-membered nonactin macrocyclic ring envelops itself around the central K^+ ion and totally shields it from the bulk solvent. Approximate cubic coordination of the K^+ ion exists in the crystal

(a)

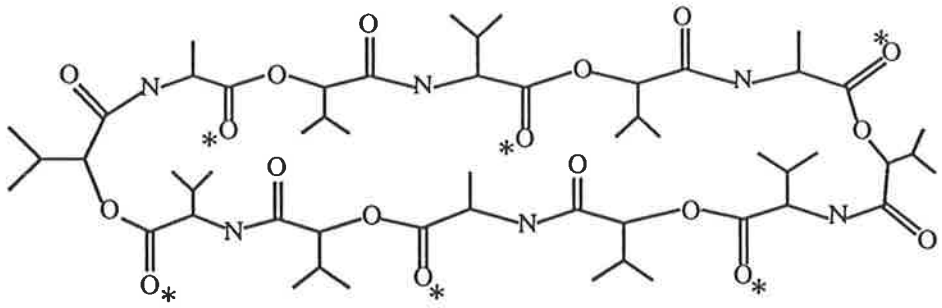

(b)

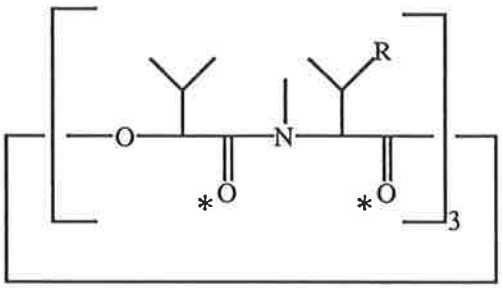

R= CH_3 : Enniatin B
R= C_2H_5 : Enniatin A

(c)

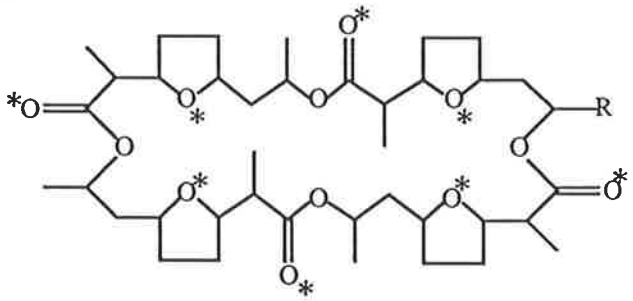

R= CH_3 : Nonactin
R= C_2H_5 : Monactin

(d)

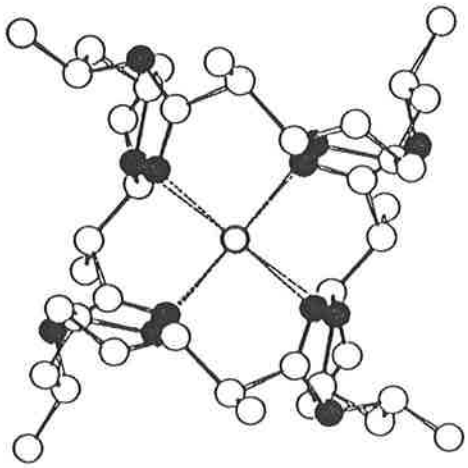

Figure 1.3 *The structures of the antibiotics (a) valinomycin, (b) enniatins A and B, (c) monactin and nonactin , and (d) the crystal structure of the K^+-nonactin complex. The coordinating atoms in (a), (b) and (c) are indicated by an asterisk (*). In the K^+-nonactin crystal structure, the carbon atoms are represented by open circles, the oxygen atoms by shaded circles and the K^+ by a heavy circle.*

stucture. It is held in place by four furane oxygen atoms and four ester carbonyl oxygen atoms (Figure 1.3(d)).

J.-M. Lehn designed and successfully synthesized diazapolyoxomacrobicyclic polyether ligands[12-15] which combined the complexing ability of the macrocyclic antibiotics with the chemical stability of the crown ethers. It was envisaged that ligands with three dimensional, spheroidal cavities that could completely encapsulate metal ions would form more stable complexes than the crown ethers, which have only two dimensional cavities. These ligands were appropriately named cryptands (derived from the Greek *κρυπτος*: hidden and Latin *crypta*: cavity, cave) and their metal complexes cryptates.[13] The presence of a third polyether chain anchored at two nitrogen bridgeheads makes the cryptands quite rigid in structure.

One of the first cryptands synthesized was 4,7,13,16,21,24-hexaoxa-1,10-diazabicyclo[8.8.8]hexacosane or C222,[12] it's trivial name indicating that there are two oxygen atoms on each of the three polyether chains. The general structural formula and abbreviated names of some typical cryptands are illustrated in Figure 1.4 along with some aliphatic bridge cryptands. The structural difference between the aliphatic bridge cryptands and the traditional three polyether bridge cryptands is that one of the polyether bridges is replaced by a pure hydrocarbon bridge.

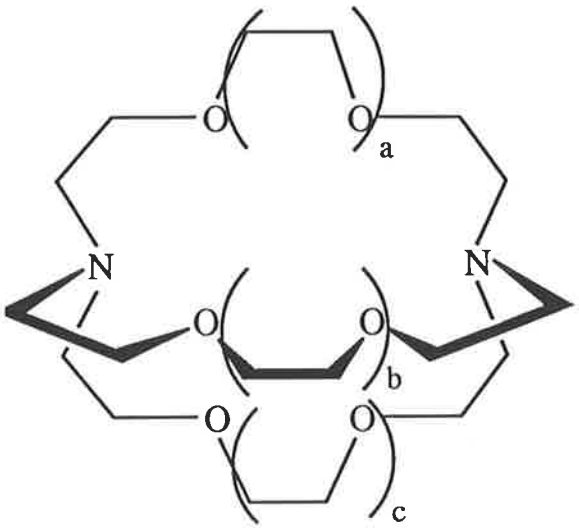

a	b	c	cryptand
0	0	0	C111
1	0	0	C211
1	1	0	C221
1	1	1	C222
2	1	1	C322
2	2	1	C332
2	2	2	C333
1	0	$(CH_2)_5$	$C21C_5$
1	1	$(CH_2)_5$	$C22C_5$
1	1	$(CH_2)_8$	$C22C_8$

Figure 1.4 *Structural formula and trivial nomenclatures for some typical cryptands, including some aliphatic bridge cryptands.*

This form of host-guest chemistry was described as supramolecular chemistry by Lehn.[15,16] Just as molecular chemistry is the chemistry of the covalent bond, supramolecular chemistry is the chemistry of the intermolecular bond. When a substrate (ie. metal cation) binds to a molecular receptor (ie. cryptand), the resultant product is a supermolecule. The substrate may be bound to the molecular receptor by various intermolecular forces including hydrogen bonding, electrostatic interactions and Van der Waals forces. Molecular receptors, which are covalently bound organic molecules, may be designed to selectively bind substrates, thus displaying molecular recognition. Basic functions other than molecular recognition which may be exhibited by supermolecules include molecular transformation and molecular translocation.

Numerous varieties of crown ethers and cryptands have since been prepared where nitrogen and sulfur have been substituted for oxygen,[3,12-14,17,18] and where the number of donor atoms have been altered, resulting in the modification of the cavity size.[19]

The crystal structures of 18-crown-6[20] and C222[21] in their uncomplexed states contain neither prearranged cavities nor binding sites. Upon complexation, the ligands binding sites must be desolvated and conformationally rearranged to create cavities in which the metal cations can be accomodated. The carbanion chemist D.J. Cram designed and synthesized a different class of ligands known as the spherands,[22-24] of which the structure shown in Figure 1.5 was the prototype.

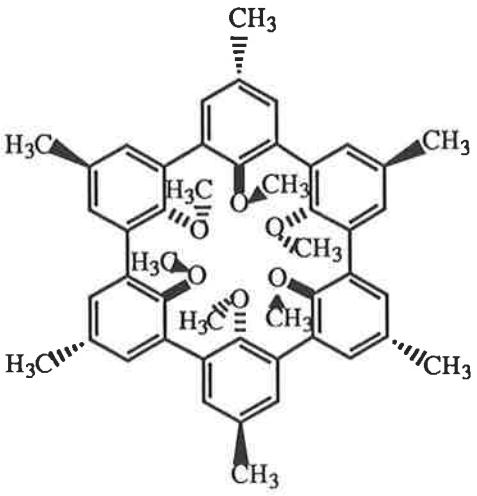

Figure 1.5 *Cram's first designed and synthesized highly preorganized spherand.*

Spherands are ligands organized for complexation during their syntheses rather than during complexation. Their unsolvated binding sites line rigid, enforced, spherical cavities which are complementary to the metal ions they accomodate. Nearly identical crystal structures are observed for the spherands in their free states and their complexed states.[24] The preorganization results in the spherands being highly selective and more powerful complexing agents than the crown ethers and cryptands.

In 1987 the Nobel Prize in chemistry was awarded to Pedersen, Lehn and Cram. Their discoveries in supramolecular chemistry has led to a new way of thinking in chemistry. The consideration of non-covalent interactions has given rise to a wide range of applications in chemistry, biochemistry, industry and other related fields, some of which will be discussed later.

While attempting to design and synthesize ligands which behave as good carriers in membrane transport like valinomycin, several factors needed to be considered. At the membrane, binding of the guest (ie. cation) should be fast and strong. Inside the hydrophobic membrane, the guest should remain strongly bound to the substrate (ie. ligand). Lastly, once on the other side of the membrane, the guest should be weakly bound and released relatively quickly. Since these contradictory prerequisites cannot all be achieved, a compromise had to be considered. The cryptands had three dimensional cavities and the binding strength required but lacked lability, whereas the crown ethers were labile but lacked both the capacity to envelop cations and the sufficient binding strength. Crown ethers possessing sidearms with or without donor atoms (lariat ethers) were developed as they appeared to occupy a niche between the crown ethers and cryptands in their metal ion complexation characteristics.[25-29]

There are two main types of lariat ethers, the carbon-pivot and nitrogen-pivot (Figure 1.6). The carbon-pivot lariat ethers have the pendant arm attached to a carbon atom in the polyether ring, whereas the nitrogen-pivot lariat ethers have a pendant arm attached to a nitrogen atom in the azacrown ring. More than one pendant arm is possible for the nitrogen-pivot lariat ethers if diaza or triaza crowns are used as the precursors. Two pendant armed systems are called **bi**bracchial **l**ariat **e**thers (or BiBLEs), likewise three pendant armed systems are called **trib**racchial **l**ariat **e**thers (or TriBLEs).[26] The type of pendant arm is varied, and some are illustrated in Figure 1.6. Since nitrogens have the ability to easily invert, they therefore make the nitrogen-pivot lariat

ethers more flexible, more dynamic and hence usually less chemically stable than the carbon-pivot lariat ethers.

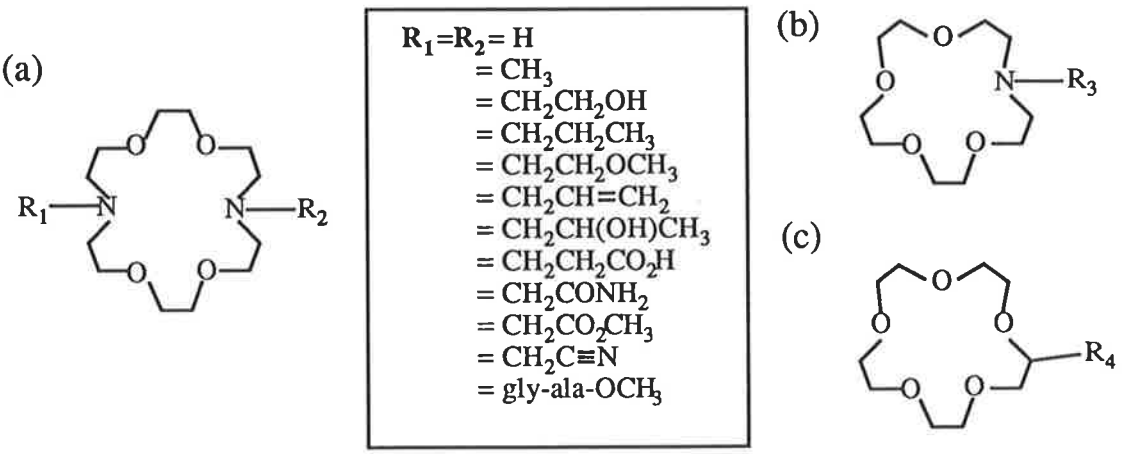

Figure 1.6 *General structures of (a) bibracchial lariat ethers, (b) Nitrogen-pivot lariat ethers, and (c) Carbon-pivot lariat ethers. A wide variety of pendant arms is shown for the 18-membered bibracchial lariat ethers (the last example is a peptide sidearm where gly and ala represent the amino acids glycine and alanine, respectively).*

The intriguing ion binding and transport abilities of these macrocyclic receptor molecules discussed have attracted a lot of interest in recent years. This study aims to improve and extend the current understanding of the equilibrium, thermodynamic, kinetic and mechanistic aspects of some monovalent and divalent cation complexes of cryptands and bibracchial lariat ethers.

1.2 : Structural Aspects of Cryptates and Lariat Ether Complexes.

An interest in the structures of synthetic macrocyclic compounds and their metal cation complexes has been generated over the years due to the ability of these compounds to surround or enclose many different cations. The structural features of such ligands determine the stability, selectivity and properties of their complexes with metal ions. Crystallographic studies of macrocyclic molecules and their complexes allows for the investigation of some of the factors which determine the type of coordination taking place. These factors include ligand cavity size and donor type, and metal cation size and type.

This study investigates the complexation properties of monovalent metal cations in a variety of trialkyl phosphate solvents with the cryptands 4,7,13,18-tetraoxa-1,10-diazabicyclo[8.5.5]eicosane, or C211, and 4,7,13-trioxa-1,10-diazabicyclo[8.5.5]eicosane, or C21C_5. The cryptand C211 has a cavity delineated by four ether oxygen and two nitrogen atoms, consequently having the capacity to hexacoordinate a metal ion upon complexation. On the other hand, the aliphatic bridge cryptand C21C_5 has one ether bridge and one electron donating oxygen atom less than C211, allowing it to only pentacoordinate a metal ion upon complexation. The third bridge in C21C_5 is a hydrocarbon chain comprising of five methylene groups. Furthermore, both C211 and C21C_5 possess similar sized cavities ($r \approx 0.8$ Å) because essentially the only difference between the two ligands is that an oxygen atom from the $-CH_2CH_2OCH_2CH_2-$ moiety in C211 is replaced by a methylene group to yield C21C_5. This intentional variation makes it possible to evaluate the effect of variation in donor atoms on the structure, stability and lability of cryptates.

Also examined in this study are the complexation characteristics of the bibracchial lariat ethers 1,7-bis(2-hydroxyethyl)-4,10,13-trioxa-1,7-diazacyclopentadecane, or BHE-C21, and 1,10-bis(2-hydroxyethyl)-4,7,13,16-tetraoxa-1,10-diazacyclooctadecane, or BHE-C22, with alkali, alkaline earth, transition and heavy metal cations in aqueous solution and a wide range of non-aqueous solvents. Both BHE-C21 and BHE-C22 possess two hydroxyethyl pendant arms, each containing an alcoholic oxygen donor atom with which they can facilitate the complexation of metal cations. The bibracchial lariat ether BHE-C21 has a smaller fifteen-membered ring and

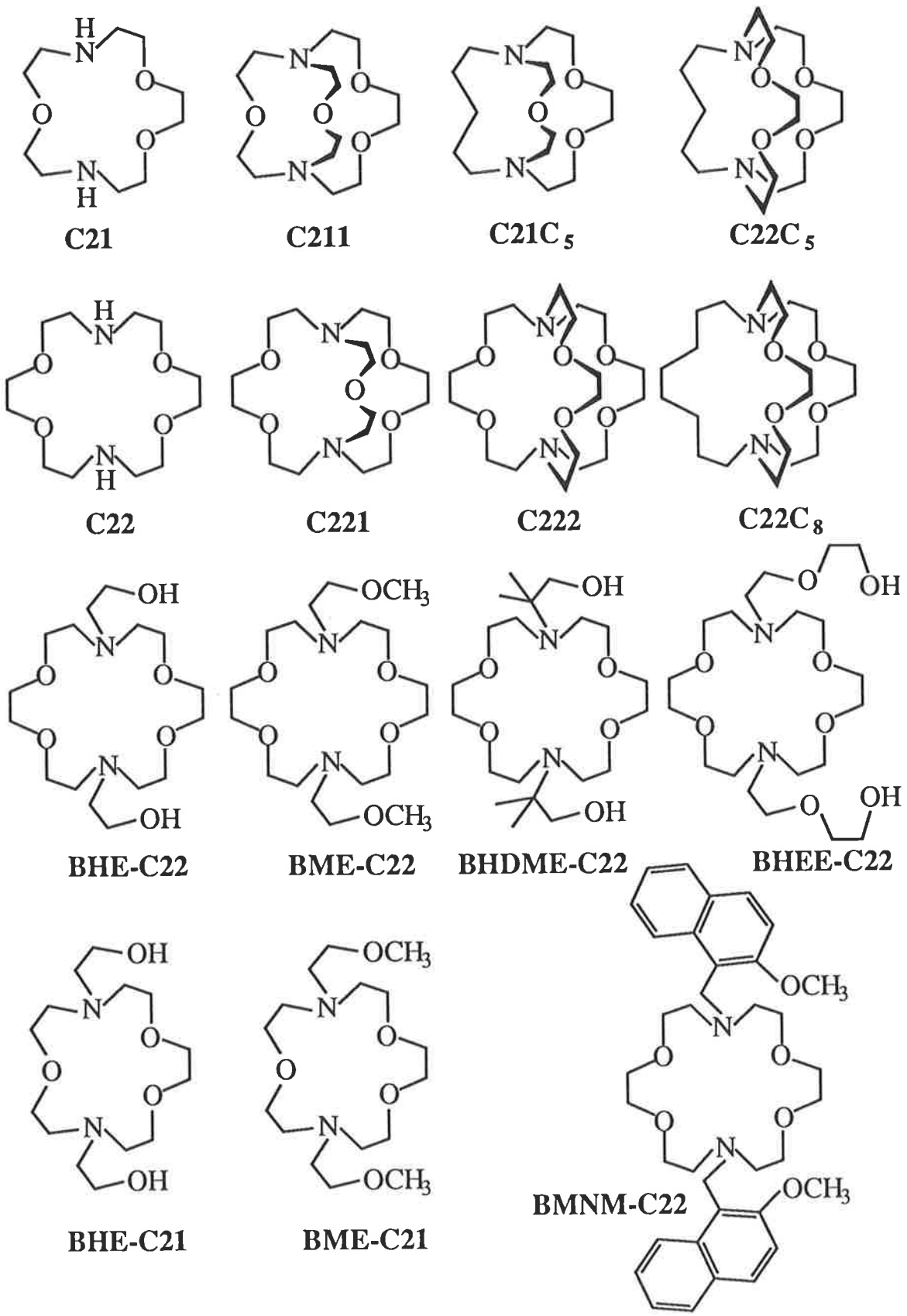

Figure 1.7 *Structure of various diaza crown ethers, cryptands and bibracchial lariat ethers used or discussed in this study.*

one less ether oxygen donor atom than BHE-C22, which has an eighteen-membered ring. Structurally, BHE-C21 and BHE-C22 are comparable to the cryptands C221 and C222 respectively, since they contain the same number of oxygen and nitrogen donor atoms. Only an ethylene bridge needs to be added to BHE-C21 and BHE-C22 to convert them exactly to their respective related cryptands. The structures of these ligands used in this study, along with some related stuctures used for discussion and comparison purposes are illustrated in Figure 1.7.

Polyoxadiazabicycloalkanes, or cryptands, contain three dimensional intramolecular cavities delineated by electon donor atoms for binding, and whose size is governed by the length of the polyether bridges. They may exist in any of three conformations (Figure 1.8) according to the configuration of the two nitrogen bridgeheads.[12] The ability for nitrogen inversion to take place gives rise to the conformers *endo-endo*, in which the lone pair of electrons on the nitrogen atoms are directed towards the inside of the intramolecular cavity, *endo-exo*, and *exo-exo*, where the lone pairs are directed away from the central cavity. The *endo-endo* form is the conformer observed in the cryptates,[30-36] since in this form all the heteroatoms may participate in complexation of the electrophilic metal cation.

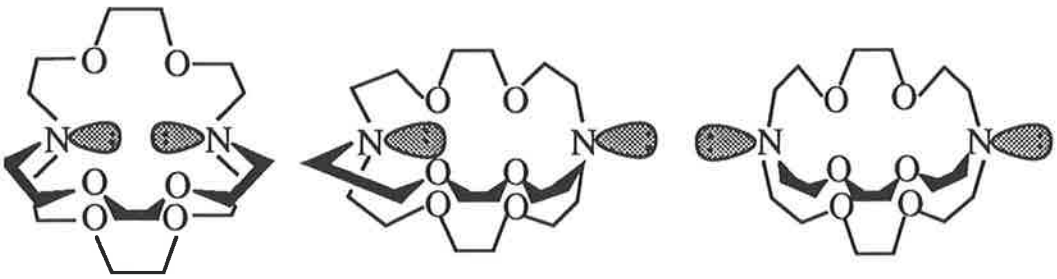

endo-endo *endo-exo* *exo-exo*

Figure 1.8 *The cryptand C222 is used to illustrate the three possible cryptand conformers.*

It would be too naive to assume that macrocycle-cation binding is the insertion of a spherical metal ion into a preformed rigid cavity. The crystal structure of the uncomplexed cryptand C222[21] is evidence of this. It exists in the *endo-endo* conformation, similar to that of cryptates, but it compensates for the vacant cavity by flattening and extending somewhat. These observations as well as the fact that some of the oxygen lone pairs in

uncomplexed C222 point away from the cavity implies that small structural changes are required during complex formation.

The intramolecular cavity radius of C222 is about 1.4 Å,[19] which is similar to the eight coordinate ionic radius of the alkali cation K^+ (r = 1.51 Å).[37] Thus the $[K.C222]^+$ cryptate formed is quite stable due to the nice fit of the cation in the centre of the intramolecular cavity. Additionally, it is formed without excessive distortion of the C222 ligand. Crystal structures of the smaller Na^+ (r = 1.18 Å) and larger Rb^+ (r = 1.61 Å) and Cs^+ (r = 1.74 Å) alkali metal cations with C222 also reveal these metal ions to be located inside the intramolecular cavity. Even though Na^+ is too small and Rb^+ and Cs^+ are too large for effective coordination, the ligand C222 exhibits some flexibility in adapting its intramolecular cavity to the ionic radius of the enclosed metal cation. These factors mentioned account for the stability of the C222-alkali metal cation cryptates being in the order $Na^+ < K^+ > Rb^+ > Cs^+$.

When cryptands complex alkali metal cations, the resulting cryptates may exist in one of two forms, either *inclusive* or *exclusive* (Figure 1.9). *Inclusive* cryptates are those in which the metal cation is totally encapsulated within the cryptand cavity, whereas *exclusive* cryptates are those in which the metal cation is located on the outside of a cryptand face, as defined by two of the nitrogen to nitrogen bridges. In *inclusive* cryptates, the first coordination spheres of the metal ions are occupied solely by the binding groups of the cryptand, and there is minimal interaction between the metal ion and the counteranion in the solid state or with the solvent in solution. Whereas, metal ions in *exclusive* cryptates are somewhat exposed and susceptible to interactions with anions or solvent molecules.

Apart from all the *inclusive* $[M.C222]^+$ cryptates mentioned previously, some other cryptates which represent *inclusive* cryptates include [Na.C221]NCS,[38] [Li.C211]I[33] and [Li.C21C5]NCS.[31] However, the complexes [K.C221.NCS],[38] [Na.C211.NCS][30] and [Na.C21C5.NCS][30] are examples of *exclusive* cryptates. All the solid state structures were determined by single-crystal X-ray diffraction methods.

The cryptand C221 has a cavity radius of about 1.1 Å, which is very close to the ionic radius of Na^+, therefore it forms *inclusive* $[Na.C221]^+$. Unlike Na^+, K^+ is too large to be accomodated inside the intramolecular cavity, and resides on the face of the eighteen-membered ring with a thiocyanate ion completing its coordination shell. Accordingly, it forms the *exclusive* cryptate $[K.C221]^+$.

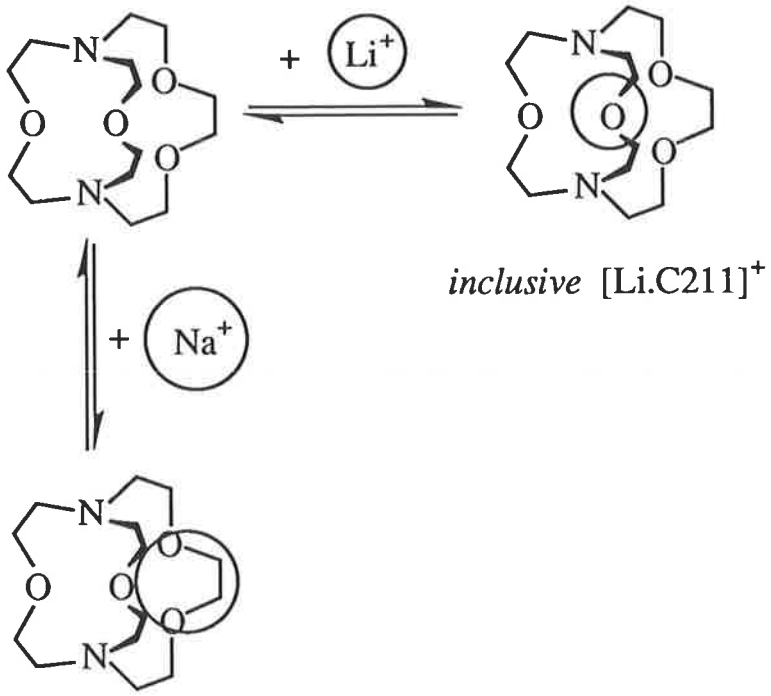

Figure 1.9 *Diagram illustrating the two extreme forms of cryptates-inclusive and exclusive.*

X-ray diffraction studies have also shown that the Li^+ cryptates of both C211 and C21C5 were *inclusive* structures and both the Na^+ cryptates of the same ligands were *exclusive* structures. Again, these observations are a consequence of Li^+ being the right size and Na^+ being too big to fit into the similarly sized intramolecular cavities of C211 and C21C5 (radius of about 0.8 Å). The extra electron donating ether oxygen in C211 provides an extra electrostatic interaction for Li^+ to enter the C211 molecular cavity as opposed to C21C5. Also in these Li^+ cryptates, the counteranions are not within bonding distance of the Li^+ ions and consequently there is no interaction between the two. In both the Na^+ cryptates of C211 and C21C5, the Na^+ ion is located 0.14 and 0.37Å respectively above the plane defined by the three oxygen atoms of the fifteen-membered 1,10-diaza-4,7,13-trioxacyclopentadecane ring. Furthermore, the Na^+ ions are within bonding distance of the nitrogen atoms in the thiocyanate anions. Here the effect of the extra oxygen donor atom in C211 is clearly evident with the greater attraction of C211 for Na^+ resulting in the closer proximity of Na^+ to the three oxygen plane of the 1,10-diaza-4,7,13-trioxacyclopentadecane ring. The space filling diagrams in Figures 1.10 and 1.11 illustrate the extent or degree to which the

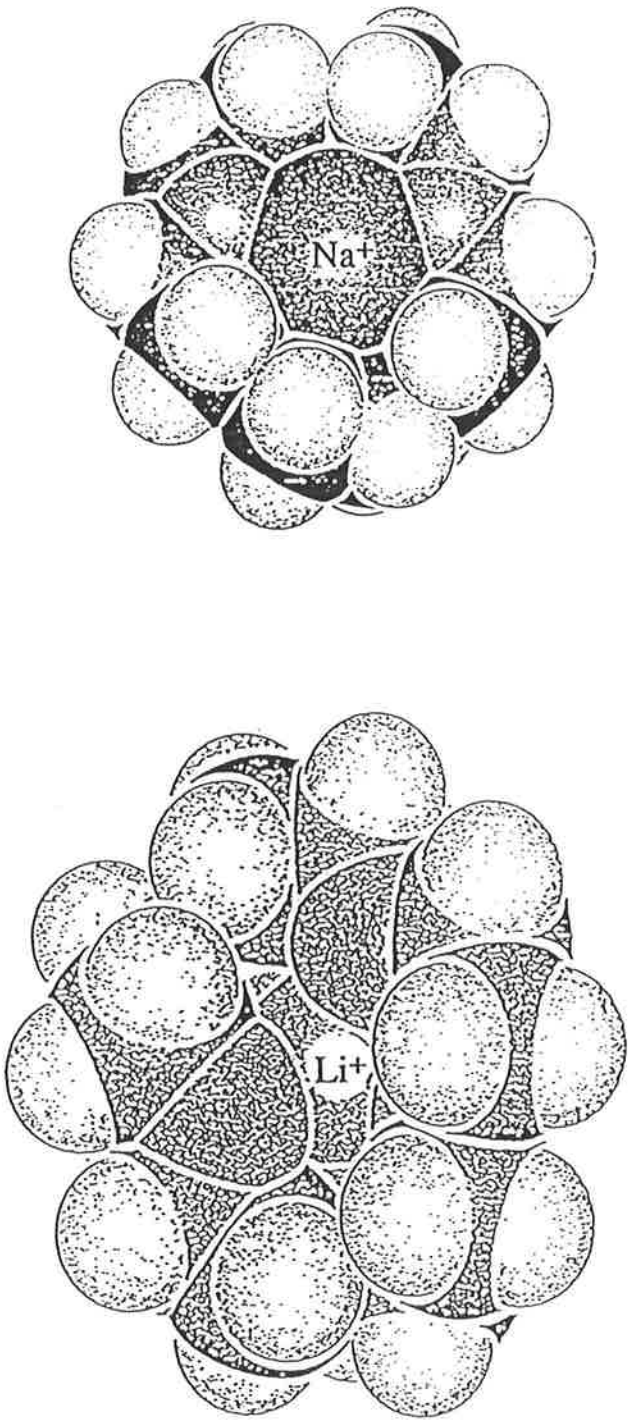

Figure 1.10 *SCHAKAL[39] plots of [Na.C211]+ [40] and [Li.C211]+ [41] showing the degree to which the alkali metal ions are included inside the intramolecular cavity of C211. All atoms are shown as spheres of appropriate radii and the anions have been omitted from view in both plots.*

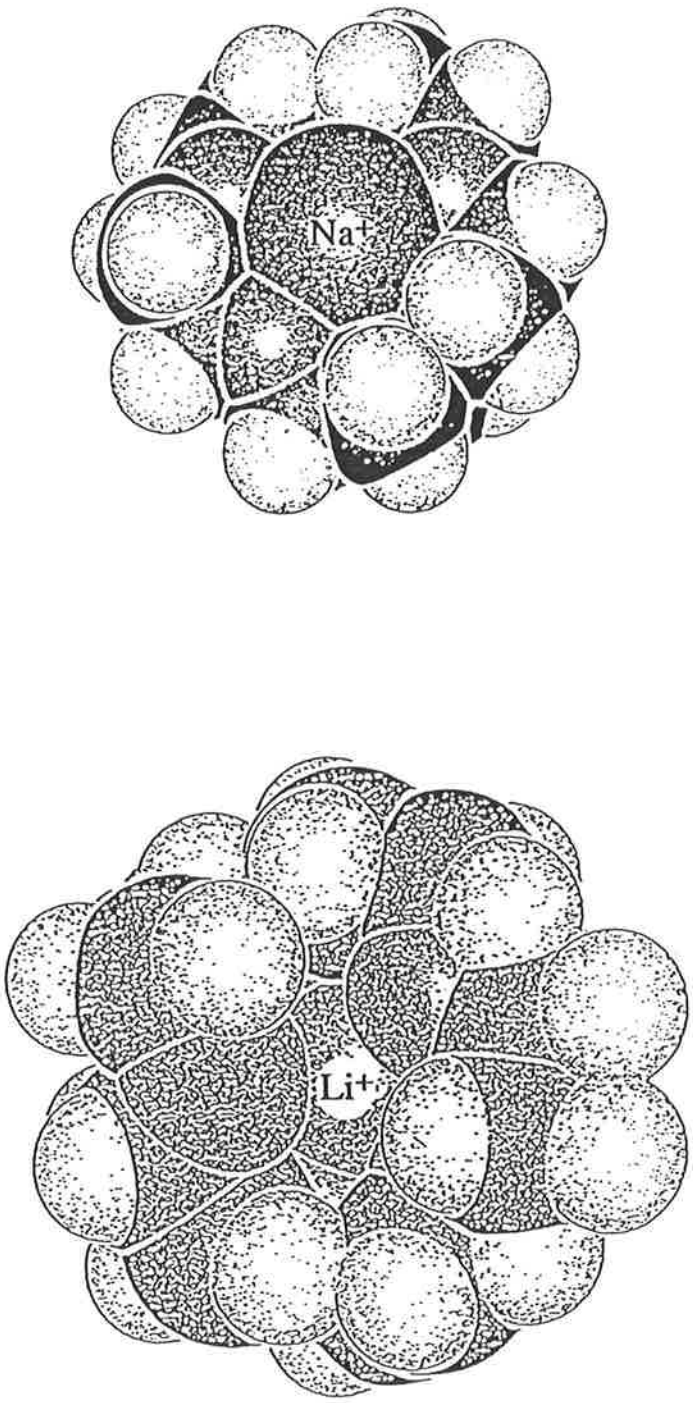

Figure 1.11 *SCHAKAL[39] plots of [Na.C21C5]+ [40] and [Li.C21C5]+ [41] showing the degree to which the alkali metal ions are included inside the intramolecular cavity of C21C5. All atoms are shown as spheres of appropriate radii and the anions have been omitted from view in both plots.*

Na^+ or Li^+ ions are included inside the intramolecular cavities of C211 and $C21C_5$.

From all the examples highlighted, it can be seen that there exists a strong correlation between cation size, cryptand cavity size and cryptate structure.[14] As a general rule, the structure of metal complexes in the solid state cannot be assumed to represent the solution state metal complex structure, since various solvational and conformational changes may occur upon dissolution. However, ^{13}C NMR studies[30,42-44] on numerous alkali metal cryptates in a variety of solvents reveal that the *inclusive* or *exclusive* nature of cryptates in the solid state are largely retained in solution. This observation assists in the mechanistic interpretation of cryptate equilibria in solution.

When contemplating the structures of bibracchial lariat ether complexes, several issues need to be considered. Firstly, are the macroring and the sidearms both involved in the coordination of the metal ion? Secondly, how many of the sidearms are involved in the complexation process? Thirdly, if both are involved, do they coordinate the metal ion from the same side or from opposite sides of the macroring? Finally, is the metal ion actually contained within the macroring?

As mentioned previously, the solid state structures are not unequivocal evidence for solution state structures. Having said that, the implication of X-ray studies are invaluable in our understanding of the interactions between metal ion and ligand. Several crystal structures of bibracchial lariat ether complexes have been determined.[45-52] They illustrate the cooperative participation of the macroring and sidearms in the binding of metal ions. Solution binding studies[53-56] and ^{13}C NMR relaxation time studies[57] have also demonstrated that sidearms and macroring cooperate in cation binding, and complement the X-ray structural studies.

All crystal structures of bibracchial lariat ether complexes determined so far have both sidearms participating in cation complexation, except those in which the sidearms lacked donor atoms[58] and no participation of sidearms is observed or expected. There have been no examples of single sidearm participation. Two different arrangements are observed in bibracchial lariat ether complexes, those which stabilize the cation with the sidearms from the same side and those from the opposite sides of the macroring. These two arrangements have been designated *syn* and *anti* respectively (Figure 1.12). There appear to be no reported solid state structures of fifteen-membered ring

bibracchial lariat ether complexes, so all discussed examples are those of eighteen-membered ring complexes.

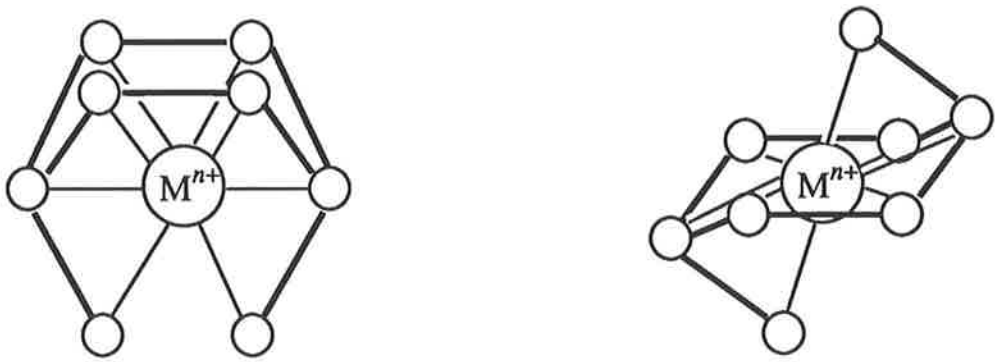

syn *anti*

Figure 1.12 *Skeletal drawings illustrating the two possible donor atom arrangements in bibracchial lariat ether complexes-syn and anti.*

The observed structure was *syn* when the sidearms were CH_2CH_2OH and the cation was either Na^+ or K^+.[45,46] The macroring donor atoms adopted a twist-boat conformation in the Na^+ complex, and the sidearm oxygen donor atoms occupied "flagpole" positions. In the K^+ complex, the macroring donor atoms were also arranged in an almost perfect boat conformation. As with the Na^+ complex, the sidearm oxygen donor atoms occupied "flagpole" positions. When the sidearms were $CH_2CH_2OCH_3$ and the cation Na^+,[47] the structure was *syn*, whereas when the cation was K^+,[46] the reported structure was *anti*. The Na^+ complex structure was very similar to the $[Na.BHE\text{-}C22]^+$ structure in that the macroring donor atoms adopted a twist-boat conformation and the sidearm oxygen donor atoms occupied "flagpole" positions. The differing K^+ complex structure had the macroring donor atoms arranged in a chair conformation and the sidearm oxygen donor atoms located above and below the plane of the macroring.

It can be seen from the skeletal drawings of $[Na.BHE\text{-}C22]^+$, $[Na.BME\text{-}C22]^+$, $[K.BHE\text{-}C22]^+$ and $[K.BME\text{-}C22]^+$ (Figure 1.13) that the alkali metal ion is not actually contained within the N_2O_4 macroring cavity in the *syn* structures, but is in *anti* $[K.BME\text{-}C22]^+$. Because of this and the fact that lariat ethers are very flexible molecules, the macroring cavity size-cation size relationship is not appropriate in the explanation of lariat ether complex chemistry as it is in cryptate chemistry. All the *syn* structures illustrate that the sidearms do not pull the metal cations towards them but rather, fill empty

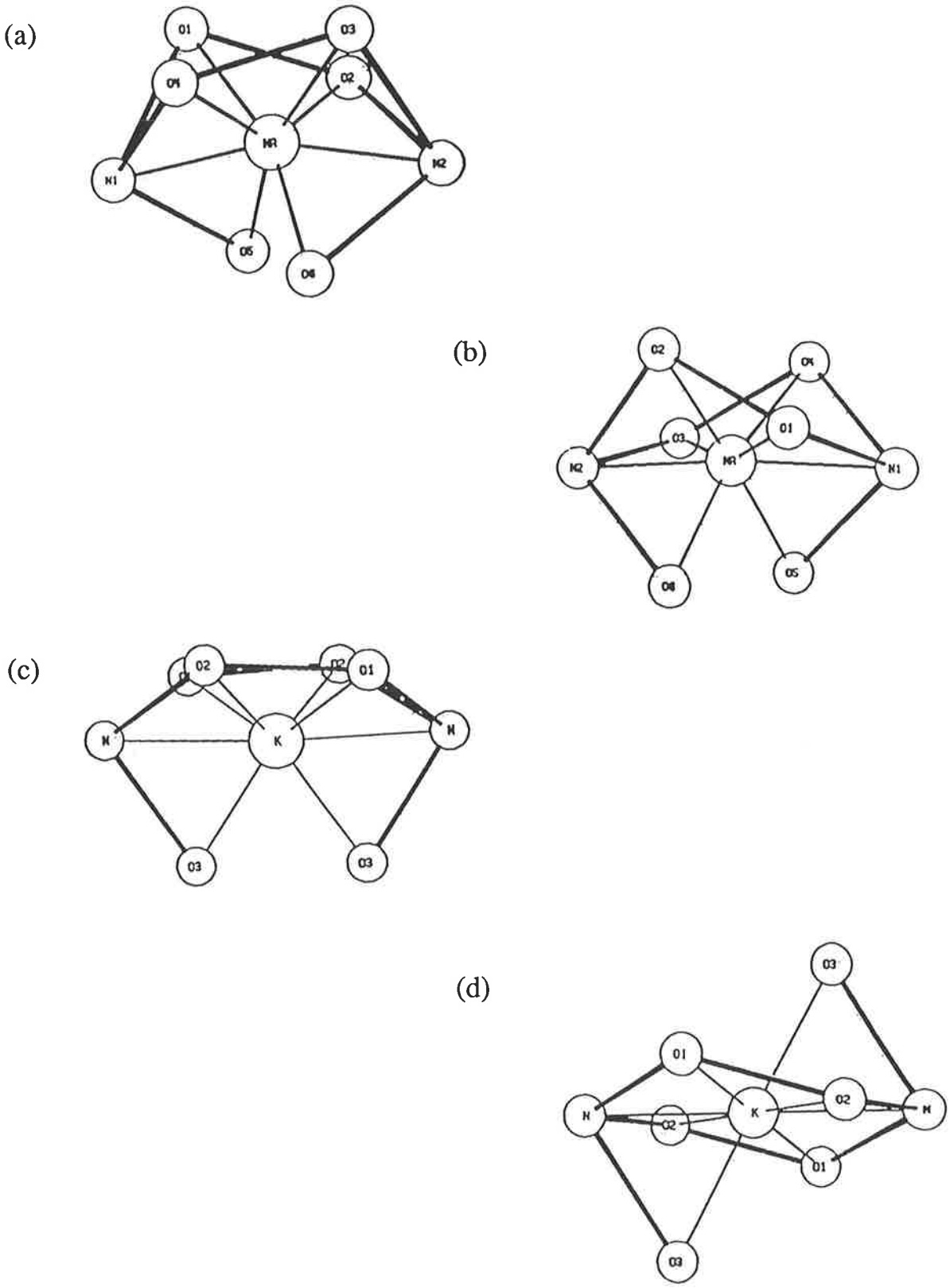

Figure 1.13 *Skeletal drawings of the sodium and potassium cation complexes of the bibracchial lariat ethers BHE-C22 and BME-C22: (a) [Na.BHE-C22]$^+$, (b) [Na.BME-C22]$^+$, (c) [K.BHE-C22]$^+$ and (d) [K.BME-C22]$^+$.*

apical positions in the cations coordination sphere. They also bear a remarkable resemblance to C222 cryptate complexes, as all the donor atoms are arranged in a three dimensional array about the metal cation.

Rather than *anti* $[K.BME\text{-}C22]^+$ being the exception, it was suggested that the odd structure was *syn* $[K.BHE\text{-}C22]^+$. All Na^+ complexes of eighteen-membered ring bibracchial lariat ethers were expected to favour the *syn* arrangement and K^+ the *anti* arrangement. The exception $[K.BHE\text{-}C22]^+$, was in the *syn* arrangement because hydrogen is such a small substituent on the sidearm alcoholic oxygens, whereas two methyl groups cause steric hindrance between the sidearms, giving rise to *anti* $[K.BME\text{-}C22]^+$.

Several recent crystal structures of eighteen-membered bibracchial lariat ether complexes have shed more light on those early structural beliefs and understandings. When the sidearms were 2-hydroxy-1,1-dimethylethyl (CMe_2CH_2OH) groups and the cation was K^+,[49] the observed structure was in the *syn* arrangement. The macroring donor atoms were in a boat conformation with very little twist. The placement of methyl groups on the ethylene bridges of a chelate ring causes less steric hindrance than placement on the actual oxygen or nitrogen donor atoms.[59] The inductive effects of the C-methyl groups, which increase the basicity of the oxygen donor atoms, appear to prevail over the steric effects. Hence, the structure of the K^+ complex is similar to *syn* $[K.BHE\text{-}C22]^+$. Unexpected observations were made when the sidearms were 2-methoxy-1-naphthylmethyl.[48] The Na^+ structure was in the *anti* arrangement with the macroring donor atoms in a chair conformation similar to *anti* $[K.BME\text{-}C22]^+$, whereas the K^+ structure was in the *syn* arrangement with the macroring donor atoms in a twisted boat conformation. These two structures are the reverse to those expected due to steric reasonns, and the *syn* K^+ complex conflicts with the idea that the methoxy methyl groups cause sidearm steric hindrance in K^+ bibracchial lariat ether complexes. The different arrangements were attributed to the different ionic radii and electron charge densities of Na^+ and K^+.

Solid state structures of the similarly sized cations K^+ and Ba^{2+} with the bibracchial lariat ether containing 2-*o*-hydroxyethyl-2-oxyethyl ($CH_2CH_2OCH_2CH_2OH$) sidearms were *anti* and *syn* respectively. The Ba^{2+} complex[51] is eleven coordinate with a water molecule accounting for the extra coordination site, as opposed to the predominant K^+ conformer[50] which is only eight or nine coordinate, with an oxygen donor atom on one or both sidearms left uncoordinated. The *anti* arrangement was adopted in

$[K.BHEE\text{-}C22]^+$ for steric and donor atom repulsion reasons. In contrast, the higher charge on Ba^{2+} led to a greater attraction for the electron donating oxygen atoms and helped counteract the mutual electrostatic repulsion between the sidearm oxygen donor atoms.

From all the above examples of eighteen-membered ring bibracchial lariat ether complexes it can be seen that the structure is a compromise between the metal cation charge, ionic radius, electron charge density and the type of macrocycle sidearm.

1.3 : Applications of Macrocyclic Chemistry.

Since the discovery of crown ethers, supramolecular chemistry has been applied to a vast range of areas, including analytical, biological and industrial fields. Some of the numerous applications of crown ethers, cryptands and lariat ethers are listed below.

(i) *Membrane transport processes*-The macrocycles act as the carrier molecules which transport the substrates (eg. cations) across membranes (Figure 1.14).[15,25,60-66]

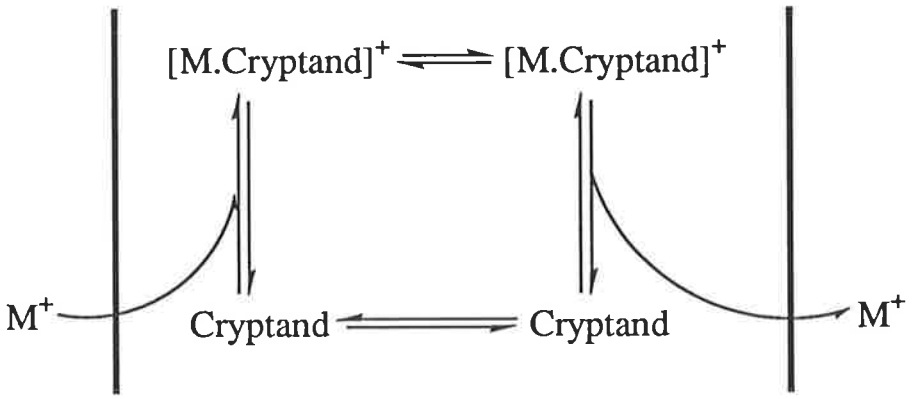

Figure 1.14 *Mechanism of carrier (ie. cryptand) mediated transport of a cation across a membrane.*

(ii) *Ion-selective electrodes*-The macrocycles behave as ion carriers.[67-70]

(iii) *Ion chromatography*-Resin-bound macrocycles facilitate the selective separation of alkali and alkaline-earth metal cations.[25,67,71,72]

(iv) *Supramolecular catalysis*-Molecular receptors containing specialized reactive groups, may bind a substrate, react with it, if its reactive groups are appropriate, and discharge the product(s).[15,16]

(v) *Binding of toxic heavy metal cations*-eg. Cd^{2+}, Pb^{2+} and Hg^{2+}.[16,27,72-76] Treatment of heavy metal poisoning is of very great concern in environmental chemistry. The economic viability for the control of these toxic metal cations in the environment is a major problem.

(vi) *Fluorescent probes*-Upon complexation of cations, certain macrocycles have an enhanced fluorescence. They have been used as fluorescent probes in membrane studies[77] and cation detection.[78-83]

(vii) *Anion recognition*-As well as cation coordination, the coordination of anionic species is possible with certain macrocyclic compounds.[84] Anionic species have both chemical and biological significance. Macrocycles which bind carboxylates and phosphates have been developed. These receptor molecules mimic biological receptors and act as anchoring sites for various biological substrates.[15]

(viii) *Isotope separation*[85,86]

(ix) *Alkalides*-eg. $Na^+(C222)Na^-$. These compounds contain anions which are negative alkali metal anions.[85,87-89] They behave as intrinsic semiconductors and have possible uses in solid-state devices and as aprotic reducing agents.

(x) *Molecular devices*-Light conversion molecular devices[15,90] are but one example. Ultraviolet light absorbed by these macrocyclic molecules is transfered to the cavity bound lanthanide cation by intramolecular energy transfer, and emitted as visible light by the complexed lanthanide cation. These complexes utilize an Absorption-Energy Transfer-Emission (A-ET-E) process. Potential biological applications include tags for monoclonal antibodies, nucleic acids and membranes.

(xi) *Chiral recognition*-Optically active macrocycles containing chiral centres exhibit enantioselectivity and are used to separate racemic mixtures into their enantiomers.[24,25,67,91-94] Chiral recognition is used in the resolution of free amino acids.[92]

(xii) *Anion activation*-When a cation is enveloped inside a macrocyclic cavity, the anion is free to do what it likes and may become reactive. Phase transfer catalysis[25] uses this idea, assisting transfer from solid to liquid or liquid to liquid. Solubilization of inorganic salts in organic solvents[2,3,25,95] by dissociating the cation-anion pair is a form of anion activation. Anion activation is also used in some industrial polymerisation processes.[85]

The examples of macrocyclic molecule applications illustrate that the applications are wide and numerous and future applications are only limited by the imagination and creativity of the research chemist.

References

1 C.J. Pedersen, *J. Am. Chem.Soc.*, **89**, 1967, 2495.

2 C.J. Pedersen, *J. Am. Chem.Soc.*, **89**, 1967, 7017.

3 C.J. Pedersen and H.K. Frensdorff, *Angew. Chem., Int. Ed. Engl.*, **11**, 1972, 16.

4 C.J. Pedersen, *J. Inclusion Phenom.*, **6**, 1988, 337.

5 Z. Stefanac and W. Simon, *Microchem. J.*, **12**, 1967,125.

6 Z. Stefanac and W. Simon, *Chimia*, **20**, 1966, 436.

7 P. Mueller and D.O. Rudin, *Biochem. Biophys. Res. Commun.*, **26**, 1967, 398.

8 C. Moore and B.C. Pressman, *Biochem. Biophys. Res. Commun.*, **15**, 1964, 562.

9 K. Neupert-Laves and M. Dobler, *Helv. Chim. Acta*, **58**, 1975, 432.

10 B.T. Kilbourn, J.D. Dunitz, L.A.R. Pioda and W. Simon, *J. Mol. Biol.*, **30**, 1967, 559.

11 M. Dobler, J.D. Dunitz and B.T. Kilbourn, *Helv. Chim. Acta*, **52**, 1969, 2573.

12 B. Dietrich, J.-M. Lehn and J.-P. Sauvage, *Tetrahedron Lett.*, 1969, 2885.

13 B. Dietrich, J.-M. Lehn and J.-P. Sauvage, *Tetrahedron Lett.*, 1969, 2889.

14 J.-M. Lehn, *Struct. Bonding (Berlin)*, **16**, 1973, 1.

15 J.-M. Lehn, *J. Inclusion Phenom.*, **6**, 1988, 351.

16 J.-M. Lehn, *Pure Appl. Chem.*, **50**, 1978, 871.

17 C.J. Pedersen, *J. Org. Chem.*, **36**, 1971, 254.

18 A.I. Popov and J.-M. Lehn: in G.A. Melson (Ed.) : "Coordination Chemistry of Macrocyclic Compounds", Plenum Press, New York, 1979.

19 J.-M. Lehn and J.-P. Sauvage, *J. Chem. Soc., Chem. Commun.*, 1971, 440.

20 J.D. Dunitz and P. Seiler, *Acta Crystallogr., Sect. B*, **B30**, 1974, 2739.

21 B. Metz, D. Moras and R. Weiss, *J. Chem. Soc., Perkin Trans. II*, 1976, 423.

22 D.J. Cram, T. Kaneda, R.C. Helgeson and G.M. Lein, *J. Am. Chem. Soc.*, **101**, 1979, 6752.

23 D.J. Cram, T. Kaneda, R.C. Helgeson, S.B. Brown, C.B. Knobler, E. Maverick and K.N. Trueblood, *J. Am. Chem. Soc.*, **107**, 1985, 3645.

24 D.J. Cram, *J. Inclusion Phenom.*, **6**, 1988, 397.

25 G.W. Gokel, "Crown Ethers and Cryptands", The Royal Society of Chemistry, Cambridge, 1991.

26 G.W. Gokel, *Chem. Soc. Rev.*, 1992, 39.

27 S. Kulstad and L.Å. Malmsten, *J. Inorg. Nucl. Chem.*, **43**, 1981, 1299.

28 P. Gramain and Y. Frère, *Nouv. J. Chim.*, **3**, 1979, 53.

29 F. Marsicano, R.D. Hancock and A. McGowan, *J. Coord. Chem.*, **25**, 1992, 85.

30 S.F. Lincoln, E. Horn, M.R. Snow, T.W. Hambley, I.M. Brereton and T.M. Spotswood, *J. Chem. Soc., Dalton Trans.*, 1986, 1075.

31 A. Abou-Hamdan, A.M. Hounslow, S.F. Lincoln and T.W. Hambley, *J. Chem. Soc., Dalton Trans.*, 1987, 489.

32 P. Clarke, J.M. Gulbis, S.F. Lincoln and E.R.T. Tiekink, *Inorg. Chem.*, **31**, 1992, 3398.

33 D. Moras and R. Weiss, *Acta Crystallogr., Sect. B*, **B29**, 1973, 400.

34 D. Moras and R. Weiss, *Acta Crystallogr., Sect. B*, **B29**, 1973, 396.

35 D. Moras, B. Metz and R. Weiss, *Acta Crystallogr., Sect. B*, **B29**, 1973, 383.

36 D. Moras, B. Metz and R. Weiss, *Acta Crystallogr., Sect. B*, **B29**, 1973, 388.

37 R.D. Shannon, *Acta Crystallogr., Sect. A: Cryst. Phys. Diffr., Theor. Gen. Crystallog.*, **A32**, 1976, 751.

38 F. Mathieu, B. Metz, D. Moras and R. Weiss, *J. Am. Chem. Soc.*, **100**, 1978, 4412.

39 E. Keller, SCHAKAL, Institüt für Anorganische Chemie der Universität Freiburg, Freiburg, Germany.

40 P. Clarke, Ph.D. Dissertation, University of Adelaide, 1992.

41 A. Abou-Hamdan, Ph.D. Dissertation, University of Adelaide, 1990.

42 E. Schmidt, J.-M. Tremillon, J.-P. Kintzinger and A.I. Popov, *J. Am. Chem. Soc.*, **105**, 1983, 7563.

43 L. Echegoyen, A. Kaifer, H.D. Durst and G.W. Gokel, *J. Org. Chem.*, **49**, 1984, 688.

44 S.F. Lincoln, I.M. Brereton and T.M. Spotswood, *J. Chem. Soc., Faraday Trans. 1*, **81**, 1985, 1623.

45 F.R. Fronczek, V.J. Gatto, R.A. Schultz, S.J. Jungk, W.J. Colucci, R.D. Gandour and G.W. Gokel, *J. Am. Chem. Soc.*, **105**, 1983, 6717.

46 R.D. Gandour, F.R. Fronczek, V.J. Gatto, C. Minganti, R.A. Schultz, B.D. White, K.A. Arnold, D. Mazzocchi, S.R. Miller and G.W. Gokel, *J. Am. Chem. Soc.*, **108**, 1986, 4078.

47 K.A. Arnold, L. Echegoyen, F.R. Fronczek, R.D. Gandour, V.J. Gatto, B.D. White and G.W. Gokel, *J. Am. Chem. Soc.*, **109**, 1987, 3716.

48 D. Wang, Y. Ge, H. Hu, K. Yu and Z. Zhou, *J. Chem. Soc., Chem. Commun.*, 1991, 685.

49 K.V. Damu, R.D. Hancock, P.W. Wade, J.C.A. Boeyens, D.G. Billing and S.M. Dobson, *J. Chem. Soc., Dalton Trans.*, 1991, 293.

50 R.D. Hancock, R. Bhavan, P.W. Wade, J.C.A. Boeyens and S.M. Dobson, *Inorg. Chem.*, **28**, 1989, 187.

51 R. Bhavan, R.D. Hancock, P.W. Wade, J.C.A. Boeyens and S.M. Dobson, *Inorg. Chim. Acta*, **171**, 1990, 235.

52 B.D. White, J. Mallen, K.A. Arnold, F.R. Fronczek, R.D. Gandour, L.M.B. Gehrig and G.W. Gokel, *J. Org. Chem.*, **54**, 1989, 937.

53 R.A. Schultz, E. Schlegel, D.M. Dishong and G.W. Gokel, *J. Chem. Soc., Chem. Commun.*, 1982, 242.

54 R.A. Schultz, D.M. Dishong and G.W. Gokel, *J. Am. Chem. Soc.*, **104**, 1982, 625.

55 V.J. Gatto, K.A. Arnold, A.M. Viscariello, S.R. Miller and G.W. Gokel, *Tetrahedron Lett.*, **27**, 1986, 327.

56 V.J. Gatto, K.A. Arnold, A.M. Viscariello, S.R. Miller, C.R. Morgan and G.W. Gokel, *J. Org. Chem.*, **51**, 1986, 5373.

57 L. Echegoyen, A. Kaifer, H.D. Durst, R.A. Schultz, D.M. Dishong, D.M. Goli and G.W. Gokel, *J. Am. Chem. Soc.*, **106**, 1984, 5100.

58 K.A. Arnold, A.M. Viscariello, M.S. Kim, R.D. Gandour, F.R. Fronczek and G.W. Gokel, *Tetrahedron Lett.*, **29**, 1988, 3025.

59 R.D. Hancock, B.S. Nakani and F. Marsicano, *Inorg. Chem.*, **22**, 1983, 2531.

60 G.W. Gokel and L. Echegoyen, *Bioorg. Chem. Frontiers*, **1**, 1990, 115.

61 T.M. Fyles, *Bioorg. Chem. Frontiers*, **1**, 1990, 71.

62 H. Tsukube, *J. Coord. Chem.*, **16**, 1987, 101.

63 B. Sesta and A. D'Aprano, *J. Solution Chem.*, **18**, 1989, 1163.

64 H. Tsukube, K. Yamashita, T. Iwachido and M. Zenki, *J. Org. Chem.*, **56**, 1991, 268.

65 H. Tsukube, K. Takagi, T. Higashiyama, T. Iwachido and N. Hayama, *J. Chem. Soc., Perkin Trans. 1*, 1986, 1033.

66 H. Tsukube, H. Adachi and S. Morosawa, *J. Chem. Soc., Perkin Trans. 1*, 1989, 1537.

67 M. Takagi and N. Nakamura, *J. Coord. Chem.*, **15**, 1986, 53.

68 E. Luboch, A. Cygan and J.F. Biernat, *Tetrahedron*, **46**, 1990, 2461.

69 E. Luboch, A. Cygan and J.F. Biernat, *Tetrahedron*, **47**, 1991, 4101.

70 R. Kataky, P.E. Nicholson, D. Parker and A.K. Covington, *Analyst*, **116**, 1991, 135.

71 Y. Frère and P. Gramain, *Makromol. Chem.*, **183**, 1982, 2163.

72 J.S. Bradshaw, K.E. Krakowiak, B.J. Tarbet, R.L. Breuning, J.F. Biernat, M. Bochenska, R.M. Izatt and J.J. Christensen, *Pure Appl. Chem.*, **61**, 1989, 1619.

73 F. Arnaud-Neu, B. Spiess and M.-J. Schwing-Weill, *Helv. Chim. Acta*, **60**, 1977, 2633.

74 B. Spiess, F. Arnaud-Neu and M.-J. Schwing-Weill, *Helv. Chim. Acta*, **63**, 1980, 2287.

75 F. Arnaud-Neu, B. Spiess and M.-J. Schwing-Weill, *J. Am. Chem. Soc.*, **104**, 1982, 5641.

76 G. Wu, W. Jiang, J.D. Lamb, J.S. Bradshaw and R.M. Izatt, *J. Am. Chem. Soc.*, **113**, 1991, 6538.

77 U. Herrmann, B. Tümmler, G. Maass, P.K.T. Mew and F. Vögtle, *Biochemistry*, **23**, 1984, 4059.

78 F. Fages, J.-P. Desvergne, H. Bouas-Laurent, J.-M. Lehn, J.P. Konopelski, P. Marsau and Y. Barrans, *J. Chem. Soc., Chem. Commun.*, 1990, 655.

79 A.P. de Silva, N. Gunaratne and K.R.A.S. Sandanayake, *Tetrahedron Lett.*, **31**, 1990, 5193.

80 F. Fages, J.-P. Desvergne, H. Bouas-Laurent, P. Marsau, J.-M. Lehn, F. Kotzyba-Hibert, A.-M. Albrecht-Gary and M. Al-Joubbeh, *J. Am. Chem. Soc.*, **111**, 1989, 8672.

81 J.P. Konopelski, F. Kotzyba-Hibert, J.-M. Lehn, J.-P. Desvergne, F. Fages, A. Castellan and H. Bouas-Laurent, *J. Chem. Soc., Chem. Commun.*, 1985, 433.

82 F. Fages, J.-P. Desvergne, H. Bouas-Laurent, J. Hinschberger and P. Marsau, *New J. Chem.*, **12**, 1988, 95.

83 A.P. de Silva and K.R.A.S. Sandanayake, *Tetrahedron Lett.*, **32**, 1991, 421.

84 B. Dietrich, J.-M. Lehn, J. Guilhem and C. Pascard, *Tetrahedron Lett.*, **30**, 1989, 4125.

85 J.-M. Lehn, *Acc. Chem. Res.*, **11**, 1978, 49.

86 S. Muñoz and L. Echegoyen, *J. Chem. Soc., Perkin Trans. II*, 1991, 1735.

87 J.L. Dye, *Pure Appl. Chem.*, **61**, 1989, 1555.

88 J.L. Dye and R.-H. Huang, *Chem. Br.*, 1990, 240.

89 R.S. Bannwart, S.A. Solin, M.G. De Backer and J.L. Dye, *J. Am. Chem. Soc.*, **111**, 1989, 5552.

90 B. Alpha, J.-M. Lehn and G. Mathis, *Angew. Chem., Int. Ed. Engl.*, **26**, 1987, 266.

91 J.S. Bradshaw, R.M. Izatt, J.J. Christensen, K.E. Krakowiak, B.J. Tarbet and R.L. Breuning, *J. Inclusion Phenom.*, **7**, 1989, 127.

92 J.-P. Joly and B. Gross, *Tetrahedron Lett.*, **30**, 1989, 4231.

93 K. Yamamoto, T. Ikeda, T. Kitsuki, Y. Okamoto, H. Chikamatsu and M. Nakazaki, *J. Chem. Soc., Perkin Trans. 1*, 1990, 271.

94 P. Huszthy, J.S. Bradshaw, C.Y. Zhu and R.M. Izatt, *J. Org. Chem.*, **56**, 1991, 3330.

95 T.Taura, *Inorg. Chim. Acta*, **162**, 1989, 105.

Chapter 2 : Equilibrium Studies of Cryptates and Lariat Ether Complexes

2.1 : Introduction

The ability of polyoxadiazabicycloalkanes, or cryptands, to form very stable and selective complexes with a wide range of cations, including alkali and alkaline-earth metal cations, has given rise to extensive binding studies to ascertain the origin of the selectivity.[1-15] When a ligand complexes with a metal cation in a solvent, an equilibrium is established between the solvated metal cation (M^+), the ligand (L) and the complex ($M.L^+$). This equilibrium may be represented by the following general equation:

$$M^{n+} + L \underset{}{\overset{K_s}{\rightleftharpoons}} [M.L]^{n+} \qquad (2.1)$$

where K_S, the concentration stability constant is defined as:

$$K_S = \frac{[M.L^{n+}]}{[M^{n+}]\,[L]} \qquad (2.2)$$

The stability constant of a complex formed between a cation and a ligand is the most important parameter for interpreting the thermodynamic properties of such constructions. The stability, lability and selective properties of the metal complexes, or cryptates, formed by cryptands are dependent on the structure of the cryptands, the number, type and arrangement of their donor atoms, and the nature of the metal cations and of the solvent.[1-17]

The stability constants of alkali and alkaline-earth metal cation cryptates are several orders of magnitude greater than those of naturally occuring or synthetic monocyclic ligands.[1,2] Some cryptates are exceptionally stable because cryptands possess three-dimensional intramolecular cavities which can accommodate metal cations of appropriate size. A prime requisite for complex stability is a good fit of metal cation to the cryptand cavity, the preferred metal cation being that whose ionic size most closely fits the cryptands intramolecular cavity. By lengthening the nitrogen to nitrogen

Table 2.1 Approximate Cavity Radii and Number of Binding Sites of Selected Cryptands and Ionic Radii of Alkali, Alkaline-Earth, Tl(I) and Ag(I) Metal Cations for Various Coordination Numbers.

Cryptand	Cavity Radius (Å)[a]	No. of Binding Sites	Cation	Ionic Radius (Å)[b] for Coordination Number 6	7	8	9	10	11
C111	0.5	5	Li^+	0.76		0.92			
C211,C21C5[c]	0.8	6,5	Na^+	1.02	1.12	1.18	1.24		
C221,C22C5[c]	1.1	7,6	K^+	1.38	1.46	1.51	1.55	1.59	
C222,C22C8[c]	1.4	8,6	Rb^+	1.52	1.56	1.61	1.63	1.66	1.69
C322	1.8	9	Cs^+	1.67		1.74	1.78	1.81	1.85
C332	2.1	10	Mg^{2+}	0.72		0.89			
C333	2.4	11	Ca^{2+}	1.00	1.06	1.12	1.18	1.23	
C21[d]	0.9[e]	5	Sr^{2+}	1.18	1.21	1.26	1.31	1.36	
C22[d]	1.4[e]	6	Ba^{2+}	1.35	1.38	1.42	1.47	1.52	1.57
			Ag^+	1.15	1.22	1.28			
			Tl^+	1.50		1.59			

[a] The estimated cavity radii were determined by the radius of the sphere which was able to be inserted into the intramolecular cavity of the space filling models of the cryptands, without distortion of the ligands. References 1, 18;

[b] Reference 19;

[c] The cavity radii of the aliphatic bridge cryptands are based on their isostructural cryptands;

[d] C21 and C22 are monocyclic diaza crown ethers, cryptand precursors, not macrobicyclic cryptands;

[e] Reference 4.

bridges of a cryptand, it is possible to gradually increase the intramolecular cavity (Table 2.1) and alter the cation selectivity (Table 2.2). It is also seen from Table 2.1 that the ionic radii of the metal cations vary with coordination number. Smaller cryptands are quite rigid and display "peak selectivity". This means that they are able to discriminate against metal cations which are either too small or too large to optimally fit into their intramolecular cavities. Thus, the cryptands C211, C221 and C222 of increasing cavity size, preferentially bind Li^+, Na^+ and K^+ respectively. However, with cryptands larger than C222, the selectivity is less evident and "plateau selectivity" is exhibited (see stability constants for the cryptand C332 in Table 2.2). This result is due to the larger cryptands being rather flexible.

From Table 2.2 the various factors which affect the stability constants of cryptates can be examined. The general rule that cryptands form the most stable cryptates with the metal ions whose ionic radii best match the intramolecular radius of the cryptand is demonstrated well by the cryptand C221. The cryptand C221 (cavity radius of about 1.1 Å[18]) forms stable, *inclusive* $[Na.C221]^+$, as it can entirely encompass the Na^+ ion (r = 1.12 Å[19]) within its intramolecular cavity. Whereas, the K^+ ion (r = 1.46 Å) is too large to be accommodated inside the C221 cavity and forms *exclusive* $[K.C221]^+$ in which the K^+ ion resides on the face of the eighteen-membered, N_2O_4 ring.[20] Additionally, since the variation of stability constants is in the order $Li^+ < Na^+ > K^+$, this may imply that Li^+ (r = 0.76 Å-the six coordinate radius is quoted here as no seven coordinate Li^+ radius is reported in the literature) forms an *inclusive* structure with C221 with the Li^+ being much too small to establish optimal bonding distances.

Another way to alter selectivity is to change the number of binding sites on the cryptand while maintaining the same intramolecular cavity size. This is achieved by replacing electron donating oxygen atoms by methylene, $-CH_2-$, groups. The aliphatic bridge cryptands $C21C_5$, $C22C_5$ and $C22C_8$ have one, one and two oxygen atoms less than their respective similarly sized traditional cryptands, C211, C221 and C222. Comparing the stability constant data in Table 2.2 for these similarly sized cryptands, it can be seen that the stabilities of C211, C221 and C222 are generally greater than their respective aliphatic bridge cryptands, $C21C_5$, $C22C_5$ and $C22C_8$. The effect on stability can be quite marked, for example, the stabilities of the Na^+ and K^+ cryptates of C222

Table 2.2 Apparent Stability Constants for Selected Cryptands and Diaza Crown Ethers with Alkali Metal Cations in Methanol and Aqueous Solution.

Cryptand	Cavity Radius (Å)[a]	Solvent	log (K_s / dm^3 mol^{-1}) Li$^+$	Na$^+$	K$^+$	Rb$^+$	Cs$^+$
C211	0.8	MeOH	8.04[b]	6.64[c]	2.36[c]	2.50[c]	2.50[c]
			7.90[c]	6.1[d]	2.3[d]	1.9[d]	<2.0[e]
		H_2O	5.3[d]	2.8[d]	<2.0[d]	<2.0[d]	<2.0[d]
			5.5[e]	3.2[e]			
$C21C_5$	0.8	MeOH	3.00[f]	3.76[g]			
C221	1.1	MeOH	5.38[b]	9.65[b]	8.54[b]	6.74[b]	4.33[b]
			4.69[c]	9.71[c]	8.40[c]	7.35[c]	4.32[c]
		H_2O	2.5[d]	5.4[d]	3.95[e]	2.55[d]	<2.0[d]
$C22C_5$	1.1	MeOH	2.30[h]	5.41[i]	5.8[h]	5.7[h]	4.8[h]
		H_2O	2.08[h]	2.58[h]	3.41[h]	3.28[h]	3.31[h]
$C22C_8$	1.4	MeOH	2.2[d]	3.5[d]	5.2[d]	3.4[d]	2.7[d]
			<2.0[e]				
		H_2O	<2[j]	<2[j]	<2[j]	<2[j]	<2[j]
C222	1.4	MeOH	2.65[d]	7.98[b]	10.41[b]	8.98[b]	3.95[c]
			2.46[c]	7.97[c]	10.49[c]	9.10[c]	4.4[d]
		H_2O	<2.0[d]	3.9[d]	5.4[d]	4.35[d]	<2.0[d]
			0.99[k]				
C332	2.1	MeOH		3.2[d]	6.0[d]	6.15[d]	6.5[d]
							>6.0[e]
		H_2O	<2.0[d]	<2.0[d]	<2.0[d]	<0.7[d]	<2.0[d]
C21	0.9[c]	MeOH		<1.5[l]	<1.5[l]		
C22	1.4[c]	MeOH	1.07[m]	1.0[d]	2.04[n]	1.2[d]	
				1.50[l]	1.80[l]	<1[c]	

[a] Reference 18; [b] Reference 21; [c] Reference 4; [d] Reference 1; [e] Reference 2; [f] Reference 12; [g] Reference 11; [h] Reference 15; [i] Reference 22; [j] Reference 23; [k] Reference 24; [l] Reference 25; [m] Reference 26. This value was determined in 95% methanol/5% water; [n] Reference 27.

are greater than those of C22C8 by a factor of 10^4-10^5 in methanol,[2] which is a factor of about 10^2 per oxygen binding site removed. Another observation from Table 2.2 is the stability constants of the diaza crown ethers C21 and C22 are much lower and less varied with different alkali metal ions than those of the cryptands C211 and C221, respectively. This may be accounted for by the fact that the diaza crown ethers are only monocyclic, the extra oxygen donor atom in the extra nitrogen to nitrogen ether bridge in the cryptands, and also the fact the diaza crown ethers possess greater structural flexibility than the cryptands.

The formation of a complex between a ligand and a metal cation involves the substitution of solvent molecules from the first coordination sphere of the metal cation. Ligands must therefore compete with solvent molecules for the cations in solution. Consequently, the nature of the solvent must affect cryptate stability, and indeed, numerous equilibrium studies have shown that stability constants of cryptate formation are very sensitive to solvent variation.[6,7,10,13,14,16,17] All the cryptands in Table 2.2 exhibit greater stabilities in methanol than in water. This is a direct result of water (D_N = 18.0[28] and 33.0[29,30]) being a better electron donor than methanol (D_N = 19.0 and 23.5), that is, water competes more strongly for the metal cations than methanol. A widely used parameter which expresses the donor strength of a solvent is the Gutmann donor number, D_N. It is defined as the magnitude of the negative enthalpy of complex formation, ΔH, between a donor solvent and the acceptor antimony (V) chloride, $SbCl_5$, in the inert medium 1,2-dichloroethane.

$$\text{Solvent} + SbCl_5 \xrightarrow{CH_2ClCH_2Cl} \text{Solvent}.SbCl_5 \qquad D_N = |-\Delta H| \quad \textbf{(2.3)}$$

Cryptate stability tends to decrease with decrease in the electron donating ability of the solvent (ie. as D_N decreases). The D_N values for some selected solvents are listed in Table 2.3.

In the case of water two D_N values, 18.0 and 33.0, are quoted, and also in the case of methanol D_N values of 19.0 and 23.5, are quoted.[29,30] The first value in each case is that obtained with dilute solutions of the protic solvent in 1,2-dichloroethane solution, and the second value is that obtained when the protic solvent is the bulk. Anomalies are observed in alkali metal ion cryptate stability and lability variations with the type of solvent when the first D_N values are used, but are largely eliminated when the second values are used. It has been argued that the reason for this is that the second D_N values reflect

Table 2.3 The Gutmann Donor Number, D_N, for Several Selected Solvents.

Solvent	D_N[a]
Acetonitrile	14.1
Propylene Carbonate	15.1
Methanol	19.0, 23.5[b]
Trimethyl Phosphate	23.0
Tri-*n*-butyl Phosphate	23.7
Triethyl Phosphate	26.0[c]
N,N-Dimethylformamide	26.6
Dimethyl Sulfoxide	29.8
Water	18.0, 33.0[b]

[a] Reference 28

[b] References 29, 30

[c] Reference 31

the intermolecular hydrogen bonded structure of the protic solvents which is important when they are the bulk solvent and is disturbed in the presence of 1,2-dichloroethane.[10,12,13] Since the second D_N values appear to better represent the electron donating power of the protic solvents, it was desirable to test this assertion by selecting an aprotic solvent with a D_N value close to the second value of the protic solvents. Appropriately, trimethyl phosphate (D_N = 23.0) was the solvent selected. It also appears that the trimethyl phosphate has not been previously used as a solvent in cryptate studies, hence it would extend the data available on the influence of the solvent on cryptate chemistry. In addition to trimethyl phosphate (V_S = 115.5 cm^3 mol^{-1})[32], two other trialkyl phosphate solvents were selected to be investigated, namely triethyl phosphate (V_S = 170.6 cm^3 mol^{-1}) and tri-*n*-butyl phosphate (V_S = 272.9 cm^3 mol^{-1}). These three trialkyl phosphate solvents are all oxygen donors, possess similar tetrahedral geometry, but have very different molar volumes, V_S, which allowed the examination of the influence of solvent molecular size on cryptate stability and lability.

The cryptands C211 and $C21C_5$ used in this study have similarly sized intramolecular cavities. The fact that C211 has one more oxygen donor atom than $C21C_5$ affords us an opportunity to study the effect of the number of cryptand donor atoms on the stabilities of the Li^+, Na^+, Ag^+ and Tl^+ cryptates in the trialkyl phosphate solvents. The metal ions, Na^+ and Li^+, were chosen as their C211 and $C21C_5$ cryptates have been well characterised in other solvents.[10-12,33] The soft acid cations, Ag^+ and Tl^+, were chosen to provide a contrast with the the hard acid characteristics of Li^+ and Na^+.[34,35]

Cyclic ligands such as crown ethers produce much more stable complexes than their corresponding open-chain counterparts.[27] This is called the macrocyclic effect. The stability constant of the K^+ complex of 18-crown-6 in methanol is greater by a factor of about 10^4 than the K^+ complex of its non-cyclic polyether analogue pentaglyme, $CH_3(OCH_2CH_2)_5OCH_3$ (Figure 2.1). An even greater increase in stability is observed for bicyclic cryptand complexes over their monocyclic, isostructural lariat ether complexes. Since the macrobicyclic topology of the cryptands greatly enhances the stability of the complexes, this effect was labelled the macrobicyclic cryptate effect. The stability of $[K.C222]^+$ is higher by a factor of 10^5 (in 95:5 methanol:water) than the stability of the K^+ complex of the bibracchial lariat ether which results from the opening of one of the C222 polyether bridges (Figure 2.1).[3]

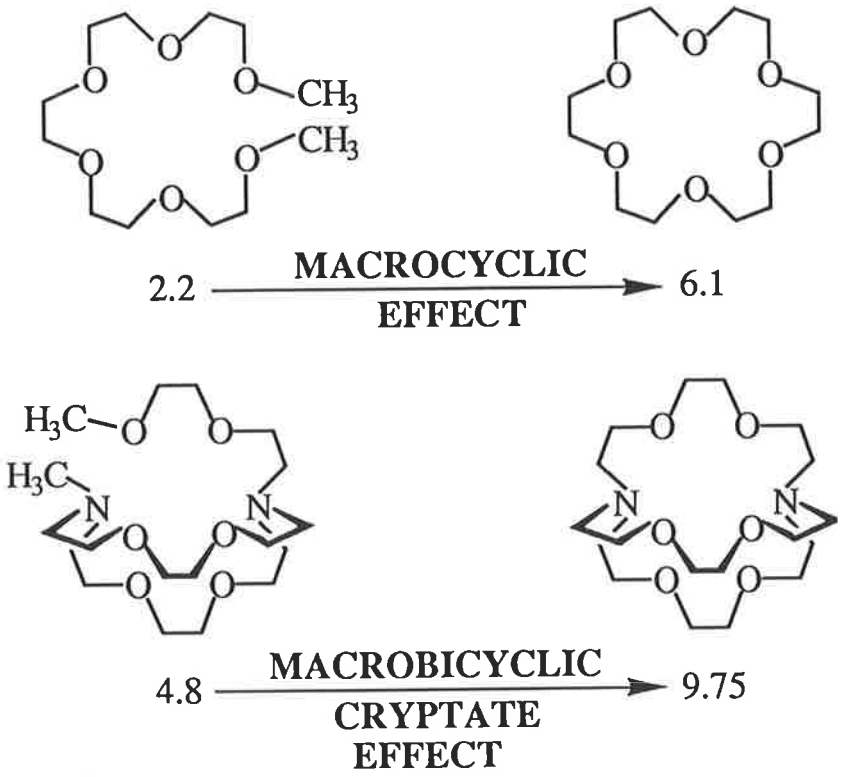

Figure 2.1 *The K^+ stability constants, log K_s, of several ligands illustrating the macrocyclic (in methanol) and macrobicyclic cryptate (in 95:5 methanol:water) effect.*

An adjustment to cation selectivity by varying factors other than cavity size and the number of donor atoms can be achieved with lariat ethers by use of their pendant arms. The selective metal ion complexation properties of lariat ethers has been well investigated.[25,36-41] On the basis of their topology and complexation characteristics bibracchial lariat ethers lie at the borderline between crown ethers and cryptands. In this study we examine the equilibrium aspects of the bibracchial lariat ethers and their monovalent and divalent metal ion complexes through a study of 1,7-bis(2-hydroxyethyl)-4,10,13-trioxa-1,7-diazacyclopentadecane (BHE-C21) and 1,10-bis(2-hydroxyethyl)-4,7,13,16-tetraoxa-1,10-diazacyclooctadecane (BHE-C22) in aqueous solution and a variety of non-aqueous solvents. The study of BHE-C21 and BHE-C22 also enhances our understanding of the extent of the macrobicyclic cryptate effect by comparison with C221 and C222, respectively, as they possess the same number of oxygen and nitrogen donor atoms.

The stabilities of bibracchial lariat ether complexes are dependant on most of the factors which affect cryptate stabilities, although the general concept that the highest stability is achieved when the metal ion size best matches the cavity size is not always applicable to bibracchial lariat ether complex chemistry. If the structure is *anti*, that is, the pendant arms coordinate the metal ion from opposite sides of the macroring, then cation binding selectivity may be dependant on the cation size-diaza crown ether cavity size concept because the metal ion is contained within the parent diaza crown ether cavity. Whereas, if the structure is *syn*, that is, both pendant arms coordinate the metal ion from the same side of the macroring, then the cation size-macroring cavity size concept will no longer hold as the metal ion is not contained within the parent diaza crown ether cavity. The donor atoms in the latter *syn* structure are arranged in a three-dimensional array about the metal ion which gives rise to cryptand-like behaviour. Thus, it is the spatial relationship rather than the cation size-macroring cavity size relationship which is of fundamental importance in determining the cation selectivity of bibracchial lariat ether complexes.

2.2 : Stability Constant Determination Techniques

Several experimental techniques have been employed in the study and determination of cryptate and lariat ether complex stability constants. These methods include conductance,[42] calorimetry,[9,42] nuclear magnetic resonance (NMR),[24,43] potentiometric titrations (ion selective electrode),[42,44,45] pH-metric titrations (pH electrode),[2,15,18] fast atom bombardment (FAB) mass spectrometry[46,47] and electrochemistry.[48,49] The technique employed usually depends on the system being studied and the availability of time, money, expertise and equipment. Two techniques were used in this study, potentiometric titrations and pH-metric titrations. These methods are described in the following sections in detail.

2.2.1 : The Potentiometric Titration Technique

The potentiometric titration technique was employed for studies in non-aqueous solvents. It is a very versatile technique allowing the stability constant determination of many metal ions. This method is best suited to stabilities in the range $10 < K_S > 10^6$.[2] When complex stability gets too high, the concentration of the free metal ion being studied in solution becomes too low to be detected by the ion selective electrode. In this instance, an alternative, indirect, competitive approach was employed, allowing the measurement of metal complex stability constants greater than 10^6.[50] The competitive method was also developed to increase the number of solvents in which stability data could be obtained.

The direct potentiometric titration technique involves the titration of a metal ion solution by a solution of ligand (cryptand or bibracchial lariat ether). This method was employed for the measurement of Na^+ and Ag^+ complex stability constants, using Na^+ and Ag^+ ion selective electrodes, respectively. The limit of detectability of the free metal ion concentration by the ion selective electrodes is dependant upon the medium in which the complex is being studied. From experience, reliable and reproducible results are obtained with the Na^+ ion selective electrode when the stability constants are in the range $10^2 < K_S > 10^7$, and with the Ag^+ ion selective electrode when the stability constants are in the range $10^2 < K_S > 10^{12}$. The Na^+ ion selective electrode was also used to determine the stability constant of $[Li.BHE\text{-}C21]^+$ in acetonitrile with high reproducibility, even though the electrode is meant to

be about 0.01 as sensitive to $[Li^+]$ as to $[Na^+]$. Calibration of the Na^+ ion selective electrode using acetonitrile solutions of both Na^+ and Li^+ are shown in Figure 2.2. These plots also illustrate the electrodes response to both Na^+ and Li^+ is Nernstian.

The electrode potential is directly proportional to the logarithm of the free, solvated metal ion concentration, as described by the abbreviated Nernst equation:

$$E = E_0 + c\ln[M^{n+}] \tag{2.4}$$

The parameters E_0 and c are determined by calibrating the ion selective electrode. Calibration involves the titration of a known concentration of metal ion solution into a known volume of background electrolyte solution. The experimental values of these two parameters vary depending on the solvent. It was found that the values for the coefficient c fall between 19.5 and 28.0 (where e.m.f. is in mV), similar to that cited in the literature.

The thermodynamic stability constant, K_{th}, for the formation of a 1:1 ligand-cation complex is defined as:

$$K_{th} = \frac{f_{M.L^{n+}}\,[M.L^{n+}]}{f_L\,[L]\,f_{M^{n+}}\,[M^{n+}]} \tag{2.5}$$

where f_L, $f_{M^{n+}}$ and $f_{M.L^{n+}}$ are the activity coefficients of the uncomplexed ligand, uncomplexed metal ion and of the complex formed, respectively. If the ionic strength varies during the titration, then activity corrections need to be considered. Since cryptands and lariat ethers are neutral molecules, the complexation process (as in Equation 2.1) does not involve the separation of charges, thus activity corrections are generally not taken into account. Also, it may be assumed that the activity coefficients of the complex and cation are equal ($f_{M.L^{n+}} = f_{M^{n+}}$) and that of the neutral ligand is zero ($f_L = 0$) in dilute solutions. Hence, the activity coefficients cancel out and need not be taken into account. Alternatively, the potentiometric titrations were carried out at a high ionic strength using an inert supporting electrolyte (tetraalkylammonium salts) so that the ionic strength was maintained nearly constant throughout

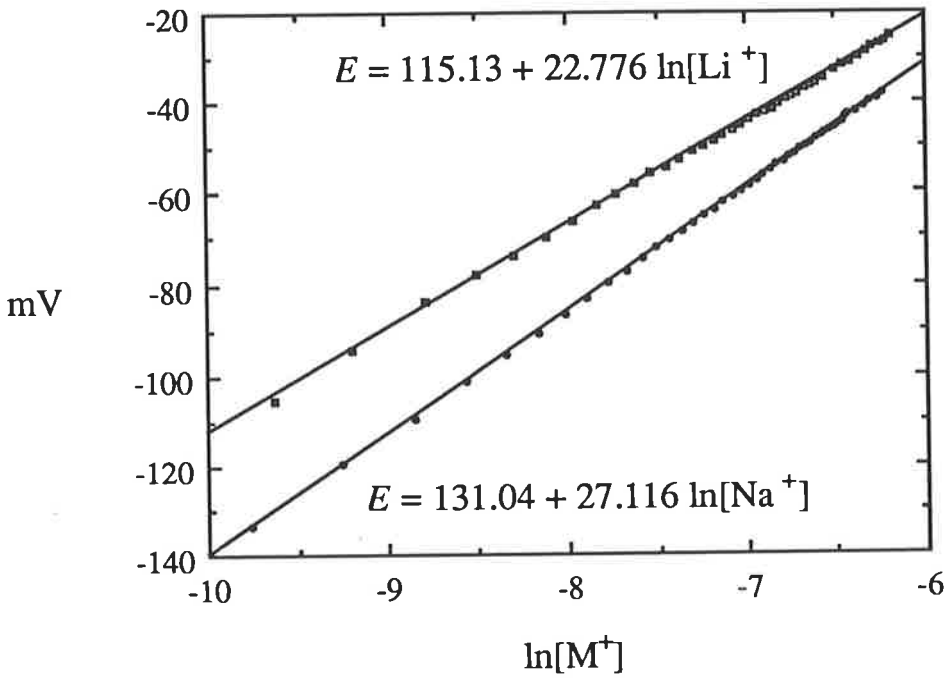

Figure 2.2 *Calibration of the Na^+ ion selective electrode with acetonitrile solutions of Na^+ (circles) and Li^+ (squares) at 298.2 K. A 20 cm^3 solution of 5.000 × 10^{-2} mol dm^{-3} NEt_4ClO_4 (background electrolyte) was titrated with a solution of 9.719 × 10^{-3} mol dm^{-3} $NaClO_4$/5.000 × 10^{-2} mol dm^{-3} NEt_4ClO_4 and similarly with a solution of 1.025 × 10^{-2} mol dm^{-3} $LiClO_4$/5.000 × 10^{-2} mol dm^{-3} NEt_4ClO_4. The values of the parameters E_0 and c are shown on the graph.*

the titration. The stability constants quoted in this study are concentration stability constants, K_S, defined as:

$$K_S = K_{th} \frac{f_L f_{M^{n+}}}{f_{M.L^{n+}}} = \frac{[M.L^{n+}]}{[M^{n+}]\,[L]} \qquad (2.6)$$

Once the parameters E_0 and c have been determined, it is then relatively easy to calculate the concentration of free, solvated metal ion in a cation-ligand solution after equilibrium has been established using Equation 2.4. Knowing the initial, or total, metal ion and ligand concentrations allows the calculation of the concentration stability constants, K_S, of the complex.

Indirect, competitive potentiometric titrations were employed for metal ions where no ion selective electrodes were available. The stability constants of the complexes where the metal ions were Li^+ (except for the [Li.BHE-C21]$^+$/acetonitrile system), K^+, Cs^+, Rb^+ and Tl^+ were determined by this method. A silver electrode was used to measure the equilibrium concentration of free, solvated Ag^+ and the equilibrium constant, K_e, for the competitive reaction:

$$[M.L]^+ + Ag^+ \overset{K_e}{\rightleftharpoons} [Ag.L]^+ + M^+ \qquad (2.7)$$

in which Ag^+ ions compete for a ligand in the presence of another metal ion, M^+, and where the equilibrium constant, K_e, is defined as:

$$K_e = \frac{[Ag.L^+]\,[M^+]}{[M.L^+]\,[Ag^+]} \qquad (2.8)$$

Any metal ion, not only Ag^+, for which an ion selective electrode is available can be used as the auxiliary ion so long as its complex is more stable than that of the other competing metal ion, M^+. If the reverse is true, the concentration of free, solvated Ag^+ will be negligible, if not zero, and the electrode potential will not change significantly during the titration to allow the monitoring of the competitive equilibrium. This was the problem when trying to determine the stability constant for [Li.BHE-C21]$^+$ in acetonitrile using Ag^+ as the auxiliary ion.

To be able to calculate the equilibrium constant, K_e, for the competitive reaction 2.7, the stability constant of the Ag^+ complex, $K_{s(Ag)}$, which is defined as:

$$Ag^+ + L \overset{K_{s(Ag)}}{\rightleftharpoons} [Ag.L]^+ \qquad (2.9)$$

where $$K_{s(Ag)} = \frac{[Ag.L^+]}{[Ag^+]\,[L]} \qquad (2.10)$$

must first be determined by a direct potentiometric titration. Combining Equations 2.8 and 2.10 gives an equation for the stability constant of the competing metal ion, $K_{s(M)}$:

$$K_{s(M)} = \frac{K_{s(Ag)}}{K_e} = \frac{[M.L^+]}{[M^+]\,[L]} \qquad (2.11)$$

The equilibrium constant, K_e, is then determined by titrating a solution of $[M.L]^+$ (with M^+ in excess) into a solution of standard Ag^+. As the initial concentrations of $[M.L]^+$, Ag^+ and M^+ are known and the equilibrium concentration of Ag^+ is determined from the electrode potential of the Ag^+ ion selective electrode, then the equilibrium concentrations of the species required to calculate K_e (Equation 2.8) can be determined. The total metal ion concentration ($Ag^+ + M^+$) was always greater than the total cryptand concentration (about a 5-fold excess) so that the concentration of the uncomplexed cryptand at equilibrium was assumed to be negligible. The reference electrode in both the direct and competitive titrations was a Ag/Ag^+ electrode.

The FORTRAN-77 program called STAB[51] was used to extract the stability constant from the experimental titration data using the linear solution method, as described by Rossotti and Rossotti.[52] The program carries out numerous calculations for each data point which by hand would be quite laborious. These calculations which eventually derive the value of K_s are now described below.

In the direct potentiometric titration case, the total concentrations of the metal and ligand are defined as:

$$[M^+_{TOT}] = [M^+] + [M.L^+] \qquad (2.12)$$

and $$[L_{TOT}] = [L] + [M.L^+] \qquad (2.13)$$

Since the total concentrations of the cation and ligand are known, the concentration of the complex formed and of the free ligand can be calculated.

Rearranging Equations 2.12 and 2.13:

$$[M.L^+] = [M^+_{TOT}] - [M^+] \quad \textbf{(2.12a)}$$

and

$$[L] = [L_{TOT}] - [M.L^+] \quad \textbf{(2.13a)}$$

$$= [L_{TOT}] - [M^+_{TOT}] + [M^+] \quad \textbf{(2.13b)}$$

Substituting Equation 2.12a into Equation 2.2 yields:

$$K_S = \frac{[M^+_{TOT}] - [M^+]}{[M^+]\,[L]} \quad \textbf{(2.14)}$$

Equation 2.14 may be rearranged and expressed as:

$$\frac{1 - \alpha_1}{\alpha_1} = K_S\,[L] \quad \textbf{(2.15)}$$

where $\alpha_1 = \frac{[M^+]}{[M^+_{TOT}]}$, the mole fraction of free, solvated metal ion.

Therefore by calculating the values of $\frac{1 - \alpha_1}{\alpha_1}$ and the free ligand concentration, [L], for each data point in the direct titration, a plot of $\frac{1 - \alpha_1}{\alpha_1}$ vesus [L] (Equation 2.15) could be obtained where the slope of the straight line was K_S.

In the competitive potentiometric titration case, Equation 2.8 can be rewritten as:

$$K_e = \frac{[Ag^+_{TOT}] - [Ag^+]}{[Ag^+]} \times \frac{[M^+]}{[M.L^+]} \quad \textbf{(2.16)}$$

where

$$[Ag.L^+] = [Ag^+_{TOT}] - [Ag^+]$$

Equation 2.16 may be rearranged and expressed as:

$$\frac{1 - \alpha_1}{\alpha_1}\,[M^+] = K_e\,[M.L^+] \quad \textbf{(2.17)}$$

where $\alpha_1 = \frac{[Ag^+]}{[Ag^+_{TOT}]}$, the mole fraction of free, solvated Ag^+.

$$[M^+] = [M^+_{TOT}] - [M.L^+]$$

and
$$[M.L^+] = [L_{TOT}] - [Ag.L^+] - [L] \quad \textbf{(2.18)}$$
$$= [L_{TOT}] - [Ag^+_{TOT}] + [Ag^+] - [L] \quad \textbf{(2.18a)}$$

As mentioned previously, [L] is negligible at equilibrium because the total metal ion concentration is always greater than the total ligand concentration ($[M^+_{TOT}] > [L_{TOT}]$), therefore:

$$[M.L^+] = [L_{TOT}] - [Ag^+_{TOT}] + [Ag^+] \quad \textbf{(2.18b)}$$

Plotting $\frac{1 - \alpha_1}{\alpha_1} \times [M^+]$ vesus $[M.L^+]$ yields a straight line of slope K_e. In both the direct and competitive titration cases, K_s and K_e, respectively, were calculated by linear regression of the slopes. Once K_e and $K_{s(Ag)}$ are known, the stability constant of the competing metal ion, $K_{s(M)}$, can be calculated from Equation 2.11 which becomes:

$$\log K_{s(M)} = \log K_{s(Ag)} - \log K_e \quad \textbf{(2.19)}$$

Before the equivalence point, the concentration of free ligand, [L], is very small. Subsequently, the experimental errors in the parameters which use [L] in their derivation are large. Only data points after the equivalence point are therefore used to determine the stability constants.

An example of a direct and competitive titration are illustrated in Figures 2.3 and 2.5, respectively. The data calculated by the progrm STAB are shown in Tables 2.4 and 2.5, and their straight line plots are illustrated in Figures 2.4 and 2.6.

Table 2.4 Experimental Data for the Stability Constant Determination of $[Na.C211]^+$ in Trimethyl Phosphate.

Titre	e.m.f.	$[Na^+]$ $\times 10^6$	$[Na^+]_{total}$ $\times 10^4$	[C211] $\times 10^4$	$\frac{1 - \alpha_1}{\alpha_1}$
(cm^3)	(mV)	(mol dm^{-3})	(mol dm^{-3})	(mol dm^{-3})	
2.02	-482.5	212.916	9.355	2.956	3.394
2.08	-486.7	176.034	9.322	2.990	4.295
2.14	-490.4	148.875	9.296	3.018	5.244
2.20	-494.6	123.087	9.271	3.059	6.532
2.26	-499.0	100.848	9.246	3.133	8.168
2.32	-503.5	82.254	9.221	3.243	10.211
2.38	-508.1	66.785	9.197	3.382	12.771
2.46	-514.9	49.082	9.164	3.594	17.670
2.52	-519.4	40.033	9.139	3.794	21.829
2.58	-523.4	33.399	9.115	4.016	26.291
2.64	-527.3	27.992	9.091	4.249	31.477
2.70	-530.9	23.780	9.067	4.493	37.127
2.76	-534.8	19.930	9.043	4.738	44.374
2.84	-538.2	17.086	9.011	5.086	51.742
2.92	-541.6	14.647	8.980	5.435	60.308
2.98	-544.2	13.020	8.956	5.698	67.789
3.04	-546.3	11.839	8.933	5.963	74.455
3.10	-548.5	10.716	8.910	6.228	82.144
3.18	-551.2	9.483	8.879	6.581	92.635
3.24	-553.1	8.701	8.856	6.845	100.786
3.30	-554.6	8.129	8.833	7.111	107.661
3.38	-556.2	7.561	8.803	7.464	115.427
3.44	-557.5	7.129	8.781	7.728	122.172
3.52	-559.1	6.630	8.751	8.078	130.978
3.58	-560.3	6.280	8.729	8.339	137.995

3.66	-561.8	5.867	8.699	8.685	147.263
3.74	-563.3	5.482	8.670	9.030	157.151
3.80	-564.4	5.216	8.650	9.287	164.810
3.88	-565.8	4.895	8.619	9.628	175.072
3.96	-566.9	4.657	8.590	9.967	183.448
4.04	-568.2	4.391	8.562	10.304	193.983
4.10	-569.2	4.196	8.540	10.556	202.509
4.18	-570.3	3.993	8.512	10.890	212.196
4.24	-571.2	3.833	8.491	11.138	220.516
4.32	-572.2	3.663	8.463	11.469	230.017
4.38	-572.9	3.549	8.442	11.715	236.871
4.46	-573.9	3.392	8.415	12.041	247.078
4.52	-574.5	3.301	8.394	12.285	253.289
4.60	-575.4	3.169	8.367	12.608	263.007
4.66	-576.1	3.070	8.346	12.849	270.848
4.74	-576.9	2.961	8.319	13.169	279.966
4.82	-577.6	2.869	8.293	13.487	288.082
4.88	-578.4	2.766	8.273	13.723	298.025
4.98	-579.2	2.668	8.239	14.116	307.816

Result: log $K_S = 5.43 \pm 0.01$.

A 20 cm^3 solution of 1.029×10^{-3} mol dm^{-3} $NaClO_4$ ($[Na^+]_{initial}$) in trimethyl phosphate was titrated with a solution of 1.120×10^{-2} mol dm^{-3} C211 in trimethyl phosphate. Both solutions were 0.05 mol dm^{-3} in NEt_4ClO_4 (supporting electrolyte). Only the data points which fall in the most accurate region of the titration curve, as described by Rossotti and Rossotti,[52] were used in the calculations. The values for solvated $[Na^+]$ were derived from a calibration which yielded the calibration parameters E_0 = -295.8 mV and c = 22.08 mV. $[Na^+]_{total}$ was determined from the mass balance equation: $[Na^+]_{total} = 20.00/(20.00 + x) \times [Na^+]_{initial}$, where x is the volume in cm^3 of added titrant and 20.00 is the initial volume in cm^3. Likewise, $[C211]_{total} = x/(20.00 + x) \times [C211]_{initial}$. The stability constant, K_S, was determined from the slope of the $(1 - \alpha_1)/\alpha_1$ versus [C211] plot.

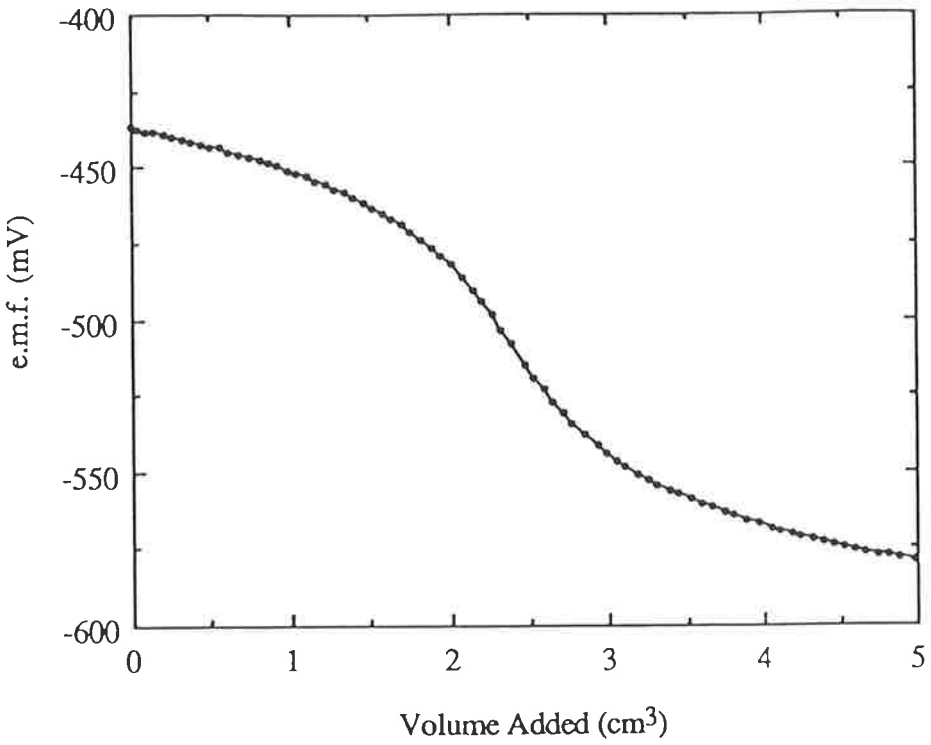

Figure 2.3 *Plot of volume added (cm^3) against e.m.f. (mV) measured for the titration of Na^+ with [C211] in trimethyl phosphate. The stability constant log K_s = 5.43 ±0.01.*

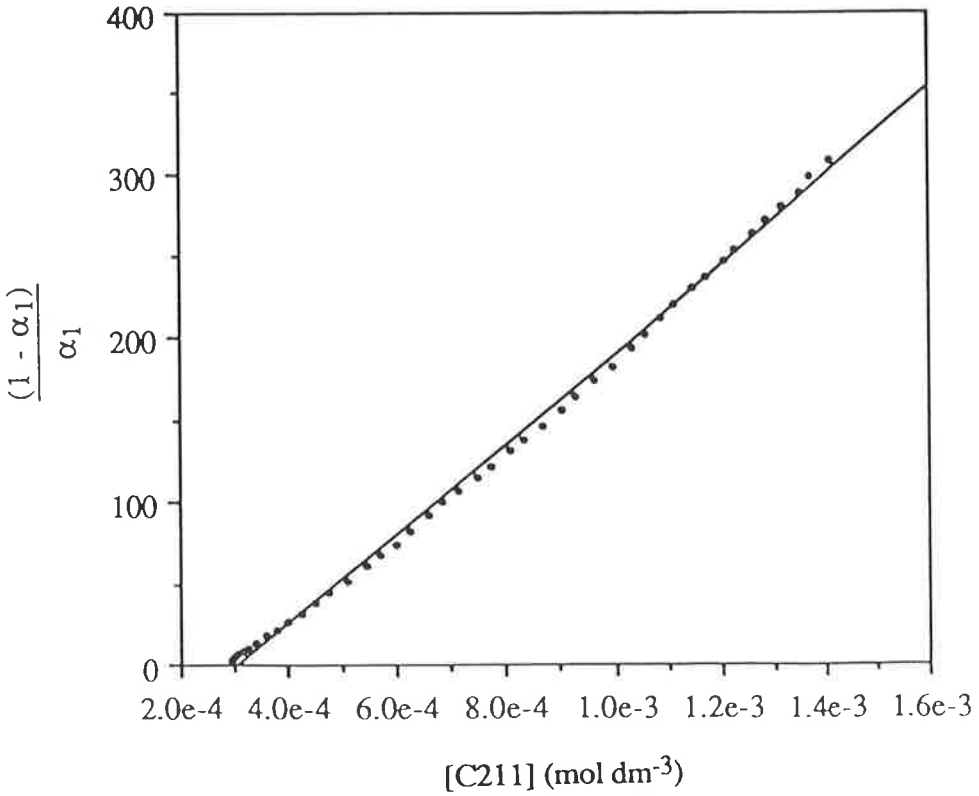

Figure 2.4 *Plot of* $\frac{1 - \alpha_1}{\alpha_1}$ *versus [C211] for the stability constant determination of [Na.C211]⁺ in trimethyl phosphate. The solid line represents the line of best fit.*

Table 2.5 Experimental Data for the Stability Constant Determination of $[K.BHE\text{-}C21]^+$ in N,N-Dimethylformamide.

Titre	e.m.f.	$[Ag^+]$ $\times 10^9$	$[K^+]$ $\times 10^3$	$[K.BHE\text{-}C21^+]$ $\times 10^4$	$\frac{1-\alpha_1}{\alpha_1} \times [K^+]$
(cm^3)	(mV)	(mol dm^{-3})	(mol dm^{-3})	(mol dm^{-3})	
2.80	-330.2	5.792	3.021	1.588	237.038
2.90	-333.0	5.120	3.100	1.799	273.877
3.00	-335.7	4.546	3.177	2.009	314.790
3.10	-338.0	4.108	3.254	2.216	355.218
3.20	-340.0	3.762	3.330	2.422	395.286
3.30	-342.0	3.445	3.405	2.626	439.569
3.40	-343.8	3.182	3.480	2.828	484.206
3.50	-345.3	2.979	3.554	3.028	526.048
3.60	-346.8	2.788	3.628	3.227	571.168
3.70	-348.1	2.633	3.701	3.424	614.374
3.80	-349.3	2.498	3.773	3.619	657.595
3.90	-350.4	2.379	3.845	3.813	700.408
4.00	-351.5	2.267	3.916	4.005	745.649
4.10	-352.5	2.169	3.986	4.196	789.959
4.21	-353.5	2.076	4.063	4.404	837.625
4.31	-354.4	1.995	4.132	4.591	882.707
4.40	-355.1	1.935	4.194	4.758	920.564
4.50	-355.9	1.868	4.262	4.943	965.129
4.60	-356.6	1.811	4.330	5.126	1007.034
4.70	-357.4	1.748	4.397	5.307	1055.025
4.80	-358.1	1.695	4.464	5.487	1100.074
4.90	-358.8	1.644	4.530	5.666	1146.675
5.00	-359.4	1.601	4.595	5.843	1189.627

Results: $\log K_e = 6.35 \pm 0.01$ and $\log K_{s(K)} = 2.99$ ($= \log K_{s(Ag)} - \log K_e$).

A 20 cm^3 solution of 5.180×10^{-4} mol dm^{-3} $AgNO_3$ ($[Ag^+]_{initial}$) in N,N-dimethylformamide was titrated with a solution containing 4.993×10^{-3} mol dm^{-3} BHE-C21 and 2.590×10^{-2} mol dm^{-3} $KClO_4$ in N,N-dimethylformamide. Both solutions were 0.05 mol dm^{-3} in NEt_4ClO_4 (supporting electrolyte). Only the data points which fall in the most accurate region of the titration curve, as described by Rossotti and Rossotti,[52] were used in the calculations. The values for solvated $[Ag^+]$ were derived from a calibration which yielded the calibration parameters $E_0 = 100.4$ mV and $c = 22.71$ mV. $[Ag^+]_{total}$ was determined from the mass balance equation: $[Ag^+]_{total} = 20.00/(20.00 + x) \times [Ag^+]_{initial}$, where x is the volume in cm^3 of added titrant and 20.00 is the initial volume in cm^3. Likewise, $[K.BHE\text{-}C21^+]_{total} = x/(20.00 + x) \times [K.BHE\text{-}C21^+]_{initial}$.and [BHE-C21] was assumed to be zero. The equilibrium constant, K_e, was determined from the slope of the $(1 - \alpha_1)/\alpha_1 \times [K^+]$ versus $[K.BHE\text{-}C21^+]$ plot.

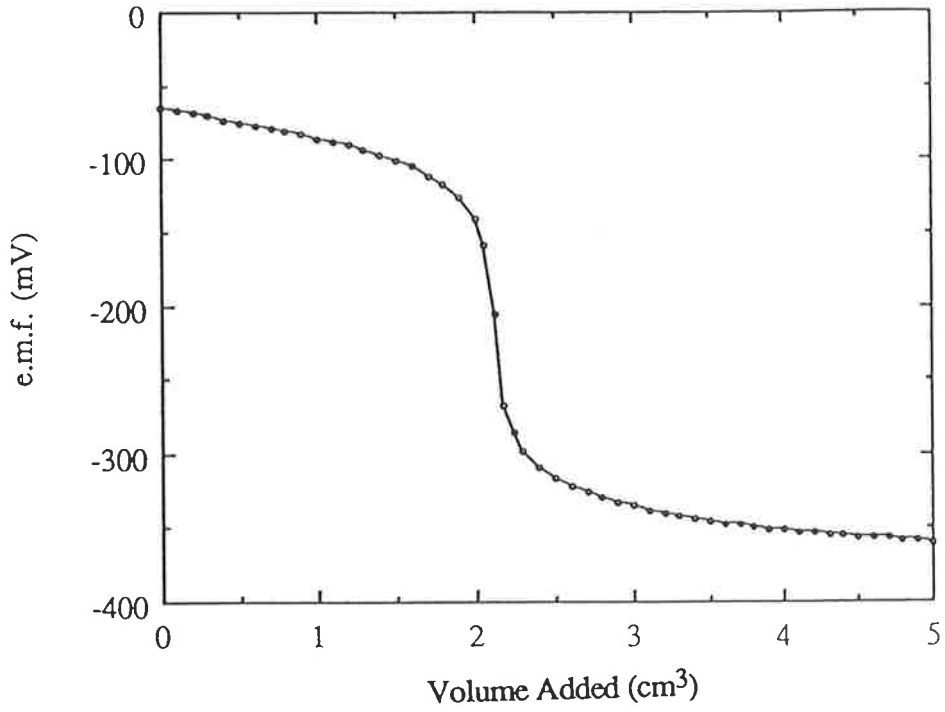

Figure 2.5 *Plot of volume added (cm^3) against e.m.f. (mV) measured for the titration of Ag^+ with $[K.BHE\text{-}C21]^+$ in N,N-dimethylformamide. The equilibrium constant log K_e = 6.35 ± 0.01 and the stability constant of $[K.BHE\text{-}C21]^+$ log $K_{s(K)}$ = log $K_{s(Ag)}$ - log K_e = 9.34 - 6.35 = 2.99.*

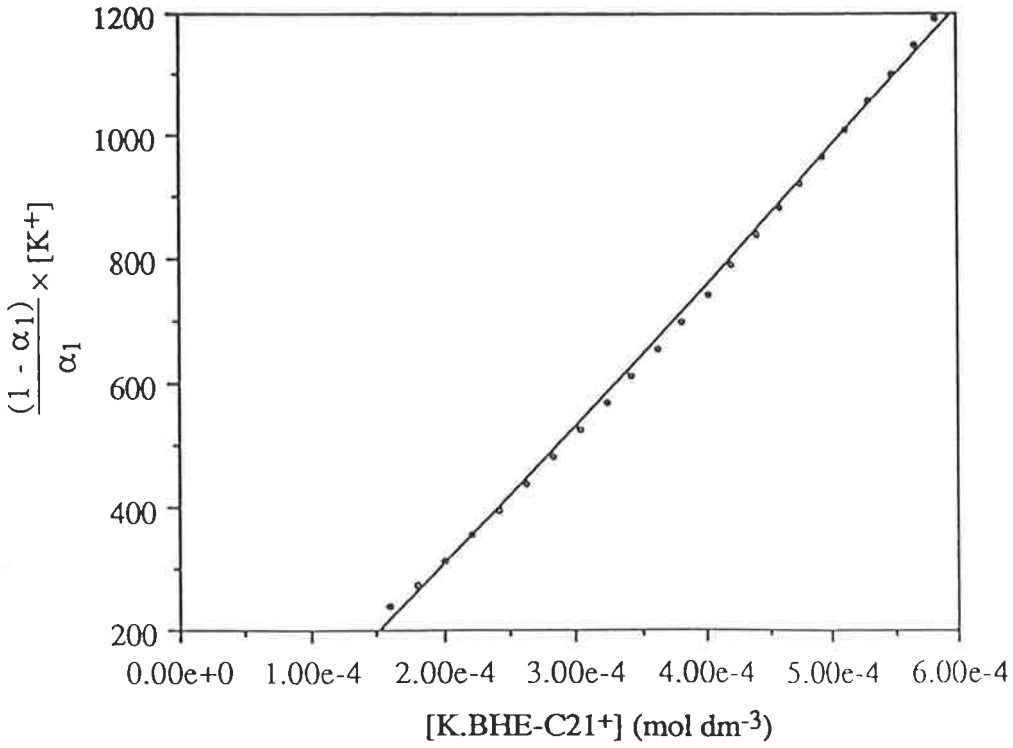

Figure 2.6 *Plot of* $\frac{1 - \alpha_1}{\alpha_1} \times [K^+]$ *versus* $[K.BHE\text{-}C21^+]$ *for the stability constant determination of* $[K.BHE\text{-}C21]^+$ *in N,N-dimethylformamide. The solid line represents the line of best fit.*

2.2.2 : The pH-Metric Titration Technique

The pH-metric titration technique was employed for stability studies of divalent metal ions with the bibracchial lariat ethers BHE-C21 and BHE-C22 in aqueous solution. This technique uses a pH electrode to determine the concentration of H^+ in solution rather than an ion selective electrode to determine the concentration of free metal ion in solution. It is best suited to higher stability constants ie. log $K_s \geq 2$.[2] The monovalent alkali metal ions were not investigated as they were expected to produce complexes too unstable in water with the two bibracchial lariat ethers for accurate enough measurement of their stability constants. Bibracchial lariat ethers are dibasic due to their two pivotal nitrogen atoms. The basicity or pH of a solution of these ligands can be altered by the complexation of a metal ion (Figure 2.7). Thus, by a comparison and analysis of the pH-metric titration curves of a ligand in the presence and absence of a metal ion, the apparent stability constant, K_s, for the complex can be determined.

The pH electrode was calibrated on a regular basis by titration of $HClO_4$ with NEt_4OH to determine its standard potential, E_0 (from the Nernst equation), and the ion product constant for water, pK_w, which may vary slightly between titration runs. The apparent protonation constants, K_1 and K_2, were then determined from the acquired titration data using the FORTRAN program MINIQUAD,[53] for the two stepwise protonation reactions:

$$H^+ + L \overset{K_1}{\rightleftharpoons} HL^+ \qquad \textbf{(2.20)}$$

$$H^+ + HL^+ \overset{K_2}{\rightleftharpoons} H_2L^{2+} \qquad \textbf{(2.21)}$$

where the stepwise apparent protonation constants are defined as:

$$K_1 = \frac{[HL^+]}{[H^+]\,[L]} \qquad \textbf{(2.22)}$$

$$K_2 = \frac{[H_2L^{2+}]}{[H^+]\,[HL^+]} \qquad \textbf{(2.23)}$$

and where L = BHE-C21 and BHE-C22.

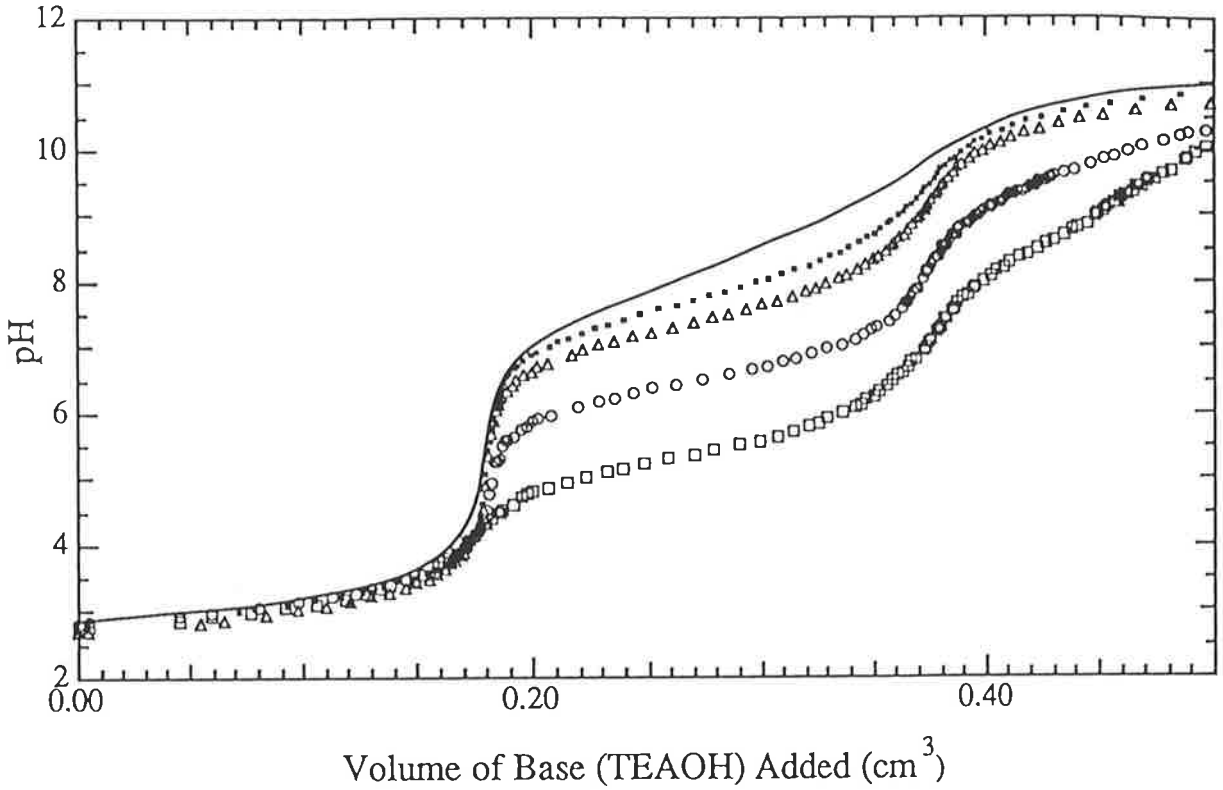

Figure 2.7 *The pH-metric titration of BHE-C21 in aqueous solution at 298.2 K in the absence of a metal ion (line) and in the presence of Pb^{2+} (squares), Co^{2+} (circles), Ca^{2+} (triangles) and Ba^{2+} (dots). The stability constant titration curve deviates from the protonation constant titration curve more as the complex stability increases. Not all the data points were used to determine the stability constants, especially those at high pH were $M(OH)_2$ species precipitate out. The stability constant experimental data points between 0.17 and 0.34 cm^3 were generally used as these gave the best fit with the protonation and complexation models. An "R Factor" less than 0.004 implies a good fit.*

$\log K_1$ (BHE-C21) = 8.822 ± 0.005; $\log K_2$ (BHE-C21) = 7.556 ± 0.009;
R Factor = 0.00140.
$\log K_s$ ($[Pb.BHE\text{-}C21]^{2+}$) = 8.886 ± 0.009; R Factor = 0.00218.
$\log K_s$ ($[Co.BHE\text{-}C21]^{2+}$) = 6.633 ± 0.008; R Factor = 0.00179.
$\log K_s$ ($[Ca.BHE\text{-}C21]^{2+}$) = 4.780 ± 0.024; R Factor = 0.00329.
$\log K_s$ ($[Ba.BHE\text{-}C21]^{2+}$) = 3.891 ± 0.019; R Factor = 0.00268.

After the stepwise protonation constants, K_1 and K_2, E_0 and pK_w were determined, the apparent stability constant, K_s, of a complex could be determined from the experimental titration data in the presence of the appropriate metal cation, using again the program MINIQUAD. The complexation of a divalent metal cation by a bibracchial lariat ether can be represented by the following reaction:

$$M^{2+} + L \overset{K_s}{\rightleftharpoons} [M.L]^{2+} \qquad (2.24)$$

where the apparent stability constant is defined as:

$$K_s = \frac{[M.L^{2+}]}{[M^{2+}]\,[L]} \qquad (2.25)$$

and where $M^{2+} = Mg^{2+}$, Ca^{2+}, Sr^{2+},Ba^{2+}, Mn^{2+}, Co^{2+}, Ni^{2+}, Cu^{2+}, Zn^{2+}, Cd^{2+}, Hg^{2+} and Pb^{2+}.

Methodical analyses of these titration curves revealed that there were no other species formed ($[M.L_2]^{2+}$, $[M_2.L]^{4+}$, $[M.HL]^{3+}$ or $[M(OH).L]^{+}$) other than the 1:1 complexes.

2.3 : Results and Discussion

2.3.1 : Complexation of Monovalent Metal Ions by the Cryptands C211 and C21C5 in Trialkyl Phosphate Solvents

The apparent stability constants, K_S, of $[M.C211]^+$ and $[M.C21C5]^+$, where $M^+ = Li^+$, Na^+, Ag^+ and Tl^+, were determined in three trialkyl phosphate solvents of varying molecular size. It can be seen from Table 2.6 that the apparent stability constants characterizing $[M.C211]^+$ are greater than those of $[M.C21C5]^+$ for all the four metal ions studied in all three trialkyl phosphate solvents. The apparent stability constants for both $[M.C211]^+$ and $[M.C21C5]^+$ vary considerably with the nature of M^+ and solvent, and the stability of both cryptates is moderately greater in trimethyl phosphate than in triethyl or tri-*n*-butyl phosphate.

The observation that the stability constants of $[M.C211]^+$ and $[M.C21C5]^+$ vary with the nature of M^+ may be explained by the structural variations of the various cryptates. In the solid state $[Li.C211]^+$ and $[Li.C21C5]^+$ exist as *inclusive* cryptates,[54,55] where the Li^+ ion resides in the cryptand intramolecular cavities consistent with an optimal fit of Li^+ (six coordinate radius = 0.76 Å) into the C211 and C21C5 cavities ($r \approx 0.8$ Å). It has been demonstrated by NMR studies that $[Li.C211]^+$ largely retains its *inclusive* structure in solution,[24] whereas $[Li.C21C5]^+$ appears to exist in a dynamic equilibrium between the *inclusive* and *exclusive* cryptates.[12] In the latter case, the Li^+ ion is largely outside the C21C5 intramolecular cavity and resides on the face of the fifteen-membered ring delineated by two nitrogen and three oxygen donor atoms. Both $[Na.C211]^+$ and $[Na.C21C5]^+$ exist as exclusive cryptates in the the solid state[56] owing to the larger Na^+ ion (six coordinate radius = 1.02 Å) being too big to be accommodated inside the intramolecular cavities of either cryptand. The fact that Li^+ has an optimal fit in the C211 cavity accounts for the greater K_S observed for $[Li.C211]^+$ in the trialkyl phosphate solvents and other solvents (Table 2.7) in comparison to $[Na.C211]^+$. The smaller magnitude of K_S for $[M.C21C5]^+$ than that for $[M.C211]^+$ is a direct consequence of the replacement of an electron donating ether oxygen atom by a methylene group resulting in a decreased electrostatic interaction between M^+ and C21C5 (see Figure 2.8). In all three trialkyl phosphate solvents the stability of the C21C5 cryptates are in the order $Li^+ > Na^+$. This relative order of stability is reversed in the other solvents listed in

Table 2.6 Apparent Stability Constants of $[M.C211]^+$ and $[M.C21C_5]^+$ in Trialkyl Phosphate Solvents at 298.2 K

	log (K_S / dm^3 mol^{-1})		
Cryptate	Trimethyl Phosphate (D_N = 23.0 [a])	Triethyl Phosphate (D_N = 26.0 [b])	Tri-*n*-butyl Phosphate [c] (D_N = 23.7 [a])
$[Li.C211]^+$	6.98 ± 0.05	6.44 ± 0.01	- [d]
$[Na.C211]^+$ [e]	5.38 ± 0.05	4.72 ± 0.01	4.94 ± 0.01
$[Ag.C211]^+$ [f]	9.82 ± 0.02	9.34 ± 0.10	7.83 ± 0.05 [g]
$[Tl.C211]^+$	3.95 ± 0.02	2.97 ± 0.10	3.36 ± 0.10 [g,h]
$[Li.C21C_5]^+$	2.40 ± 0.10	1.99 ± 0.10	2.36 ± 0.10 [g,i]
$[Na.C21C_5]^+$ [e]	1.90 ± 0.05	< 2 [j]	1.55 ± 0.10
$[Ag.C21C_5]^+$ [f]	6.04 ± 0.02	5.68 ± 0.10	4.94 ± 0.08 [g]
$[Tl.C21C_5]^+$	2.42 ± 0.10 [i]	2.18 ± 0.10 [i]	

All the stability constants quoted are derived from this study-errors represent one standard deviation.

[a] Reference 28; [b] Reference 31; [c] Tri-*n*-butyl phosphate titration solutions were 0.05 mol dm^{-3} in NBu_4ClO_4, whereas the solutions of the other two solvents were 0.05 mol dm^{-3} in NEt_4ClO_4. The supporting electrolyte NEt_4ClO_4 was not very soluble in tri-*n*-butyl phosphate; [d] The cryptate $[Li.C211]ClO_4$ was insufficiently soluble for study; [e] The Na^+ cryptate stability constants were determined directly using a Na^+ ion selective electrode; [f] The Ag^+ cryptate stability constants were determined directly using an Ag^+ ion selective electrode. All other stability constants were determined competitively using an Ag^+ ion selective electrode; [g] $AgClO_4$ was used instead of $AgNO_3$ (used in the other two solvents) as the source of Ag^+ due to the low solubility of $AgNO_3$ in tri-*n*-butyl phosphate; [h] The concentration of all solutions were 1/10th the normal experimental concentrations (see Experimental section); [i] The concentration of all solutions were 1/2 the normal experimental concentrations (see Experimental section); [j] The small change in e.m.f. (≈10 mV) during the titration made the accurate measurement of the $[Na.C21C_5]^+$ stability constant in triethyl phosphate very difficult.

Table 2.7 Apparent Stability Constants for Cryptates Formed by Some Monovalent Metal Ions and 4,7,13,18-tetraoxa-1,10-diazabicyclo[8.5.5]eicosane (C211) and 4,7,13-trioxa-1,10-diazabicyclo[8.5.5]eicosane (C21C5) in Various Solvents at 298.2 K.

Solvent	D_N	V_s[a]	log (K_s / dm^3 mol^{-1})			
		cm^3 mol^{-1}	[Li.C211]$^+$	[Na.C211]$^+$	[Ag.C211]$^+$	[Tl.C211]$^+$
Acetonitrile	14.1[b]	52.5	> 10[c]	9.8[d] 8.74[f]	7.70[c] 7.74[f]	7.02[e]
Propylene Carbonate	15.1[b]	85.9	12.44[c] 13.7[g]	8.76[c] 8.90[g]	14.44[c]	6.58[e]
Methanol	19.0[b] 23.5[h]	40.5	8.04[c] 7.90[i]	6.7[d] 6.64[i]	10.60[c] 10.46[f]	5.65[e]
Trimethyl Phosphate	23.0[b]	115.5	6.98 ± 0.05[j]	5.38 ± 0.05[j]	9.82 ± 0.02[j]	3.95 ± 0.02[j]
Triethyl Phosphate	26.0 [k]	170.6	6.44 ± 0.01[j]	4.72 ± 0.01[j]	9.34 ± 0.10[j]	2.97 ± 0.10[j]
Tri-*n*-butyl Phosphate	23.7[b]	272.9	.[l]	4.94 ± 0.01[j]	7.83 ± 0.05[j]	3.36 ± 0.10[j]
N,N-Dimethyl-formamide	26.6[b]	77.4	6.99[c]	5.23[c]	8.60[c]	3.15[e]
Dimethyl sulfoxide	29.8[b]	71.0	5.84[c]	4.63[c] 4.3[d]	6.17[c]	1.44[e]
Water	18.0[b] 33.0[h]	18.1	5.5[c]	2.8[m] 3.2[c]	8.52[n]	3.19[e]

			$[Li.C21C_5]^+$	$[Na.C21C_5]^+$	$[Ag.C21C_5]^+$	$[Tl.C21C_5]^+$
Acetonitrile	14.1[b]	52.2	4.15[o]	5.08[p]	4.29[o]	
Methanol	19.0[b] 23.5[h]	40.5	3.00[o]	3.76[p]	7.69[o]	
Trimethyl Phosphate	23.0[b]	115.5	2.40 ± 0.10[j]	1.90 ± 0.05[j]	6.04 ± 0.02[j]	2.42 ± 0.10[j]
Triethyl Phosphate	26.0[k]	170.6	1.99 ± 0.10[j]	< 2[j]	5.68 ± 0.10[j]	2.18 ± 0.10[j]
Tri-*n*-butyl Phosphate	23.7[b]	272.9	2.36 ± 0.10[j]	1.55 ± 0.10[j]	4.94 ± 0.08[j]	
N,N-Dimethyl-formamide	26.6[b]	77.4	1.80[o]	2.87[p]	5.23[o]	

[a] Molar volumes were calculated from the densities of acetonitrile, propylene carbonate, methanol, trimethyl, triethyl, and tri-*n*-butyl phosphate, dimethylformamide, dimethyl sulfoxide and water = 0.786, 1.189, 0.791, 1.213, 1.068, 0.976, 0.944, 1.101 and 0.997 g cm^{-3}, respectively; [b] Reference 28; [c] Reference 6 and references therein; [d] Reference 57; [e] Reference 7 and references therein; [f] Reference 5 and references therein; [g] Reference 58; [h] References 29,30; [i] Reference 4; [j] This work-errors represent one standard deviation; [k] Reference 31; [l] The cryptate $[Li.C211]ClO_4$ was insufficiently soluble for study; [m] Reference 1; [n] Reference 8; [o] Reference 12; [p] Reference 11.

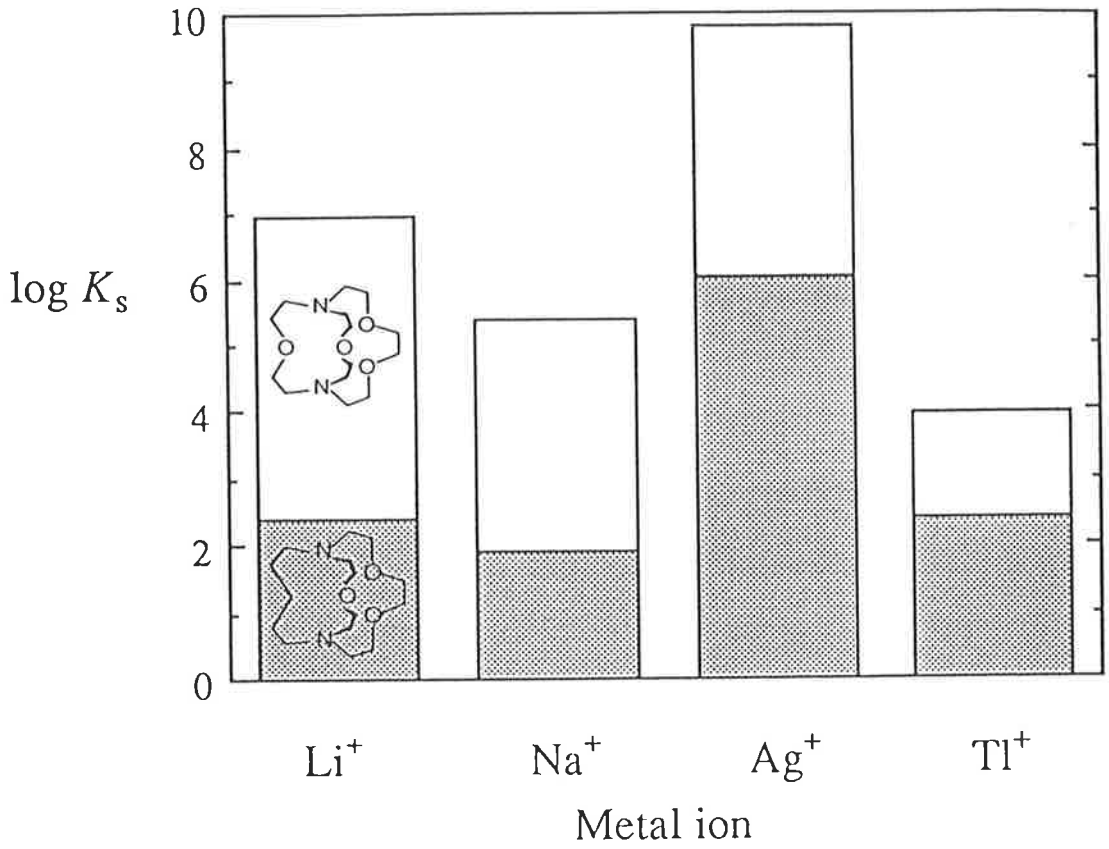

Figure 2.8 *The stability constants of C211 with Li^+, Na^+, Ag^+ and Tl^+ (shaded + clear area) are greater than the analogous $C21C_5$ complexes (shaded area) in trimethyl phosphate due to the extra oxygen donor atom of C211.*

Table 2.7, and may indicate the varying proportions of $[Li.C21C_5]^+$ existing in the *inclusive* and *exclusive* forms and its consequent variation in overall stability relative to $[Na.C21C_5]^+$.

The cryptates $[Ag.C211]^+$ and $[Ag.C21C_5]^+$ exhibit stability constants considerably greater than their Li^+ and Na^+ analogues in the trialkyl phosphate solvents and other oxygen donor solvents. These extraordinarily high Ag^+ cryptate stabilities are also observed for other cryptands such as C221, $C22C_5$ and C222 as well as for the diaza crown ethers C21 and C22. This is attributable to the soft acid characteristics of Ag^+ and its tendency to preferentially bind nitrogen donor atoms rather than oxygen donor atoms.[34,35] Therefore hard base oxygen donor solvents do not compete as effectively with the cryptand for Ag^+ as they do for the hard acid Li^+ and Na^+ ions, and this contributes to the greater stability of the Ag^+ cryptates. (Ag^+ also displays an inclination for forming two strong bonds in linear array[59] which may be approximately achieved through bonding with the two cryptand nitrogen bridgehead atoms). This same reasoning can be used to explain why in the nitrogen donor solvent acetonitrile there is a reversal in stability whereby the Ag^+ cryptates become less stable than their Li^+ and Na^+ analogues. Pearson's extensive classification[34,35] of metal ions as hard or soft acids, and ligands as hard or soft bases depending on their degree of polarizability (reducing power, degree of unsaturation) is an attempt to find a general relationship which may indicate the overall stabilities of complexes. The most important generalization about complex stabilities is that soft ligands form stable complexes with soft metal ions, and hard ligands form stable complexes with hard metal ions. Hard ion-soft ligand or soft ion-hard ligand complexes are expected to be less stable.

The Tl^+ complex of C211, $[Tl.C211]^+$, in all of the solvents listed in Table 2.7 is less stable than its Li^+, Na^+ and Ag^+ analogues, except in water where its stability is comparable to that of $[Na.C211]^+$. This suggests that the soft acid Tl^+, unlike Ag^+, does not interact strongly with the C211 nitrogen donor atoms. Also the relatively large size of Tl^+ (r = 1.50 Å) would be expected to give rise to the formation of an *exclusive* cryptate with C211. This structural assumption is based on the knowledge that the smaller metal ion Na^+ (r = 1.02 Å) forms *exclusive* $[Na.C211]^+$ in the solid state.[56] Likewise, $[Ag.C211]^+$ may also exist in the *exclusive* form on account of Ag^+ (r = 1.15 Å) also having an ionic radius greater than that of Na^+. The interaction between Tl^+ and the oxygen donor atom in the $-(CH_2)_2O(CH_2)_2-$ moiety

opposite the fifteen-membered ring delineated by two nitrogens and three oxygens where Tl^+ probably resides in *exclusive* $[Tl.C211]^+$, is not great and results in low stabilities for $[Tl.C211]^+$. The extremely low stability constant for $[Tl.C211]^+$ in dimethyl sulfoxide is probably a reflection of the ambidentate nature of the solvent whereby it may bond through either hard oxygen to hard acids or soft sulfur to soft acids.[60] Since Tl^+ is a soft acid it is possible that dimethyl sulfoxide competes rather effectively with C211 for Tl^+ by binding through its sulfur atom. This rationale may also account for the low K_S observed for $[Ag.C211]^+$ in the same solvent. In both trimethyl and triethyl phosphate the stability constant of $[Tl.C21C_5]^+$ is similar to that of its Na^+ and Li^+ analogues. This may indicate that the advantage emanating from the ability of the latter two metal ions to closely approach and interact with the six donor atoms of C211, on account of their smaller sizes, is lost in $C21C_5$ where all five donor atoms are distributed around one fifteen-membered cryptand ring (N_2O_3).

The stability constants of $[M.C211]^+$ and $[M.C21C_5]^+$ in trimethyl phosphate are the highest observed in the three trialkyl phosphate solvents examined. This indicates that trimethyl phosphate competes the least effectively for Li^+, Na^+, Ag^+ and Tl^+. The three trialkyl phosphate solvents are of significantly different molecular sizes with the solvent size increasing in the order TBP > TEP > TMP. If solvent molecular size played a role in determining cryptate stabilities then it should be quite evident from a stability study in these three solvents. Tri-*n*-butyl phosphate, by virtue of having the largest molar volume (V_S) of the three trialkyl phosphates, would be expected to exhibit the largest K_S values if increased solvent molecular size hindered competition for the metal ion. However, this is not the case as seen from the results in Table 2.6. The K_S values in tri-*n*-butyl phosphate are smaller than those observed in trimethyl phosphate, most markedly so in the case of Ag^+. The slight difference in cryptate stabilities between the two solvents may be attributed to the slight difference in their D_N values.

A comparison of the stability constants observed for $[M.C211]^+$ and $[M.C21C_5]^+$ in all the solvents listed in Table 2.7 broadly indicates that the ability of the trialkyl phosphate solvents to compete with the cryptands for the metal ions Li^+, Na^+, Ag^+ and Tl^+ is greater than that of acetonitrile (except for the Ag^+ cryptates, as explained earlier), propylene carbonate and methanol, similar to that of N,N-dimethylformamide, and less than that of dimethyl sulfoxide as anticipated from their D_N values. These results are in agreement with the general concept that cryptate stability in solution

decreases with the increasing electron donating power (D_N value) of the solvent. However, water competes most effectively with C211 for Li^+ and Na^+ than all the other solvents (consistent with D_N = 33.0), but it competes less effectively than dimethyl sulfoxide for both Ag^+ and Tl^+, tri-*n*-butyl phosphate for Ag^+ and triethyl phosphate for Tl^+. It is also worth noting that trimethyl phosphate competes significantly more effectively with the two cryptands for Li^+, Na^+, Ag^+ and Tl^+ than does methanol despite trimethyl phosphate (D_N = 23.0) having a slightly lower D_N value than methanol (D_N = 23.5 for bulk methanol). This may suggest that a $D_N < 23.5$ for methanol might be more appropriate as deduced from these cryptate systems. These examples of stability variations imply that D_N values are suggestive of broad trends rather than absolute trends in stability variations. Other solvent effects such as the nature of metal to solvent bonding or steric effects may superimpose on the broad trend to give stability variations not consistent with the D_N values.

2.3.2 : Complexation of Alkali and Ag(I) Metal Ions by the Lariat Ethers BHE-C21 and BHE-C22 in Non-Aqueous Solvents

The apparent stability constants, K_S, of $[M.BHE\text{-}C21]^+$, where $M^+ = Li^+$, Na^+ and Ag^+, were determined in acetonitrile, methanol, trimethyl phosphate and N,N-dimethylformamide. In addition, the K^+, Rb^+ and Cs^+ bibracchial lariat ether complex stabilities were determined in N,N-dimethylformamide. This would provide a complete range of alkali metal $[M.BHE\text{-}C21]^+$ complex stabilities from which the most selective alkali metal ion could be deduced. The same stability constants were determined with the larger bibracchial lariat ether BHE-C22, except no stabilities were measured in acetonitrile and the stability of the Na^+ complex in methanol was not measured as it had already been previously determined. All the results are tabulated in Table 2.8.

The order in which the stability constants of $[M.BHE\text{-}C21]^+$ and $[M.BHE\text{-}C22]^+$ vary with M^+ in N,N-dimethylformamide at 298.2 K is $Li^+ < Na^+ > K^+ > Rb^+ > Cs^+$ and $Li^+ < Na^+ < K^+ > Rb^+ > Cs^+$, respectively, with the Ag^+ complex of both ligands being 2-4 times greater than that of the alkali metal ion complexes (Table 2.8). These alkali metal ion selectivity patterns are the same as those of the cryptands C221 and C222 (Table 2.11), respectively, although the magnitudes of the stabilities of the cryptates including those of the Ag^+ cryptates are greater than the stabilities of the bibracchial lariat ether complexes (except $[Cs.BHE\text{-}C22]^+$). The aliphatic bridge cryptands $C22C_5$ and $C22C_8$ possess similar cavity sizes to those of C221 and C222, respectively, but have one and two oxygen donor atoms less than their similarly sized traditional cryptands. The stabilities of $[M.C22C_5]^+$ are significantly lower than those of their $[M.C221]^+$ analogues with the variation of stabilities in the sequence $Li^+ < Na^+ < K^+ \approx Rb^+ > Cs^+$. The complexes of $C22C_8$ are characterized by even lower stabilities than those of $C22C_5$, and lower stabilities than those of its related cryptand C222. It exhibits a selectivity for the K^+ ion similar to C222 and the bibracchial lariat ether BHE-C22. If the pendant arm hydroxy protons in BHE-C21 and BHE-C22 are replaced by methyl groups, the bibracchial lariat ethers BME-C21 and BME-C22 are formed. These methoxyethyl pendant armed bibracchial lariat ethers form complexes which are mostly less stable than their similarly sized hydroxyethyl pendant armed bibracchial lariat ethers. These observations are now discussed in more detail.

Table 2.8 Apparent Stability Constants of [M.BHE-C21]$^+$ and [M.BHE-C22]$^+$ in Selected Solvents at 298.2 K

	log (K_s / dm^3 mol^{-1})			
Complex	Acetonitrile (D_N = 14.1[a])	Methanol (D_N = 19.0[a] or 23.5[b])	Trimethyl Phosphate (D_N = 23.0[a])	N,N-Dimethyl-formamide (D_N = 26.6[a])
[Li.BHE-C21]$^+$	8.61 ± 0.01[c]	2.85 ± 0.05	2.30 ± 0.04	2.36 ± 0.03
[Na.BHE-C21]$^+$[c]	7.00 ± 0.01	4.71 ± 0.01	3.82 ± 0.01	3.93 ± 0.01
[K.BHE-C21]$^+$				3.08± 0.08[d]
[Rb.BHE-C21]$^+$				2.50 ± 0.03[d]
[Cs.BHE-C21]$^+$				2.11 ± 0.06[d]
[Ag.BHE-C21]$^+$[e]	6.24 ± 0.01	9.36 ± 0.03	11.87 ± 0.01	9.34 ± 0.01
[Li.BHE-C22]$^+$		2.08 ± 0.03	2.12 ± 0.01	2.29 ± 0.04
[Na.BHE-C22]$^+$		4.87[f]	3.92 ± 0.06[c]	3.65 ± 0.03[c]
[K.BHE-C22]$^+$		5.08[f]		4.66 ± 0.01[d]
[Rb.BHE-C22]$^+$				3.56 ± 0.01[d]
[Cs.BHE-C22]$^+$				3.36 ± 0.01[d]
[Ag.BHE-C22]$^+$[e]		10.86 ± 0.01	7.23 ± 0.01	9.13 ± 0.09

All solutions were 0.05 mol dm^{-3} in NEt_4ClO_4.

[a] Reference 28; [b] References 29,30; [c] The Na^+ complex stability constants were determined directly using a Na^+ ion selective electrode; [d] The concentration of all solutions were 1/2 the normal experimental concentrations (see Experimental section); [e] The Ag^+ complex stability constants were determined directly using a Ag^+ ion selective electrode. All other stability constants were determined competitively using a Ag^+ ion selective electrode; [f] Reference 36. All the other stability constants were derived from this study-errors represent one standard deviation.

Table 2.9 Apparent Stability Constants for the Complexation of Monovalent Metal Ions by Several Macrocyclic and Macrobicyclic Ligands in N,N-Dimethylformamide at 298.2 K

	log (K_s / dm^3 mol^{-1})					
Complex	Li^+	Na^+	K^+	Rb^+	Cs^+	Ag^+
[M.BHE-C21]$^+$[a]	2.36 ± 0.03	3.93 ± 0.01	3.08 ± 0.08	2.50 ± 0.03	2.11 ± 0.06	9.34 ± 0.01
[M.BHE-C22]$^+$[a]	2.29 ± 0.04	3.65 ± 0.03	4.66 ± 0.01	3.56 ± 0.01	3.36 ± 0.01	9.13 ± 0.09
[M.C221]$^+$[b]	3.58	7.93	6.66	5.35	3.61	12.41
[M.C222]$^+$[b]		6.17	7.98	6.78	2.16	10.07
[M.C22C5]$^+$	2.21[c]	3.66[d]	3.85[c]	3.82[c]	2.90[c]	9.40[c]
[M.C22C8]$^+$[e]	1.90	2.3	2.6	2.2	2.0	7.7
[M.C21]$^+$[f]		2.1				
[M.C22]$^+$	≈ 0[g]	< 2[h]	< 2[h]		0.61[g]	9.91[i]
[M.BME-C21]$^+$[j]	2.23	3.50	3.31	2.84	2.31	8.37
[M.BME-C22]$^+$[j]	1.93	3.31	3.82	3.08	2.38	8.28

[a] This work; [b] Reference 6; [c] Reference 15; [d] Rference 22; [e] Reference 23; [f] Reference 61; [g] Reference 62; [h] Reference 63; [i] Reference 64; [j] Reference 65.

In the solid state, the complexes [Na.BHE-C22]$^+$ and [K.BHE-C22]$^+$ adopt a *syn* conformation whereby the pendant arms coordinate the metal ions from the same side of the macroring.[66,67] The metal ions are octacoordinate in both cases (two nitrogen and six oxygen donors), as both pendant arms are involved in the coordination of the metal ions. The donor atoms are arranged in a three-dimensional fashion about the central metal ions with the crystal structures of these bibracchial lariat ether complexes bearing a remarkable resemblance to the *inclusive* cryptate [K.C222]$^+$.[68] The cryptand C222 has an approximate spherical cavity of radius about 1.4 Å[18] and when compared to eight coordinate radii of 0.92, 1.18, 1.51, 1.61 and 1.74 Å[19] for Li^+, Na^+, K^+, Rb^+ and Cs^+, respectively, it can be seen that the alkali metal ion with the best cavity fit is K^+. On account of the K^+ ions close to optimal fit into the C222 intramolecular cavity, the cryptate [K.C222]$^+$ is the most stable alkali metal ion cryptate of C222 in N,N-dimethylformamide (Table 2.9), Similar logic can be used to explain why [K.BHE-C22]$^+$ is the most stable alkali metal ion complex of BHE-C22. The ligand BHE-C22 due to its pseudocryptate arrangement of donor atoms about K^+, is capable of forming a cavity of approximately 1.4 Å in radius as it has the same number of donor atoms as C222. Thus [K.BHE-C22]$^+$ is the least strained alkali metal ion complex of BHE-C22 and exhibits the highest stability.

In the literature there appear to be no records of any [M.BHE-C21]$^+$ solid state structures which makes the discussion of BHE-C21 complexes speculative. Nevertheless, some predictions can be made from the examination of related ligand complex structures. The bibracchial lariat ether BHE-C21 can be formed when an ethylene linkage from a $-(CH_2)_2O(CH_2)_2O(CH_2)_2-$ moiety in C221 is removed. It is known that the cryptand C221 has an approximate cavity radius of 1.1 Å which compares with the six coordinate radii of 0.76, 1.02 (1.12), 1.38 (1.46), 1.52 (1.56) and 1.67 for Li^+, Na^+, K^+, Rb^+ and Cs^+, respectively. (Ideally the seven coordinate metal radii should be used for discussion purposes, but as they are not available for all the alkali metal ions the six coordinate radii are quoted. Those seven coordinate radii which are available are quoted in brackets). The Na^+ ion has the closest to optimal fit into the C221 intramolecular cavity and forms *inclusive* [Na.C221]$^+$,[20] whereas the other alkali metal ions are either too large or too small. Accordingly, [Na.C221]$^+$ is the most stable alkali metal cryptate of C221 in N,N-dimethylformamide (Table 2.9). The fact that Na^+ also forms the most stable alkali metal [M.BHE-C21]$^+$ complex in

N,N-dimethylformamide suggests that BHE-C21 forms a cavity similar to C221, approximately 1.1 Å in radius, if it assumes the *syn* conformation.

The observation that the stability constants of $[M.C221]^+$, where M^+ = alkali metal ions and Ag^+, are significantly higher than their $[M.BHE\text{-}C21]^+$ analogues and the $[M.C222]^+$ cryptates are significantly more stable than their $[M.BHE\text{-}C22]^+$ analogues (except Cs^+) can in part be attributed to the greater flexibility of the bibracchial lariat ethers. It appears that the solvent can better compete with the more flexible bibracchial lariat ethers than with the rigid cryptands for the metal ions. The additional complex stability accompanying ring closure as achieved by linking the two hydroxyethyl pendant arms of BHE-C21 and BHE-C22 with an ethylene bridge to form C221 and C222, respectively, is the macrobicyclic cryptate effect. This increased stability may also be due to the greater Lewis basicity of the cryptand ether oxygens as compared with the bibracchial lariat ether pendant arm alcoholic oxygens. The higher basicity of the ether oxygens can be attributed to the positive inductive effect of the ethylene bridge which increases the electron density on the ether oxygen atoms, thereby making them better donor atoms than the alcoholic oxygen atoms.

From Table 2.9 it can be seen that decreasing the number of donor atoms in C221 and C222 by one and two oxygen atoms, respectively, to yield $C22C_5$ and $C22C_8$ results in the $[M.C22C_5]^+$ and $[M.C22C_8]^+$ complexes being characterized by lower stabilities than their analogous $[M.C221]^+$ and $[M.C222]^+$ complexes, and by stabilities even lower than those characterizing $[M.BHE\text{-}C21]^+$ and $[M.BHE\text{-}C22]^+$, when $M^+ = Li^+$, Na^+ and K^+ (except in the case of $[K.BHE\text{-}C21]^+$ and $[K.C22C_5]^+$). This illustrates the destabilizing effect of decreasing the number of donor atoms while retaining the relatively rigid cryptand structure in th cases of $C22C_5$ and $C22C_8$, and also of retaining the same number of donor atoms while increasing the flexibility of the structure in the cases of BHE-C21 and BHE-C22. These stability variations become less apparent when the metal ions become considerably larger than the cavities formed by the ligands. A prime example of this is the Cs^+ complexes, where the stabilities become very similar. The alkali metal ion selectivity of the N_2O_4-based ligands in N,N-dimethylformamide are illustrated in Figure 2.9.

The parent diaza crown ethers C21 and C22, from which the bibracchial lariat ethers BHE-C21 and BHE-C22 are derived, exhibit alkali metal ion complex

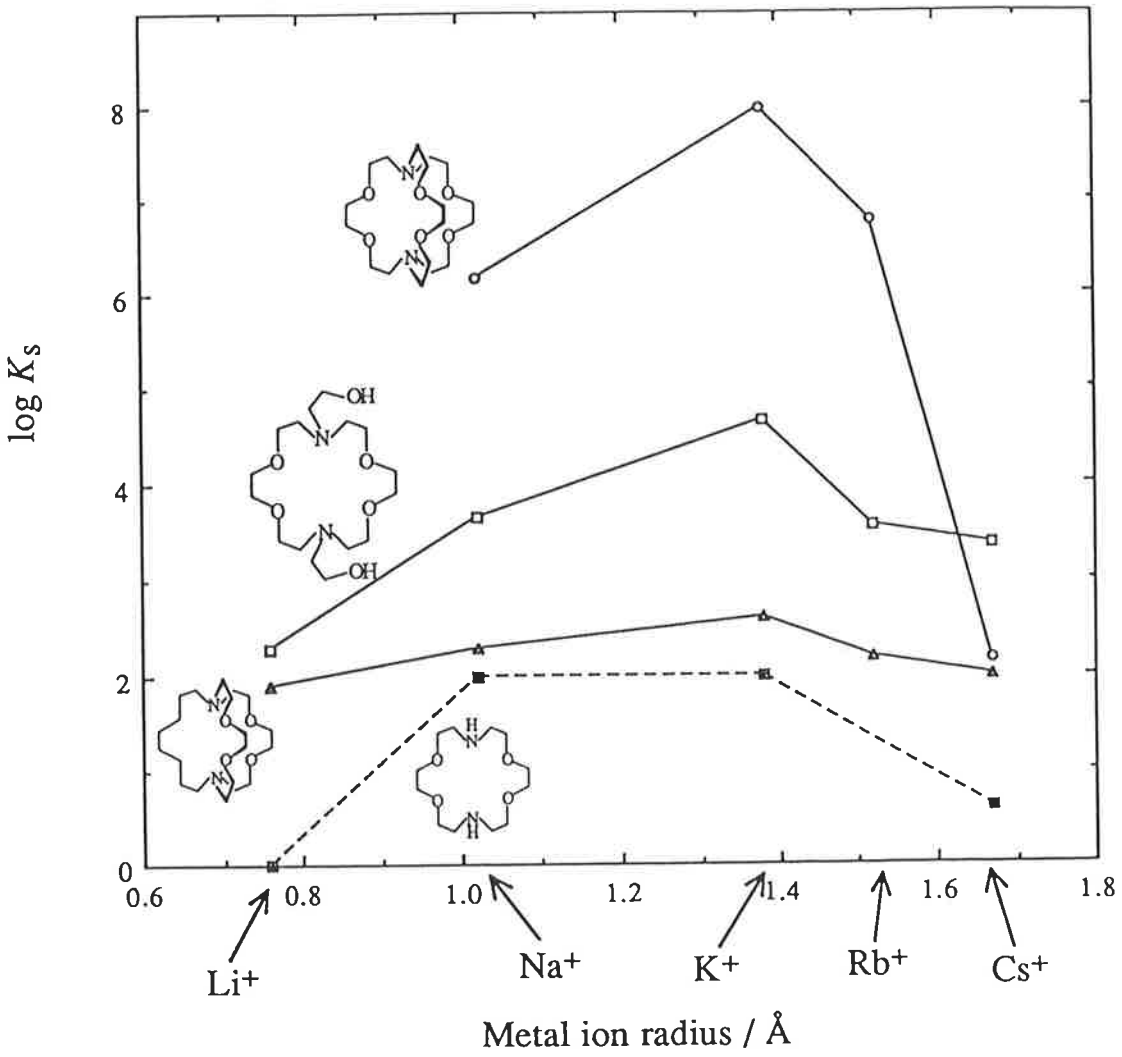

Figure 2.9 *Complexation of the alkali metal ions in N,N-dimethylformamide by the ligands C22 (square-cross), C22C8 (triangle), BHE-C22 (square) and C222 (circle). The six coordinate radii for the alkali metal ions were used as these would be the minimum appropriate ionic radii.*

stability constants much lower than those of their $[M.BHE\text{-}C21]^+$ and $[M.BHE\text{-}C22]^+$ analogues (Table 2.9). The increase in stability implies that the pendant arms facilitate the coordination of the metal ions. This may be due to the greater Lewis basicity of the alcoholic oxygen atoms of the bibracchial lariat ether pendant arms as compared with the oxygen donors of the solvent, N,N-dimethylformamide. Marsicano *et al* suggested that the increase in stability was largely an entropy effect, associated with the desolvation of the pendant arm hydroxy groups.[69] A free **bi**bracchial **l**ariat ether (BiBLE) due to its two pendant arm hydroxy groups, is more solvated in N,N-dimethylformamide than a free diaza crown ether, which has no hydrogen bonding hydroxy groups. Thus the complexation of an alkali metal ion by a bibracchial lariat ether leads to a greater release of solvent than the complexation of an alkali metal ion by a diaza crown ether. This greater net release of solvent molecules would lead to a more favourable positive change in entropy, ΔS, contribution for the substitution reaction:

$$M^+_{(s)} + BiBLE_{(s)} \overset{K_s}{\rightleftharpoons} [M.BiBLE]^+_{(s)} + \text{solvent released} \qquad \textbf{(2.26)}$$

which would inturn lead to a greater negative value for the Gibbs free energy of complexation, ΔG, and hence a greater K_S value (from Equations 2.27 and 2.28).

$$\Delta G = \Delta H - T\Delta S \qquad \textbf{(2.27)}$$

$$\Delta G = -RT\ln K_S \qquad \textbf{(2.28)}$$

where ΔH is the change in enthalpy;

R is the gas constant 8.314 J K^{-1} mol^{-1}, and

T is the temperature in Kelvin.

However, $[Ag.C22]^+$ is slightly more stable than $[Ag.BHE\text{-}C22]^+$ in N,N-dimethylformamide which may imply that the hydroxyethyl pendant arms of BHE-C22 do not facilitate the coordination of Ag^+ or that the hydroxyethyl pendant arms do not allow the parent diaza crown ether ring to adopt a conformation similar to that of the C22 ligand. This makes sense as it is well known that Ag^+ has a tendency to coordinate linearly to two donors.[59]

The hydroxyethyl pendant arms of BHE-C22 therefore may cause steric hindrance to the Ag^+ ion which results in the lower stability.

The observation that the methoxyethyl pendant armed BME-C21 produces complexes of lower stabilities with Li^+, Na^+ and Ag^+ than BHE-C21, and BME-C22 produces complexes of lower stabilities with Li^+, Na^+, K^+, Rb^+, Cs^+ and Ag^+ than BHE-C22 in N,N-dimethylformamide is a consequence of the steric hindrance produced by the pendant arm O-methyl groups (Table 2.9). However, in the case of $[M.BME\text{-}C21]^+$, when $M^+ = K^+$, Rb^+ and Cs^+, the stabilities are slightly greater than their analogous $[M.BHE\text{-}C21]^+$ complexes. This may reflect a structural difference between the complexes of the two bibracchial lariat ethers. Again, stability correlations become less distinct when the metal ions are much larger than the cavities formed by the ligands.

The stabilities of the Ag^+ complexes of both BHE-C21 and BHE-C22 are considerably greater than their alkali metal ion analogues in all the solvents listed in Table 2.8 (except $[Ag.BHE\text{-}C21]^+$ in acetonitrile). As mentioned previously in section 2.3.1 for cryptates, this result is attributable to the tendency of soft acid Ag^+ to preferentially bind nitrogen donor atoms.[34,35] Thus, the nitrogen donor solvent acetonitrile competes more effectively with BHE-C21 for Ag^+ than for Li^+ or Na^+ and results in a lower stability constant for $[Ag.BHE\text{-}C21]^+$ than the Li^+ or Na^+ analogues. Also, the rather high K_S value for $[Ag.C221]^+$ in N,N-dimethylformamide is probably a consequence of the ionic radius of Ag^+ ($r = 1.22$ Å) closely matching that of the intramolecular cavity of C221.

An examination of the stability constants for $[M.BHE\text{-}C21]^+$ in Table 2.8 reveals that the stabilities of the Li^+ and Na^+ complexes vary with the nature of solvent in the order: acetonitrile > methanol > N,N-dimethylformamide. This stability sequence is in accordance with that expected from the solvent D_N values, where stabilities increase with a decrease in D_N. When the trimethyl phosphate stabilities are also taken into account, no stability correlations with the solvent donor power can be made. A noteworthy observation is the change in relative stabilities from $[Na.BHE\text{-}C21]^+ > [Li.BHE\text{-}C21]^+$ in methanol, trimethyl phosphate and N,N-dimethylformamide to $[Li.BHE\text{-}C21]^+ > [Na.BHE\text{-}C21]^+$ in acetonitrile. No such change in metal ion selectivity with change in solvent has been reported for the alkali metal cryptates where the optimal fit of the alkali metal ion into the cryptand cavity governs the relative stability. It appears the greater

structural flexibility of BHE-C21 allows the nature of the solvent to have a greater effect on the metal ion selectivity of $[M.BHE\text{-}C21]^+$ than in the case of the cryptates. The higher atomic number of Na^+ renders it a less hard acid than Li^+ and it may therefore bind more strongly with the borderline hard base nitrogen of acetonitrile resulting in $[Li.BHE\text{-}C21]^+ > [Na.BHE\text{-}C21]^+$. It is possible for intramolecular hydrogen bonding between the pendant arm hydroxy groups to occur and would lead to suppressed segmental motion in the pendant arms. The solvents methanol, trimethyl phosphate and N,N-dimethylformamide have hydrogen bonding capabilities which would reduce the amount of intramolecular hydrogen bonding in bibracchial lariat ethers and result in a more open structure with enhanced segmental freedom for the pendant arms. Acetonitrile on the other hand has no hydrogen bonding capability and would allow greater intramolecular hydrogen bonding resulting in a more closed structure which may be more compatible with the smaller Li^+ ion than Na^+. However, it is highly unlikely that hydrogen bonding is the cause of the change in relative stabilities as the complexes of the methoxy analogue of BHE-C21, 1,7-bis(2-methoxyethyl)-4,10,13-trioxa-1,7-diazacyclopentadecane, BME-C21, are also characterized by the relative stabilities $[Li.BME\text{-}C21]^+ > [Na.BME\text{-}C21]^+$, which is the reverse order of that observed in methanol and N,N-dimethyformamide.[65]

A comparison of the stability constants for $[M.BHE\text{-}C22]^+$ in methanol, trimethyl phosphate and N,N-dimethylformamide also does not show any trend with the solvent D_N values. This emphasizes the point made earlier in section 2.3.1 for cryptates, that the D_N values of solvents are indicative of broad trends in stability variations on which more specific characteristics may superimpose.

2.3.3 : Protonation of BHE-C21 and BHE-C22 in Aqueous Solution

The bibracchial lariat ethers are dibasic species in water due to their two tertiary amine nitrogen atoms, hence two protonation constants are observed in water at 298.2 K and $I = 0.10$ (NEt_4ClO_4). All four bibracchial lariat ethers listed in Table 2.10 have similar K_1 values which indicates that the size of the parent macrocycle, the number of oxygen donor atoms and the type of pendant arms do not greatly influence the basicity of their tertiary amine nitrogens. The same observation can be made on the basicity of the cryptands and diaza crown ethers.

Table 2.10 Protonation Constants for BHE-C21, BHE-C22 and Related Ligands at 298.2 K and $I = 0.10$ (NEt_4ClO_4) in Water.

Ligand	log K_1	log K_2
C21	9.26 [a] 8.76 [b]	8.12 [a] 8.04 [b]
BHE-C21	8.79 ± 0.02 [c]	7.57 ± 0.02 [c]
BME-C21	8.64 [d]	7.16 [d]
C221	11.02 [b]	7.74 [b]
$C22C_5$	11.43 [e]	8.13 [e]
C22	9.30 [a] 9.20 [b] 9.245 [f] 9.08 [g]	8.15 [a] 8.02 [b] 8.225 [f] 7.94 [g]
BHE-C22	8.60 ± 0.01 [c] 8.702 [f]	7.20 ± 0.03 [c] 7.468 [f]
BME-C22	8.42 [d] 8.540 [f]	7.07 [d] 7.430 [f]
C222	10.00 [b]	7.53 [b]
$C22C_8$	11.1 [h]	8.41 [h]

All protonation constants quoted were determined in solutions containing 0.10 mol dm^{-3} NEt_4ClO_4 as the supporting electrolyte, except where stated otherwise.

[a] Reference 70; [b] Reference 8; [c] This work, errors represent one standard deviation; [d] Reference 65; [e] Reference 15; [f] Reference 40, $I = 0.500$ $LiClO_4$; [g] Reference 26; [h] Reference 23.

The addition of a second positive charge, H^+, causes repulsion between the two protonic charges and results in $K_2 < K_1$ for the bibracchial lariat ethers as well as for the cryptands and diaza crown ethers. The K_1 values of the bibracchial lariat ethers are slightly less than those characterizing the diaza crown ethers and substantially less than those characterizing the cryptands. This implies that the nitrogen protonation sites of the bibracchial lariat ethers compete less with water for a proton than the nitrogen protonation sites of the diaza crown ethers and cryptands. That is, the Lewis basicity of the cryptand tertiary amine nitrogens is substantially greater than that of the diaza crown ether secondary amine nitrogens and the N-substituted tertiary amines of the bibracchial lariat ethers. The Lewis basicity of the N-substituted tertiary amines of the bibracchial lariat ethers are marginally influenced by the pendant arm end-groups and follow the order OH > OCH_3 ie. the K_1 and K_2 values of BHE-C21 and BHE-C22 are slightly greater than those of BME-C21 and BME-C22, respectively.

The rather high K_1 values for the cryptands suggests that the first coordinated proton is held inside the cryptand cavity with the nitrogen atom in the *endo* conformation. This conformation would only allow a minimal solvent interaction with the nitrogen protonation site. This suggestion is verified by the solid state crystal structure of mono-protonated $C22C_5$,[15] where the lone pair of electrons on both nitrogens are directed towards the centre of the cryptand cavity. The destabilizing effect of the close proximity of the two protonic charges in the *endo-endo* cryptand conformation may lead to one or both of the nitrogen lone pairs assuming the *exo* cinformation. In this nitrogen conformation the proton is vulnerable to solvent interaction and is indicated by $K_2 < K_1$. The similar K_2 values for the cryptands and diaza crown ethers also supports the proposition that the second proton is exposed to solvent interaction.

The aliphatic bridge cryptands $C22C_5$ and $C22C_8$ display slightly higher K_1 and K_2 values than their size related cryptands C221 and C222, respectively. It appears that the extra one and two ether oxygens in C221 and C222, respectively, cause a decrease in Lewis basicity of the tertiary amine nitrogens.

2.3.4 : Complexation of Divalent Metal Ions by the Lariat Ethers BHE-C21 and BHE-C22 in Aqueous Solution

The apparent stability constants of BHE-C21 and BHE-C22 with alkaline-earth, some first row transition and heavy divalent metal ions were determined in aqueous solution at 298.2 K and I = 0.10 ($NEtClO_4$). These divalent metal ions have greater surface charge densities and a wider variation in their hard/soft characteristics than the alkali metal ions previously discussed and studied. From Table 2.11 it can be seen that the magnitude of K_S varies considerably with the nature of M^{2+}. The size and hard/soft nature of the divalent metal ions, crystal field effects, and the size of the pseudocryptate cavities which can be formed by BHE-C21 and BHE-C22 if the *syn* conformation is adopted may all influence the magnitude of K_S.

The stability constants of the alkaline-earth complexes of BHE-C21 and BHE-C22 vary with M^{2+} in the sequence: $Mg^{2+} < Ca^{2+} > Sr^{2+} > Ba^{2+}$ and $Mg^{2+} < Ca^{2+} < Sr^{2+} < Ba^{2+}$, respectively (Table 2.11). These stability sequences are a direct result of the ionic radii of the alkaline-earth metal ions and the stereochemistry of donor atoms in both bibracchial lariat ethers. A comparison of the alkaline-earth stability constants of $[M.C22]^{2+}$ and $[M.BHE\text{-}C22]^{2+}$ reveals that $[M.BHE\text{-}C22]^{2+} > [M.C22]^{2+}$ which indicates that the hydroxyethyl arms of BHE-C22 participate in the coordination of the alkaline-earth metal ions (Table 2.11). A similar comparison of the alkaline-earth complexes of C21 and BHE-C21 cannot be made as there is no available data for C21. As C221 and C222 exhibit identical selectivity patterns as BHE-C21 and BHE-C22, respectively, it suggests that BHE-C21 and BHE-C22 form cavities of radius 1.1 and 1.4 Å, respectively, if they adopt the *syn* conformation. Thus Ca^{2+} (r = 1.06 Å) and Ba^{2+} (r = 1.42 Å) have the closest to optimal fits in the BHE-C21 and BHE-C22 cavities, respectively. As a consequence, $[Ca.BHE\text{-}C21]^{2+}$ and $[Ba.BHE\text{-}C22]^{2+}$ are the most stable alkaline-earth $[M.BHE\text{-}C21]^{2+}$ and $[M.BHE\text{-}C22]^{2+}$ complexes, respectively.

The alkaline-earth metal ions are hard acids and preferentially bind oxygen donor atoms.[34,35] Therefore water is expected to compete well with the bibracchial lariat ethers for the alkaline-earth metal ions and produce low K_S values in comparison with the K_S characterizing transition and heavy metal bibracchial lariat ether complexes. This theory explains the stabilities of the

Table 2.11 Apparent Stability Constants for the Complexation of Divalent Metal Ions by BHE-C21, BHE-C22 and Related Ligands at 298.2 K and I = 0.10 (NEt_4ClO_4) in Water.

	Ionic Radius[a]	log (K_s / dm^3 mol^{-1})							
M^{2+}	(Å)	$[M.C21]^{2+}$	$[M.BHE\text{-}C21]^{2+}$[b]	$[M.BME\text{-}C21]^{2+}$[c]	$[M.C221]^{2+}$	$[M.C22]^{2+}$	$[M.BHE\text{-}C22]^{2+}$	$[M.BME\text{-}C22]^{2+}$	$[M.C222]^{2+}$
Mg^{2+}	0.72 (6) 0.89 (8)		≈2	< 2	< 2.0[d]	1.3[e]	< 2[f]	< 2[c]	1.7[e] < 2.0[d]
Ca^{2+}	1.00 (6) 1.06 (7) 1.12 (8)		4.86 ± 0.14	2.8	6.95[d]	1.8[e] 1.74[g]	4.08[f]	2.4[c]	4.57[e] 4.4[d] 4.91[h]
Sr^{2+}	1.18 (6) 1.21 (7) 1.26 (8)		4.15 ± 0.12	3.62	7.35[d]	2.8[e]	4.29 ± 0.08[b]	3.64[c]	8.0[d] 8.26[e]
Ba^{2+}	1.35 (6) 1.38 (7) 1.42 (8)		3.99 ± 0.10	3.45	6.30[d]	2.65[e]	5.33 ± 0.06[b]	4.36[c]	9.5[d] 9.7[e]
Mn^{2+}	0.83 (6) 0.90 (7) 0.96 (8)		5.28 ± 0.07	4.08			2.88 ± 0.11[b]	2.78[c]	
Co^{2+}	0.75 (6) 0.90 (8)	5.05[i] 5.22[j]	6.62 ± 0.01	3.76	5.40[i]	≤ 2.5[i] 3.25[j]	2.80 ± 0.08[b]	2.68[c]	≤ 2.5[i]
Ni^{2+}	0.69 (6)	3.73[i] 4.05[j]	4.73 ± 0.03	3.33	4.28[i]	≤ 2.5[i] 3.43[j]	2.69 ± 0.01[b]	2.32[c]	≤ 3.5[i]
Cu^{2+}	0.73 (6)	7.17[i] 8.15[j]	8.11 ± 0.01	5.38	7.56[i]	6.18[i] 7.59[j]	6.60[f]	5.89[c]	6.81[i]

Zn^{2+}	0.74 (6) 0.90 (8)	5.19[i] 5.34[j]	6.18 ± 0.02	3.79	5.41[i]	3.19[i] 4.31[j]	3.03 ± 0.02[b]	2.58[c]	≤ 2.5[i]
Cd^{2+}	0.95 (6) 1.03 (7) 1.10 (8)	6.46[i]	7.70 ± 0.01	5.69	10.04[i]	5.59[f] 5.31[i] 5.25[e]	7.96[f]	5.01[f] 4.72[c]	7.10[i] 6.8[e]
Hg^{2+}	1.02 (6) 1.14 (8)	16.65[k]	15.07 ± 0.08	15.2	19.97[k]	17.85[e]	14.58 ± 0.20[b]	14.1[c]	18.2[e]
Pb^{2+}	1.19 (6) 1.23 (7) 1.29 (8)	5.85[i]	8.91 ± 0.01	8.12	13.12[i]	7.01[f] 6.90[i]	9.20[f]	8.39[f] 8.18[c]	12.72[i] 12.36[e] 12.0[d]

[a] Reference 19. The ionic radii for the coordination numbers 6, 7 and 8 (in brackets) are quoted; [b] This work-errors represent one standard deviation; [c] Reference 65; [d] Reference 2; [e] Reference 71; [f] Reference 40; [g] Reference 72; [h] Reference 73; [i] Reference 8; [j] Reference 70; [k] Reference 16.

BHE-C21 complexes, however, the alkaline-earth metal $[M.BHE\text{-}C22]^{2+}$ complexes are more stable than the transition metal $[M.BHE\text{-}C22]^{2+}$ complexes (except $[Mg.BHE\text{-}C22]^{2+}$ and $[Cu.BHE\text{-}C22]^{2+}$). A possible explanation is that the smaller ionic radii of the transition metal ions in comparison with the alkaline-earth metal ions are less compatible with the larger cavity possibly formed by BHE-C22 causing strained structures and hence complexes of lower stabilities. A comparison of the transition metal $[M.BHE\text{-}C22]^{2+}$ complexes with the analogous $[M.C22]^{2+}$ complexes reveals that the stabilities of the transition metal complexes of $[M.C22]^{2+}$ are greater or similar to the analogous $[M.BHE\text{-}C22]^{2+}$ complexes. This indicates that the hydroxyethyl pendant arms of BHE-C22 do not facilitate the coordination of the transition metal ions and therefore probably cause steric hindrance to the transition metal ions or it may be possible that the hydroxyethyl pendant arms do not allow the parent diaza crown ether ring to adopt a conformation similar to that of the C22 ligand. The possibility that the hydroxyethyl pendant arms facilitate the coordination of the alkaline-earth metal ions but not the transition metal ions may account for the greater K_S values characterizing the alkaline-earth metal $[M.BHE\text{-}C22]^{2+}$ complexes in comparison with the K_S values characterizing the transition metal $[M.BHE\text{-}C22]^{2+}$ complexes.

From Table 2.11 it can be noted that the stabilities of the transition metal $[M.BHE\text{-}C21]^{2+}$ complexes are greater than the stabilities of the analogous $[M.C21]^{2+}$ complexes (Cu^{2+} is less apparent) which indicates that the pendant arms of BHE-C21 do facilitate the coordination of the transition metal ions. The participation of the pendant arms of BHE-C21 in coordinating the transition metal ions and the non-participation of the pendant arms of BHE-C22 accounts for the greater stabilities of the transition metal complexes of BHE-C21 in comparison to the analogous BHE-C22 complexes.

The variation in apparent stability constants for $[M.BHE\text{-}C21]^{2+}$ and $[M.BHE\text{-}C22]^{2+}$, where $M^{2+} = Mn^{2+}$, Co^{2+}, Ni^{2+}, Cu^{2+} and Zn^{2+}, is $Mn^{2+} < Co^{2+} > Ni^{2+} < Cu^{2+} > Zn^{2+}$ and $Mn^{2+} \approx Co^{2+} > Ni^{2+} < Cu^{2+} > Zn^{2+}$, respectively. For simple ligands, the stability of complexes formed with the first-row transition metal ions (M^{2+}) follows the Irving-Williams series[74,75], $Mn^{2+} < Co^{2+} < Ni^{2+} < Cu^{2+} > Zn^{2+}$, which arises as a consequence of ligand dipole-metal ion electrostatic effects and crystal field effects. The transition metal ion stability constants of $[M.BHE\text{-}C21]^{2+}$ and $[M.BHE\text{-}C22]^{2+}$ follow the Irving-Williams series except for Ni^{2+}. This exception may reflect the

small size of Ni^{2+} which would result in a more strained structure. A similar inversion in the order of stability of the Co^{2+} and Ni^{2+} complexes was observed for BME-C21, BME-C22[65] and C22.[70] The Cu^{2+} complexes of both bibracchial lariat ethers are the most stable transition metal complexes perhaps because Cu^{2+} also exhibits soft acid characteristics sometimes and is capable of strong interaction with nitrogen[76] whereas the other transition metal ions are borderline between hard and soft acids.[34,35]

The heavy metal ions Cd^{2+}, Hg^{2+} and Pb^{2+} produce very stable complexes with both BHE-C21 and BHE-C22. This is due to their soft acid nature and their tendency to preferentially bind nitrogen donor atoms.[34,35] Thus the bibracchial lariat ethers compete more effectively for the heavy metal ions than water. The Hg^{2+} complexes of both BHE-C21 and BHE-C22 are the most stable heavy metal complexes even though it appears that the pendant arms do not coordinate Hg^{2+} since the parent diaza crown ether-Hg^{2+} complexes are more stable than the bibracchial lariat ether-Hg^{2+} complexes. The higher Hg^{2+} bibracchial lariat ether complex stabilities imply that the common two-coordinate Hg^{2+} linear geometry[59] is achieved and satisfied through bonding with the two pivotal amine nitrogens (similar to Ag^{+}). No formation of mercuric oxide was observed during the titration of BHE-C21 and BHE-C22 in the presence of Hg^{2+}, consistent with the high stability of the $[Hg.BHE\text{-}C21]^{2+}$ and $[Hg.BHE\text{-}C22]^{2+}$ complexes. Whereas a similar comparison of the Pb^{2+} and Cd^{2+} complexes of BHE-C21, C21, BHE-C22 and C22 indicates that the pendant arms are involved in the complexation of these heavy metal ions.

It is worth noting that the stabilities of the $[M.C221]^{2+}$ and $[M.C222]^{2+}$ are not always greater than the analogous $[M.BHE\text{-}C21]^{2+}$ and $[M.BHE\text{-}C22]^{2+}$ complexes, respectively, as anticipated by the macrobicyclic cryptate effect. Also, the stabilities of the BME-C21 and BME-C22 complexes are always lower than their analogous BHE-C21 and BHE-C22 complexes (except in the case of $[Hg.BHE\text{-}C21]^{2+}$ and $[Hg.BME\text{-}C22]^{2+}$, where the stabilities are similar). This illustrates that the greater steric crowding at the donor oxygen of the methoxyethyl pendant arms makes the hydroxyethyl arms sterically more efficient for coordination of metal ions. Even in the cases where it appears that the pendant arms do not participate in the coordination process, the slightly larger methoxyethyl pendant arms will again cause more steric hindrance to the incoming metal ion than the hydroxyethyl pendant arms resulting in lower complex stabilities for BME-C21 and BME-C22.

Without knowing the structures of the complexes in solution it is very difficult trying to explain the experimental results in terms of the coordination number of the metal ions. It is possible that coordination numbers greater than that expected arises in solution as it is possible that some water molecules occupy some coordination sites in the metal complexes. An example of this is the eleven-coordinate $[Ba.BHEE\text{-}C22.H_2O]^{2+}$ complex,[77] where a water molecule occupies the eleventh coordination site. Many factors were used to interpret the stability constant data and very rarely is it possible to explain stability data in terms of only one factor. Usually it is necessary to apply several factors when discussing experimental stability results.

References

1 J.-M. Lehn, *Struct. Bonding (Berlin)*, **16**, 1973, 1.

2 J.-M. Lehn and J.-P. Sauvage, *J. Am. Chem. Soc.*, **97**, 1975, 6700.

3 J.-M. Lehn, *Acc. Chem. Res.*, **11**, 1978, 49.

4 H.-J. Buschmann, *Inorg. Chim. Acta*, **125**, 1986, 31.

5 H.-J. Buschmann, *Inorg. Chim. Acta*, **120**, 1986, 125.

6 B.G. Cox, J. Garcia-Rosas and H. Schneider, *J. Am. Chem. Soc.*, **103**, 1981, 1384.

7 B.G. Cox, J. Stroka, I. Schneider and H. Schneider, *J. Chem. Soc., Faraday Trans. I*, **85**, 1989, 187.

8 F. Arnaud-Neu, B. Spiess and M.-J. Schwing-Weill, *Helv. Chim. Acta*, **60**, 1977, 2633.

9 H.-J. Buschmann, *J. Solution Chem.*, **15**, 1986, 453.

10 S.F. Lincoln, I.M. Brereton and T.M. Spotswood, *J. Am. Chem. Soc.*, **108**, 1986, 8134.

11 S.F. Lincoln, B.J. Steel, I.M. Brereton and T.M. Spotswood, *Polyhedron*, **5**, 1986, 1597.

12 S.F. Lincoln and A. Abou-Hamdan, *Inorg. Chem.*, **29**, 1990, 3584.

13 A. Abou-Hamdan and S.F. Lincoln, *Inorg. Chem.*, **30**, 1991, 462.

14 S.F. Lincoln and A.K.W. Stephens, *Inorg. Chem.*, **30**, 1991, 3529.

15 P. Clarke, J.M. Gulbis, S.F. Lincoln and E.R.T. Tiekink, *Inorg. Chem.*, **31**, 1992, 3398.

16 F. Arnaud-Neu, B. Spiess and M.-J. Schwing-Weill, *J. Am. Chem. Soc.*, **104**, 1982, 5641.

17 B.G. Cox, N.V. Truong and H. Schneider, *J. Am. Chem. Soc.*, **106**, 1984, 1273.

18 J.-M. Lehn and J.-P. Sauvage, *J. Chem. Soc., Chem. Commun.*, 1971, 440.

19 R.D. Shannon, *Acta Crystallogr., Sect. A: Cryst. Phys. Diffr., Theor. Gen. Crystallog.*, **A32**, 1976, 751.

20 F. Mathieu, B. Metz, D. Moras and R. Weiss, *J. Am. Chem. Soc.*, **100**, 1978, 4412.

21 B.G. Cox, H. Schneider and J. Stroka, *J. Am. Chem. Soc.*, **100**, 1978, 4746.

22 P. Clarke, S.F. Lincoln and E.R.T. Tiekink, *Inorg. Chem.*, **30**, 1991, 2747.

23 S.F. Lincoln and A.K.W. Stephens, *Inorg. Chem.*, **31**, 1992, 5067.

24 Y.M. Cahen, J.L. Dye and A.I. Popov, *J. Phys. Chem.*, **79**, 1975, 1289.

25 V.J. Gatto, K.A. Arnold, A.M. Viscariello, S.R. Miller and G.W. Gokel, *Tetrahedron Lett.*, **27**, 1986, 327.

26 G. Anderegg, *Helv. Chim. Acta*, **64**, 1981, 1790.

27 H.K. Frensdorff, *J. Am. Chem. Soc.*, **93**, 1971, 600.

28 V. Gutmann, "Coordination Chemistry in Non-Aqueous Solutions", Springer, Vienna, 1968.

29 R.H. Erlich, E. Roach and A.I. Popov, *J. Am. Chem. Soc.*, **92**, 1970, 4989.

30 W.J. DeWitte and A.I. Popov, *J. Solution Chem.*, **5**, 1976, 231.

31 Y. Marcus, *J. Solution Chem.*, **13**, 1984, 599.

32 The molar volumes of the trialkyl phosphates were calculated from the molar densities of trimethyl, triethyl and tri-*n*-butyl phosphate = 1.213, 1.068 and 0.976 g cm^{-3}, respectively.

33 A. Abou-Hamdan, I.M. Brereton, A.M. Hounslow, S.F. Lincoln and T.M. Spotswood, *J. Inclusion Phenom.*, **5**, 1987, 137.

34 R.G. Pearson, *J. Am. Chem. Soc.*, **85**, 1963, 3533.

35 R.G. Pearson, *Coord. Chem. Rev.*, **100**, 1990, 403.

36 V.J. Gatto, K.A. Arnold, A.M. Viscariello, S.R. Miller, C.R. Morgan and G.W. Gokel, *J. Org. Chem.*, **51**, 1986, 5373.

37 R.A. Schultz, D.M. Dishong and G.W. Gokel, *J. Am. Chem. Soc.*, **104**, 1982, 625.

38 R.A. Schultz, E. Schlegel, D.M. Dishong and G.W. Gokel, *J. Chem. Soc., Chem. Commun.*, 1982, 242.

39 P. Gramain and Y. Frère, *Nouv. J. Chim.*, **3**, 1979, 53.

40 S. Kulstad and L.Å. Malmsten, *J. Inorg. Nucl. Chem.*, **43**, 1981, 1299.

41 K.V. Damu, R.D. Hancock, P.W. Wade, J.C.A. Boeyens, D.G. Billing and S.M. Dobson, *J. Chem. Soc., Dalton Trans.*, 1991, 293.

42 H.-J. Buschmann, *Inorg. Chim. Acta*, **195**, 1992, 51.

43 E. Mei, L. Liu, J.L. Dye and A.I. Popov, *J. Solution Chem.*, **6**, 1977, 771.

44 T. Nakamura, Y. Yumoto and K. Izutsu, *Bull. Chem. Soc. Jpn.*, **55**, 1982, 1850.

45 K.A. Arnold and G.W. Gokel, *J. Org. Chem.*, **51**, 1986, 5015.

46 G. Bonas, C. Bonas and M.R. Vignon, *J. Inclusion Phenom.*, **7**, 1989, 637.

47 T. Takahashi, A. Uchiyama, K. Yamada, B.C. Lynn and G.W. Gokel, *Tetrahedron Lett.*, **33**, 1992, 3825.

48 J. Stroka, B.G. Cox, H. Schneider, *J. Electroanal. Chem.*, **266**, 1989, 337.

49 E.L. Lee, O.A. Gansow and M.J. Weaver, *J. Am. Chem. Soc.*, **102**, 1980, 2278.

50 J. Gutknecht, H. Schneider and J. Stroka, *Inorg. Chem.*, **17**, 1978, 3326.

51 P. Clarke, STAB, University of Adelaide, Australia.

52 F.J.C. Rossotti and H. Rossotti, "The Determination of Stability Constants", Chapter 5, McGraw-Hill, New York, 1961.

53 A. Sabatini, A. Vacca and P. Gans, *Talanta*, **21**, 1974, 53.

54 D. Moras and R. Weiss, *Acta Crystallogr., Sect. B*, **B29**, 1973, 400.

55 A. Abou-Hamdan, A.M. Hounslow, S.F. Lincoln and T.W. Hambley, *J. Chem. Soc., Dalton Trans.*, 1987, 489.

56 S.F. Lincoln, E. Horn, M.R. Snow, T.W. Hambley, I.M. Brereton and T.M. Spotswood, *J. Chem. Soc., Dalton Trans.*, 1986, 1075.

57 M.-F. Lejaille, M.-H. Livertoux, C. Guidon and J. Bessière, *Bull. Soc. Chim. Fr.*, 1978, I373.

58 H.-J. Buschmann, *J. Inclusion Phenom.*, **7**, 1989, 581.

59 F.A. Cotton and G. Wilkinson, "Advanced Inorganic Chemistry", Interscience, New York, 3rd Edn., 1980.

60 Y. Ducommun, L. Helm, A.E. Merbach, B. Hellquist and L.I. Elding, *Inorg. Chem.*, **28**, 1989, 377.

61 P. Clarke, A. Abou-Hamdan, A.M. Hounslow and S.F. Lincoln, *Inorg. Chim. Acta*, **154**, 1988, 83.

62 M. Shamsipur and A.I. Popov, *Inog. Chim. Acta*, **43**, 1980, 243.

63 I. Marolleau, J.-P. Gisselbrecht, M. Gross, F. Arnaud-Neu and M.-J. Schwing-Weill, *J. Chem. Soc., Dalton Trans.*, 1989, 367.

64 B.G. Cox, P. Firman, H. Horst and H. Schneider, *Polyhedron*, **2**, 1983, 343.

65 J.B. Lucas, Unpublished results.

66 F.R. Fronczek, V.J. Gatto, R.A. Schultz, S.J. Jungk, W.J. Colucci, R.D. Gandour and G.W. Gokel, *J. Am. Chem. Soc.*, **105**, 1983, 6717.

67 R.D. Gandour, F.R. Fronczek, V.J. Gatto, C. Minganti, R.A. Schultz, B.D. White, K.A. Arnold, D. Mazzocchi, S.R. Miller and G.W. Gokel, *J. Am. Chem. Soc.*, **108**, 1986, 4078.

68 D. Moras, B. Metz and R. Weiss, *Acta Crystallogr., Sect. B*, **B29**, 1973, 383.

69 F. Marsicano, R.D. Hancock and A. McGowan, *J. Coord. Chem.*, **25**, 1992, 85.

70 E. Luboch, A. Cygan and J.F. Biernat, *Inorg. Chim. Acta*, **68**, 1983, 201.

71 G. Anderegg, *Helv. Chim. Acta*, **58**, 1975, 1218.

72 R.D. Hancock, R. Bhavan, M.S. Shaikjee, P.W. Wade and A. Hearn, *Inorg. Chim. Acta*, **112**, 1986, L23.

73 B.G. Cox, J. Stroka and H. Schneider, *Inorg. Chim. Acta*, **128**, 1987, 207.

74 H. Irving and R.J.P. Williams, *Nature (London)*, **162**, 1948, 746.

75 H. Irving and R.J.P. Williams, *J. Chem. Soc.*, 1953, 3182.

76 M. Herceg and R. Weiss, *Inorg. Nucl. Chem. Lett.*, **6**, 1970, 435.

77 R. Bhavan, R.D. Hancock, P.W. Wade, J.C.A. Boeyens and S.M. Dobson, *Inorg. Chim. Acta*, **171**, 1990, 235.

Chapter 3 : Metal Ion Exchange on Cryptates and Lariat Ether Complexes

3.1 : Introduction

The kinetic aspects of alkali metal cryptates have been well investigated.[1-32] These kinetic studies were catalysed by the ability of naturally occuring macrocycles, like valinomycin,[33] to induce the transport of cations through artificial and biological membranes by behaving as cation carriers.[34,35] A better understanding of naturally occuring membrane transport would be provided by the elucidation of the mechanism of complex formation of alkali metal ions with cryptands. Furthermore, kinetic studies of alkali metal cryptates enable the determination of the kinetic origins of the selectivity of the cryptands.

Kinetic and equilibrium factors are interrelated. This can be illustrated by the simple complexation reaction exemplified in Equation 3.1, where the stability constant, K_S, may be expressed in terms of the complexation rate constant, k_c, and the decomplexation rate constant, k_d:

$$M^+ + \text{Cryptand} \underset{k_d}{\overset{k_c}{\rightleftharpoons}} [\text{M.Cryptand}]^+ \qquad \textbf{(3.1)}$$

where $$K_S = \frac{k_c}{k_d} \qquad \textbf{(3.2)}$$

Cryptate lability is controlled by a number of factors including cryptand cavity size, the number, type and arrangement of cryptand donor atoms, cryptand structural flexibility, the size and nature of the metal ion and also the type of solvent. Kinetic studies have shown that the selectivity of cryptands towards certain metal cations is primarily due to variations in the decomplexation rate constant.[6,9,11,18-21,23,29,31,36-39] The stability and decomplexation rate constants determine whether a cryptand functions as a metal cation receptor or a metal cation carrier. Several studies have shown that the decomplexation rate constants of cryptates are influenced more strongly by solvent variation than the complexation rate constants.[9,18-21,23,39] The greater stabilities of the cryptates over the crown ether complexes, which is referred to as the macrobicyclic cryptate effect, is kinetic in origin and due to the slower rate of decomplexation of the cryptates.[11,40]

Two mechanisms for the complexation of a metal cation by a macrobicyclic ligand have been proposed, namely the Chock[41] and Eigen-Winkler[11,42,43] mechanisms. The Chock mechanism (Equations 3.3 and 3.4) involves a fast conformational change in the ligand (L) followed by the reaction of one of the ligand conformers (L_2) with a cation (M^+). The slow rate determining step is the complexation step.

$$L_1 \underset{k_{-0}}{\overset{k_0}{\rightleftharpoons}} L_2 \qquad \textit{fast} \tag{3.3}$$

$$M^+ + L_2 \underset{k_{-1}}{\overset{k_1}{\rightleftharpoons}} [M.L_2]^+ \qquad \textit{slow} \tag{3.4}$$

The Eigen-Winkler multistep mechanism (Equation 3.5) is the generally accepted mechanism which best interprets the complexation process of cryptands. The first step involves the metal ion (M^+) and the cryptand (C_0, the subscript number indicates how many metal ion-cryptand donor atom bonds have been formed) coming together at a diffusion-controlled rate to form an encounter complex with both the metal ion and cryptand retaining their inner coordination sphere. The ensuing step involves the partial desolvation of the metal ion, the partial conformational rearrangement of the cryptand and the formation of the first metal ion-cryptand bond. A series of steps follow in which the remaining solvent molecules in the inner coordination sphere of the metal ion are replaced sequentially by the donor atoms of the cryptand. Hence, after several steps of metal ion desolvation, cryptand conformational rearrangement and metal ion-cryptand bond formation the cryptate ($[M.C_n]^+$) is formed. In this mechanism, identification of the rate determining step is complicated due to the different cryptand conformational changes and metal ion desolvation which may occur in each step and contribute differently to the energetics of each step.

$$M^+ + C_0 \underset{k_{-1}}{\overset{k_1}{\rightleftharpoons}} M^+\cdots C_0 \underset{k_{-2}}{\overset{k_2}{\rightleftharpoons}} M.C_1^+ \underset{k_{-3}}{\overset{k_3}{\rightleftharpoons}} \cdots\cdots \underset{k_{-n}}{\overset{k_n}{\rightleftharpoons}} [M.C_n]^+ \tag{3.5}$$

Shchori *et al* proposed two mechanisms which describe the exchange metal ions undergo between the solvated, uncomplexed state and the complexed state.[44,45] The first exchange mechanism is the monomolecular dissociative mechanism. This mechanism may be described by Equation 3.1, where a

metal ion must be completely decomplexed from the cryptand before another metal ion may complex the cryptand.

$$M^+ + \text{Cryptand} \underset{k_d}{\overset{k_c}{\rightleftharpoons}} [\text{M.Cryptand}]^+ \qquad \textbf{(3.1)}$$

The rate law for this mechanism is independent of the solvated metal ion concentration but dependent on the cryptate concentration:

$$\text{rate of exchange} = k_d[\text{M.Cryptand}^+] \qquad \textbf{(3.6)}$$

The mean lifetime of the cryptate, τ_c, is defined as:

$$\tau_c = \frac{1}{k_d} = \frac{\tau_s \chi_c}{\chi_s} \qquad \textbf{(3.7)}$$

where τ_s is the mean lifetime of the solvated metal ion;

χ_c is the mole fraction of the metal ion in the complexed state, and

χ_s is the mole fraction of the metal ion in the solvated state.

The second exchange mechanism is the bimolecular mechanism. In this mechanism the leaving metal ion decomplexes and solvates concurrently with the complexation and desolvation of an entering metal ion (the asterisk is a typographical distinction only), and may be represented by the following equation:

$$^*M^+ + [\text{M.Cryptand}]^+ \underset{k_b}{\overset{k_b}{\rightleftharpoons}} M^+ + [^*\text{M.Cryptand}]^+ \qquad \textbf{(3.8)}$$

where k_b is the bimolecular exchange rate constant.

The rate law for this bimolecular exchange mechanism is dependent on both the solvated metal ion and cryptate concentrations:

$$\text{rate of exchange} = k_b[\text{M.Cryptand}^+][M^+] \qquad \textbf{(3.9)}$$

The mean lifetime of the cryptate, τ_c, is now defined as:

$$\tau_c = \frac{1}{k_b[M^+]} = \frac{\chi_s}{\tau_s \chi_c} \qquad \textbf{(3.10)}$$

If both the monomolecular and bimolecular mechanisms operate in parallel,[24] the overall rate law will be:

$$\text{rate of exchange} = k_{obs}[\text{M.Cryptand}]^+ = (k_d + k_b[M^+])[\text{M.Cryptand}^+] \quad \textbf{(3.11)}$$

where τ_c is defined as:

$$\tau_c = \frac{1}{k_{obs}} = \frac{1}{(k_d + k_b[M^+])} \quad \textbf{(3.12)}$$

The monomolecular mechanism is the more commonly observed exchange mechanism in cryptates.[13,17-24] The electrostatic repulsion which would be experienced by the two positively charged reacting species in the bimolecular mechanism renders the monomolecular mechanism more favourable. However, the cation-cation electrostatic repulsion can be reduced if the ligand-cation interaction is sufficiently strong.[46] It is reasonable to assume that the bimolecular mechanism would prefer a cryptand conformation which enables the simultaneous entrance of a free metal ion and exit of the complexed metal ion to occur with minimal ligand rearrangement. Relatively rigid cryptands satisfy this conformational condition for the bimolecular mechanism better than the flexible cryptands. The monomolecular mechanism is exemplified by $[Li.C222]^+$ in acetonitrile, acetone and propylene carbonate, whereas the bimolecular mechanism is exemplified by $[Li.C221]^+$ in acetonitrile and propylene carbonate.[24]

Cryptates exhibit a wide range of complexation and decomplexation rate constants, thus a number of different kinetic techniques are used in the kinetic studies of cryptates. These include the stopped-flow technique,[5-10,16,29-32,36-39,47,48] the ultrasonic relaxation technique,[49] the temperature-jump relaxation technique[50,51] and the NMR technique.[12-15,17-24,27,52] The NMR technique is a very powerful and sensitive tool which enables the study of the different metal ion chemical environments in numerous solvents and is the method employed in this kinetic study. It also enables a wide range of k_c and k_d to be determined. An NMR kinetic study of $[Na.C211]^+$, $[Na.C21C_5]^+$, $[Li.C211]^+$ and $[Li.C21C_5]^+$ in trimethyl, triethyl and tri-*n*-butyl phosphate provides a better understanding of the cryptate metal ion exhange mechanisms and the factors which influence cryptate lability.

The cryptands form highly stable and selective cation complexes but the release rate of the cations is extremely slow in comparison to valinomycin. In contrast, crown ethers form labile cation complexes similar to valinomycin

due to their structural flexibility but lack the three-dimensionality of valinomycin and the cryptands. For a synthetic compound to behave as a good specific cation carrier like valinomycin, it must be a flexible, three-dimensional ligand capable of completely enveloping the cation with sufficient binding stength. Both the cryptands and crown ethers lack one of the criteria which creates a good cation carrier. The paradox of cation transport is that the carrier should bind the cation strongly and rapidly at the membrane but bind the cation weakly and release it rapidly on the the other side of the membrane. These contradictory criteria can be attained with the right balance of structural flexibility and three-dimensionality. Lariat ethers were developed to mimic the cation transport properties of valinomycin. The attachment of one or more pendant arms to a crown ether ring provides the macrocycle with the three-dimensional binding character of the cryptands, and the mobility of the pendant arms and flexibility of the parent crown ether ring provides it with the necessary lability of the crown ethers which is required for efficient cation transport.

Although the lariat ethers were specifically designed to be more labile than the cryptands and to act as cation carriers, only a few kinetic studies of lariat ether complexes have been reported.[53,54] Consequently this study seeks to extend the understanding of the kinetic aspects of the lariat ethers and their monovalent metal ion complexes through a study of 1,7-bis(2-hydroxyethyl)-4,10,13-trioxa-1,7-diazacyclopentadecane, BHE-C21, and 1,10-bis(2-hydroxyethyl)-4,7,13,16-tetraoxa-1,10-diazacyclooctadecane, BHE-C22, which have the same number of oxygen and nitrogen donor atoms as the cryptands 4,7,13,16,21-pentaoxa-1,10-diazabicyclo[8.8.5]tricosane, C221, and 4,7,13,16,21,24-hexaoxa-1,10-diazabicyclo[8.8.8]hexacosane, C222, respectively. Additionally, the ligands BHE-C22 and C222 appear to coordinate alkali metal ions with a similar disposition of donor atoms.[55,56]

Eyring and Petrucci demonstrated, using the ultrasonic relaxation technique, that the complexation of Na^+ by 1-methoxyethoxyethyl-4,7,10,13-tetraoxa-1-monoazacyclopentadecane in methanol at 298.2 K takes place in two steps.[53] The first step involves the formation of an encounter complex with Na^+ residing outside the parent crown ether ring and the second step involves a ligand conformational change, entry of the Na^+ into the macroring and the complexation of Na^+ by the methoxyethoxyethyl pendant arm. The proposed reaction scheme is illustrated in Figure 3.1. The kinetic and equilibrium parameters determined for the two steps were: $k_1 = 9.0 \times 10^{10}$ dm^3 mol^{-1} s^{-1}, $k_{-1} = 2.1 \times 10^8$ s^{-1}, $K_1 = 429$ dm^3 mol^{-1} ($=k_1/k_{-1}$), $k_2 = 1.2 \times 10^7$ s^{-1}, $k_{-2} = 1.5$

$\times 10^5$ s^{-1} and $K_2 = 80$ dm^3 mol^{-1} ($= k_2/k_{-2}$). The overall equilibrium constant, K_s, can be calculated from K_1 and K_2 as $K_s = K_1(1 + K_2) = 3.47 \times 10^4$ dm^3 mol^{-1} ($\log K_s = 4.54$) which proved to be the same as that reported in the literature previously.[57] This data is evidence that lariat ethers are labile as well as relatively strong cation binders.

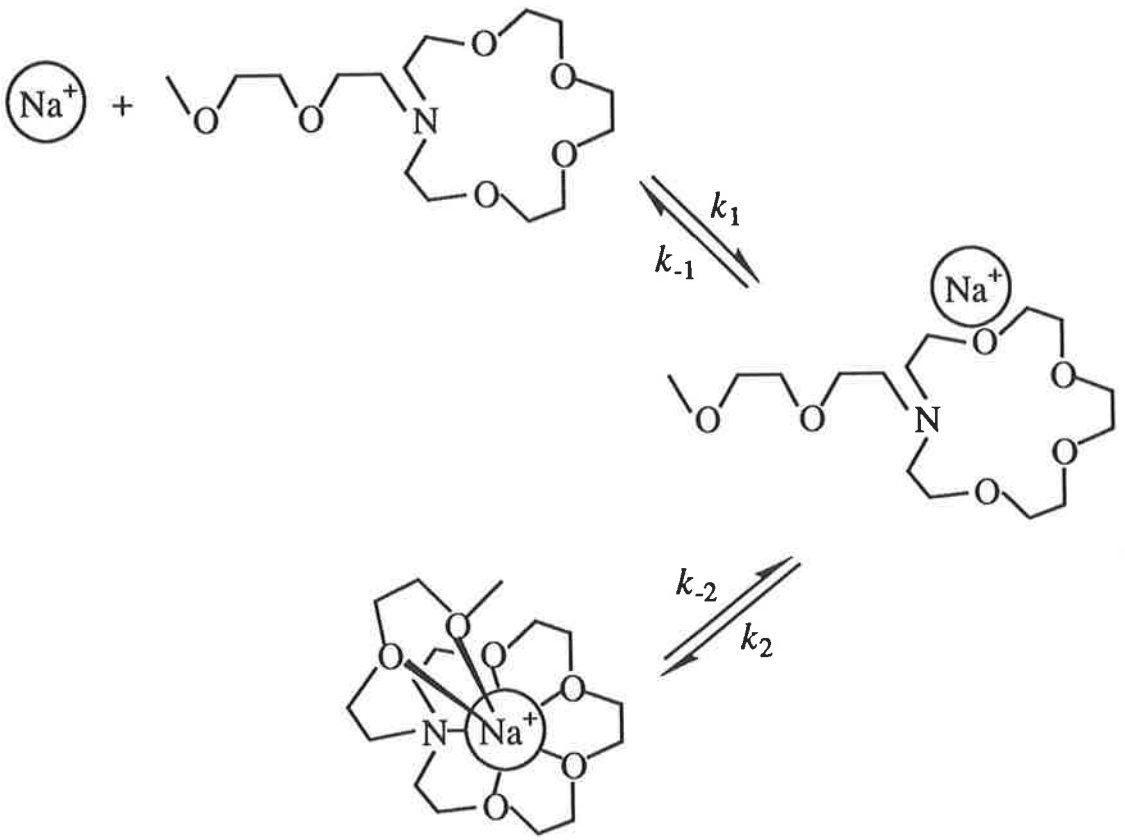

Figure 3.1 *The proposed two step complexation mechanism of Na^+ by 1-methoxyethoxyethyl-4,7,10,13-tetraoxa-1-monoazacyclopentadecane in methanol at 298.2 K.*

3.2 : Results and Discussion

3.2.1 : Exchange Kinetics of Na^+ on $[Na.C211]^+$

The temperature dependent coalescence of the ^{23}Na resonances corresponding to solvated Na^+ and $[Na.C211]^+$ in trimethyl (Figure 3.2), triethyl and tri-*n*-butyl phosphate generates the kinetic parameters for the decomplexation of $[Na.C211]^+$ (Equation 3.13) displayed in Table 3.1.

$$Na^+ + C211 \underset{k_d}{\overset{k_c}{\rightleftharpoons}} [Na.C211]^+ \qquad \textbf{(3.13)}$$

where k_c is the complexation rate constant, and

k_d is the decomplexation rate constant.

These kinetic parameters are derived from the temperature variation of the mean lifetime of $[Na.C211]^+$, τ_c, through Equation 6.27. The τ_c values are obtained by complete lineshape analysis[58] of the coalescing ^{23}Na resonances observed for solutions i - x (Table 3.1), as exemplified by solution iii in Figure 3.2. The coalescing spectra of at least three solutions of different solvated Na^+ to $[Na.C211]^+$ ratios and constant total Na^+ concentration were lineshaped for each system. The temperature range over which τ_c (= $1/k_d$) values were calculated in each of the three trialkyl phosphate solvents was within 336-387 K. The k_d values at two temperatures are quoted in Table 3.1. One is at a temperature in the midst of the coalescence region where modification to the lineshapes due to chemical exchange is at a maximum and hence where the most reliable values for k_d may be obtained. The other is at 298.2 K, for the purpose of comparison with other systems. The plots of $\ln(T\tau_c)$ against $1/T$ for the four solutions of $[Na.C211]^+$ in trimethyl phosphate and each of the three solutions of $[Na.C211]^+$ in triethyl and tri-*n*-butyl phosphate are indistinguishable (Figure 3.3). This indicates that τ_c is independent of the solvated Na^+ concentration (Table 3.1). Thus, solvated Na^+ does not participate in the rate-determining step of the predominant pathway for Na^+ exchange on $[Na.C211]^+$ which is consistent with the operation of a monomolecular mechanism for the decomplexation of Na^+ from C211.

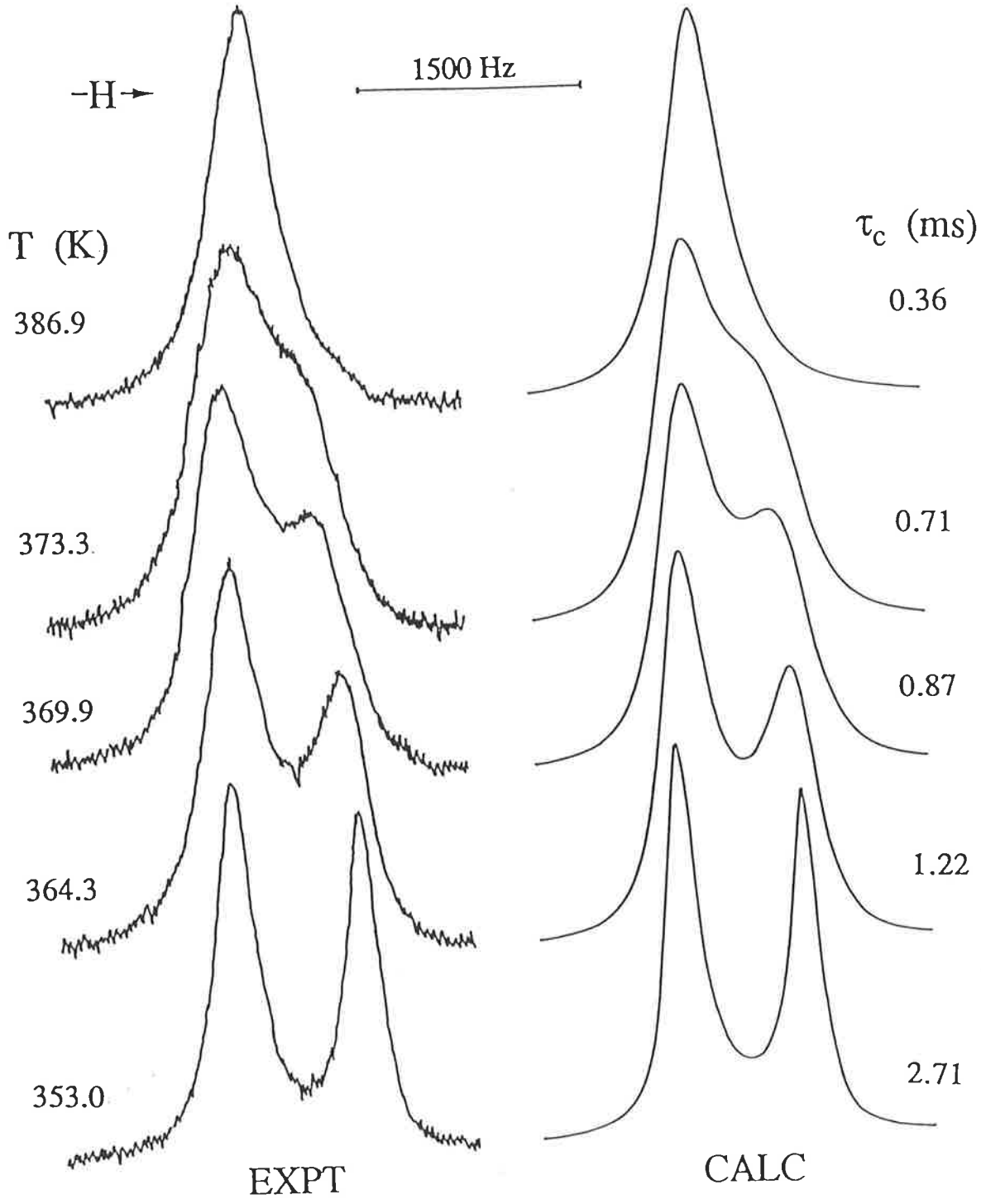

Figure 3.2 *Typical exchange modified 79.39 MHz ^{23}Na NMR spectra of a trimethyl phosphate solution of $NaClO_4$ (0.1002 mol dm^{-3}) and C211 (0.0571 mol dm^{-3}). Experimental temperatures and spectra appear to the left of the figure and the best fit calculated lineshapes and corresponding τ_c values appear to the right. The resonance of $[Na.C211]^+$ appears downfield from that of solvated Na^+.*

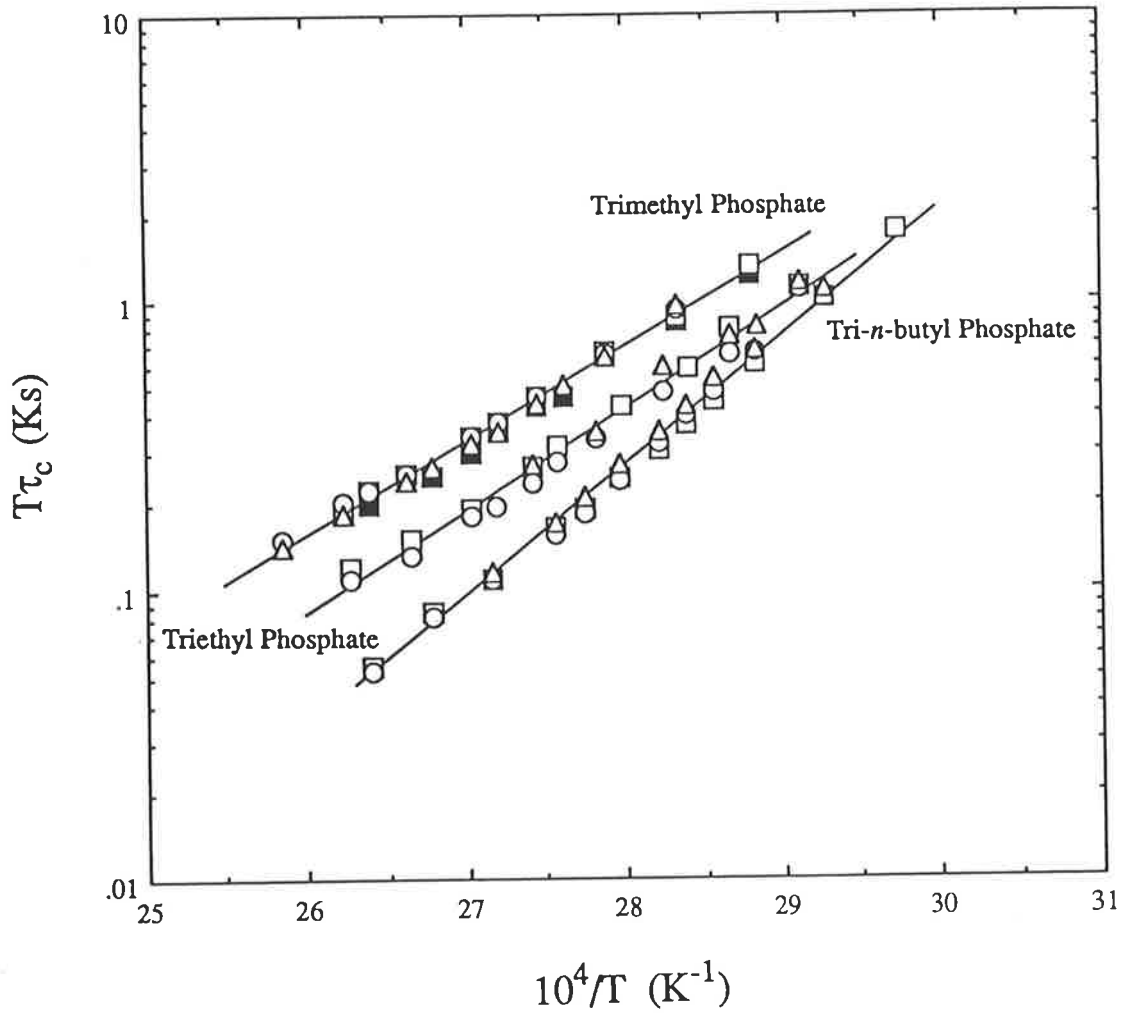

Figure 3.3 *The temperature variation of τ_c for Na^+ exchange on $[Na.C211]^+$ in trimethyl, triethyl and tri-n-butyl phosphate. Data points for the trimethyl phosphate solutions (i) - (iv) are represented by circles, squares, triangles and solid squares, respectively. The data points for the triethyl phosphate solutions (v) - (vii) and the tri-n-butyl phosphate solutions (viii) - (x) are both represented by circles, squares and triangles, respectively. For all three sets of data the solid line represents the best fit of the combined data for each set of solutions to Equation 6.27.*

Table 3.1 Kinetic Parameters and Solution Compositions for the Exchange of Na^+ on $[Na.C211]^+$ in Trimethyl (TMP), Triethyl (TEP) and Tri-*n*-butyl Phosphate (TBP).

Solution	Solvent	$[Na^+_{solvated}]$ mol dm^{-3}	$[Na.C211^+]$ mol dm^{-3}	k_d (coalescence)[a] s^{-1}	k_d (298.2K) s^{-1}	$\Delta H_d^{\ddagger}$ kJ mol^{-1}	$\Delta S_d^{\ddagger}$ J K^{-1} mol^{-1}
				(373.0K)			
i	TMP	0.0735	0.0272	1270 ± 15	7.44 ± 0.62	60.7 ± 1.1	-24.6 ± 3.1
ii	"	0.0541	0.0461	1280 ± 15	6.69 ± 0.54	62.2 ± 1.0	-20.6 ± 3.1
iii	"	0.0431	0.0571	1340 ± 20	6.47 ± 0.78	63.1 ± 1.5	-17.6 ± 4.5
iv	"	0.0340	0.0661	1400 ± 25	6.88 ± 0.87	62.9 ± 1.6	-17.9 ± 4.9
(i - iv)	"			1325 ± 15	6.92 ± 0.50	62.2 ± 0.9	-20.3 ± 2.7
				(365.0K)			
v	TEP	0.0806	0.0254	1490 ± 30	8.89 ± 1.28	66.6 ± 1.9	-3.4 ± 5.8
vi	"	0.0530	0.0530	1335 ± 25	8.27 ± 0.99	66.1 ± 1.6	-5.7 ± 4.9
vii	"	0.0127	0.0933	1400 ± 40	7.78 ± 1.04	67.6 ± 2.1	-1.2 ± 6.4
(v - vii)	"			1415 ± 20	8.17 ± 0.79	67.0 ± 1.4	-2.6 ± 4.1
				(352.0K)			
viii	TBP	0.0672	0.0331	885 ± 26	3.97 ± 0.64	84.9 ± 2.7	51.3 ± 6.8
ix	"	0.0522	0.0481	884 ± 20	4.15 ± 0.49	84.2 ± 2.0	49.3 ± 5.1
x	"	0.0341	0.0642	805 ± 6	2.62 ± 0.15	89.7 ± 1.1	64.1 ± 2.8
(viii - x)	"			859 ± 12	3.61 ± 0.30	84.7 ± 1.4	50.5 ± 3.7

[a] Temperature in the midst of the coalescence region where the most reliable kinetic data are obtained.

All the errors represent one standard deviation from the least-squares fit of the experimental τ_c data to Equation 6.27.

3.2.2 : Exchange Kinetics of Li^+ on $[Li.C21C5]^+$

In trimethyl phosphate and triethyl phosphate (Figure 3.4) a temperature dependent coalescence of the ^7Li resonances arising from solvated Li^+ and $[Li.C21C5]^+$ yields the kinetic parameters for the decomplexation of $[Li.C21C5]^+$ (Equation 3.14) shown in Table 3.2.

$$Li^+ + C21C5 \underset{k_d}{\overset{k_c}{\rightleftharpoons}} [Li.C21C5]^+ \qquad (3.14)$$

These parameters are derived from the temperature variation of the mean lifetime of $[Li.C21C5]^+$, τ_c, through Equation 6.27. The τ_c values were determined by complete lineshape analysis[58] of the coalescing ^7Li resonances observed for solutions i - vi (Table 3.2), as illustrated by solution iv in Figure 3.4. In trimethyl phosphate and triethyl phosphate the rate of Li^+ exchange on $[Li.C21C5]^+$ was sufficient for complete lineshape analysis between 300 K and 342 K and between 280 K and 328 K, respectively. The coalescing spectra of three solutions of varying solvated Li^+ and $[Li.C21C5]^+$ concentrations but constant total Li^+ concentration were lineshaped for each solvent. The derived k_d (= $1/\tau_c$) values at 298.2 K and at the coalescence temperature, the solution compositions, $\Delta H_d^{\ddagger}$ and $\Delta S_d^{\ddagger}$ are given in Table 3.2.

From Figure 3.5 it can be seen that the magnitude and temperature variation of τ_c for each of the three $[Li.C21C5]^+$ solutions studied in trimethyl and triethyl phosphate are very similar. These results indicate that τ_c is independent of the solvated Li^+ concentration (Table 3.2) consistent with the non-participation of the solvated Li^+ in the rate-determining step of the dominant pathway for Li^+ exchange on $[Li.C21C5]^+$, and the operation of a monomolecular mechanism for the decomplexation of Li^+ from $[Li.C21C5]^+$.

3.2.3 : Qualitative Study of the Exchange Kinetics for $[Li.C211]^+$ and $[Na.C21C5]^+$ in Trialkyl Phosphate Solvents

Metal ion exchange on $[Li.C211]^+$ and $[Na.C21C5]^+$ is in the very slow and very fast extreme of the NMR time scale, respectively, in trimethyl and triethyl phosphate which prevented quantitative kinetic characterization. The study of Na^+ exchange on $[Na.C21C5]^+$ was also made difficult by the precipitation of $[Na.C21C5]ClO_4$ upon lowering the temperature below room

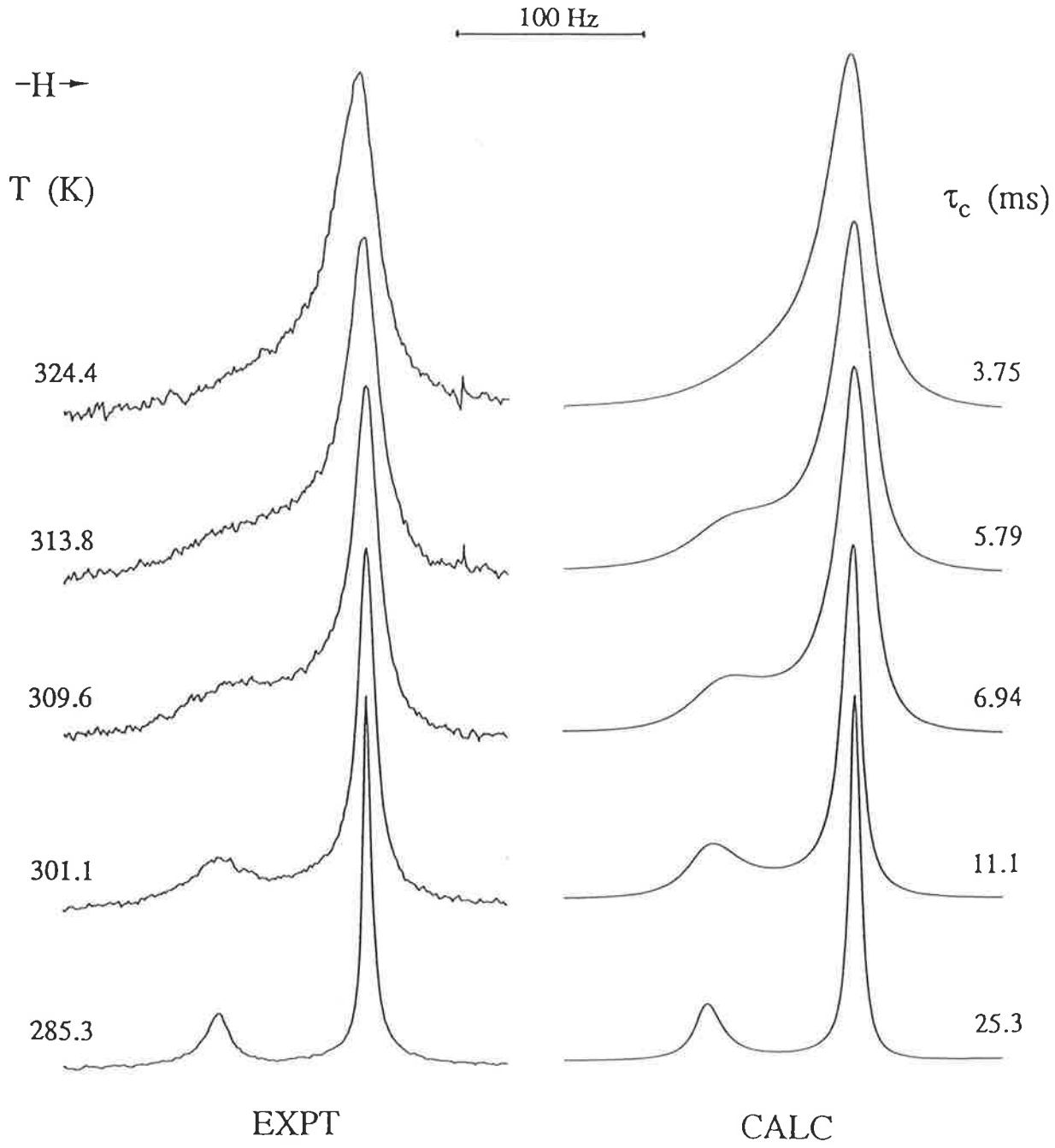

Figure 3.4 *Typical exchange modified 116.64 MHz ^7Li NMR spectra of a triethyl phosphate solution of $LiClO_4$ (0.0204 mol dm^{-3}) and C211 (0.0057 mol dm^{-3}). Experimental temperatures and spectra appear to the left of the figure and the best fit calculated lineshapes and corresponding τ_c values appear to the right. The resonance of $[Li.C21C_5]^+$ appears downfield from that of solvated Li^+.*

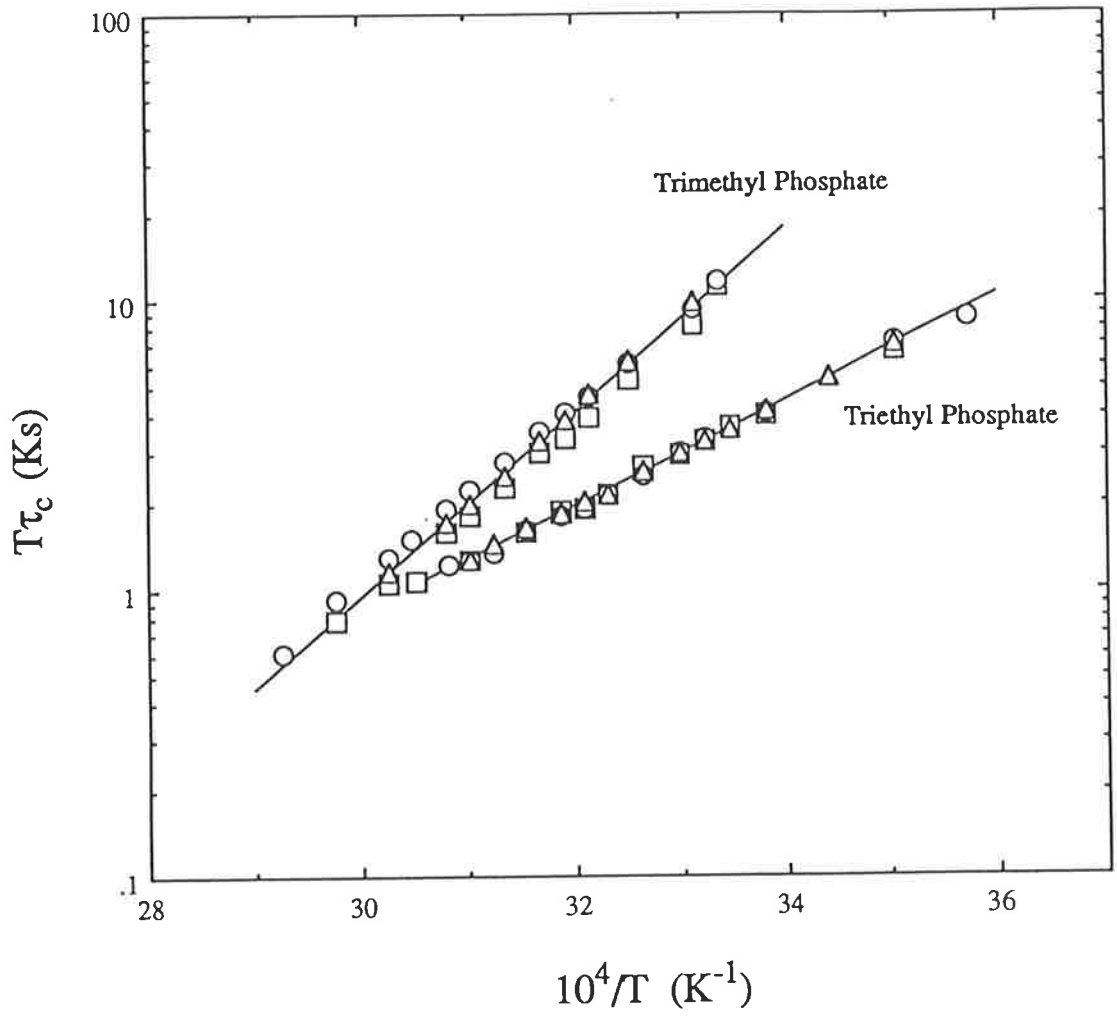

Figure 3.5 *The temperature variation of τ_c for Li^+ exchange on $[Li.C21C5]^+$ in trimethyl and triethyl phosphate. Data points for the trimethyl phosphate solutions (i) - (iii) are represented by circles, squares and triangles, respectively. The data points for the triethyl phosphate solutions (iv) - (vi) are also represented by circles, squares and triangles, respectively. For both sets of data the solid line represents the best fit of the combined data for each set of solutions to Equation 6.27.*

Table 3.2 Kinetic Parameters and Solution Compositions for the Exchange of Li^+ on $[Li.C21C5]^+$ in Trimethyl (TMP) and Triethyl (TEP) Phosphate.

Solution	Solvent	$[Li^+_{solvated}]$ mol dm^{-3}	$[Li.C21C5^+]$ mol dm^{-3}	k_d (coalescence)[a] s^{-1}	k_d (298.2K) s^{-1}	$\Delta H_d^{\ddagger}$ kJ mol^{-1}	$\Delta S_d^{\ddagger}$ J K^{-1} mol^{-1}
				(325.0K)			
i	TMP	0.0139	0.0075	180 ± 2	23.0 ± 0.4	59.4 ± 0.6	-19.8 ± 2.0
ii	"	0.0102	0.0111	210 ± 4	25.9 ± 0.9	61.1 ± 1.3	-13.1 ± 4.2
iii	"	0.0079	0.0134	193 ± 2	22.6 ± 0.6	61.7 ± 1.0	-12.1 ± 3.4
(i - iii)	"			195 ± 3	23.3 ± 0.4	61.2 ± 1.1	-13.6 ± 3.6
				(310.0K)			
iv	TEP	0.0147	0.0057	144 ± 1	81.1 ± 1.0	34.8 ± 0.6	-91.7 ± 1.9
v	"	0.0106	0.0098	143 ± 1	81.2 ± 1.1	34.3 ± 0.7	-93.4 ± 2.4
vi	"	0.0090	0.0114	142 ± 1	79.5 ± 0.5	35.1 ± 0.4	-90.9 ± 1.3
(iv - vi)	"			143 ± 1	80.5 ± 0.5	34.7 ± 0.3	-91.9 ± 1.1

[a] Temperature in the midst of the coalescence region where the most reliable kinetic data are obtained.

All the errors represent one standard deviation from the least-squares fit of the experimental τ_c data to Equation 6.27.

temperature. Quantitative NMR studies of the labilities of $[Li.C211]^+$, $[Li.C21C_5]^+$ and $[Na.C21C_5]^+$ in tri-*n*-butyl phosphate were inhibited by the low solubilities of their perchlorate salts.

Two distinct ^7Li resonances were observed for $[Li.C211]^+$ in trimethyl and triethyl phosphate over the temperature range 298-390 K. A conservative upper limit can be obtained for these systems in the very slow extreme of the NMR time scale using the slow exchange approximation at 298.2 K[59]:

$$k_d \leq 1.5\pi W_{1/2obs} - \pi W_{1/2obs} = 0.5\pi W_{1/2obs} \qquad \textbf{(3.15)}$$

where $1.5\pi W_{1/2obs}$ is the linewidth at half-height (Hz) which would be observed if the rate of exchange was sufficient to increase the natural linewidth at half-height, $W_{1/2obs}$, by half. An upper limit of $k_d \leq 4\ s^{-1}$ was calculated for $[Li.C211]^+$ in trimethyl phosphate and $k_d \leq 3.2\ s^{-1}$ for $[Li.C211]^+$ in triethyl phosphate. The linewidths used to calculate these estimates are listed in Table 3.3.

Only a single ^{23}Na resonance was observed for $[Na.C21C_5]^+$ in trimethyl and triethyl phosphate from 298.2 K down to approximately the freezing point of the solvent in question ie. 230 K and 220 K, respectively. At temperatures below 250 K the resonance begins to broaden rather dramatically and phasing of the lineshapes on the NMR spectrometer becomes difficult. This broadening at low temperatures is probably due to viscosity effects. An approximate k_d can be calculated for these rapidly exchanging systems using the fast exchange approximation at 298.2 K[59]:

$$\pi W_{1/2obs} \geq \chi_c \pi W_{1/2c} + \chi_s \pi W_{1/2s} + \chi_c^2 \chi_s^2 4\pi^2 (\nu_c - \nu_s)^2 (\tau_c + \tau_s) \qquad \textbf{(3.16)}$$

where $W_{1/2obs}$ is the observed linewidth at half-height of the single resonance arising from the environmental averaging of the complexed and solvated metal cation resonances, $W_{1/2c}$ and $W_{1/2s}$ are the linewidths at half-height of the complexed and solvated metal cation resonances, respectively, χ_c and χ_s are the mole fractions of these respective species, $(\nu_c - \nu_s)$ is the chemical shift difference between the complexed and solvated metal cation resonances and τ_c $(= 1/k_d)$ and τ_s $(= \tau_c\chi_s/\chi_c)$ are their respective mean lifetimes. The parameters $W_{1/2c}$, $W_{1/2s}$, ν_c and ν_s were obtained from solutions of $[Na.C21C_5]^+$ and $Na^+_{solvated}$ alone at the same total Na^+ concentration as the exchanging solutions which provide $W_{1/2obs}$, χ_c and χ_s. At 298.2 K, $k_d \geq 10^4\ s^{-1}$ was calculated for $[Na.C21C_5]^+$ in trimethyl phosphate and

$k_d \geq 2 \times 10^4$ s^{-1} for $[Na.C21C5]^+$ in triethyl phosphate. The parameters used to calculate these estimations are listed in Table 3.3.

Table 3.3 Parameters Used to Calculate the Slow and Fast Exchange Limit k_d Values at 298.2 K.

Cryptate	Solvent	k_d (s^{-1})	$W_{1/2obs}$ (Hz)	$W_{1/2c}$ (Hz)	$W_{1/2s}$ (Hz)	χ_c	χ_s	$(\nu_c-\nu_s)$ (Hz)
$[Na.C21C5]^+$	TMP	$\geq 10^{4a}$	364	351	93	0.45	0.55	932
$[Na.C21C5]^+$	TEP	$\geq 2 \times 10^{4a}$	295	345	147	0.50	0.50	804
$[Li.C211]^+$	TMP	$\leq 4^b$	2.56					
$[Li.C211]^+$	TEP	$\leq 3.2^b$	2.06					

[a] Estimated from the fast exchange approximation (Equation 3.16); [b] Estimated from the slow exchange approximation (Equation 3.15).

3.2.4 : General Conclusions for the $[M.C211]^+$ and $[M.C21C5]^+$ Systems in Various Solvents

The decomplexation rate constant, k_d, increases in the sequence: $[Li.C211]^+ < [Na.C211]^+ < [Li.C21C5]^+ < [Na.C21C5]^+$ in the three trialkyl phosphate solvents at 298.2 K. It is seen from Table 3.4 that a similar sequence to this is observed in other solvents. Knowledge of the stability constant, K_s, of a cryptate and its k_d value allows the determination of the complexation reate constant, k_c, from $K_s = k_c/k_d$ (Table 3.4). Generally, the magnitude of k_d reflects the influence of the optimisation of fit between the metal cation and the cryptand intramolecular cavity, the number and type of cryptand donor atoms, and the nature of the metal cation and cryptand on the decomplexation process. The $[Li.C211]^+$ cryptate is more stable and less labile than the $[Li.C21C5]^+$ cryptate because of the greater electrostatic interaction between the six donor atoms of C211 and Li^+ in comparison with the five donor atoms of C21C5 and Li^+. The optimal fit between Li^+ and C211 results in *inclusive* $[Li.C211]^+$,[60] whereas $[Li.C21C5]^+$, as a consequence of possessing one less oxygen donor atom, exists partially in the *exclusive* form[19] which is part way to the formation of the decomplexation transition state. The major reasons why $[Na.C211]^+$ is more labile than $[Li.C211]^+$ is its *exclusive* nature[61] and

Table 3.4 Kinetic Parameters for Li^+ and Na^+ Exchange in Several Cryptates in a Range of Solvents.

Solvent	D_N	$10^{-5}k_c$ (298.2 K)[a] $dm^3\ mol^{-1}\ s^{-1}$	k_d (298.2 K) s^{-1}	$\Delta H_d^{\ddagger}$ $kJ\ mol^{-1}$	$\Delta S_d^{\ddagger}$ $J\ K^{-1}\ mol^{-1}$
		[Li.C211]$^+$			
Methanol[b]	19.0[c] 23.5[d]	4.8	0.0044		
Trimethyl Phosphate[e]	23.0[c]		≤ 4		
Triethyl Phosphate[e]	26.0[f]		≤ 3.2		
N,N-Dimethyl-formamide[g]	26.6[c]	1.27	0.0130	64.4	-64.8
		[Li.C21C5]$^+$			
Acetonitrile[h]	14.1[c]	-	slow		
Propylene Carbonate[h]	15.1[c]	-	slow		
Acetone[h]	17.0[c]	-	slow		
Methanol[h]	19.0[c] 23.5[d]	0.221	21.6	36.1	-98.4
Trimethyl Phosphate[e]	23.0[c]	0.058	23.3	61.2	-13.6
Triethyl Phosphate[e]	26.0[f]	0.079	80.5	34.8	-91.9
N,N-Dimethyl-formamide[h]	26.6[c]	0.073	116	38.4	-76.5
		[Na.C211]$^+$			
Propylene Carbonate[i]	15.1[c]	210	0.036		
Methanol[i]	19.0[c] 23.5[d]	31.0	2.5		
Trimethyl Phosphate[e]	23.0[c]	16.6	6.92	62.2	-20.3

Triethyl Phosphate[e]	26.0[f]	4.3	8.2	67.0	-2.6
Tri-*n*-butyl Phosphate[e]	23.7[c]	3.1	3.6	84.7	50.5
N,N-Dimethyl-formamide[j]	26.6[c]	19.2	12.1	83.5	55.9
			$[Na.C21C_5]^+$		
Acetonitrile[k]	14.1[c]	100	84.8	57.9	-13.8
Propylene Carbonate[k]	15.1[c]	25.5	19.4	70.3	15.3
Acetone[k]	17.0[c]	84	878	54.4	-6.1
Methanol[k]	19.0[c] 23.5[d]	104	1800	44.9	-31.9
Trimethyl Phosphate[e]	23.0[c]		≥ 10000		
Triethyl Phosphate[e]	26.0[f]		≥ 20000		
N,N-Dimethyl-formamide[k]	26.6[c]	214	28800	40.0	-25.3

[a] $k_c = k_d K_s$; [b] Reference 10; [c] Reference 62. The dielectric constants from the same reference are: acetonitrile 38.0, propylene carbonate 69.0, acetone 20.7, methanol 32.6, trimethyl phosphate 20.6 and N,N-dimethylformamide 36.1; [d] References 63 and 64; [e] This work; [f] Reference 65; [g] Reference 15; [h] Reference 19; [i] Reference 9; [j] Reference 17; [k] Reference 18.

the lower surface charge density of Na^+. A combination of the *exclusive* nature[61] of $[Na.C21C5]^+$ and a decrease by one in the number of donor atoms of C21C5 results in this cryptate being the most labile of the four cryptates studied.[18] Solid state X-ray diffraction studies have shown that the centre of the Na^+ ion in *exclusive* [Na.C211.NCS] and *exclusive* [Na.C21C5.NCS] is 14 and 37 pm, respectively, above the common plane of the N_2O_3 fifteen membered cryptand ring, with a thiocyanate nitrogen in bonding distance in both cryptates.[61] These *exclusive* structures are expected to be retained in solution with the thiocyanate interactions replaced by interactions with one or more solvent molecules.

From the k_d sequence mentioned earlier for the four cryptates studied, $[Li.C21C5]^+$ would be expected to be more stable than $[Na.C21C5]^+$. The relative order of stability $[Li.C21C5]^+ > [Na.C21C5]^+$ holds in the trialkyl phosphate solvents but is the reverse in the other solvents. This is a consequence of a much larger increase in k_c than in k_d for $[Na.C21C5]^+$ in comparison with $[Li.C21C5]^+$. For example, in N,N-dimethylformamide $[Na.C21C5]^+$ possesses a 2900 fold greater k_c and only a 250 fold greater k_d than $[Li.C21C5]^+$. The smaller magnitude of k_c for $[Li.C21C5]^+$ reflects the greater electrostatic interaction between the smaller Li^+ and the solvent, which results in an increase in the activation energy required to sequentially desolvate the Li^+ in the complexation process. Likewise, the smaller magnitude of k_d for $[Li.C21C5]^+$ reflects the greater electrostatic interaction between Li^+ and C21C5, which results in an increase in the activation energy required to dissociate Li^+ from C21C5 in the decomplexation process.

The three trialkyl phosphate solvents of similar electron donating strength exhibit a 2.36 fold variation in their molar volumes. A maximum of 5 fold variation in the magnitudes of k_d and k_c characterizing $[Li.C21C5]^+$ and $[Na.C211]^+$ is observed with change in trialkyl phosphate solvent. Hence, variation of solvent molecular size results in only a minor influence on the rate determining steps of the decomplexation and complexation reactions.

It can be seen from Table 3.4 that the variation of k_d with solvent is markedly greater than that of k_c in a variety of solvents, as exemplified by the $[Na.C21C5]^+$ system. Thus, variation in K_s is largely a consequence of variation in k_d, and is consistent with the transition state for the rate determining decomplexation process more closely resembling the solvated metal ion and the free cryptand than the cryptate. A simple model in which the free energy of activation of complexation, $\Delta G_c^{\ddagger}$, is held constant and the

free energy of activation of decomplexation, $\Delta G_d^{\ddagger}$, varies with solvent may be used to explain the variation in k_d with solvent. In the absence of solvent interaction, the free energy change arising from structural rearrangement in a given cryptate on going from the ground state to the transition state, $\Delta G_r^{\ddagger}$, is constant, and the free energy change arising from the involvement of solvent in the activation process, $\Delta G_s^{\ddagger}$, decreases the free energy of the transition state such that:

$$\Delta G_d^{\ddagger} = \Delta G_r^{\ddagger} - \Delta G_s^{\ddagger} \qquad \textbf{(3.17)}$$

Since the magnitude of $\Delta G_r^{\ddagger}$ is independent of solvent, an increase in solvent D_N will result in a decrease in $\Delta G_d^{\ddagger}$ and an increase in k_d (Figure 3.6).[18] The cryptates $[Li.C21C5]^+$, $[Na.C211]^+$ and $[Na.C21C5]^+$ generally show an increase in k_d with an increase in the solvent D_N. However, there appears to be no obvious correlation between the variation in k_d and the solvent dielectric constant (Table 3.4). The $\Delta H_d^{\ddagger}$ and $\Delta S_d^{\ddagger}$ contributions to $\Delta G_d^{\ddagger}$ vary irregularly between systems and probably indicate the underlying contributions of the conformational and solvational changes associated with the decomplexation process.

Finally, one of the original aims of cryptate studies has been the design of effective cation carrier molecules for membrane transport as well as the design of cation receptor molecules. A cryptand can be transformed from a cation receptor into a cation carrier by simple structural changes. Replacement of a cryptand oxygen donor atom with a methylene group generally produces a more effective carrier molecule for transport of alkali metal ions across membranes.[4] In all the solvents listed in Table 3.4 the Na^+ and Li^+ cryptates of C21C5 are more labile than their respective analogous C211 cryptates making C21C5 a more efficient carrier for Na^+ and Li^+ than C211. Similarly, C22C5 is substantially a more efficient Na^+ carrier than C221.[22]

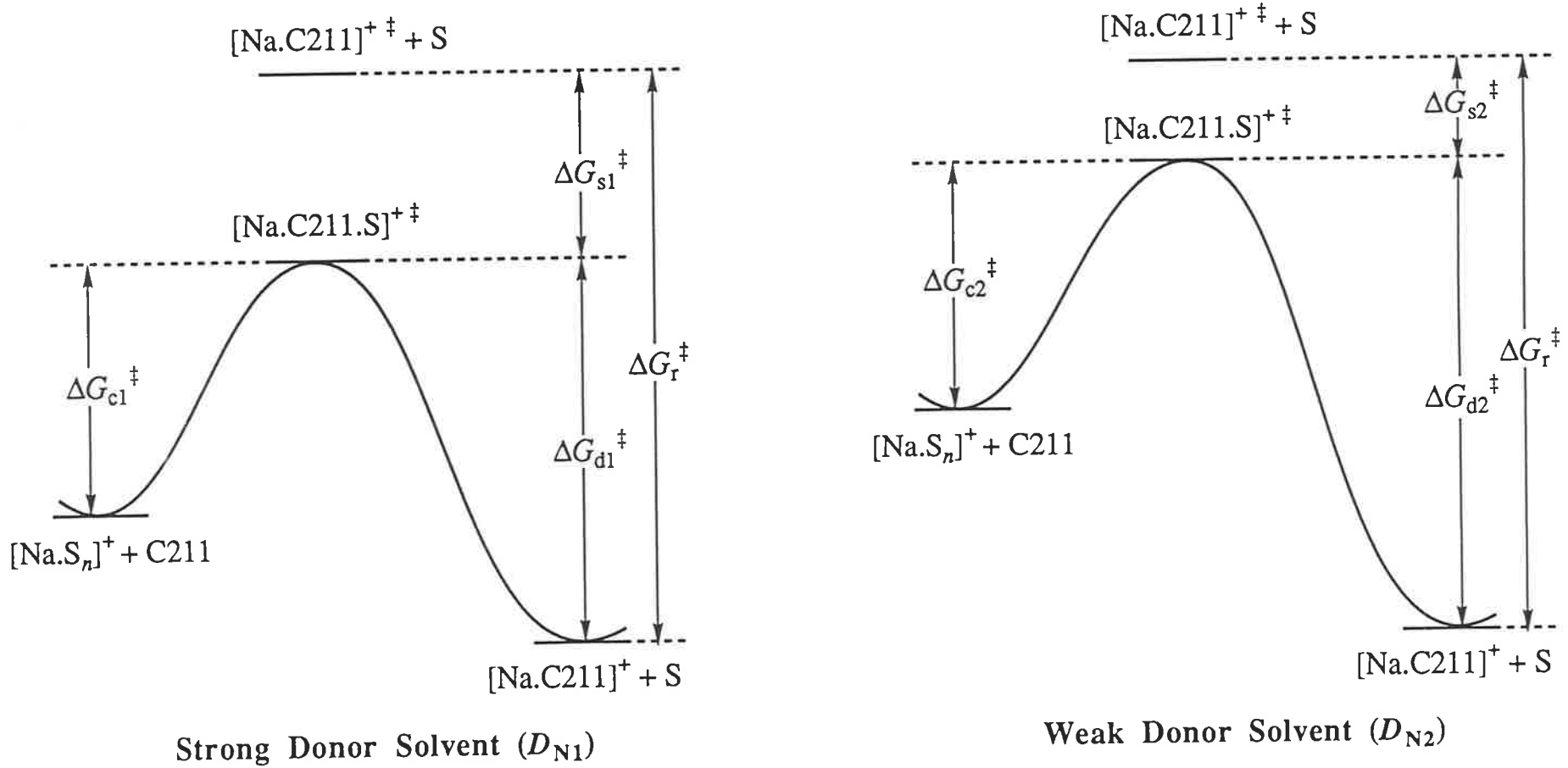

Figure 3.6 *Simplified reaction profiles for the complexation and decomplexation of [Na.C211]$^+$ in two solvents of different D_N ($D_{N1} > D_{N2}$). They illustrate the significant variation in k_d and little variation in k_c with the nature of solvent (S). The free energies of the [Na.C211]$^+$ + S ground states in both solvents are normalized to the same value in both profiles. The free energies of the transition-states [Na.C211]$^{+\ddagger}$ is the same value in both profiles as it is the trnsition-state in the absence of solvent participation in the activation process. The [Na.S$_n$]$^+$ species represent the ground state solvated cations. Since $D_{N1} > D_{N2}$, $\Delta G_{s1}^{\ddagger} > \Delta G_{s2}^{\ddagger}$ and therefore $\Delta G_{d1}^{\ddagger} < \Delta G_{d2}^{\ddagger}$ ($\Delta G_{c1}^{\ddagger} = \Delta G_{c2}^{\ddagger}$).*

3.2.5 : Exchange Kinetics of Na^+ on $[Na.BHE\text{-}C21]^+$ in Acetonitrile and $[Na.BHE\text{-}C22]^+$ in Methanol

Complete lineshape analyses of the temperature dependent coalescence of the ^{23}Na resonances arising from solvated Na^+ and $[Na.BHE\text{-}C21]^+$ in acetonitrile (Figure 3.7) and from solvated Na^+ and $[Na.BHE\text{-}C22]^+$ in methanol yields τ_c, the mean lifetime of Na^+ in $[Na.BHE\text{-}C21]^+$ and $[Na.BHE\text{-}C22]^+$. The activation parameters presented in Table 3.5 for solutions i - vi characterizing the decomplexation of $[Na.BHE\text{-}C21]^+$ (Equation 3.18) in acetonitrile and $[Na.BHE\text{-}C22]^+$ (Equation 3.19) in methanol are derived from the temperature variation of τ_c for the respective complexes through Equation 6.27.

$$Na^+ + \text{BHE-C21} \underset{k_d}{\overset{k_c}{\rightleftharpoons}} [Na.BHE\text{-}C21]^+ \qquad \textbf{(3.18)}$$

$$Na^+ + \text{BHE-C22} \underset{k_d}{\overset{k_c}{\rightleftharpoons}} [Na.BHE\text{-}C22]^+ \qquad \textbf{(3.19)}$$

The τ_c values for Na^+ exchange on $[Na.BHE\text{-}C21]^+$ in acetonitrile and for Na^+ exchange on $[Na.BHE\text{-}C22]^+$ in methanol were determined over the temperature ranges 283-326 K and 246-273 K, respectively. In the $[Na.BHE\text{-}C21]^+$ system in acetonitrile, two well resolved ^{23}Na resonances were observed at the lower temperatures. However, it was not possible to fully separate the two ^{23}Na resonances of the $[Na.BHE\text{-}C22]^+$ system in methanol, even at 210 K where the system was in the extreme limit of slow exchange. This is due to a combination of broad ^{23}Na resonances and a small chemical shift difference between the two Na^+ chemical environments. Plots of $\ln(T\tau_c)$ against $1/T$ for the three solutions of $[Na.BHE\text{-}C21]^+$ in acetonitrile and the three solutions of $[Na.BHE\text{-}C22]^+$ in methanol are indistinguishable (Figure 3.8), and the derived activation parameters for the three solutions of each system are consequently indistinguishable also (Table 3.5). This suggests that the exchange rate in both systems is independent of the solvated Na^+ concentration (see Equation 3.6) consistent with the predominant decomplexation mechanism being the monomolecular mechanism in both cases.

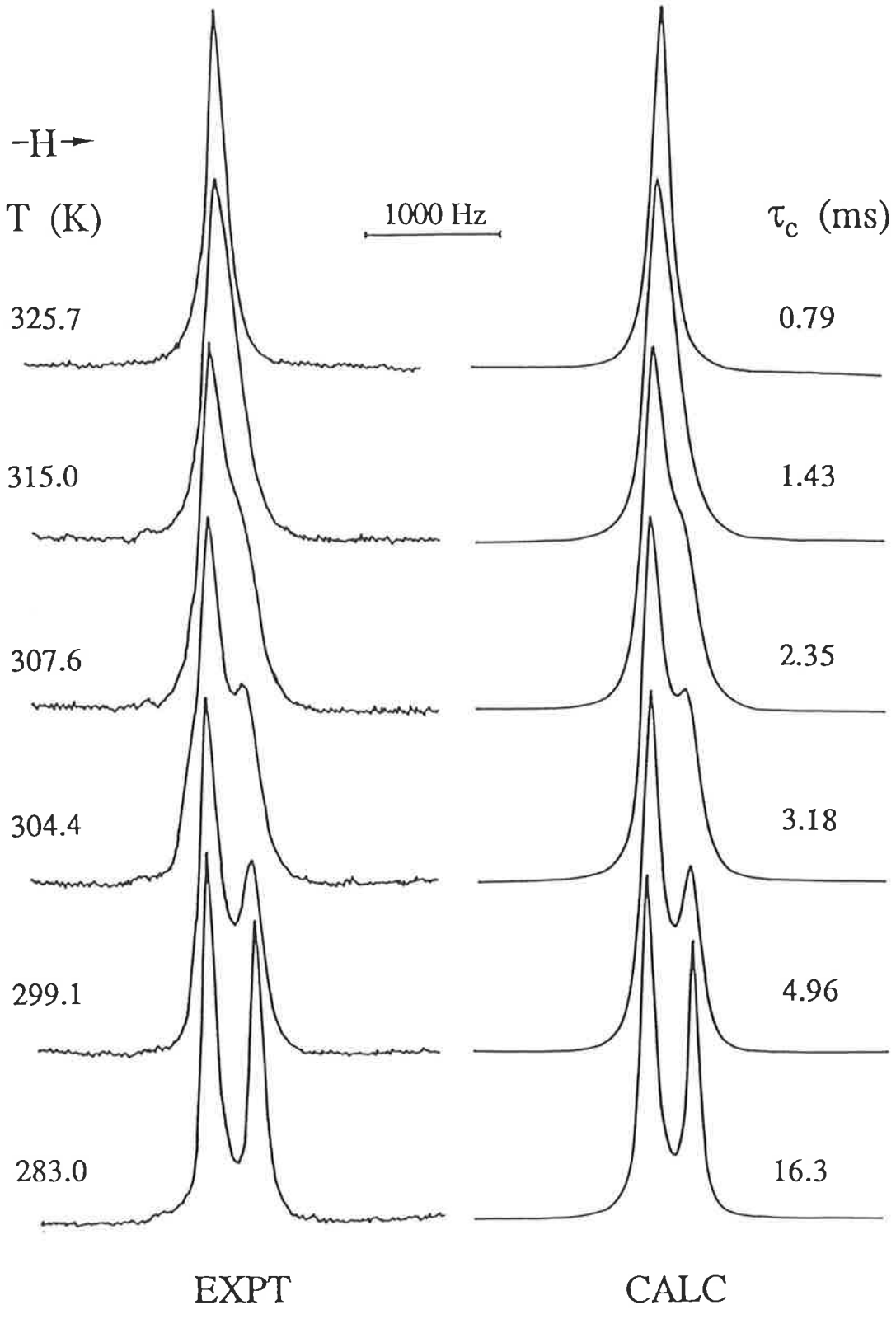

Figure 3.7 *Typical exchange modified 79.39 MHz ^{23}Na NMR spectra of an acetonitrile solution of $NaClO_4$ (0.1008 mol dm^{-3}) and BHE-C21 (0.0625 mol dm^{-3}). Experimental temperatures and spectra appear to the left of the figure and the best fit calculated lineshapes and corresponding τ_c values appear to the right. The resonance of $[Na.BHE\text{-}C21]^+$ appears downfield from that of solvated Na^+.*

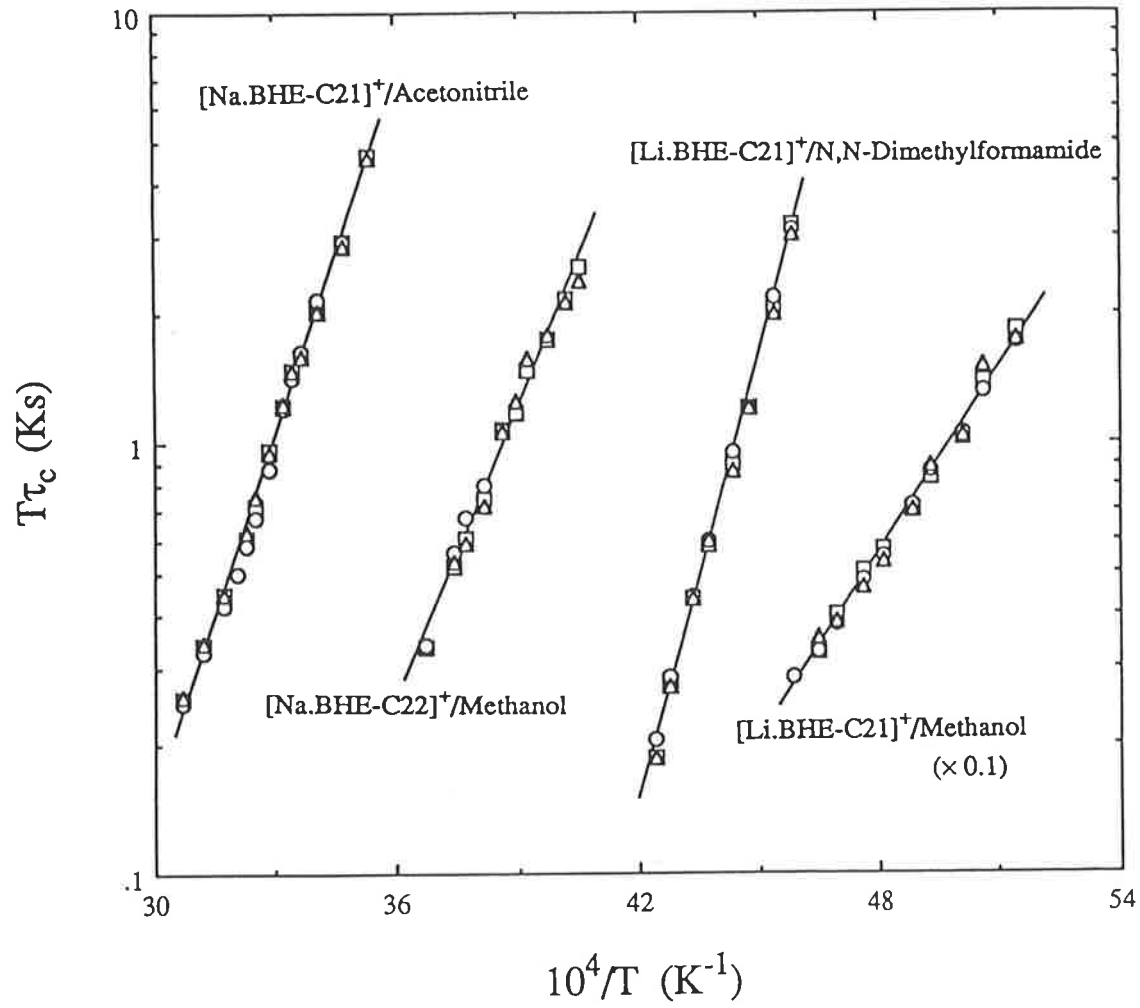

Figure 3.8 *The temperature variation of τ_c for (a) Na^+/[Na.BHE-C21]$^+$/acetonitrile solutions (i) - (iii), (b) Na^+/[Na.BHE-C22]$^+$/methanol solutions (iv) - (vi), (c) Li^+/[Li.BHE-C21]$^+$/N,N-dimethylformamide solutions (i) - (iii), and (d) Li^+/[Li.BHE-C21]$^+$/methanol solutions (iv) - (vi)(τ_c/10 in this case). The data points for the three solutions of each system are represented by circles, squares and triangles, respectively. The solid lines represent the best fits of the combined data to Equation 6.27 for each group of solutions.*

Table 3.5 Kinetic Parameters and Solution Compositions for the Exchange of Na^+ on $[Na.BiBLE]^+$ in Acetonitrile (AN) and Methanol (MeOH).

Solution	Solvent	$[Na^+_{solvated}]$ mol dm^{-3}	$[Na.BiBLE^+]$ mol dm^{-3}	k_d (coalescence)[a] s^{-1}	k_d (298.2K) s^{-1}	$\Delta H_d^{\ddagger}$ kJ mol^{-1}	$\Delta S_d^{\ddagger}$ J K^{-1} mol^{-1}
			$[Na.BHE\text{-}C21^+]$	(304.0K)			
i	AN	0.0767	0.0242	325 ± 7	210 ± 6	53.7 ± 1.6	-20.2 ± 5.6
ii	"	0.0383	0.0625	313 ± 5	205 ± 4	52.3 ± 1.0	-25.4 ± 3.3
iii	"	0.0282	0.0726	312 ± 4	204 ± 3	51.8 ± 0.8	-27.0 ± 2.9
(i - iii)	"			317 ± 3	207 ± 3	52.6 ± 0.7	-24.1 ± 2.4
			$[Na.BHE\text{-}C22^+]$	(256.0K)			
iv	MeOH	0.0779	0.0220	179 ± 10	5460 ± 855	49.2 ± 3.1	-8.5 ± 12.4
v	"	0.0503	0.0545	208 ± 4	4385 ± 350	43.6 ± 1.3	-28.9 ± 5.2
vi	"	0.0280	0.0719	208 ± 6	3840 ± 600	41.6 ± 2.4	-36.6 ± 9.9
(iv - vi)	"			206 ± 3	4125 ± 275	42.8 ± 1.1	-32.0 ± 4.5

[a] Temperature in the midst of the coalescence region where the most reliable kinetic data are obtained.

All the errors represent one standard deviation from the least-squares fit of the experimental τ_c data to Equation 6.27.

3.2.6 : Exchange Kinetics of Li^+ on $[Li.BHE\text{-}C21]^+$ in N,N-Dimethylformamide and Methanol

The kinetic parameters for the decomplexation of $[Li.BHE\text{-}C21]^+$ in N,N-dimethylformamide and methanol were obtained from complete lineshape analyses of the temperature dependent coalescence of the ^7Li resonances arising from solvated Li^+ and $[Li.BHE\text{-}C21]^+$, as exemplified by $[Li.BHE\text{-}C21]^+$ in N,N-dimethylformamide in Figure 3.9. The derived mean lifetimes of $[Li.BHE\text{-}C21]^+$, τ_c $(=1/k_d)$, at 298.2 K and at the coalescence temperature of each system, $\Delta H_d^{\ddagger}$, $\Delta S_d^{\ddagger}$, and the compositions of solutions i - vi are given in Table 3.6. Complete lineshape analysis in N,N-dimethylformamide was carried out over the temperature range 218-236 K, and in methanol from 194 K to 218 K. It can be seen from Figure 3.8 and Table 3.6 that the magnitude and temperature variations of τ_c for each of the solutions studied for a given solvent are virtually identical. This implies that τ_c is independent of the solvated Li^+ concentration in both solvents consistent with the non-participation of solvated Li^+ in the rate-determining step of the dominant pathway for Li^+ exchange on $[Li.BHE\text{-}C21]^+$, and the operation of the monomolecular decomplexation mechanism as shown in Equation 3.20.

$$Li^+ + BHE\text{-}C21 \underset{k_d}{\overset{k_c}{\rightleftharpoons}} [Li.BHE\text{-}C21]^+ \qquad (3.20)$$

3.2.7 : Qualitative Study of the Exchange Kinetics for $[M.BHE\text{-}C21]^+$ and $[M.BHE\text{-}C22]^+$ in Selected Solvents

A single exchange broadened ^{23}Na NMR resonance was observed in methanol, trimethyl phosphate and N,N-dimethylformamide solutions containing solvated Na^+ and $[Na.BHE\text{-}C21]^+$ at temperatures just above the freezing point of the solvent. Thus, the rate of Na^+ exchange between the solvated and complexed Na^+ environments was in the fast exchange limit of the ^{23}Na NMR time scale. Approximate lower limits of $k_d \geq 2000$ s^{-1} in methanol, $k_d \geq 200$ s^{-1} in trimethyl phosphate and $k_d \geq 1000$ s^{-1} in N,N-dimethylformamide at 293.4 K were calculated using the fast exchange approximation equation (Equation 3.16).[59] Similarly, the rate of Na^+ exchange on $[Na.BHE\text{-}C22]^+$ in acetonitrile, propylene carbonate, trimethyl phosphate and N,N-dimethylformamide was in the fast exchange limit of the ^{23}Na NMR time scale over the solvent liquid temperature range. At 288.2 K, estimates of $k_d \geq 1000$ s^{-1}, $k_d \geq 2600$ s^{-1}, $k_d \geq 1800$ s^{-1} and $k_d \geq 1000$ s^{-1} were

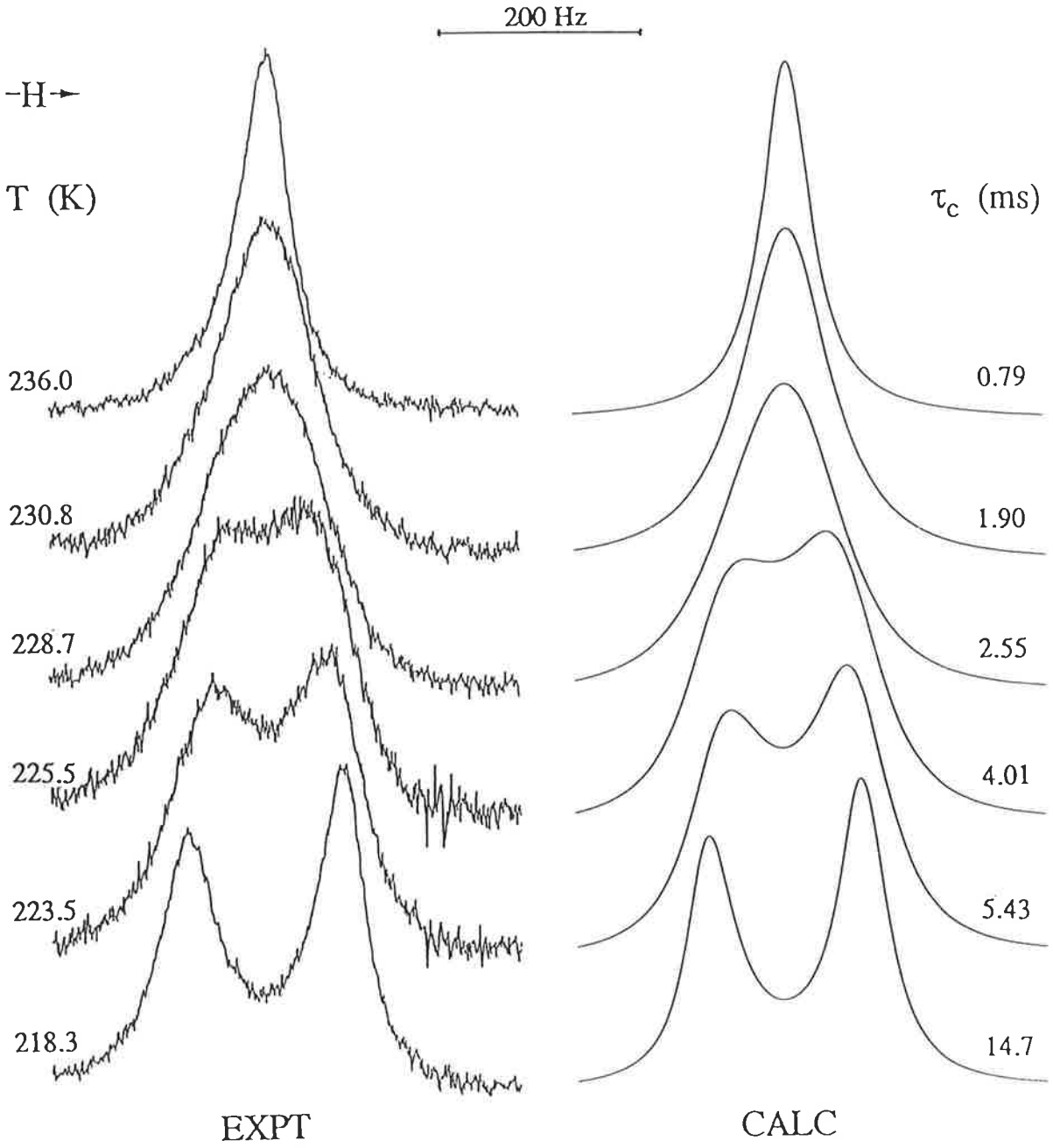

Figure 3.9 *Typical exchange modified 116.64 MHz ^7Li NMR spectra of a N,N-dimethylformamide solution of $LiClO_4$ (0.0209 mol dm^{-3}) and BHE-C21 (0.0115 mol dm^{-3}). Experimental temperatures and spectra appear to the left of the figure and the best fit calculated lineshapes and corresponding τ_c values appear to the right. The resonance of $[Li.BHE\text{-}C21]^+$ appears upfield from that of solvated Li^+.*

Table 3.6 Kinetic Parameters and Solution Compositions for the Exchange of Li^+ on $[Li.BHE\text{-}C21]^+$ in N,N-Dimethylformamide (DMF) and Methanol (MeOH).

Solution	Solvent	$[Li^+_{solvated}]$ mol dm^{-3}	$[Li.BHE\text{-}C21^+]$ mol dm^{-3}	k_d (coalescence)[a] s^{-1}	k_d (298.2K) s^{-1}	$\Delta H_d^{\ddagger}$ kJ mol^{-1}	$\Delta S_d^{\ddagger}$ J K^{-1} mol^{-1}
				(225.0K)			
i	DMF	0.0155	0.0054	218 ± 3	$1.3x10^6 \pm 0.2x10^6$	64.6 ± 1.2	89.4 ± 4.8
ii	"	0.0094	0.0115	223 ± 5	$1.6x10^6 \pm 0.3x10^6$	66.1 ± 1.7	96.1 ± 6.7
iii	"	0.0078	0.0132	228 ± 5	$1.5x10^6 \pm 0.3x10^6$	65.2 ± 1.8	92.4 ± 6.9
(i - iii)	"			223 ± 3	$1.5x10^6 \pm 0.1x10^6$	65.4 ± 0.9	92.9 ± 3.6
				(204.0K)			
iv	MeOH	0.0138	0.0074	26.9 ± 0.3	5510 ± 480	26.5 ± 0.5	-84.3 ± 2.5
v	"	0.0098	0.0115	26.5 ± 0.4	6300 ± 880	27.3 ± 0.8	-80.5 ± 3.9
vi	"	0.0076	0.0136	26.5 ± 0.6	6670 ± 1420	27.6 ± 1.3	-79.1 ± 6.0
(iv - vi)	"			26.7 ± 0.2	6070 ± 480	27.1 ± 0.5	-81.5 ± 3.6

[a] Temperature in the midst of the coalescence region where the most reliable kinetic data are obtained.

All the errors represent one standard deviation from the least-squares fit of the experimental τ_c data to Equation 6.27.

calculated for $[Na.BHE\text{-}C22]^+$ in acetonitrile, propylene carbonate, trimethyl phosphate and N,N-dimethylformamide, respectively. The rate of Li^+ exchange on $[Li.BHE\text{-}C22]^+$ in acetonitrile, methanol, trimethyl phosphate and N,N-dimethylformamide and also on $[Li.BHE\text{-}C21]^+$ in trimethyl phosphate was in the extreme limit of fast exchange at 296.5 K. Only a single environmentally-averaged resonance was observed over the solvent liquid temperature range. This prevented both a quantitative and qualitative study of k_d in these Li^+ systems. Several fast exchanging Na^+ and Li^+ systems over a broad temperature range are illustrated in Figures 3.10 and 3.11. No estimate of k_d was possible for $[Li.BHE\text{-}C21]^+$ in acetonitrile as a 1:1 solution of solvated Li^+ and $[Li.BHE\text{-}C21]^+$ at 296.5 K gave a very broad signal with poor resolution (small signal to noise ratio). This was quite unexpected as solutions containing $[Li.BHE\text{-}C21]^+$ and Li^+ alone gave well resolved singlets. The estimated k_d values are not discussed any further as they are only limiting values.

3.2.8 : General Conclusions for the $[M.BHE\text{-}C21]^+$ and $[M.BHE\text{-}C22]^+$ Systems in Various Solvents

Unfortunately due to the rate of Na^+ and Li^+ exchange on most of the $[M.BHE\text{-}C21]^+$ and $[M.BHE\text{-}C22]^+$ complexes in various solvents being in the fast extreme of the NMR time scale, only a limited comparison of the kinetic characteristics of $[M.BHE\text{-}C21]^+$ and $[M.BHE\text{-}C22]^+$ with other similar complexes could be made (Table 3.7). It can be seen from Table 3.7 that the differences in stability between $[Na.BHE\text{-}C22]^+$, $[Na.C222]^+$ and $[Na.C22C_8]^+$ in methanol are controlled by the variation in k_d. The larger k_d characterizing $[Na.C22C_8]^+$ is attributable to the ligand only having six donor atoms with which to bind the Na^+ whereas C222 and BHE-C22 have eight donor atoms. The smaller k_d and hence larger K_s ($= k_c/k_d$) of $[Na.C222]^+$ is attributable to a combination of the rigid nature of C222, its eight donor atoms and the strong shielding of Na^+ from solvent interactions. The $[Na.BHE\text{-}C22]^+$ complex has an intermediate k_d value due to its flexible nature and eight donor atoms. In methanol, $[Na.BHE\text{-}C22]^+$ is more stable than $[Na.BME\text{-}C22]^+$ due to a 3.4 fold greater k_c and only a 1.7 fold greater k_d. Similarly, the difference in stability between $[Li.BHE\text{-}C21]^+$ and $[Li.C221]^+$ in methanol is a consequence of the much greater k_d value for $[Li.BHE\text{-}C21]^+$. The lower k_d value for $[Li.C221]^+$ is consistent with the activation energy required for Li^+ to dissociate from C221 being much greater than that required for Li^+ to dissociate from BHE-C21 for the simple

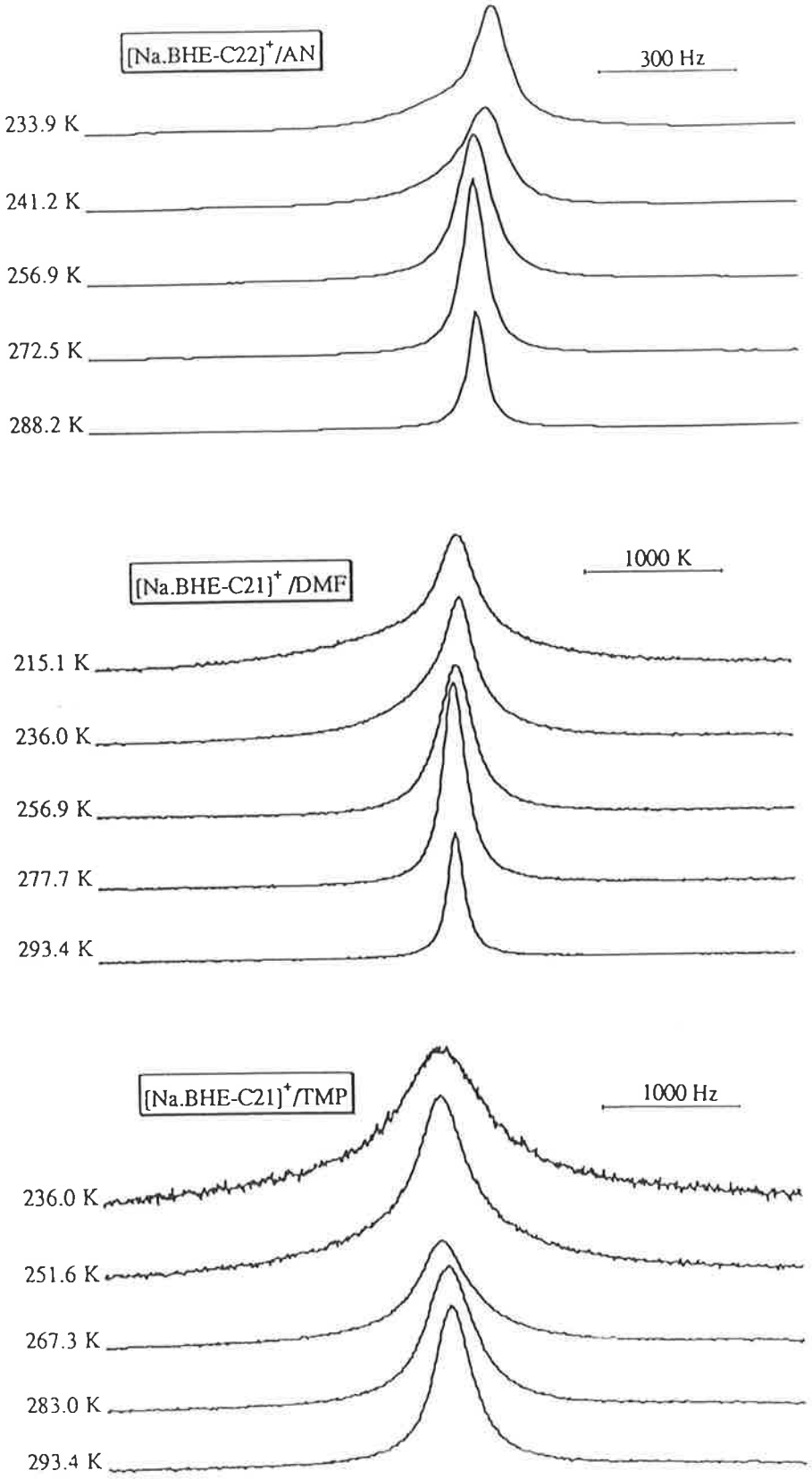

Figure 3.10 *Some fast exchanging Na^+-bibracchial lariat ether complex systems.*

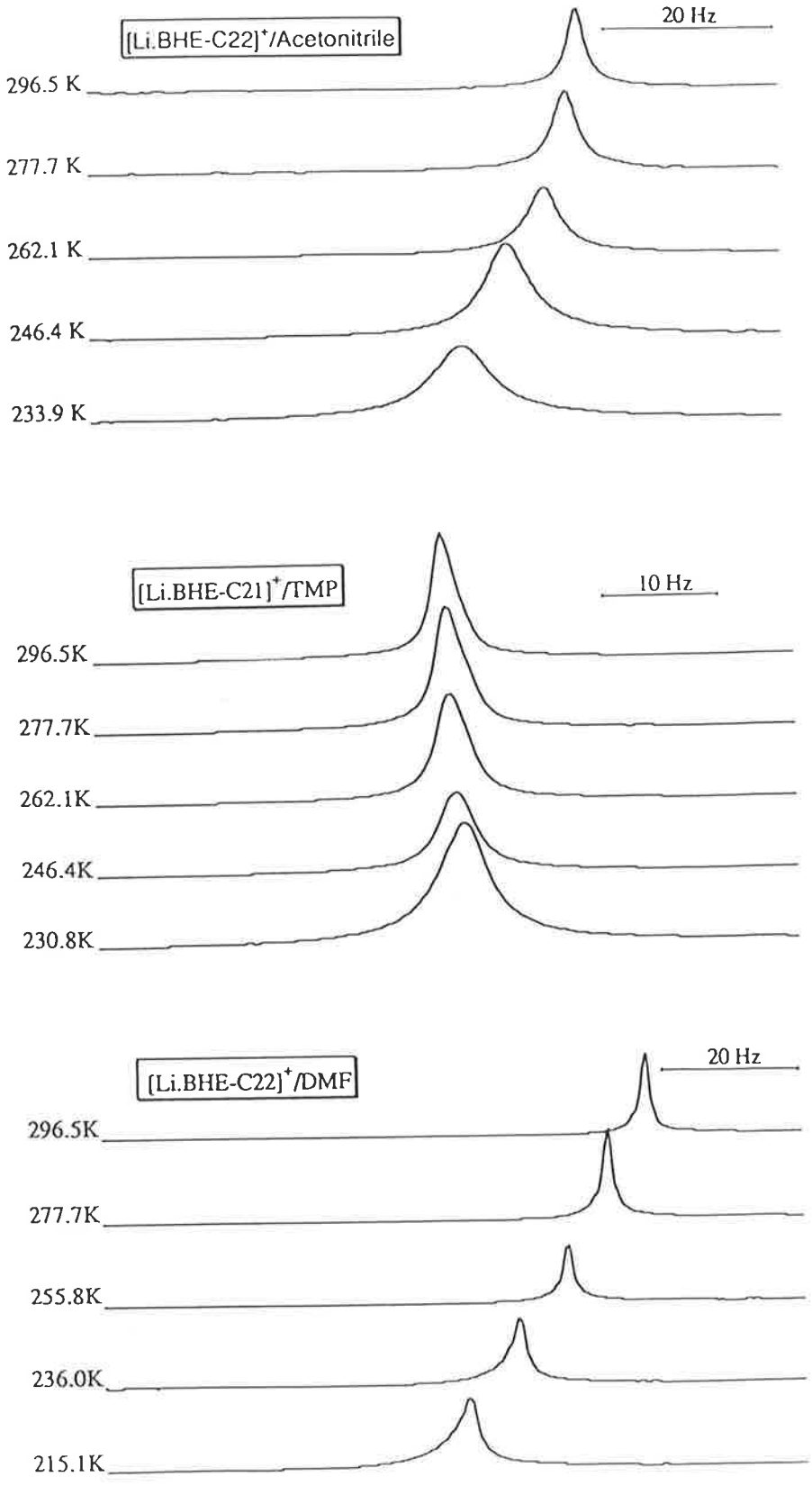

Figure 3.11 *Some fast exchanging Li^+-bibracchial lariat ether complex systems.*

Table 3.7 Kinetic Parameters for Na^+ and Li^+ Exchange on Several Cryptates and Bibracchial Lariat Ethers.

Complex	Solvent	log (K_s / dm^3 mol^{-1}) (298.2 K)	$10^{-5}k_c$ (298.2 K)[a] dm^3 mol^{-1} s^{-1}	k_d (298.2 K) s^{-1}	$\Delta H_d^{\ddagger}$ kJ mol^{-1}	$\Delta S_d^{\ddagger}$ J K^{-1} mol^{-1}
[Li.BHE-C21]$^{+}$[b]	DMF	2.36 ± 0.03	3436	1500000	65.4	92.9
[Li.BME-C21]$^{+}$[c]	DMF	2.23	55	32600	36.4	-36.5
[Li.BHE-C21]$^{+}$[b]	MeOH	2.85 ± 0.05	43	6070	27.1	-81.5
[Li.BME-C21]$^{+}$[c]	MeOH	3.01	20	1970	20.4	-113
[Li.C221]$^{+}$	MeOH	5.38[d]	188[e]	78.4[e]	23.8[e]	-129[e]
[Na.BHE-C21]$^{+}$[b]	AN	7.00 ± 0.01	20700	207	52.6	-24.1
[Na.BME-C21]$^{+}$[c]	AN	8.17	183409	124	43.2	-60.0
[Na.BHE-C22]$^{+}$	MeOH	4.87[f]	3058[b]	4125[b]	42.8[b]	-32.0[b]
[Na.BME-C22]$^{+}$[c]	MeOH	4.57	903	2430	59.9	20.8
[Na.C222]$^{+}$[d]	MeOH	7.98	2700	2.87	-	-
[Na.C22C8]$^{+}$[g]	MeOH	3.4	271	10800	46.7	-11

[a] $k_c = k_d K_s$; [b] This work; [c] Reference 66; [d] Reference 6; [e] Reference 10; [f] Reference 67; [g] Reference 23.

reason that C221 better solvates or envelops the Li^+. In addition, the greater decrease in k_d than k_c for $[Li.BME\text{-}C21]^+$ in comparison with $[Li.BHE\text{-}C21]^+$ in methanol results in $[Li.BME\text{-}C21]^+$ being slightly more stable than $[Li.BHE\text{-}C21]^+$.

Despite K_s characterizing $[Li.BHE\text{-}C21]^+$ in N,N-dimethylformamide being only one third of that in methanol, the k_c and k_d values observed in N,N-dimethylformamide are 80 fold and 247 fold, respectively, greater than those observed in methanol. As methanol has strong hydrogen bonding ability, it might be expected that competition between Li^+ and methanol for the hydroxyethyl pendant arms may arise. Any hydrogen bonding interaction between methanol and the hydroxyethyl pendant arms would reduce the intramolecular hydrogen bonding, if any exists, between the hydroxyethyl pendant arms and result in a more open structure.[68] Consequently Li^+ would be exposed to more solvent interactions and hence a larger k_d would be observed in methanol than N,N-dimethylformamide. However, this hydrogen bonding effect is not evident in the $[Li.BHE\text{-}C21]^+$ systems because k_d is smaller in methanol. In alkali metal cryptates, k_c values show a small variation with the nature of solvent whereas the k_d values show a substantial variation, thus K_s is essentially determined by the variation in k_d.[6,9,11,18-21,23,29,31,36-39] In contrast to this, $[Li.BHE\text{-}C21]^+$ shows a substantial variation in both k_c and k_d upon change of solvent, reflecting the greater flexibility of the bibracchial lariat ethers. Furthermore, k_d characterizing $[Li.BHE\text{-}C21]^+$ increases with the electron donating strength (D_N) of the solvent, which is observed to be the case in many cryptate systems. A comparison of $[Na.BHE\text{-}C21]^+$, $[Na.BHE\text{-}C22]^+$ and $[Li.BHE\text{-}C21]^+$ with their respective analogous BME-C21 and BME-C22 complexes reveals that the hydroxyethyl armed complexes are more labile but not necessarily less stable than the methoxyethyl armed complexes.

A possible mechanism for the complexation of Na^+ by BHE-C22 is illustrated in Figure 3.12. Some of the sequential solvation, coordination and conformation changes involved in the complexation and decomplexation of Na^+ or Li^+ by BHE-C21 or BHE-C22 are indicated in Figure 3.12. Since it is known from solid state X-ray diffraction studies that $[Na.BHE\text{-}C22]^+$ adopts a *syn* conformation,[69] this mechanism assumes that the *syn* conformation is retained in solution. The first step, characterized by k_1 and k_{-1}, involves the diffusion-controlled formation of an encounter complex in which a direct interaction between Na^+ and BHE-C22 exists but Na^+ resides outside the BHE-C22 sixteen-membered ring. This is followed by the entry of Na^+ into

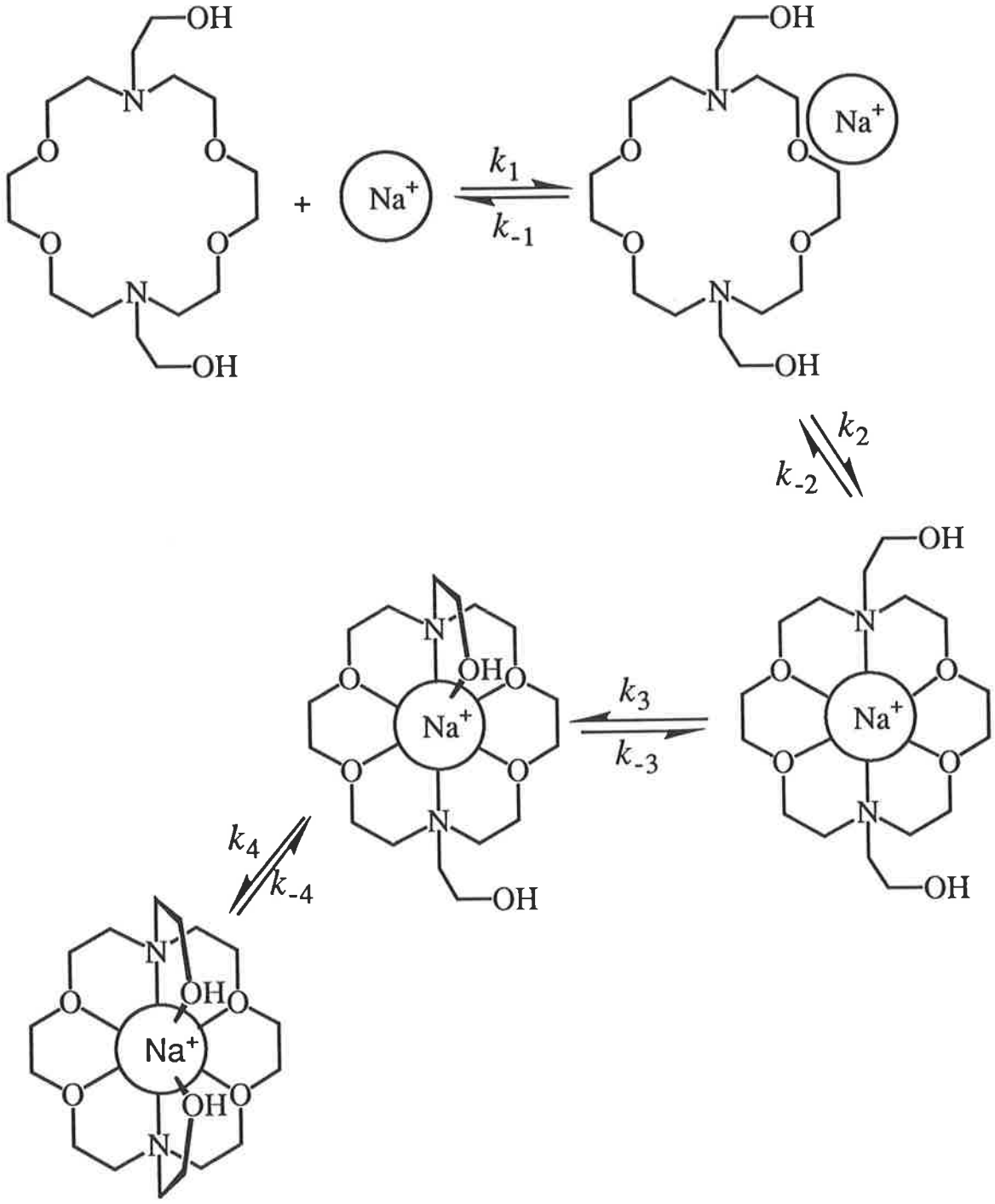

Figure 3.12 *A possible mechanism for the complexation of Na^+ by BHE-C22, assuming the syn conformation observed in the solid state is retained in solution.*

the BHE-C22 ring and the coordination of Na^+ by the ring donor atoms, characterized by k_2 and k_{-2}. Subsequent steps involve the coordination of the two hydroxy groups of the two hydroxyethyl pendant arms, characterized by k_3 ,k_{-3}, k_4 and k_{-4}, to produce eight coordinate Na^+ in $[Na.BHE\text{-}C22]^+$. This mechanism is very similar to the Eigen-Winkler mechanism (Equation 3.5) in which an initial diffusion-controlled complexation step is followed by slower conformational changes in the ligand.[11,42,43] On the basis of the data obtained by alkali nuclei NMR it is not possible to rule out other alternative mechanisms in which one or both of the pendant arms coordinate the Na^+ in an earlier step.

As mentioned earlier in section 3.1, a two step complexation process has been detected in an ultrasonic relaxation study of the complexation of Na^+ by 1-methoxyethoxyethyl-4,7,10,13-tetraoxa-1-monoazacyclopentadecane in methanol at 298.2 K.[53] The first step which involves the formation of an encounter complex is characterized by $k_1 = 9.0 \times 10^{10}$ dm^3 mol^{-1} and $k_{-1} = 2.1 \times 10^8$ s^{-1} and the second step which involves the entry of Na^+ into the ring and the complexation of Na^+ by the ring donor atoms and the methoxyethoxyethyl arm is characterized by $k_2 = 1.2 \times 10^7$ s^{-1} and $k_{-2} = 1.5 \times 10^5$ s^{-1}. Another ultrasonic relaxation study involving the complexation of Na^+ by 1,4,7,10,13,16-hexaoctadecane (18-crown-6) in methanol at 298.2 K is also best interpreted by the Eigen-Winkler mechanism. The entry of Na^+ into the ring from the encounter complex is characterized by $k_2 = 2.8 \times 10^8$ s^{-1} and a later conformational change in the complex is characterized by $k_3 = 1.6 \times 10^6$ s^{-1}.[70,71] A subsequent ^{23}Na NMR study on the same system yielded a decomplexation rate constant, k_d, of 7.2×10^4 s^{-1} which was assigned k_{-3}, the reverse of the complex conformational change characterized by k_3.[72] Thus k_d calculated for $[Na.BHE\text{-}C22]^+$ by ^{23}Na NMR in this study probably represents one of the slower steps in the mechanism shown in Figure 3.12, most likely k_{-3} or k_{-4}. It is conceivable that the k_d values characterizing $[Na.BHE\text{-}C21]^+$ and $[Li.BHE\text{-}C21]^+$ (Table 3.7) represent similar slow steps. Generally, the magnitude of the k_c values (Table 3.7) appear to be too low to correspond to the fast initial encounter complex forming step (diffusion-controlled processes are ~10^{10} dm^3 mol^{-1} s^{-1} [26]). Thus, the second order complexation rate constants, k_c (= $k_d K_s$), are most likely to be composite rate constants incorporating the several sequential rate processes of the complexation mechanism.

References

1 J.-M. Lehn, *Struct. Bonding (Berlin)*, **16**, 1973, 1.

2 J.-M. Lehn and J.-P. Sauvage, *J. Am. Chem. Soc.*, **97**, 1975, 6700.

3 J.-M. Lehn, *Acc. Chem. Res.*, **11**, 1978, 49.

4 J.-M. Lehn, *Pure Appl. Chem.*, **51**, 1979, 979.

5 B.G. Cox and H. Schneider, *J. Am. Chem. Soc.*, **99**, 1977, 2809.

6 B.G. Cox, H. Schneider and J. Stroka, *J. Am. Chem. Soc.*, **100**, 1978, 4746.

7 B.G. Cox and H. Schneider, *J. Am. Chem. Soc.*, **102**, 1980, 3628.

8 B.G. Cox, J. Garcia-Rosas and H. Schneider, *J. Phys. Chem.*, **84**, 1980, 3178.

9 B.G. Cox, J. Garcia-Rosas and H. Schneider, *J. Am. Chem. Soc.*, **103**, 1981, 1054.

10 B.G. Cox, I. Schneider and H. Schneider, *Ber. Bunsenges. Phys. Chem.*, **84**, 1980, 470.

11 B.G. Cox and H. Schneider, *Pure Appl. Chem.*, **62**, 1990, 2259.

12 J.M. Ceraso and J.L. Dye, *J. Am. Chem. Soc.*, **95**, 1973, 4432.

13 J.M. Ceraso, P.B. Smith, J.S. Landers and J.L. Dye, *J. Phys. Chem.*, **81**, 1977, 760.

14 Y.M. Cahen, J.L. Dye and A.I. Popov, *J. Phys. Chem.*, **79**, 1975, 1289.

15 Y.M. Cahen, J.L. Dye and A.I. Popov, *J. Phys. Chem.*, **79**, 1975, 1292.

16 G.W. Liesegang, *J. Am. Chem. Soc.*, **103**, 1981, 953.

17 S.F. Lincoln, I.M. Brereton and T.M. Spotswood, *J. Chem. Soc., Faraday Trans. 1*, **81**, 1985, 1623.

18 S.F. Lincoln, I.M. Brereton and T.M. Spotswood, *J. Am. Chem. Soc.*, **108**, 1986, 8134.

19 S.F. Lincoln and A. Abou-Hamdan, *Inorg. Chem.*, **29**, 1990, 3584.

20 A. Abou-Hamdan and S.F. Lincoln, *Inorg. Chem.*, **30**, 1991, 462.

21 S.F. Lincoln and A.K.W. Stephens, *Inorg. Chem.*, **30**, 1991, 3529.

22 P. Clarke, S.F. Lincoln and E.R.T. Tiekink, *Inorg. Chem.*, **30**, 1991, 2747.

23 S.F. Lincoln and A.K.W. Stephens, *Inorg. Chem.*, **31**, 1992, 5067.

24 M. Shamsipur and A.I. Popov, *J. Phys. Chem.*, **90**, 1986, 5997.

25 R. Gresser, D.W. Boyd, A.M. Albrecht-Gary and J.P. Schwing, *J. Am. Chem. Soc.*, **102**, 1980, 651.

26 G.W. Liesegang and E.M. Eyring: in R.M. Izatt and J.J. Christensen (Ed.): "Synthetic Multidentate Macrocyclic Compounds", Academic Press, New York, Chapter 5, 1978.

27 E. Mei, A.I. Popov and J.L. Dye, *J. Phys. Chem.*, **81**, 1977, 1677.

28 B.G. Cox, D. Knop and H. Schneider, *J. Am. Chem. Soc.*, **100**, 1978, 6002.

29 B.G. Cox, D. Knop and H. Schneider, *J. Phys. Chem.*, **84**, 1980, 320.

30 B.G. Cox, P. Firman, I. Schneider and H. Schneider, *Inorg. Chim. Acta*, **49**, 1981, 153.

31 B.G. Cox, J. Garcia-Rosas and H. Schneider, *Ber. Bunsenges. Phys. Chem.*, **86**, 1982, 293.

32 K. Ishihara, H. Miura, S. Funahashi and M. Tanaka, *Inorg. Chem.*, **27**, 1988, 1706.

33 C. Moore and B.C. Pressman, *Biochem. Biophys. Res. Commun.*, **15**, 1964, 562.

34 Z. Stefanac and W. Simon, *Microchem. J.*, **12**, 1967,125.

35 P. Mueller and D.O. Rudin, *Biochem. Biophys. Res. Commun.*, **26**, 1967, 398.

36 V.M. Loyola, R. Pizer and R.G. Wilkins, *J. Am. Chem. Soc.*, **99**, 1977, 7185.

37 B.G. Cox, N.V. Truong and H. Schneider, *J. Am. Chem. Soc.*, **106**, 1984, 1273.

38 B.G. Cox, J. Garcia-Rosas, H. Schneider and N.V. Truong, *Inorg. Chem.*, **25**, 1986, 1165.

39 B.G. Cox, J. Stroka, I. Schneider and H. Schneider, *J. Chem. Soc., Faraday Trans. I*, **85**, 1989, 187.

40 J.D. Lamb, R.M. Izatt, J.J. Christensen and D.J. Eatough: in G.A. Melson (Ed.): "Coordination Chemistry of Macrocyclic Compounds", Plenum Press, New York, 1979.

41 P.B. Chock, *Proc. Natl. Acad. Sci. U.S.A.*, **69**, 1972, 1939.

42 E. Grell, T. Funck and F. Eggers, in G. Eisenman (Ed.): "Membranes", Marcel Dekker, New York, Chapter 1, **3**, 1975.

43 L.J. Rodriguez, M. Xu, E.M. Eyring and S. Petrucci, *Pure Appl. Chem.*, **61**, 1989, 1593.

44 E. Shchori, J. Jagur-Grodzinski, Z. Luz and M. Shporer, *J. Am. Chem. Soc.*, **93**, 1971, 7133.

45 E. Shchori, J. Jagur-Grodzinski and M. Shporer, *J. Am. Chem. Soc.*, **95**, 1973, 3842.

46 Y. Hou and A.I. Popov, *Spectroscopy Lett.*, **22**, 1989, 87.

47 V.M. Loyola, R.G. Wilkins and R. Pizer, *J. Am. Chem. Soc.*, **97**, 1975, 7382.

48 B.G. Cox, J. Stroka, and H. Schneider, *Inorg. Chim. Acta*, **147**, 1988, 9.

49 T. Tanaka, T. Hida, S. Funahashi and M. Tanaka, *J. Am. Chem. Soc.*, **113**, 1991, 1259.

50 B. Tümmler, G. Maass, E. Weber, W. Wehner and F. Vögtle, *J. Am. Chem. Soc.*, **99**, 1977, 4683.

51 K. Henco, B. Tümmler and G. Maass, *Angew. Chem. Int. Ed. Engl.*, **16**, 1977, 538.

52 L. Echegoyen, A. Kaifer, H.D. Durst and G.W. Gokel, *J. Org. Chem.*, **49**, 1984, 688.

53 L. Echegoyen, G.W. Gokel, M.S. Kim, E.M. Eyring and S. Petrucci, *J. Phys. Chem.*, **91**, 1987, 3854.

54 L. Echegoyen, A. Kaifer, H.D. Durst, R.A. Schultz, D.M. Dishong, D.M. Goli and G.W. Gokel, *J. Am. Chem. Soc.*, **106**, 1984, 5100.

55 R.D. Gandour, F.R. Fronczek, V.J. Gatto, C. Minganti, R.A. Schultz, B.D. White, K.A. Arnold, D. Mazzocchi, S.R. Miller and G.W. Gokel, *J. Am. Chem. Soc.*, **108**, 1986, 4078.

56 K.A. Arnold, L. Echegoyen, F.R. Fronczek, R.D. Gandour, V.J. Gatto, B.D. White and G.W. Gokel, *J. Am. Chem. Soc.*, **109**, 1987, 3716.

57 R.A. Schultz, D.M. Dishong and G.W. Gokel, *J. Am. Chem. Soc.*, **104**, 1982, 625.

58 S.F. Lincoln, *Prog. React. Kinetics*, **9**, 1977,1.

59 F.A. Bovey, "Nuclear Magnetic Resonance Spectroscopy", Academic Press, San Diego, CA, 2nd Edn., 1988.

60 D. Moras and R. Weiss, *Acta Crystallogr., Sect. B*, **B29**, 1973, 400.

61 S.F. Lincoln, E. Horn, M.R. Snow, T.W. Hambley, I.M. Brereton and T.M. Spotswood, *J. Chem. Soc., Dalton Trans.*, 1986, 1075.

62 V. Gutmann, "Coordination Chemistry in Non-Aqueous Solutions", Springer, Vienna, 1968.

63 R.H. Erlich, E. Roach and A.I. Popov, *J. Am. Chem. Soc.*, **92**, 1970, 4989.

64 W.J. DeWitte and A.I. Popov, *J. Solution Chem.*, **5**, 1976, 231.

65 Y. Marcus, *J. Solution Chem.*, **13**, 1984, 599.

66 J.B. Lucas, Unpublished results.

67 V.J. Gatto, K.A. Arnold, A.M. Viscariello, S.R. Miller, C.R. Morgan and G.W. Gokel, *J. Org. Chem.*, **51**, 1986, 5373.

68 D.S.B. Grace and J. Krane, *J. Chem. Res. (S)*, 1983, 162.

69 F.R. Fronczek, V.J. Gatto, R.A. Schultz, S.J. Jungk, W.J. Colucci, R.D. Gandour and G.W. Gokel, *J. Am. Chem. Soc.*, **105**, 1983, 6717.

70 C.C. Chen and S. Petrucci, *J. Phys. Chem.*, **86**, 1982, 2601.

71 W. Wallace, C. Chen, E.M. Eyring and S. Petrucci, *J. Phys. Chem.*, **89**, 1985, 1357.

72 S.F. Lincoln, A. White and A.M. Hounslow, *J. Chem. Soc., Faraday Trans. 1*, **83**, 1987, 2459.

Chapter 4 : The Study of a Fluorescent Sulfonamidoquinoline Probe for Zinc(II)

4.1 : Introduction

The first row transition metal ion Zn^{2+} is quite common in biology and is involved in inhibitory control as well as catalysis.[1] Zinc(II) is an essential cofactor in many enzymes, including carbonic anhydrase, carboxypepsidase, alcohol dehydrogenase, β-lactamase and phospholipase, and it is also associated with some non-enzyme proteins such as insulin and metallothionine.[1] However, there is little clear understanding of the precise biological role of Zn^{2+}. Since several medical disorders, including the neurobehavioural disorders epilepsy and anorexia,[2] are considered to be associated with abnormal Zn^{2+} levels, it is important that the biological role of Zn^{2+} be understood. Zinc(II) ionophores, chelators and isotopes (^{65}Zn) have been used to indirectly detect intracellular Zn^{2+}.[3-5] However, the inability to quantify intracellular Zn^{2+} levels has been an impediment to the understanding of its biological role. In an attempt to try and solve this problem, a Zn^{2+} specific probe which could simply, inexpensively, rapidly and directly measure intracellular Zn^{2+} in living cells has been sought.

Over the past decade several fluorescent probes, namely Quin-2, Indo-1, Fura-2 and Fura-3, have been developed for the measurement of intracellular free Ca^{2+}.[6,7] These Ca^{2+} fluorescent probes are quite sensitive to free Ca^{2+} concentrations and the method of fluorescence allows the measurement of low Ca^{2+} concentrations. Due to the unavailability of Zn^{2+} specific microelectrodes it was envisaged that a similarly operating Zn^{2+} specific fluorescent probe would be an appropriate method for measuring intracellular Zn^{2+}.

A Zn^{2+} specific probe must satisfy several criteria. Firstly, the probe must obviously possess a relatively high specificity for Zn^{2+} over the other biologically relevant cations such as Mg^{2+}, Ca^{2+}, Na^{+} and K^{+}. That is, the stability constant for the Zn^{2+} complex must be greater than the stability constants for the complexes formed with Mg^{2+}, Ca^{2+}, Na^{+} and K^{+}. This can be accomplished by selecting a ligand with nitrogen donor atoms rather than oxygen donor atoms. Since the competitor metal ions Mg^{2+}, Ca^{2+}, Na^{+} and K^{+} are hard acids according to Pearson's hard and soft acids and bases concept,[8,9] they are expected to exhibit a preference for oxygen donor atoms.

Zinc(II) is borderline between a hard and a soft acid and would therefore be expected to have a tendency to preferentially bind nitrogen donor atoms. It is also preferable to use a nitrogen donor ligand because it is known that most of the Zn^{2+} enzymes possess nitrogen donor atoms in their active sites.[1] In addition to the probe not binding the competitor metal ions it should also not bind to the cell membrane. Secondly, the binding of Zn^{2+} must not be too strong such that the cell is destroyed. Thus, the Zn^{2+} specific probe should measure only the intracellular cytoplasmic free Zn^{2+} concentration rather than the total Zn^{2+} concentration as the removal of bound Zn^{2+} from certain enzymes or proteins may result in the destruction of the cell. Thirdly, the Zn^{2+} complex must fluoresce much more strongly than the probe itself with a good fluorescence yield to enable the accurate measurement of low Zn^{2+} concentrations. A good fluorescence yield would also prevent the loading of large quantities of the probe into the living cell and thus prevent possible serious toxic side effects. Fourthly, if both the Zn^{2+}-free and Zn^{2+}-bound forms of the probe fluoresce then it is preferable that they do so at different wavelengths. This is because incomplete entry of the probe into the cell or a loss of some of the fluorescent probe from inside the cell would not permit an accurate Zn^{2+} calibration curve to be established. Consequently, the free Zn^{2+} concentration would have to be measured as a change in fluorescence intensity. If the Zn^{2+}-free and Zn^{2+}-bound forms of the probe fluoresced at different wavelengths then the ratio of the fluorescences at the two wavelengths would enable the measurement of the free Zn^{2+} concentration without a requirement for separate calibration. Fifthly, a nondisruptive loading procedure of the Zn^{2+} specific probe into the cell is required. The Zn^{2+} specific probe must be able to readily permeate the cells hydrophobic lipid bilayer and once inside the cell it must not leak from the cell or enter membrane bound subcellular organelles such as mitochondria and vesicles. This can be achieved by using a nonpolar ligand with an ester functional group as the probe. The nonpolar ligand should be able to readily permeate the cell hydrophobic lipid bilayer and enter the cell. Esterases in the cells cytoplasm may then hydrolyze the nonpolar ligand into its membrane-impermeant carboxylate form. The trapped nonpolar hydrolyzed ligand is then able to bind the cytoplasmic free Zn^{2+}. This process of loading a cell with a Zn^{2+} specific fluorescent probe (L) is illustrated in Figure 4.1. Finally, it would be preferable if the rate of complexation of intracellular free Zn^{2+} was rapid. Generally, Zn^{2+} complexes with simple ligands are usually labile.[10-12]

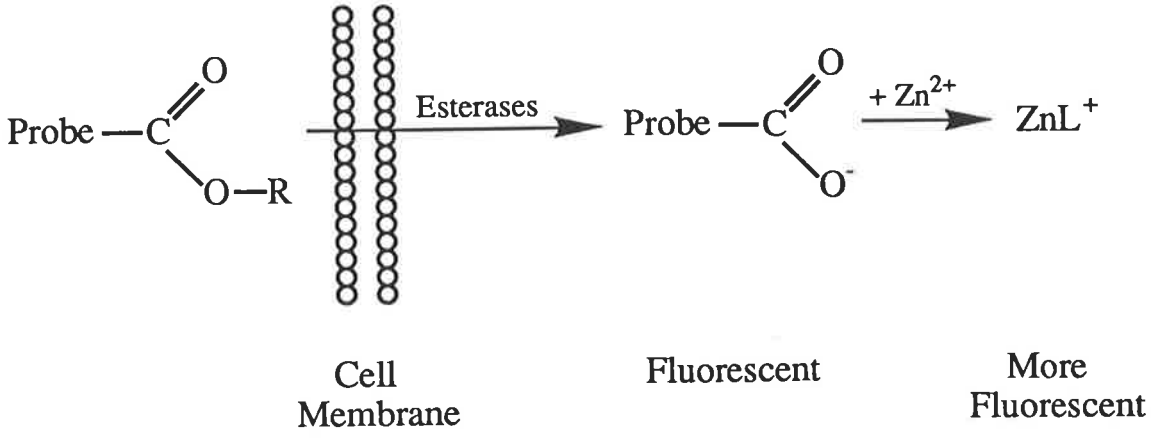

Figure 4.1 *The procedure of loading a fluorescent Zn^{2+} specific probe into a living cell. The cell is loaded with the intracellularly hydrolyzable ester form of the Zn^{2+} specific probe by incubation. Inside the cell, the membrane permeability of the hydrolyzed Zn^{2+} specific probe is low. Thus, it is trapped in the cytoplasm where it can bind the cytoplasmic free Zn^{2+}.*

The chelator 8-hydroxyquinoline is known to produce fluorescent complexes with the biologically relevant cations Zn^{2+}, Ca^{2+} and Mg^{2+}.[13] However, it is expected to preferentially bind Zn^{2+} in the presence of the other biologically relevant cations because its stability constant with Zn^{2+} (10^8) is much greater than that with Mg^{2+} (10^4) or Ca^{2+} (10^3).[14] Mahanand and Houck[15] showed that even in a large excess concentration of Mg^{2+} and Ca^{2+} only Zn^{2+} formed a fluorescent complex at pH 8.0 with 8-hydroxyquinoline. This ligand was first used as a fluorescent probe for histochemically detecting Zn^{2+} by Smith *et al* in 1969.[16] Since that time, numerous derivatives of quinoline have been prepared and tested for the possible use as fluorescent Zn^{2+} probes.[2,17,18] The most potentially useful ligand found was 6-methoxy-8-(*p*-toluenesulfonamido)quinoline (MTS-Q).[18] It displays a high selectivity for the chelation of Zn^{2+} and a good fluorescence yield is obtained for the Zn^{2+} complex. MTS-Q has been predominantly used as a fluorescent histochemical probe for Zn^{2+} in sections of the brain, where it is thought to bind only a minor fraction of the non-metalloenzyme and non-metalloprotein Zn^{2+}.[2] However, its use as a fluorescent Zn^{2+} specific probe is limited by its poor cellular retention.

Sulfonamidoquinolines, of which MTS-Q is one of, have recently attracted attention because of their strong metal cation chelating properties.[19,20] They complex metal cations through their quinolinium and amide nitrogen atoms, thus creating a five-membered ring with the complexed metal cation. A five-membered ring usually creates stable Zn^{2+} and other transition metal cation complexes as it approaches the optimum ring size for the transition metal cations.[21]

In view of the histochemical studies mentioned and the strong chelating ability of the sulfonamidoquinolines, the sulfonamidoquinoline ligand 2-methyl-8-*p*-toluenesulfonamido-6-quinolyloxyacetic acid (MTS-QAA) was examined to ascertain its possible effectiveness as a fluorescent Zn^{2+} specific probe (Figure 4.2). MTS-QAA possesses a carboxyl functional group which can be converted into an ester functional group, thus making loading into cells

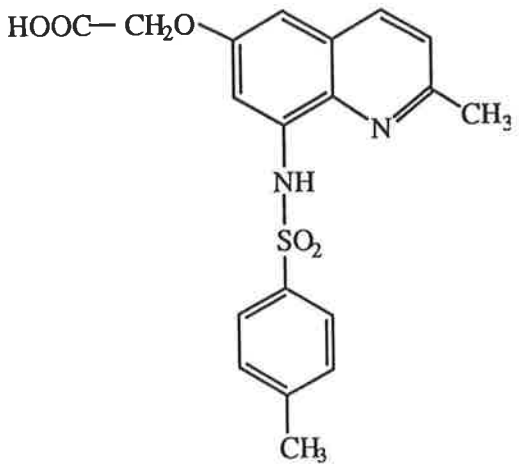

Figure 4.2 *The sulfonamidoquinoline ligand 2-methyl-8-p-toluenesulfonamido-6-quinolyloxyacetic acid (MTS-QAA).*

possible. In this study, the spectral and kinetic properties of MTS-QAA with Zn^{2+} were explored as well as its complexation properties with Zn^{2+} and several other divalent metal cations. However, no histochemical testing of MTS-QAA was carried out in this study. The objectives of this study was to identify and determine the stability constants of all the Zn^{2+} complexes formed in solution with MTS-QAA and to determine their fluorescence yields. In addition, the kinetic study of the Zn^{2+} complexes of MTS-QAA would provide an insight into their complexation and decomplexation mechanisms.

4.2 Complexation Properties of MTS-QAA

4.2.1 Protonation and Stability Constant Determination

In this study, the protonation constants for MTS-QAA and the stability constants for all the complexes formed between MTS-QAA and Zn^{2+}, Co^{2+}, Ni^{2+}, Cu^{2+}, Cd^{2+} and Mg^{2+} were determined by direct potentiometric back titration with a strong base (NaOH) in 50% ethanol/50% water at 298.2 K and $I = 0.10$ ($NaClO_4$). The concentration of H^+ was monitored with a glass pH electrode.

All the potentiometric titrations of MTS-QAA were carried out in a 50% ethanol/50% water solvent mixture because MTS-QAA was not sufficiently soluble in water alone. Below 50% water content MTS-QAA was insufficiently soluble for convenient study by the methods described here. It is necessary to have a reasonable water content in a mixed water/organic solvent system to ensure the glass bulb of the pH electrode does not dehydrate and thus prevent unstable and slow electrode response. This method of determining the protonation and stability constants is best suited to values greater than $10^{2.22}$

The glass pH electrode was calibrated regularly (every 3 titrations) by titrating a $HClO_4$ solution with a standardized NaOH solution to determine its standard potential, E_0, and the ion product constant for water, pK_w, which may vary slightly over days. Glass pH electrodes do not measure pH directly but rather a potential difference (e.m.f.). The e.m.f. is directly proportional to the H^+ concentration through the Nernst equation:

$$E = E_0 + \frac{RT}{F}\ln[H^+] \qquad (4.1)$$

where E is the observed potential (Volts);

E_0 is the standard potential for the electrode (Volts);

R is the gas constant, 8.314 J K^{-1} mol^{-1};

T is the temperature (Kelvin);

F is Faraday's constant, 9.6487×10^4 Coulombs mol^{-1}, and

$[H^+]$ is the hydrogen ion concentration.

By measuring the e.m.f. in millivolts rather than volts, converting to common logs (logarithm to base 10) and considering only the experimental temperature of 298.2 K, the Nernst equation becomes:

$$E = E_0 - 59.15\text{pH} \tag{4.2}$$

which upon rearrangement becomes:

$$\text{pH} = \frac{E_0 - E}{59.15} \tag{4.3}$$

where pH = -log[H^+]

An experimental value for pK_w may be determined from:

$$\text{p}K_w = \frac{E_0 - E}{59.15} + \text{pOH} \tag{4.4}$$

where pK_w = pH + pOH and pOH = -log[OH^-].

The average pK_w determined in 50% ethanol/50% water at I = 0.10 ($NaClO_4$) was 14.263. In water with I = 0.0, pK_w is 14.00. The presence of ethanol suppresses the dissociation of water such that the equilibrium:

$$H_2O \rightleftharpoons H^+ + OH^- \qquad K_w = [H^+][OH^-] \tag{4.5}$$

is shifted to the left. Therefore K_w will be smaller and pK_w (=-logK_w) will be larger in 50% ethanol/50% water than in water.

A more detailed description of the experimental conditions and procedures is given in Chapter 5.

4.2.2 Results and Discussion

MTS-QAA is tribasic in 50% ethanol/50% water at 298.2 K and I = 0.10 ($NaClO_4$). The three apparent protonation constants, K_1, K_2 and K_3, determined for MTS-QAA are described by the following three stepwise reactions:

$$H^+ + \text{MTS-QAA}^{2-} \overset{K_1}{\rightleftharpoons} \text{HMTS-QAA}^- \tag{4.6}$$

$$H^+ + \text{HMTS-QAA}^- \overset{K_2}{\rightleftharpoons} H_2\text{MTS-QAA} \tag{4.7}$$

$$H^+ + H_2MTS\text{-}QAA \overset{K_3}{\rightleftharpoons} H_3MTS\text{-}QAA^+ \quad \textbf{(4.8)}$$

where the three apparent stepwise protonation constants are defined as:

$$K_1 = \frac{[HMTS\text{-}QAA^-]}{[H^+][MTS\text{-}QAA^{2-}]} \quad \textbf{(4.9)}$$

$$K_2 = \frac{[H_2MTS\text{-}QAA]}{[H^+][HMTS\text{-}QAA^-]} \quad \textbf{(4.10)}$$

$$K_3 = \frac{[H_3MTS\text{-}QAA^+]}{[H^+][H_2MTS\text{-}QAA]} \quad \textbf{(4.11)}$$

At low pH, MTS-QAA is fully protonated and possesses a single positive charge, whereas at high pH it is fully deprotonated and possesses a dinegative charge. The first protonation reaction characterized by log $K_1 = 10.01 \pm 0.02$ (pK_{a1}) refers to the association of the amide (-SO_2-NH-) proton. The second protonation reaction characterized by log $K_2 = 3.72 \pm 0.03$ (pK_{a2}) refers to the association of the carboxyl (-COOH) proton. Finally, the third protonation reaction characterized by log $K_3 = 1.87 \pm 0.10$ (pK_{a3}) refers to the association of the quinolinium proton. All three protonation constants were found to be highly reproducible and the values quoted are the averages of three separate titrations. The value for log K_3 falls slightly below 2, the lower limit for accurate measurement, and should therefore be treated with caution. However, since this value was highly reproducible, it was adopted as a real constant when calculating the stability constants for the complexes formed between MTS-QAA and the divalent metal cations Zn^{2+}, Co^{2+}, Ni^{2+}, Cu^{2+}, Cd^{2+} and Mg^{2+}. The placement of an electron donating methyl group in the 2-position of the quinoline moiety increases the basicity of the quinoline nitrogen and is probably the reason why the protonation constant for the quinolinium proton (log K_3) was measurable. A species distribution for MTS-QAA in 50% ethanol/50% water over the pH range 2 - 12 is shown in Figure 4.3.

The pK_as of several similar sulfonamidoquinolines were determined in 75% dioxane/25% water.[20] They exhibited amide and quinolinium proton pK_as comparable to MTS-QAA, 11.9 - 12.9 and < 2, respectively. A recent study of several MTS-QAA precursor sulfonamidoquinolines in 75% ethanol/25% water also demonstated comparable amide and quinolinium proton pK_as.[23] The quinolinium proton pK_as of 8-(benzenesulfonamido)quinoline (BS-Q),

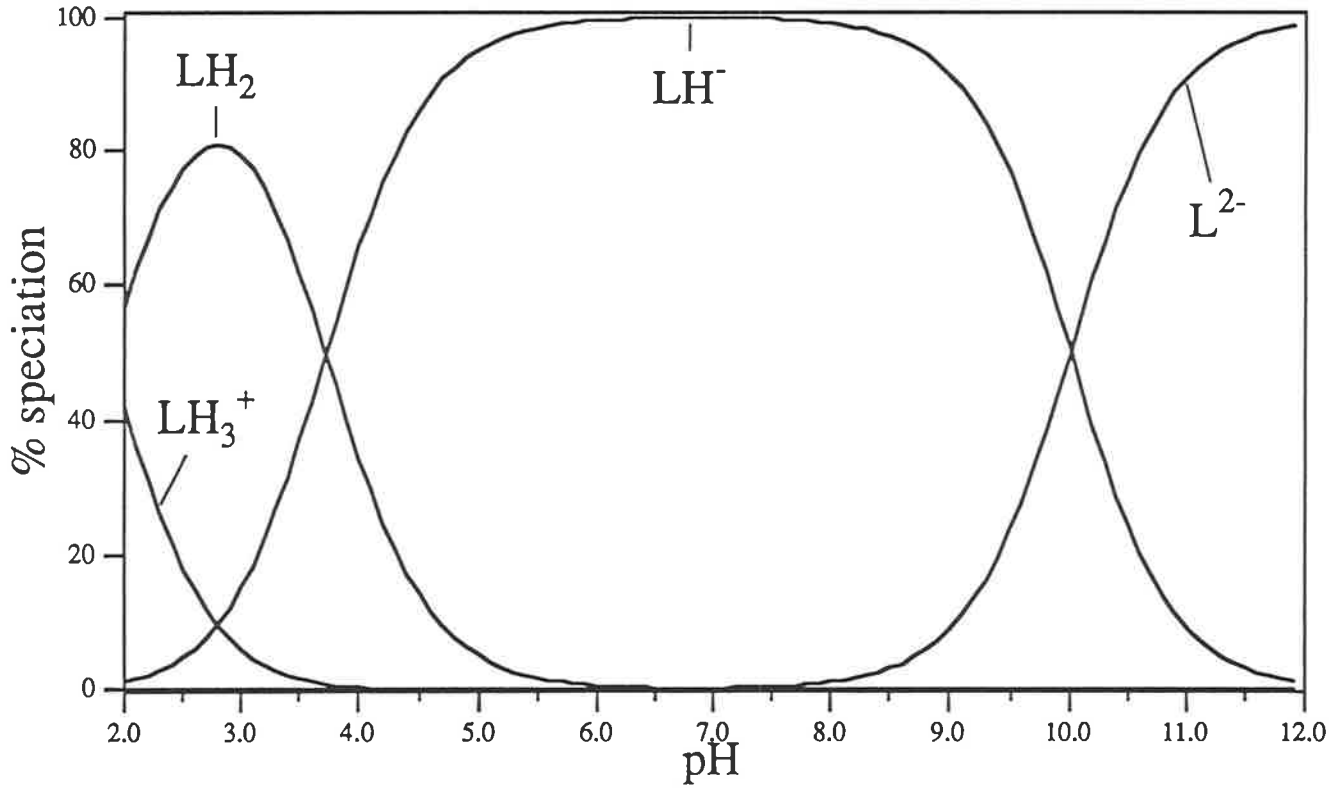

Figure 4.3 *Speciation curves for MTS-QAA (L) protonation in 50% ethanol/50% water at 298.2 K and I = 0.10 ($NaClO_4$). Total MTS-QAA concentration = 4.94×10^{-3} mol dm^{-3}.*

8-(*p*-toluenesulfonamido)quinoline (TS-Q) and 2-methyl-6-methoxy-8-(*p*-toluenesulfonamido)quinoline (MMTS-Q) all fell below 2 and could not be accurately determined, whereas the amide proton pK_as were 9.70, 10.00 and 10.19, respectively. A more detailed discussion and comparison of the pK_as of MTS-QAA with those of similar sulfonamidoquinolines is not possible as no other sulfonamidoquinoline studies in 50% ethanol/50% water have been reported.

The complex formation equilibria of MTS-QAA with M^{2+} in 50% ethanol/50% water at 298.2 K and I = 0.10 ($NaClO_4$) can generally be expressed by the following equations:

$$M^{2+} + \text{MTS-QAA}^{2-} \overset{K_{110}}{\rightleftharpoons} [\text{M.MTS-QAA}] \qquad \textbf{(4.12)}$$

$$M^{2+} + 2\text{MTS-QAA}^{2-} \overset{K_{120}}{\rightleftharpoons} [\text{M.MTS-QAA}_2]^{2-} \qquad \textbf{(4.13)}$$

$$M^{2+} + 3\text{MTS-QAA}^{2-} \overset{K_{130}}{\rightleftharpoons} [\text{M.MTS-QAA}_3]^{4-} \qquad \textbf{(4.14)}$$

where the apparent stepwise stability constants are defined as:

$$K_{110} = \frac{[\text{M.MTS-QAA}]}{[M^{2+}][\text{MTS-QAA}^{2-}]} \qquad \textbf{(4.15)}$$

$$K_{120} = \frac{[\text{M.MTS-QAA}_2{}^{2-}]}{[M^{2+}][\text{MTS-QAA}^{2-}]^2} \qquad \textbf{(4.16)}$$

$$K_{130} = \frac{[\text{M.MTS-QAA}_3{}^{4-}]}{[M^{2+}][\text{MTS-QAA}^{2-}]^3} \qquad \textbf{(4.17)}$$

No other species such as $[M_2.\text{MTS-QAA}]^{2+}$, $[\text{M.HMTS-QAA}]^{+}$ or $[\text{M(OH).MTS-QAA}]^{-}$ were detected upon comparison and analysis of the pH-metric titration curves of the ligand in the absence and presence of the divalent metal cations Zn^{2+}, Co^{2+}, Ni^{2+}, Cu^{2+}, Cd^{2+} and Mg^{2+}. The stability constants of all the species detected in solution for each divalent metal cation are listed in Table 4.1. All values quoted are the averages of at least three separate titrations.

Table 4.1 Apparent Stability Constants for the Complexation of Divalent Metal Ions by the Sulfonamidoquinoline ligand MTS-QAA at 298.2 K and $I = 0.10$ ($NaClO_4$) in 50% Ethanol/50% Water.

$\log \beta_n$ [a] (mol dm^{-3})	Co^{2+}	Ni^{2+}	Cu^{2+}	Zn^{2+}	Cd^{2+} [b]	Mg^{2+}
$\log \beta_1$	8.12 ± 0.20	< 8 [c]	11.96 ± 0.02	9.65 ± 0.02	8.44 ± 0.50	< 2 [d]
$\log \beta_2$	17.06 ± 0.11	15.73 ± 0.03	21.40 ± 0.03	19.11 ± 0.06	15.38 ± 0.40	
$\log \beta_3$	25.56 ± 0.11					

[a] $\log \beta_n = \log K_{110} + \log K_{120} + \ldots\ldots + \log K_{1n0}$; [b] Tentative values only; [c] The stability of the [Ni.MTS-QAA] complex was not very reproducible because the amount formed in solution was less than 5% of the total [Ni^{2+}]; [d] The stability of the [Mg.MTS-QAA] complex was too low to be measured.

From Table 4.1 it can be seen that Ni^{2+}, Cu^{2+}, Zn^{2+} and Cd^{2+} formed both [M.MTS-QAA] and $[M.MTS\text{-}QAA_2]^{2-}$ complexes, Mg^{2+} formed a very unstable [M.MTS-QAA] complex and Co^{2+} formed [M.MTS-QAA], $[M.MTS\text{-}QAA_2]^{2-}$ and $[M.MTS\text{-}QAA_3]^{4-}$ complexes. The order of the transition metal [M.MTS-QAA] complex stabilities is $Co^{2+} > Ni^{2+} < Cu^{2+} > Zn^{2+}$, the order of Ni^{2+} and Co^{2+} being reversed from that of the Irving-Williams series.[24,25] Similar transition metal complex stability sequences were observed for 2-methyl-8-(methanesulfonamido)quinoline (MMS-Q) and 2-methyl-8-(mesitylenesulfonamido)quinoline (MMsS-Q) in 75% dioxane/25% water .[20]

Only an upper limit of < 8 could be quoted for the stability of [Ni.MTS-QAA] because the stability constant was not very reproducible due to the fact that less than 5% of the total [Ni^{2+}] formed [Ni.MTS-QAA]. It can be seen that the difference between the $\log K_{110}$ (= $\log \beta_1$) values of Ni^{2+} and Co^{2+} is smaller than the difference between the $\log K_{120}$ (= $\log \beta_2$ - $\log K_{110}$) values. This may suggest that the $[M.MTS\text{-}QAA_2]^{4-}$ complexes of Ni^{2+} and Co^{2+} adopt different geometries. The colour of the Co^{2+} and Ni^{2+} titration solutions verifies this. At the start of the titration (low pH), the Co^{2+} titration solution (Co^{2+} + MTS-QAA + H^+) was pale yellow due to the free ligand. As NaOH was added and Co^{2+} complexes were formed, the solution gradually became a dark maroon colour which implies the formation of octahedral Co^{2+}

complexes. Stable octahedral $[Co.MTS\text{-}QAA_3]^{4-}$ is formed despite the obvious steric interactions which would be expected to prevent this forming. The Ni^{2+} titration solution (Ni^{2+} + MTS-QAA + H^+) was initially pale green due to octahedral $[Ni(H_2O)_6]^{2+}$. Upon increasing pH by addition of NaOH, the solution turned a golden brown colour which implies the formation of square planar $[Ni.MTS\text{-}QAA_2]^{2-}$.

A speciation plot illustrating the percentage composition of the Zn^{2+} titration solution over the pH range 2 - 12 is shown in Figure 4.4. From Figure 4.4 it can be seen that under the experimental conditions used for the Zn^{2+} titrations (see Chapter 5) virtually all of MTS-QAA was in the $[Zn.MTS\text{-}QAA_2]^{2-}$ form at pH > 8, and the maximum quantity of [Zn.MTS-QAA] was obtained at pH ≈ 4. The presence of two different Zn^{2+}-MTS-QAA complexes would undoubtedly complicate the measurement of intracellular free $[Zn^{2+}]$. The results in Table 4.1 indicate that the [Zn.MTS-QAA] complex is slightly more stable than the $[Zn.MTS\text{-}QAA_2]^{2-}$ complex. In contrast to this, the MTS-QAA precursor TS-Q exhibited a greater stability for the $[Zn.TS\text{-}Q_2]$ complex than the $[Zn.TS\text{-}Q]^+$ complex in 75% ethanol/25% water.[23] Since the stability constants of [Zn.MTS-QAA] and $[Zn.MTS\text{-}QAA_2]^{2-}$ are not that different (stepwise stability constants are generally decreasing) the implication is that a change in the coordination number of the Zn^{2+} has occured. The [Zn.MTS-QAA] complex may be octahedral (with water molecules occupying the remaining four coordination sites) and the $[Zn.MTS\text{-}QAA_2]^{2-}$ complex may be tetrahedral. A tetrahedral geometry is highly likely in Zn^{2+} complexes as it is known that Zn^{2+} in biology has a preference for tetrahedral protein sites.[1] Only the crystal structures of the two Zn^{2+} complexes could reveal their actual geometries. Attempts to grow reasonable [Zn.MTS-QAA] and $[Zn.MTS\text{-}QAA_2]^{2-}$ crystals for crystal structure determinations have been unsuccessful. However, the crystal structure of the Cu^{2+} complex of the MTS-QAA precursor TS-Q, $[Cu.TS\text{-}Q_2]$, was found to exhibit tetrahedral geometry.[26]

At approximately pH 5 in the Cd^{2+} titrations, a precipitate appeared (possibly $Cd(OH)_2$) which only allowed the data up to that point to be used to determine the Cd^{2+} complex stability constants. Generally, data points at high pH were not used to determine the divalent metal ion MTS-QAA complex stability constants because of the formation and precipitation of $M(OH)_2$

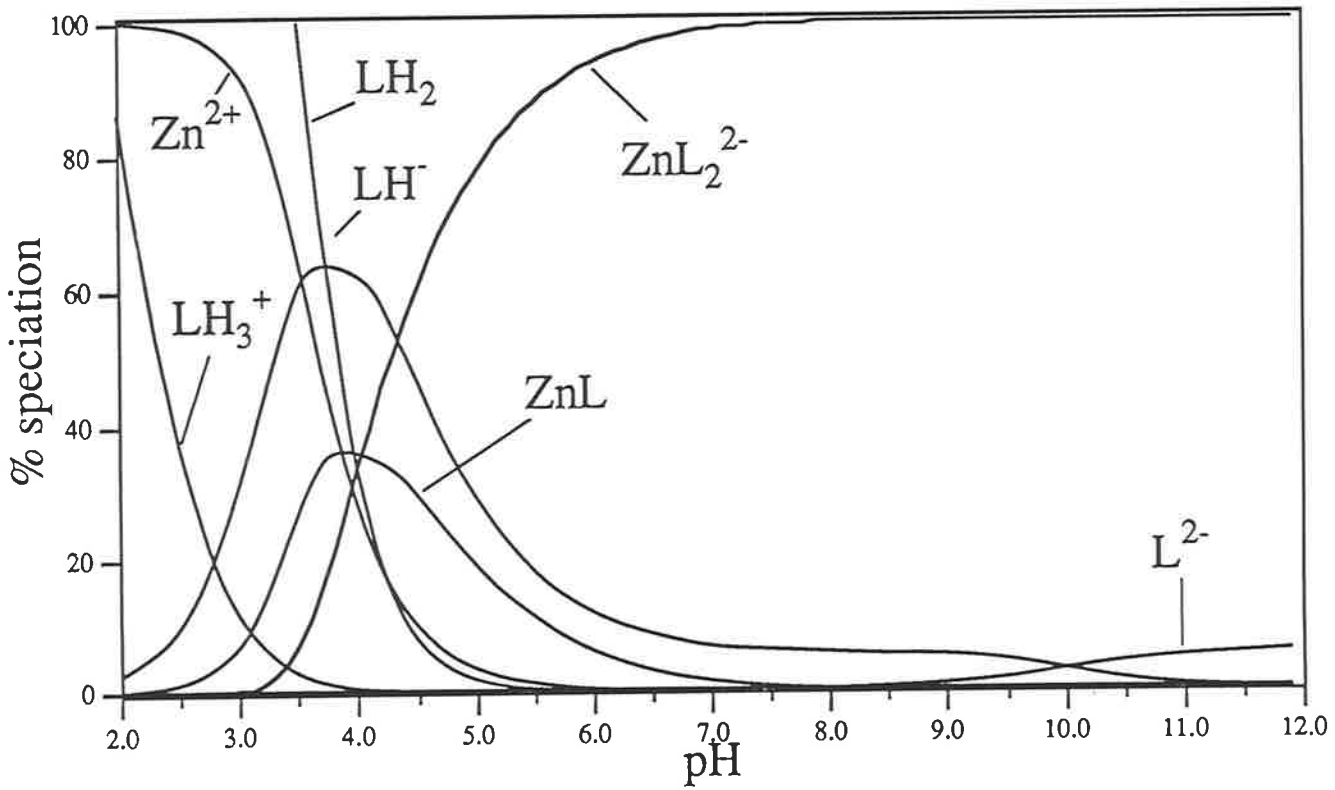

Figure 4.4 *Speciation curves for Zn^{2+} complexes of MTS-QAA (L) in 50% ethanol/50% water at 298.2 K and I = 0.10 ($NaClO_4$). Total Zn^{2+} concentration = 0.49 × 10^{-3} mol dm^{-3}, and the total MTS-QAA concentration = 1.00 × 10^{-3} mol dm^{-3}.*

species. At best, only 5% of MTS-QAA formed the $[Cd.MTS\text{-}QAA_2]^{2-}$ complex and the stability constants of both the [Cd.MTS-QAA] and $[Cd.MTS\text{-}QAA_2]^{2-}$ complexes were not very reproducible. Therefore the Cd^{2+} complex stability constants are tentative values only and should be treated with caution.

The pH-metric titration curve of MTS-QAA in the absence and presence of Mg^{2+} was virtually identical. This indicates that the [Mg.MTS-QAA] complex was not very stable and an upper limit of 2 is quoted. No attempt was made to determine the stability constants of the other biologically relevant cations Ca^{2+}, Na^{+} and K^{+} with MTS-QAA because they were expected to be similarly too low for measurement.

The formation of stable [M.MTS-QAA] species, where $M^{2+} = Co^{2+}$, Ni^{2+}, Cu^{2+} and Cd^{2+}, in principle presents an obstacle to the quantification of Zn^{2+} levels in biological systems. This problem is lessened by the expectation that these metal ions are of substantially lower concentration than Zn^{2+} in healthy cells, and also as a consequence of the effective quenching of fluorescence by Co^{2+}, Ni^{2+} and Cu^{2+} as is discussed in sections 4.3.1 and 4.3.2.

4.3 Spectral Properties of MTS-QAA

4.3.1 Principles of Fluorescence Spectroscopy

Upon the absorption of ultraviolet or visible electromagnetic radiation, molecules are elevated to an excited electronic state. Some molecules may return to their ground electronic states by emitting the absorbed energy as light of a different wavelength than that of the absorbed radiation. Two types of this deactivation process called photoluminescence may occur, namely fluorescence and phosphorescence. The two photoluminescent phenomenon are illustrated by the Jablonski energy level diagram in Figure 4.5.

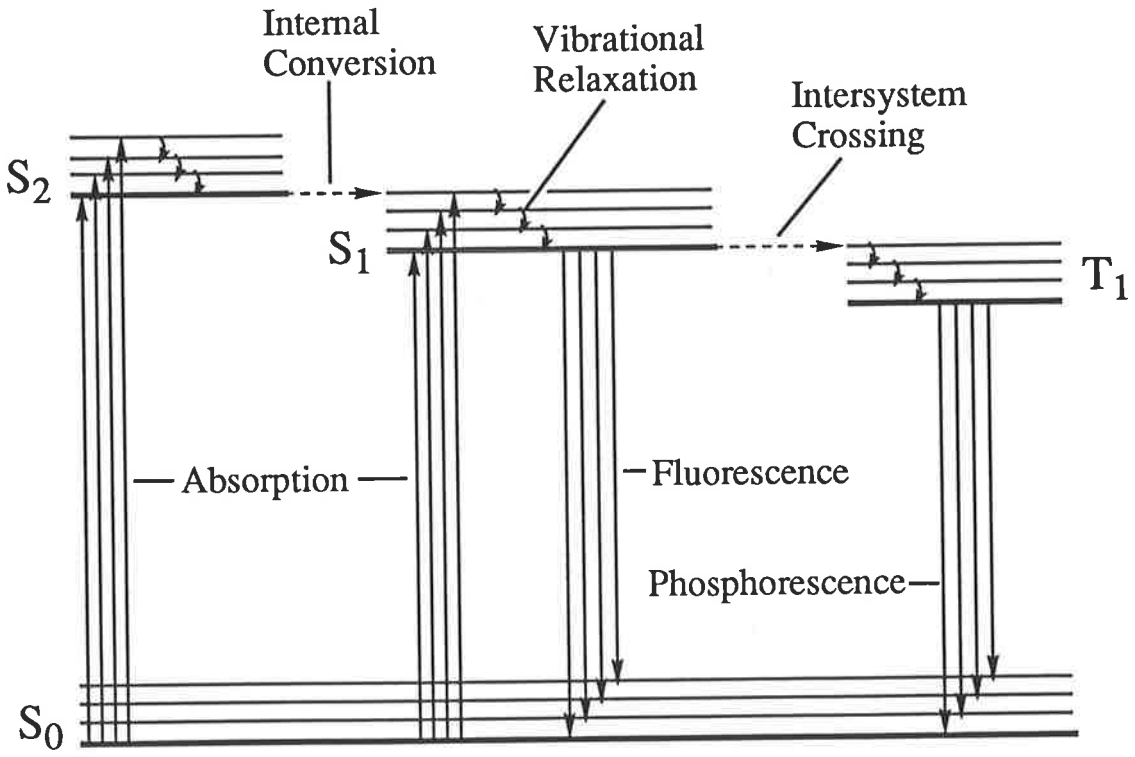

Figure 4.5 *Jablonski energy level diagram depicting absorption and emission processes.*

S_0, S_1 and S_2 denote the ground, first and second electronic singlet states, respectively. A number of vibrational energy levels (thinner horizontal lines) exist at each of these electronic singlet states. These are termed singlet states because when one of a pair of electrons of a molecule is excited to one of these higher energy levels the spin of the promoted electron remains paired with the ground state electron. T_1 represents the first electronic triplet state.

This is termed a triplet state because the spin of the excited electron to this energy level becomes unpaired with the ground state electron. Again numerous vibrational energy levels are associated with this electronic state.

The absorption of radiation is extremely rapid, taking about 10^{-15} s. During this time, a molecule is excited to a higher electronic singlet state, S_1 or S_2. As illustrated in Figure 4.5, a molecule may be excited to any one of the numerous vibrational energy levels of S_1 or S_2. From here several radiationless deactivation process may occur. Collisions between the excited molecules results in these molecules relaxing to the lowest vibrational energy level of the electronically excited singlet state and the excess vibrational energy being dissipated as heat. This process of deactivation is termed vibrational relaxation. Once an excited molecule has relaxed to the lowest vibrational energy level of the electronically excited singlet state (ie. S_2), it may then lose the excitation energy by going to an equally energetic vibrational energy level of a lower electronic singlet state (ie. S_1). This process of deactivation is termed internal conversion. Vibrational relaxation to the lowest vibrational energy level of the lower electronic singlet state (ie. S_1) then may follow as before. The two deactivation processes of vibrational relaxation and internal conversion occur quite rapidly in about 10^{-12} s.

Once the excited molecules have reached the lowest vibrational energy level of the lower electronic singlet state (ie. S_1) they may then deexcitate to the ground electronic singlet state, S_0, by the emission of photons. This process is termed fluorescence. Fluorescence generally arises as a result of electronic transitions between the S_1 and S_0 states because the closeness of the excited electronic singlet states allows efficient internal conversion to the lowest electronic excited singlet state, S_1. After excitation, fluorescence emission occurs in approximately 10^{-8} s.

Alternately, molecules in the S_1 state may deexcite to an equally energetic vibrational energy level of the lowest electronic excited triplet state, T_1. This radiationless transition of S_1 to T_1 is termed intersystem crossing. Once again vibrational relaxation may take place such that the molecules attain the lowest T_1 vibrational energy level. From this position, the molecules can deexcite to S_0 by emission of photons in a process called phosphorescence. Transitions from T_1 to S_0 are forbidden and thus result in phosphorescence being much longer lived than fluorescence (approximately 10^{-3} to 10 s). Phosphorescence and fluorescence can be lost by a process called quenching. This is the radiationless deactivation of the T_1 or S_1 state which may occur upon the

interaction of the phosphorescent or fluorescent molecules with quencher species such as paramagnetic metal ions.

4.3.2 Results and Discussion

Fluorescence spectroscopy is a very sensitive technique which has a wide concentration detection range. Thus, the measurement of the intensity of fluorescence permits the quantitative determination of a variety of organic and inorganic species in trace amounts.

The emission spectra for a series of MTS-QAA solutions with increasing Zn^{2+} concentrations at pH 6.6, I = 0.10 (NaPIPES) and 298.2 K in 50% ethanol/50% water is shown in Figure 4.6. From Figure 4.6 it can be seen that the Zn^{2+}-free and Zn^{2+}-bound forms of MTS-QAA fluoresce at the same wavelength. Thus, the intracellular [Zn^{2+}] would have to be measured as a change in fluorescence intensity. The emission spectra of some species show significant structure due to the individual vibrational energy levels of the ground and excited states. However, the emission spectra for the Zn^{2+}-MTS-QAA solutions exhibit no apparent vibrational structure. The presence of only one fluorescence emission peak is indicative of fluorescence emanating from the S_1 excited electronic singlet state to the S_0 ground electronic singlet state. These emission spectra were established by excitation at 350 nm and measuring emission between 360 and 660 nm. A filter which passes light above 390 nm was used to reduce the amount of stray and scattered light. Excitation and emission slit widths of 10 nm were also used.

Upon variation of the [Zn^{2+}]/[MTS-QAA] ratio from 0 to 50, the intensity of the fluorescence increased about sixfold, though the wavelength of the emission peak remained relatively constant at 483 nm (Table 4.2 and Figure 4.7). Fluorescence arising from the NaPIPES buffer (sodium piperazine-N,N'-bis(2-ethane-sulfonate), which maintained the pH of all solution at 6.6 and also kept the ionic strength constant at 0.10, was deducted from all the fluorescence measurements made. This fluorescence correction value was very small and may arise from < 1 ppm heavy metal impurities in NaPIPES which might be complexed by MTS-QAA.

Prior to the fluorescence measurements, a knowledge of the ultraviolet-visible absorption characteristics of MTS-QAA and its Zn^{2+} complexes was essential in selecting the excitation wavelength. The ultraviolet-visible absorption of

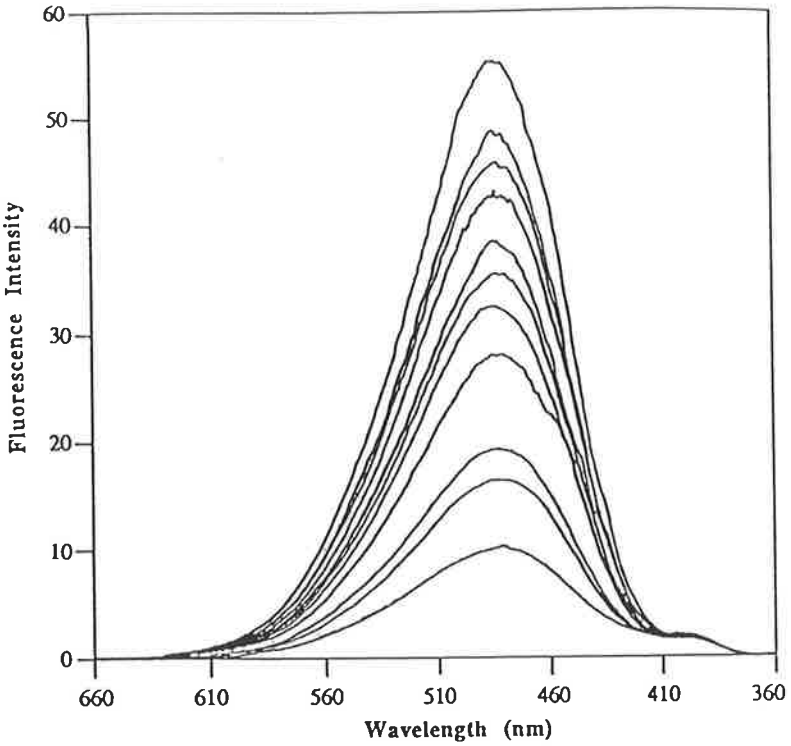

Figure 4.6 *The variation of the fluorescence emission spectrum of MTS-QAA with Zn^{2+} at pH 6.6, I = 0.10 (NaPIPES) and 298.2 K in 50% ethanol/50% water. The total [MTS-QAA] = 2.518 × 10^{-6} mol dm^{-3} and the total [Zn^{2+}] increases in the order 0, (0.002509, 0.005018, 0.01004, 0.01505, 0.02007, 0.02509, 0.05018, 0.1254, 0.2509 and 1.254) × 10^{-4} mol dm^{-3} as the maximum in successive fluorescence spectra increases. The excitation wavelength was 350 nm.*

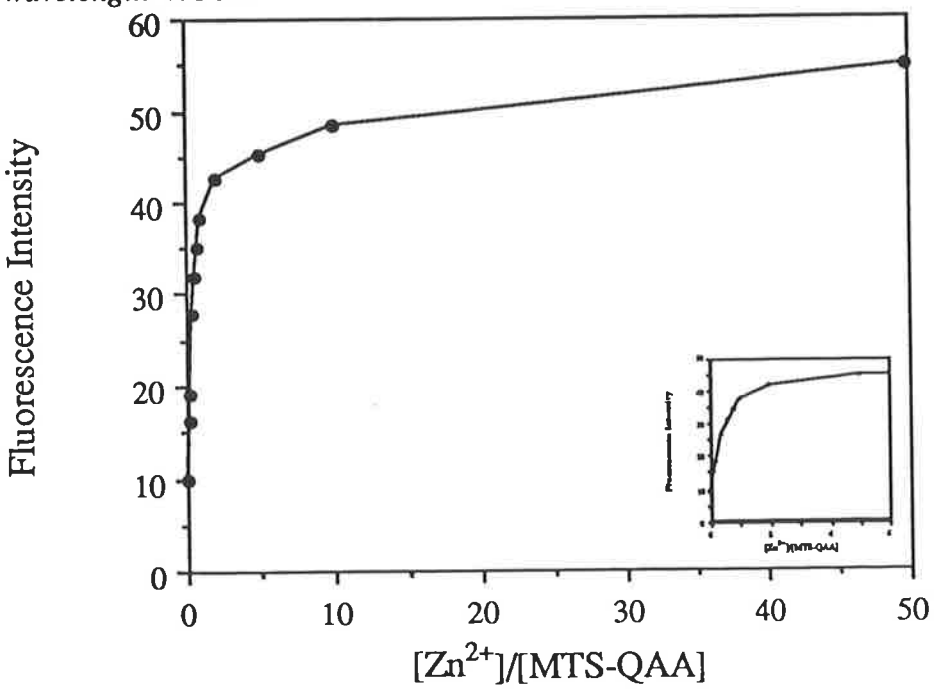

Figure 4.7 *Increase in fluorescence intensity at 483 nm upon increasing the [Zn^{2+}]/[MTS-QAA] ratio. An enlargement of the initial part of the plot is shown in the inset.*

Table 4.2 Fluorescence Solution Compositions in 50% Ethanol/50% Water at pH 6.6, 298.2 K and I = 0.10 (NaPIPES).

Solution	$[Zn^{2+}]$ (mol dm^{-3})	[L] (mol dm^{-3})	[L] in the free form	[L] in the [ZnL] form	[L] in the $[ZnL_2]^{2-}$ form	Total Fluorescence[a]	$\frac{[Zn^{2+}]}{[L]}$
i	-	2.518×10^{-6}	2.518×10^{-6}	-	-	9.3	0
ii	2.509×10^{-7}	2.518×10^{-6}	2.123×10^{-6}	6.925×10^{-8}	3.258×10^{-7}	15.6	0.10
iii	5.018×10^{-7}	2.518×10^{-6}	1.766×10^{-6}	1.528×10^{-7}	5.993×10^{-7}	18.4	0.20
iv	1.004×10^{-6}	2.518×10^{-6}	1.206×10^{-6}	3.568×10^{-7}	9.553×10^{-7}	27.1	0.40
v	1.505×10^{-6}	2.518×10^{-6}	8.531×10^{-7}	5.754×10^{-7}	1.090×10^{-6}	31.3	0.60
vi	2.007×10^{-6}	2.518×10^{-6}	6.439×10^{-7}	7.715×10^{-7}	1.103×10^{-6}	34.4	0.80
vii	2.509×10^{-6}	2.518×10^{-6}	5.144×10^{-7}	9.357×10^{-7}	1.068×10^{-6}	37.5	1.00
viii	5.018×10^{-6}	2.518×10^{-6}	2.584×10^{-7}	1.436×10^{-6}	8.239×10^{-7}	41.8	1.99
ix	1.254×10^{-5}	2.518×10^{-6}	1.073×10^{-7}	1.947×10^{-6}	4.638×10^{-7}	44.6	4.98
x	2.509×10^{-5}	2.518×10^{-6}	5.498×10^{-8}	2.195×10^{-6}	2.684×10^{-7}	47.6	9.96
xi	1.254×10^{-4}	2.518×10^{-6}	2.266×10^{-9}	2.503×10^{-6}	1.259×10^{-8}	54.2	49.82

[a] The fluorescence values quoted have been adjusted for 0.10 mol dm^{-3} NaPIPES.

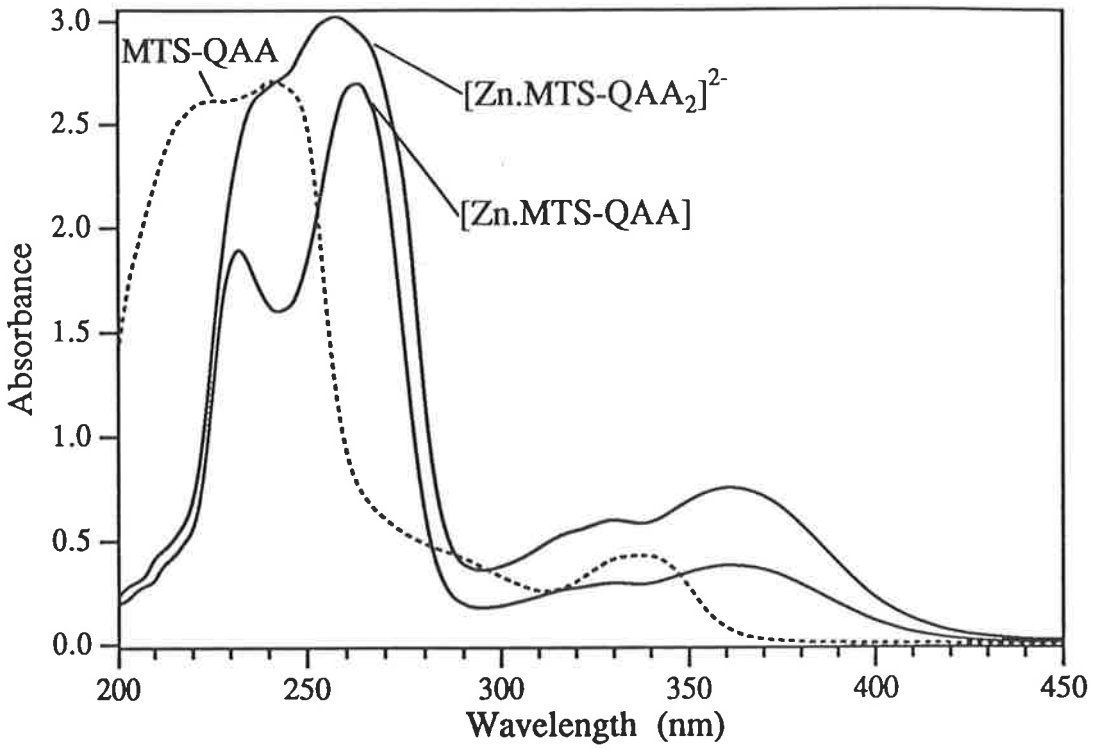

Figure 4.8 *The ultraviolt-visible spectra of MTS-QAA, [Zn.MTS-QAA] and [Zn.MTS-QAA$_2$]$^{2-}$ in 50% ethanol/50% water at pH 6.6, I = 0.10 (NaPIPES) and 298.2 K.*

Table 4.3 Location of the Absorption Maxima (λ_{max}) and their Molar Extinction Coefficient (ε) Values in the Free MTS-QAA, [Zn.MTS-QAA] and [Zn.MTS-QAA$_2$]$^{2-}$ Ultraviolet-Visible Spectra in 50% Ethanol/50% Water at pH 6.6, I = 0.10 (NaPIPES) and 298.2 K.

Species	Concentration (mol dm^{-3})	λ_{max} (nm) and ε^a (dm^3 cm^{-1} mol^{-1})			
MTS-QAA^b	1.071×10^{-4}	224 (24360)	242 (25290)	338 (4010)	
[Zn.MTS-QAA]	9.476×10^{-5}	232 (20160)	262 (28490)	332 (3170)	362 (4010)
[Zn.MTS-QAA$_2$]$^{2-}$	9.126×10^{-5}	238 (29040)	260 (33200)	332 6580)	362 (8330)

^{a} The ε values are in brackets; ^{b} At pH 6.6, the ligand is in the monoprotonated form, HMTS-QAA$^-$.

free MTS-QAA, [Zn.MTS-QAA] and $[Zn.MTS\text{-}QAA_2]^{2-}$ at pH 6.6, $I = 0.10$ (NaPIPES) and 298.2 K in 50% ethanol/50% water are shown in Figure 4.8. It was important to clarify whether the increase in fluorescence of MTS-QAA upon the addition of varying amounts of Zn^{2+} was due to the Zn^{2+} or due to the different amounts of radiation absorbed by Zn^{2+}-free MTS-QAA and Zn^{2+}-bound MTS-QAA. It can be seen that at 350 nm the free ligand solution absorbs the same amount of photons as the [Zn.MTS-QAA] complex solution. These solutions were irradiated at 350 nm and their fluorescence measured. The solution containing Zn^{2+} fluoresced much more strongly than that without the Zn^{2+}. Thus, the increase in fluorescence of MTS-QAA upon the addition of Zn^{2+} (Figures 4.6 and 4.7) is not due to different amounts of radiation absorbed by the Zn^{2+}-free MTS-QAA and Zn^{2+}-bound MTS-QAA species.

Table 4.3 lists the location of the absorption maxima (λ_{max}) and their molar extinction coefficient (ε) values in the free MTS-QAA, [Zn.MTS-QAA] and $[Zn.MTS\text{-}QAA_2]^{2-}$ ultraviolet-visible absorption spectra. Ligand to metal charge transfer (LMCT) transitions are not possible in the Zn^{2+} complexes of MTS-QAA because Zn^{2+} possesses filled d orbitals. MTS-QAA is therefore unable to donate an electron to a Zn^{2+} d orbital. For the same reason, no d-d transitions can be observed in Zn^{2+} complexes. Generally, the ultraviolet-visible absorption spectra of organic compounds are associated with transitions between a bonding (π) or lone-pair (n) orbital and an unfilled antibonding (π^*) orbital. The molar extinction coefficients for peaks associated with $n \rightarrow \pi^*$ transitions are generally quite low and range from 10 to 100 $dm^3\ cm^{-1}\ mol^{-1}$. Whereas, ε values between 1000 and 10000 $dm^3\ cm^{-1}\ mol^{-1}$ characterize $\pi \rightarrow \pi^*$ transitions and almost always signify the presence of an aromatic system. Therefore, all the peaks listed in Table 4.3 are probably due to $\pi \rightarrow \pi^*$ intraligand transitions. The two lowest wavelength peaks in each spectrum are characterized by ε values between 20000 and 35000 $dm^3\ cm^{-1}\ mol^{-1}$. This is because the quinoline aromatic ring system is substituted with an amide nitrogen atom and an ether oxygen atom which may extend the chromophore, thus giving intraligand transition absorption peaks with $\varepsilon > 10000\ dm^3\ cm^{-1}\ mol^{-1}$.

In general, fluorescent chelates are formed only by diamagnetic metal ions and not by paramagnetic metal ions. The complexation of a paramagnetic transition metal ion such as Co^{2+}, Ni^{2+} and Cu^{2+} by a fluorescent ligand results in quenching of the ligand fluorescence. This is because the rate of

intersystem crossing from the S_1 state to the T_1 state of the fluorescent ligand is greatly increased by the unpaired electrons of the paramagnetic metal ions.[27] Whereas, the complexation of a diamagnetic metal ion such as Zn^{2+}, a d^{10} metal ion, by a fluorescent ligand should result in chelation-enhanced fluorescence. The increase in fluorescence upon the complexation of a diamagnetic metal ion is probably the result of the formation of a more rigid structure. Structural rigidity has been found to be the cause of an increase in fluorescence in several chelating molecules upon the complexation of a metal ion.[28] It is expected that structural rigidity probably reduces the amount of radiationless deactivation processes such as internal conversion and vibrational relaxation.

The percentage of all the MTS-QAA species in each of the eleven fluorescence solutions can be determined using MACSPECIES.[29] MACSPECIES incorporates the protonation constants of MTS-QAA, the stability constants of [Zn.MTS-QAA] and $[Zn.MTS\text{-}QAA_2]^{2-}$, and the initial concentration of Zn^{2+} and free MTS-QAA. These results in conjunction with the fluorescence intensity values for each of the eleven solutions may be used to obtain eleven simultaneous equations of the form:

$$F_{total} = f(L_0)[L_0] + f(L_1)[L_1] + f(L_2)[L_2] \qquad \textbf{(4.18)}$$

where F_{total} is the measured total fluorescence;

$f(L_0)$ is the fluorescence of the free ligand;

$[L_0]$ is the concentration of the free ligand;

$f(L_1)$ is the fluorescence of the ligand in the [Zn.MTS-QAA] complex;

$[L_1]$ is the concentration of the ligand in the [Zn.MTS-QAA] complex;

$f(L_2)$ is the fluorescence of the ligand in the $[Zn.MTS\text{-}QAA_2]^{2-}$ complex, and

$[L_2]$ is the concentration of the ligand in the $[Zn.MTS\text{-}QAA_2]^{2-}$ complex.

The value of $f(L_0)$ can be calculated from the first fluorescence solution containing no Zn^{2+}, since $[L_1] = [L_2] = 0$. It was determined to be 3.69×10^6 $dm^3\ mol^{-1}$. Solving the remaining ten simultaneous equations using DATAFIT[30,31] yielded $f(L_1) = (2.03 \pm 0.04) \times 10^7$ $dm^3\ mol^{-1}$ and $f(L_2) =$

$(1.49 \pm 0.08) \times 10^7$ dm^3 mol^{-1}. It can therefore be noted that a MTS-QAA molecule in the [Zn.MTS-QAA] complex form fluoresces much more strongly than a MTS-QAA molecule in the free form, by a factor of 5.5. Whereas, a MTS-QAA molecule in the $[Zn.MTS\text{-}QAA_2]^{2+}$ complex form fluoresces more than a MTS-QAA molecule in the free form, by a factor of 4. This means that the 1:1 Zn^{2+} complex has a greater fluorescence yield per MTS-QAA ligand than the 1:2 Zn^{2+} complex. However, in terms of overall fluorescence, the $[Zn.MTS\text{-}QAA_2]^{2-}$ complex (2.98×10^7 dm^3 mol^{-1}) fluoresces 1.47 times more strongly than the [Zn.MTS-QAA] complex (2.03×10^7 dm^3 mol^{-1}).

4.4 Reaction Kinetics for [Zn.MTS-QAA] and $[Zn.MTS\text{-}QAA_2]^{2-}$

4.4.1 Stopped-flow Fluorescence Spectroscopy

The acid catalysed decomplexation kinetics of [Zn.MTS-QAA] and $[Zn.MTS\text{-}QAA_2]^{2-}$ and the formation kinetics of [Zn.MTS-QAA] were studied in order to formulate mechanisms for the reactions described by Equations 4.19 - 4.21:

$$Zn^{2+} + HMTS\text{-}QAA^- \rightleftharpoons [Zn.MTS\text{-}QAA] + H^+ \quad \textbf{(4.19)}$$

$$Zn^{2+} + 2HMTS\text{-}QAA^- \rightleftharpoons [Zn.MTS\text{-}QAA_2]^{2-} + 2H^+ \quad \textbf{(4.20)}$$

$$[Zn.MTS\text{-}QAA] + 3H^+ \rightleftharpoons Zn^{2+} + H_3MTS\text{-}QAA^+ \quad \textbf{(4.21)}$$

Kinetic studies of these Zn^{2+} systems were carried out on a stopped-flow fluorescence spectrometer similar to that described by Erman and Hammes.[32] Further details on the stopped-flow fluorimeter and on the acquisition of data is provided in Chapter 5. An excitation wavelength of 350 nm was used and the decrease and increase in fluorescence for the decomplexation and complexation reactions, respectively, were monitored by employing a filter which allowed $\geq 70\%$ transmission above 480 nm and $\leq 1\%$ below 450 nm. Between eight and ten reaction traces were collected for each pair of solutions studied in the three systems. Bisquare weighted least squares fitting of the averaged exponential signal to Equation 4.22 yielded the observed pseudo first order rate constants, k_{obs}.

$$A = C\exp(-k_{obs}t) \quad \textbf{(4.22)}$$

where A is the amplitude (Volts);

C is a constant (Volts);

k_{obs} is the observed first order rate constant (s^{-1}), and

t is the time (s).

The k_{obs} values were fitted to equations which best described the most likely reaction mechanism using the non-linear, weighted least squares program DATAFIT.[30,31]

In the decomplexation and complexation kinetic studies, excess $[H^+]$ and excess $[Zn^{2+}]$ were used, respectively, to generate pseudo first order conditions. The concentration of the excess reactant effectively remained invariant during the reaction. It is appropriate at this point to describe the various mechanisms of ligand substitution on metal centres and define the respective observed rate constants.

4.4.2 Ligand Substitution Mechanisms

The Langford-Gray formalism[33] has been widely used to classify the mechanisms of ligand substitution reactions on metal centres. It divides reaction mechanisms into three categories: associative (A), dissociative (D) and interchange (I). For this discussion the simple octahedral complex $[MS_6]^{m+}$, where M^{m+} represents a metal ion and S represents a solvent molecule, and the simple monodentate ligand X will be used.

An associative mechanism may be described by Equation 4.23, where a reactive intermediate of increased coordination number is formed. The reactive intermediate can survive several collisions before reacting to form $[MS_5X]^{m+}$. The rate determining step for the forward reaction is the formation of the first transition state in which a new bond between the metal ion and the ligand is virtually formed. However, the rate determining step for the reverse reaction is the formation of the second transition state.

$$[MS_6]^{m+} + X \underset{r.d.s.}{\xrightarrow{slow}} \underset{\text{first transition state}}{[S_6M^{m+}\cdots X]} \xrightarrow{fast} \underset{\text{7-coordinate reactive intermediate}}{[MS_6X]^{m+}} \qquad (4.23)$$

$$\downarrow fast$$

$$[MS_5X]^{m+} + S \xleftarrow{fast} \underset{\text{second transition state}}{[S_5XM^{m+}\cdots S]}$$

Under the experimental condition of an excess [X], the formation reaction is pseudo first order. Since the forward and reverse reactions are observed simultaneously, the observed rate constant, k_{obs}, is defined as:

$$k_{obs} = k_f[X] + k_r \tag{4.24}$$

where k_f is the second order formation rate constant and k_r is the first order decomplexation rate constant. When [X] = 0: $k_{obs} = k_r$ (see Figure 4.9 (a)).

In a dissociative mechanism, as described by Equation 4.25, a reactive intermediate of decreased coordination number is formed via a transition state in which a metal ion to solvent bond is virtually broken. The rate determining step for the forward and reverse reactions is the formation of the first and second transition states, respectively.

$$[MS_6]^{m+} + X \xrightarrow[r.d.s.]{slow} \underset{\text{first transition state}}{[S_5M^{m+}\cdots S]} + X \xrightarrow{fast} \underset{\substack{\text{5-coordinate}\\ \text{reactive}\\ \text{intermediate}}}{[MS_5]^{m+}} + S + X \tag{4.25}$$

$$\downarrow fast$$

$$[MS_5X]^{m+} + S \xleftarrow{fast} \underset{\text{second transition state}}{[S_5M^{m+}\cdots X]} + S$$

Under the pseudo first order conditions of excess [X] and under the steady state condition where $[MS_5{}^{m+}]$ is very small and invariant with time, the observed rate constant for the approach to equilibrium is defined as:

$$k_{obs} = \frac{k_1[X] + k_{-1}k_{-2}/k_2}{k_{-1}/k_2 + [X]} \tag{4.26}$$

where k_1 is the forward $[MS_5]^{m+}$ formation rate constant;

k_2 is the forward $[MS_5X]^{m+}$ formation rate constant;

k_{-1} is the reverse $[MS_6]^{m+}$ formation rate constant, and

k_{-2} is the reverse $[MS_5X]^{m+}$decomplexation rate constant (as shown in Equation 4.27).

$$[MS_6]^{m+} + X \underset{k_{-1}}{\overset{k_1}{\rightleftharpoons}} [MS_5]^{m+} + S + X \underset{k_{-2}}{\overset{k_2}{\rightleftharpoons}} [MS_5X]^{m+} + S \tag{4.27}$$

When [X] « k_{-1}/k_2: $k_{obs} \approx \frac{k_1 k_2[X]}{k_{-1}} + k_{-2}$,

but when [X] » k_{-1}/k_2: $k_{obs} \approx k_1 + \frac{k_{-1}k_{-2}}{k_2[X]}$,

and when [X] = 0: $k_{obs} = k_{-2}$ (see Figure 4.9 (b)).

In an interchange mechanism, as described by Equation 4.28, the incoming (X) and leaving (S) ligands participate equally in the formation of the only transition state. Since the incoming and leaving ligands interchange positions synchronously, the incoming ligand must be in position in the second coordination sphere of the metal ion before interchange can occur. Thus, an encounter complex is formed at a diffusion-controlled rate prior to the formation of the transition state. In contrast to the associative and dissociative mechanisms, no kinetically detectable reactive intermediate is formed.

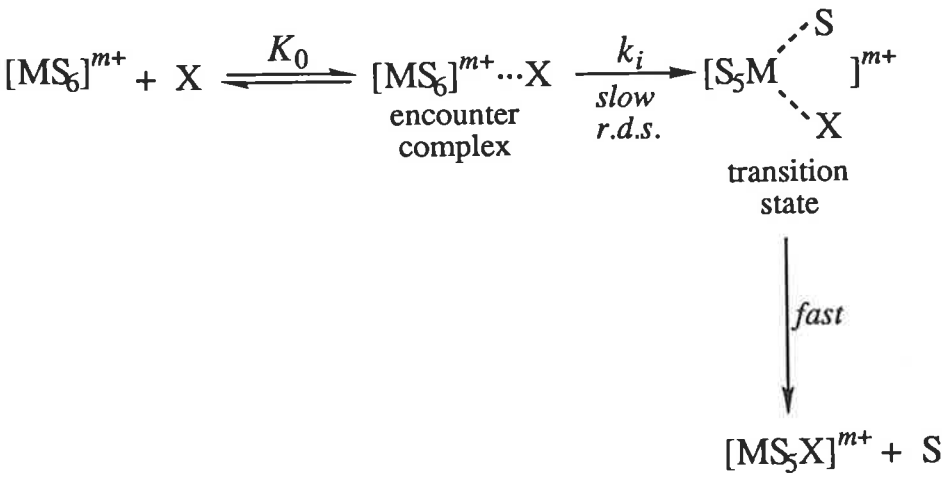

(4.28)

The interchange mechanism category is further subdivided into two groups: associative interchange (I_a) and dissociative interchange (I_d). In an I_d mechanism there is only weak bonding to the incoming and leaving ligands, bond breaking processes dominate the rate determining step and the interchange rate constant, k_i, is independent of the nature of the incoming ligand. Whereas in an I_a mechanism there is considerable bonding to the incoming and leaving ligands, bond making processes dominate the rate determining step and k_i, shows a dependence on the nature of the incoming ligand.

Under the pseudo first order conditions of excess [X], the observed rate constant is defined as:

$$k_{obs} = \frac{k_i K_0[X]}{(1 + K_0[X])} + k_{-i} \qquad (4.28)$$

where k_i is the first order forward interchange rate constant;

K_0 is the stability constant of the encounter complex, and

k_{-i} is the first order interchange rate constant for the reverse reaction.

When $1 \gg K_0[X]$: $k_{obs} \approx k_i K_0[X] + k_{-i}$,

but when $1 \ll K_0[X]$: $k_{obs} \approx k_i + k_{-i}$,

and when $[X] = 0$: $k_{obs} = k_{-i}$ (see Figure 4.9 (c))

Figures 4.9 (a), (b) and (c) show the rate profiles for the associative, dissociative and interchange mechanisms, respectively.

The ligand substitution reactions of the divalent first row transition metal ions have been extensively studied because they usually fall within the stopped-flow and NMR time scales. Merbach *et al* demonstrated, using high pressure NMR methods, that a gradual gradual changeover in mechanism from I_a to I_d occured for solvent exchange on divalent solvated metal ions in going from V^{2+} to Ni^{2+} along the first row transition metal series.[34-38] The trend was rationalized in terms of metal ion atomic d orbital occupancy. For octahedral complexes, in the absence of π bonding, the e_g orbitals are antibonding and the t_{2g} orbitals are nonbonding. From Mn^{2+} to Ni^{2+}, the occupancy of the e_g orbitals remains constant, whereas the occupancy of the t_{2g} orbitals is gradually increased. Thus, the approach of a seventh molecule towards the face of an octahedron becomes less and less electrostatically favourable and may explain the tendency towards more and more dissociative character. However, from V^{2+} to Mn^{2+}, it was supposed that the gradual increase in the antibonding e_g orbital occupancy (t_{2g} orbital occupancy remains constant) would produce a decreased associative character. It has also been demonstrated that a similar changeover in mechanism from I_a to I_d occurs for complex formation reactions on the divalent first row transition metal ions.[37,39-41]

In two recent studies, the complex formation reactions of 2,2'-bipyridine and 2-chloro-1,10-phenanthroline with $[Zn(H_2O)_6]^{2+}$ were both found to proceed via an I_d mechanism.[42,43] The I_d mechanism prevails because the Zn^{2+} ion is

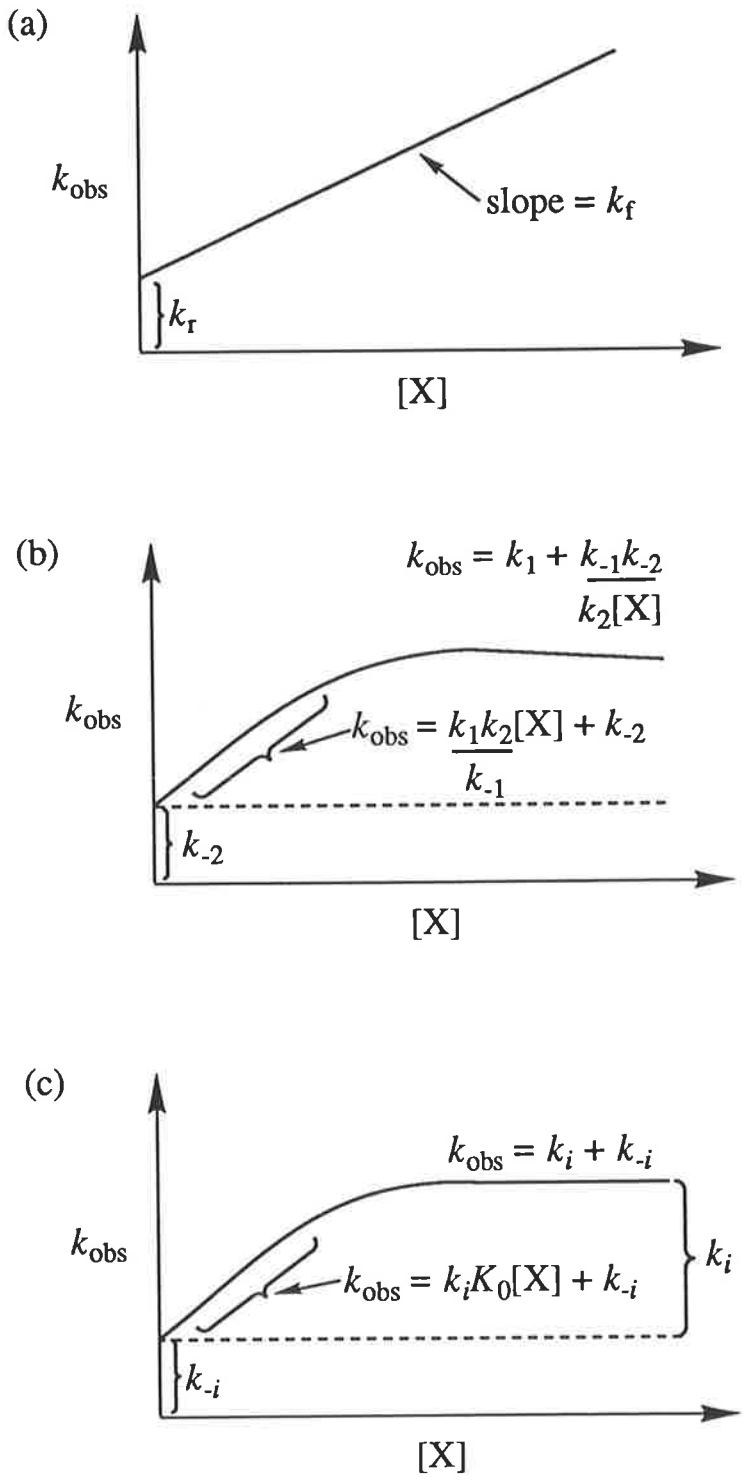

Figure 4.9 *The variation of k_{obs} with [X], which is in excess, in an (a) associative, (b) dissociative and (c) interchange mechanism.*

not large enough to accommodate a seventh molecule at the transition state. Both of these bulky ligands are bidentate, thus complex formation requires an extra coordination step of ring closure. The second coordination or ring closure step is rapid and statistically more probable than the first coordination step. Therefore it is generally considered that the first coordination step is the rate determining step. MTS-QAA is a bulky bidentate ligand which coordinates Zn^{2+} through a -N-C-C-N- structural unit like 2,2'-bipyridine and 2-chloro-1,10-phenanthroline, thus it was anticipated that MTS-QAA substitution on Zn^{2+} may also proceed via an I_d mechanism.

4.4.3 Results and Discussion

4.4.3.1 Acid Catalysed Decomplexation of [Zn.MTS-QAA]

The acid catalysed decomplexation study of [Zn.MTS-QAA] (Equation 4.30) was carried out in 50% ethanol/50% water at 298.2 K and I = 0.10 ($NaClO_4$).

$$[\text{Zn.MTS-QAA}] + H^+ \text{(excess)} \underset{k_{c1}}{\overset{k_{d1}}{\rightleftharpoons}} Zn^{2+} + H_3\text{MTS-QAA}^+ \quad \textbf{(4.30)}$$

For comparison purposes, the acid catalysed decomplexation of [Zn.MTS-QAA] was also examined in 75% ethanol/25% water at 298.2 K and I = 0.10 ($NaClO_4$). To ensure the presence of only the [Zn.MTS-QAA] complex, a twenty times excess [Zn^{2+}] was used in the complex solution. The complex solution comprised 8.028×10^{-4} mol dm^{-3} Zn^{2+}, 4.029×10^{-5} mol dm^{-3} MTS-QAA and 0.10 mol dm^{-3} $NaClO_4$. This complex solution was treated with a series of nine acid solutions ranging in concentration from 0.020 mol dm^{-3} to 0.100 mol dm^{-3}. The [H^+] was in excess to maintain pseudo first order conditions. In addition, the acid solutions contained varying concentrations of $NaClO_4$ to maintain the ionic strength at 0.10. All concentrations given were those prior to the reaction of the complex and acid solutions in the mixing chamber of the stopped-flow fluorimeter.

A typical averaged reaction trace for the acid catalysed decomplexation of [Zn.MTS-QAA] is shown in Figure 4.10. An increase in voltage represents a decrease in fluorescence. The observed pseudo first order rate constant, k_{obs}, deduced by fitting the averaged reaction trace for each pair of solutions in

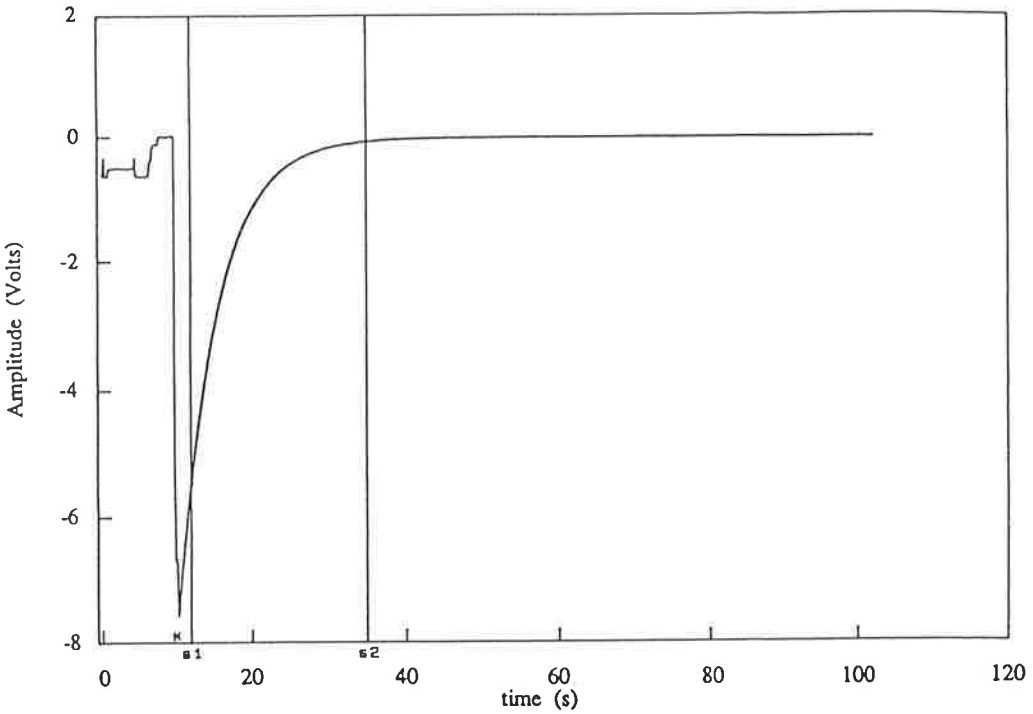

Figure 4.10 *Reaction trace for the acid catalysed decomplexation of [Zn.MTS-QAA] with $[H^+]$ = 0.015 mol dm^{-3} in 50% ethanol/50% water at 298.2 K and I = 0.10 ($NaClO_4$).*

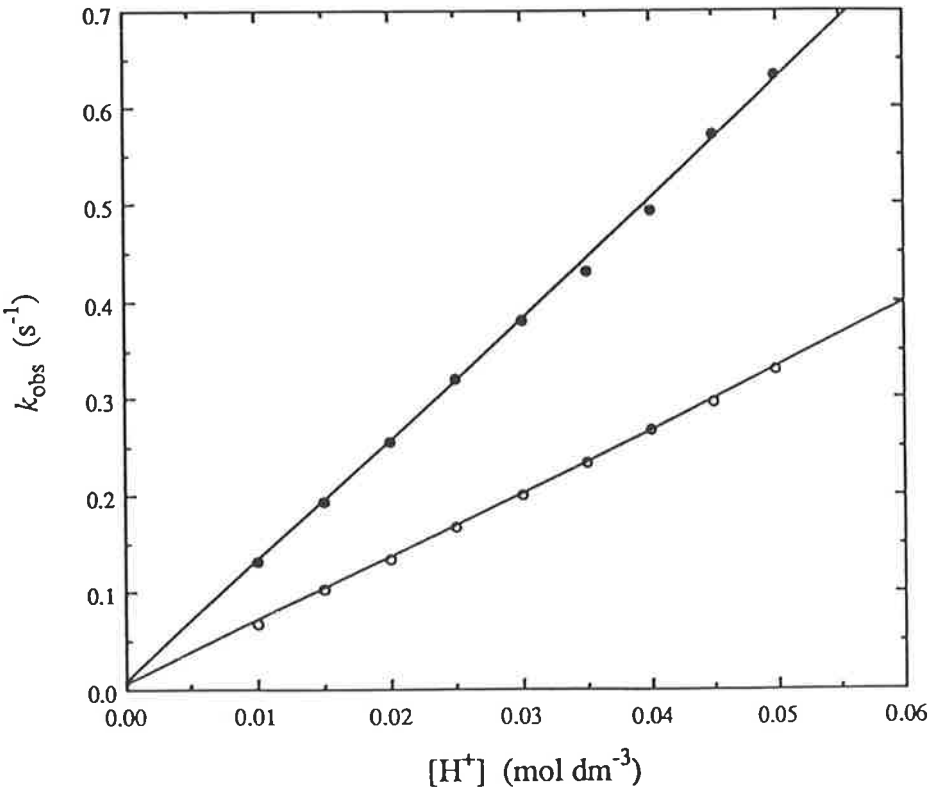

Figure 4.11 *Acid concentration dependence of the observed pseudo first order rate constants, k_{obs}, for the acid catalysed decomplexation of [Zn.MTS-QAA] in 50% ethanol/50% water (•) and 75% ethanol/25% water (°) at 298.2 K and I = 0.10 ($NaClO_4$). The solid curves represent the non-linear least squares fits to Equation 4.31.*

both 50% ethanol/50% water and 75% ethanol/25% water to Equation 4.22 are listed in Table 4.3.

Table 4.3 The observed pseudo first order rate constants, k_{obs}[a], for the acid catalysed decomplexation of [Zn.MTS-QAA] in 50% ethanol/50% water and 75% ethanol/25% water at 298.2 K and I = 0.10 ($NaClO_4$).

$[H^+]$[b] (mol dm^{-3})	k_{obs} 50% ethanol/50% water (s^{-1})	k_{obs} 75% ethanol/25% water (s^{-1})
0.010	0.13	0.07
0.015	0.19	0.10
0.020	0.26	0.14
0.025	0.32	0.17
0.030	0.38	0.20
0.035	0.43	0.23
0.040	0.49	0.27
0.045	0.57	0.30
0.050	0.63	0.33

[a] The individual k_{obs} values have experimental errors within ± 0.1%.

[b] The H^+ concentrations quoted are those in the mixing chamber of the stopped-flow fluorimeter.

From the rate profile in Figure 4.11 it can be seen that k_{obs} has a linear acid dependence in both solvent mixtures. Under the pseudo first order conditions employed, k_{obs} is characterized by:

$$k_{obs} = k_{d1}[H^+] + k_0 \qquad \textbf{(4.31)}$$

The second order acid catalysed decomplexation rate constant, k_{d1}, and the first order uncatalysed decomplexation rate constant, k_0, were determined by fitting the k_{obs} values obtained for each solvent mixture (Table 4.3) to Equation 4.31 using the non-linear, weighted least squares program DATAFIT.[30,31] In 50% ethanol/50% water, k_{d1} = 12.40 ± 0.17 dm^3 mol^{-1} s^{-1} and k_0 = 0.006 ± 0.006 s^{-1}, and in 75% ethanol/50% water, k_{d1} = 6.54 ± 0.04

$dm^3\ mol^{-1}\ s^{-1}$ and $k_0 = 0.004 \pm 0.001\ s^{-1}$. The errors quoted represent one standard deviation. In both solvent mixtures, the value of k_0 was essentially zero within experimental error. This does not mean that k_0 was zero, but that k_0 was too small to be reliably measured by extrapolation. The large shift in equilibrium to the right in Equation 4.30, as a consequence of the excess $[H^+]$ used, was expected to result in very small if not negligible values of k_{c1} in both solvent mixtures. A higher k_{d1} was observed in 50% ethanol/50% water than 75% ethanol/25% water because water ($D_N = 33.0$[44,45]) is a stronger electron donor solvent than ethanol ($D_N = 30.0$[45]). Hence, the solvent mixture containing more water is able to compete more with the ligand for the Zn^{2+} ions. A similar acid catalysed decomplexation stopped-flow fluorescence study of $[Zn.TS\text{-}Q]^+$ in 75% ethanol/25% water yielded $k_{d1} = 2.19 \times 10^4\ dm^3\ mol^{-1}\ s^{-1}$ and $k_0 \approx 0\ s^{-1}$.[23] The difference between the two sulfonamidoquinoline ligands is that MTS-QAA possesses two electron donating groups, namely $-CH_3$ and $-OCH_2COOH$, on the quinoline moiety. These electron donating groups increase the basicity of the quinoline nitrogen and bring about greater binding of the Zn^{2+} ion. The overall effect on the kinetics is a lower k_{d1} value for [Zn.MTS-QAA].

A possible mechanism for the acid catalysed decomplexation of [Zn.MTS-QAA] is illustrated in Figure 4.12. The first step involves the protonation of the most acidic nitrogen atom, the amide nitrogen, at a diffusion-controlled rate to form a reactive intermediate. The amide nitrogen atom in the reactive intermediate must posses a tetrahedral arrangement of atoms about its centre. This is probably an unfavourable arrangement of atoms about the amide nitrogen as it is known from the [Cu.TS-Q_2] crystal structure that the stereochemistry about both of the amide nitrogens is between tetrahedral and trigonal planar, almost trigonal planar.[26] Furthermore, the crystal structure of the closely related sulfonamidoquinoline ligand 2-methyl-6-hydroxy-8-(*p*-toluenesulfonamido)quinoline (MHTS-Q) in the uncomplexed form also exhibited a stereochemistry between tetrahedral and trigonal planar (almost trigonal planar) about the amide nitrogen.[26] From these crystal structures, it can be concluded that the amide nitrogen atoms in sulfonamidoquinoline ligands prefer an almost trigonal planar arrangement of atoms about their centres. It also implies that the non bonding, lone pair of electrons on the amide nitrogens (contained in a *p* orbital) have a tendency to become delocalized in the molecules. Hence, an extention of the conjugated systems occurs with the delocalization of the amide nitrogen lone pair of

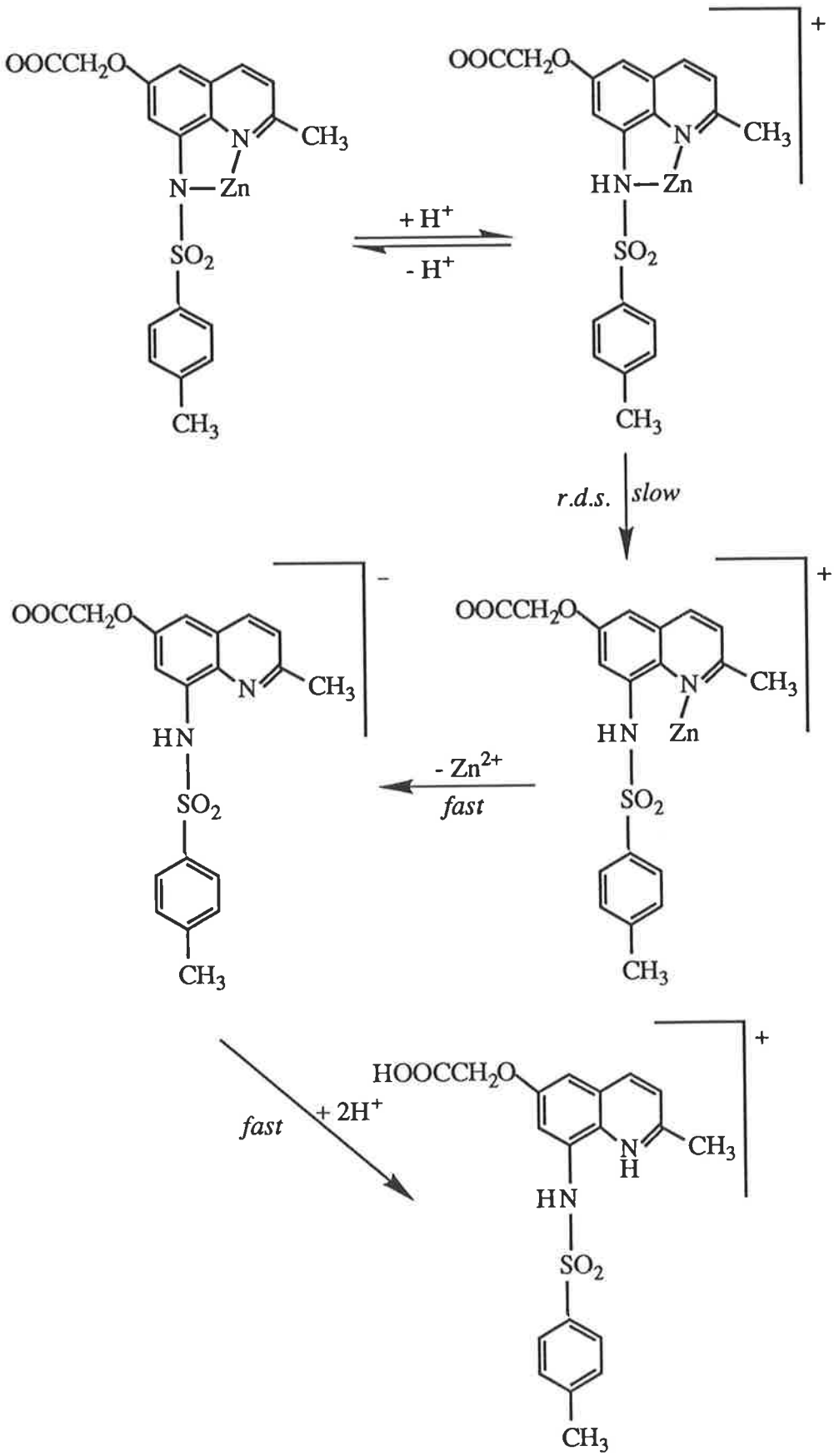

Figure 4.12 *The proposed mechanism for the acid catalysed decomplexation of [Zn.MTS-QAA].*

electrons. The second step in the mechanism therefore involves the cleavage of the amide nitrogen to Zn^{2+} bond such that the stereochemistry about the amide nitrogen atom becomes trigonal planar again. Subsequent steps involve the cleavage of the quinolinium nitrogen to Zn^{2+} bond and the further protonation of the ligand. On the basis of the data obtained by stopped-flow fluorescence it is not possible to rule out other alternative mechanisms in which simultaneous protonation and bond cleavage occurs. The principle of microscopic reversibility states that the forward and reverse reactions follow the same path but in opposite directions. Thus, the third step of cleavage of the second ligand to Zn^{2+} bond might be expected to be the rate determining step since the first coordination of a bidentate ligand in complex formation is generally considered to be the rate determining step. However, from the formation kinetics of [Zn.MTS-QAA], discussed later, it can be seen that the second step of ring closure must be the rate determining step.

4.4.3.2 Acid Catalysed Decomplexation of $[Zn.MTS\text{-}QAA_2]^{2-}$

The acid catalysed decomplexation of $[Zn.MTS\text{-}QAA_2]^{2-}$ (Equation 4.32) was studied in 50% ethanol/50% water at 298.2 K and $I = 0.10$ ($NaClO_4$). The excess acid solutions were the same as those used in the acid catalysed decomplexation of [Zn.MTS-QAA]. However, the complex solution in this case comprised 2.007×10^{-5} mol dm^{-3} Zn^{2+}, 4.029×10^{-4} mol dm^{-3} MTS-QAA and 0.10 mol dm^{-3} $NaClO_4$. A twenty times excess of ligand was necessary to ensure the presence of only the $[Zn.MTS\text{-}QAA_2]^{2-}$ complex. All concentrations given were those prior to the reaction of the complex and acid solutions in the mixing chamber of the stopped-flow fluorimeter.

$$[Zn.MTS\text{-}QAA_2]^{2-} + H^+ \text{ (excess)} \underset{k_c}{\overset{k_d}{\rightleftharpoons}} Zn^{2+} + 2H_3MTS\text{-}QAA^+ \quad \textbf{(4.32)}$$

The reaction traces for the acid catalysed decomplexation of $[Zn.MTS\text{-}QAA_2]^{2-}$ appeared as single exponentials (Figure 4.13) and were virtually identical to the analogous reaction traces for the acid catalysed decomplexation of [Zn.MTS-QAA] (Figure 4.10). Table 4.4 lists the k_{obs} values obtained by fitting the reaction traces to Equation 4.22.

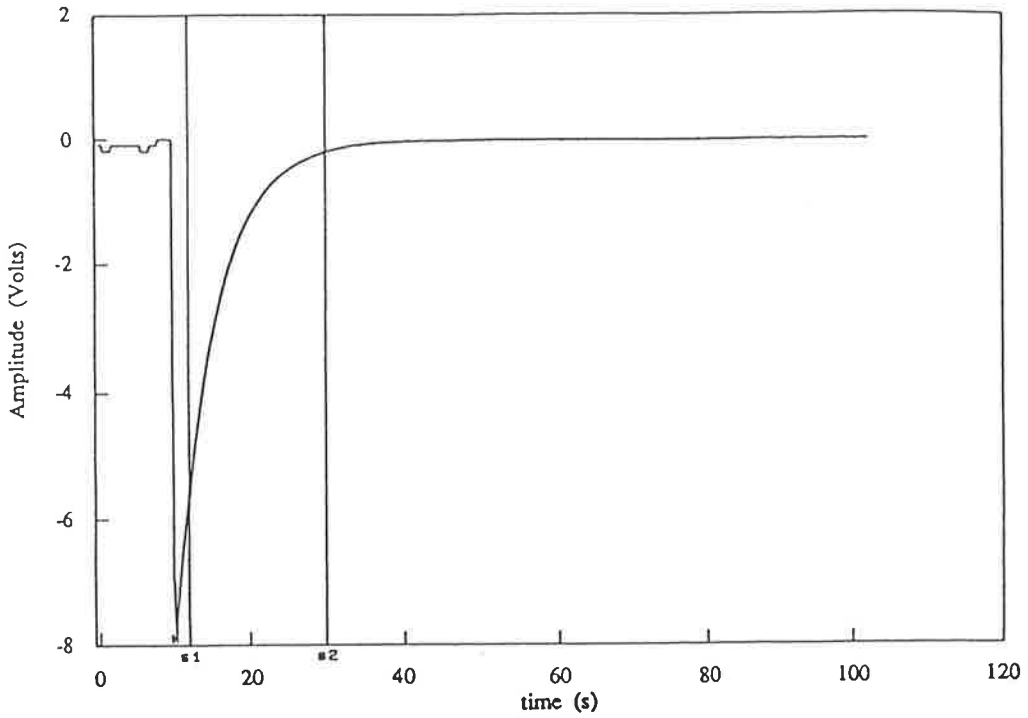

Figure 4.13 *Reaction trace for the acid catalysed decomplexation of $[Zn.MTS\text{-}QAA_2]^{2-}$ with $[H^+]$ = 0.015 mol dm^{-3} in 50% ethanol/50% water at 298.2 K and I = 0.10 ($NaClO_4$).*

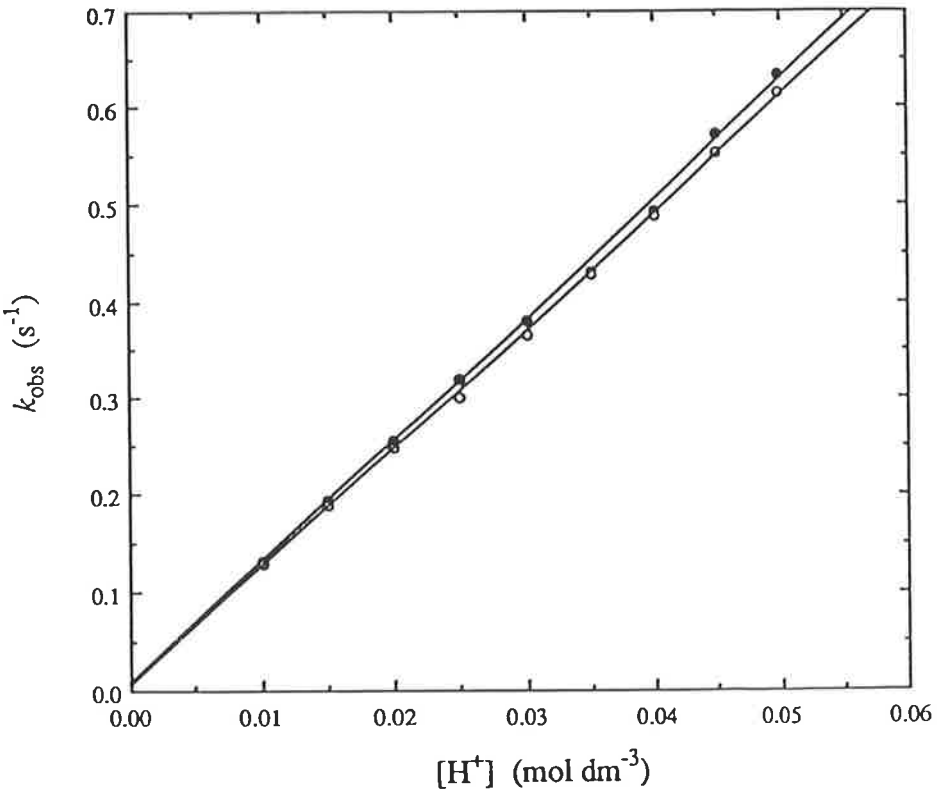

Figure 4.14 *Acid concentration dependence of the observed pseudo first order rate constants, k_{obs}, for the acid catalysed decomplexation of $[Zn.MTS\text{-}QAA_2]^{2-}$ (°) and [Zn.MTS-QAA] (•) in 50% ethanol/50% water at 298.2 K and I = 0.10 ($NaClO_4$). The solid curves represent the non-linear least squares fits to Equation 4.33.*

Table 4.4 The observed pseudo first order rate constants, k_{obs}[a], for the acid catalysed decomplexation of $[Zn.MTS\text{-}QAA_2]^{2-}$ in 50% ethanol/50% water at 298.2 K and I = 0.10 ($NaClO_4$).

$[H^+]$[b] (mol dm^{-3})	k_{obs} 50% ethanol/50% water (s^{-1})
0.010	0.13
0.015	0.19
0.020	0.25
0.025	0.30
0.030	0.37
0.035	0.43
0.040	0.49
0.045	0.55
0.050	0.62

[a] The individual k_{obs} values have experimental errors within ± 0.1%.

[b] The H^+ concentrations quoted are those in the mixing chamber of the stopped-flow fluorimeter.

Figure 4.14 illustrates the linear variation of k_{obs} with $[H^+]$ for the acid catalysed decomplexation of $[Zn.MTS\text{-}QAA_2]^{2-}$ and its similarity with that of the acid catalysed decomplexation of [Zn.MTS-QAA]. Under the pseudo first order conditions of excess $[H^+]$, k_{obs} is characterized by:

$$k_{obs} = k_d[H^+] + k_{0'} \qquad \textbf{(4.33)}$$

Non-linear, weighted least squares fitting[30,31] of the data in Table 4.4 to Equation 4.33 produced the second order acid catalysed decomplexation rate constant, k_d = 12.12 ± 0.10 dm^3 mol^{-1} s^{-1}, and the first order uncatalysed decomplexation rate constant, $k_{0'}$ = 0.004 ± 0.003 s^{-1}. The errors quoted represent one standard deviation. The value of $k_{0'}$ was essentially zero within experimental error because it was too small to be reliably measured by extrapolation.

Equation 4.32 may be rewritten as two stepwise equations:

$$[Zn.MTS\text{-}QAA_2]^{2-} + H^+ \text{ (excess)} \underset{k_{c2}}{\overset{k_{d2}}{\rightleftharpoons}} [Zn.MTS\text{-}QAA] + H_3MTS\text{-}QAA^+ \quad \textbf{(4.34)}$$

$$[Zn.MTS\text{-}QAA] + H^+ \text{ (excess)} \underset{k_{c1}}{\overset{k_{d1}}{\rightleftharpoons}} Zn^{2+} + H_3MTS\text{-}QAA^+ \quad \textbf{(4.35)}$$

Only one of these decomplexation processes was observed in the acid catalysed decomplexation of $[Zn.MTS\text{-}QAA_2]^{2-}$ because the reaction traces showed only a single exponential, consistent with the observation of only one process. Furthermore, since the decomplexation rate constant for the acid catalysed decomplexation of $[Zn.MTS\text{-}QAA_2]^{2-}$, k_d, was virtually identical to that of the acid catalysed decomplexation of [Zn.MTS-QAA], k_{d1}, and since the fluorescence decrease in both the acid catalysed decomplexation of [Zn.MTS-QAA] and $[Zn.MTS\text{-}QAA_2]^{2-}$ were virtually identical, it is highly likely that the same process was observed in both kinetic studies ie. that described in Equation 4.35. This can occur if the decomplexation process described in Equation 4.34 was too rapid to be observed by the stopped-flow fluorimeter. Application of a very small time sweep did not reveal any other decomplexation process. The decomplexation process described in Equation 4.34 may in fact be so rapid that it occurs in the deadtime of the stopped-flow fluorimeter (ie. time of the manual push plus the allowed delay time, 100 ms). A 35% smaller decrease in fluorescence is expected for the decomplexation process described in Equations 4.34 than the decomplexation process described in Equation 4.35 (see section 4.3.2). However, the decrease in fluorescence characterized by k_{d2} is not small enough to be masked by the decrease in fluorescence characterized by k_{d1}. Alternatively, if $k_{d2} \approx k_{d1}$, then the decrease in fluorescence observed would be due to the sequential decomplexation of $[Zn.MTS\text{-}QAA_2]^{2-}$ and thus, k_d would be a composite decomplexation rate constant incorporating both of the sequential decomplexation rate constants, k_{d2} and k_{d1}. This is the least likely scenario because k_{d2} and k_{d1} characterize two different chemical environments in $[Zn.MTS\text{-}QAA_2]^{2-}$ and [Zn.MTS-QAA], respectively. The greater electrostatic attraction between $[Zn.MTS\text{-}QAA_2]^{2-}$ and H^+ than [Zn.MTS-QAA] and H^+ may give rise to a larger k_{d2} than k_{d1}.

4.4.3.3 Formation of [Zn.MTS-QAA]

The formation of [Zn.MTS-QAA] (Equation 4.36) was examined in 50% ethanol/50% water at pH 6.6, 298.2 K and I = 0.10 ($NaClO_4$). A ligand solution containing 4.029×10^{-5} mol dm^{-3} MTS-QAA, 1.00×10^{-3} mol dm^{-3} NaPIPES and 0.10 mol dm^{-3} $NaClO_4$ was mixed with a series of eleven Zn^{2+} solutions of varying [Zn^{2+}]. The Zn^{2+} solutions had a [Zn^{2+}] range of 8.028×10^{-4} mol dm^{-3} to 1.204×10^{-2} mol dm^{-3} and they also contained 1.00×10^{-3} mol dm^{-3} NaPIPES and 0.10 mol dm^{-3} $NaClO_4$. At pH 6.6, all of the ligand was in the HMTS-QAA$^-$ form. Under the pseudo first order conditions of a twenty to three hundred times excess [Zn^{2+}], predominantly [Zn.MTS-QAA] was formed. The concentrations quoted are those prior to the reaction of the ligand and Zn^{2+} solutions in the mixing chamber of the stopped-flow fluorimeter.

$$Zn^{2+} + \text{HMTS-QAA}^- \underset{k_r}{\overset{k_f}{\rightleftharpoons}} [\text{Zn.MTS-QAA}] + H^+ \qquad \textbf{(4.36)}$$

A typical averaged reaction trace for the formation of [Zn.MTS-QAA] is shown in Figure 4.15. A decrease in voltage represents an increase in fluorescence. It is quite apparent from this reaction trace that two processes occurred. Initially, a rapid process characterized by a large increase in fluorescence occured followed by a slower process characterized by a small decrease in fluorescence. The initial rapid process corresponds to the formation of [Zn.MTS-QAA]. Whereas the later slower process may be the result of the formation of a small amount of $[Zn.MTS\text{-}QAA_2]^{2-}$. Using MACSPECIES[29], it was found that under the experimental condition used between 1% and 6% of the total ligand forms $[Zn.MTS\text{-}QAA_2]^{2-}$. From the fluorescence study in section 4.3 it is known that a ligand molecule in [Zn.MTS-QAA] fluoresces 36% more than a ligand molecule in $[Zn.MTS\text{-}QAA_2]^{2-}$. However, conversion of two [Zn.MTS-QAA] complexes into one $[Zn.MTS\text{-}QAA_2]^{2-}$ complex actually results in a 27% decrease in fluorescence. Thus, the formation of a small amount of $[Zn.MTS\text{-}QAA_2]^{2-}$ would result in an overall decrease in fluorescence. An alternative explanation for the later slower process may be that the [Zn.MTS-QAA] complex undergoes an octahedral-tetrahedral structural change. If a structurally less rigid complex is formed upon conversion of octahedral $[(H_2O)_4Zn.MTS\text{-}QAA]$ to tetrahedral $[(H_2O)_2Zn.MTS\text{-}QAA]$, then the

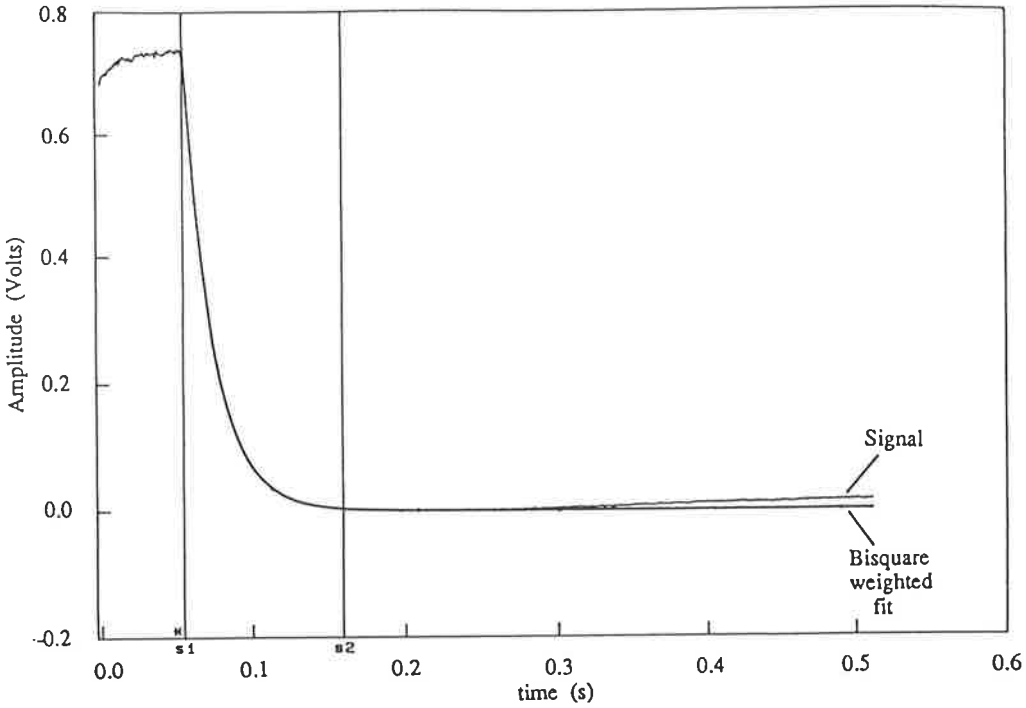

Figure 4.15 *Reaction trace for the formation of [Zn.MTS-QAA] in 50% ethanol/50% water at 298.2 K and I = 0.10 ($NaClO_4$). The $[Zn^{2+}] = 5.018 \times 10^{-3}$ mol dm^{-3} and the [MTS-QAA] = 2.014×10^{-5} mol dm^{-3} in the mixing chamber of the stopped-flow fluorimeter.*

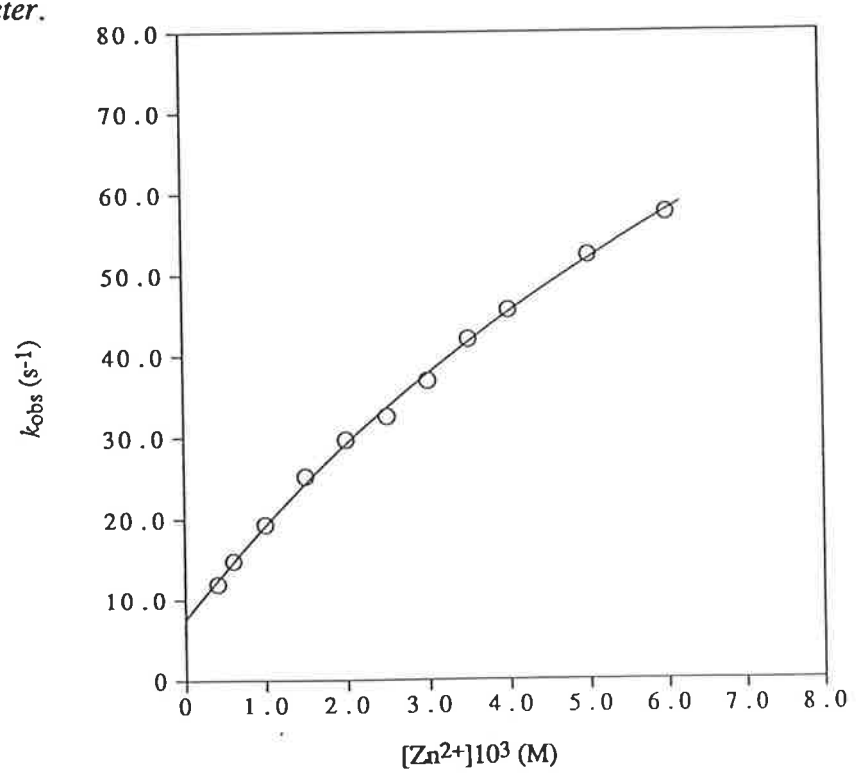

Figure 4.16 *Zn^{2+} concentration dependence of the observed pseudo first order rate constants, k_{obs}, for the formation of [Zn.MTS-QAA] in 50% ethanol/50% water at pH 6.6, 298.2 K and I = 0.10 ($NaClO_4$). The solid curve represents the non-linear least squares fit to Equation 4.37.*

amount of vibrational relaxation would be expected to be increased, and in turn a decrease in fluorescence would be expected to be observed. A temperature-jump relaxation study was carried out on the Zn^{2+}-chlorophenol red system in an attempt to detect an octahedral-tetrahedral equilibrium for the Zn^{2+} aquo ion.[46] However, no evidence for tetrahedral $[Zn(H_2O)_4]^{2+}$ was found, and it was concluded that Zn^{2+} assumes a tetrahedral arrangement only after two or more sites are occupied by ligands other than water.

Bisquare weighted least squares fitting of the exponential corresponding to the formation of [Zn.MTS-QAA] only (denoted by two vertical lines in Figure 4.15) to Equation 4.22 yielded the pseudo first order rate constants, k_{obs}, listed in Table 4.5.

Table 4.5 The observed pseudo first order rate constants, k_{obs}, for the formation of [Zn.MTS-QAA] in 50% ethanol/50% water at pH 6.6, 298.2 K and $I = 0.10$ ($NaClO_4$).

$[Zn^{2+}]$ *a* (mol dm^{-3})	k_{obs} (s^{-1})
4.014×10^{-4}	11.95 ± 0.01
6.021×10^{-4}	14.85 ± 0.03
1.004×10^{-3}	19.34 ± 0.02
1.505×10^{-3}	25.17 ± 0.05
2.007×10^{-3}	29.64 ± 0.04
2.509×10^{-3}	32.52 ± 0.04
3.011×10^{-3}	36.92 ± 0.05
3.512×10^{-3}	41.98 ± 0.07
4.014×10^{-3}	45.55 ± 0.03
5.018×10^{-3}	52.38 ± 0.06
6.021×10^{-3}	57.57 ± 0.06

a The Zn^{2+} concentrations quoted are those in the mixing chamber of the stopped-flow fluorimeter.

A plot illustrating k_{obs} as a function of $[Zn^{2+}]$ is shown in Figure 4.16. The shape of this curve and the knowledge that the divalent first row transition

metal ions generally form complexes via interchange mechanisms is evidence that [Zn.MTS-QAA] complex formation probably also proceeds via an interchange mechanism (see Figure 4.9 (c)). From the rate profile alone, it is not possible to predict whether the interchange mechanism is I_a or I_d. However, it has been shown that Zn^{2+} complexation kinetics favour an I_d mechanism.[42,43]

A proposed mechanism for the complexation of $[Zn(H_2O)_6]^{2+}$ by HMTS-QAA$^-$ is illustrated in Figure 4.17. The oppositely charged species associate in an encounter complex at a diffusion-controlled rate. This is followed by the rate determining interchange of a water molecule with the incoming HMTS-QAA$^-$ ligand. The formation of the first coordinate bond involves the quinolinium nitrogen atom because the lone pair of electrons on this nitrogen atom are more readily available for bonding than those on the amide nitrogen atom. Those electrons are thought to be involved in extending the conjugated system by becoming delocalized in the ligand molecule. Finally, the last step involves rapid formation of the second coordinate bond or ring closure.

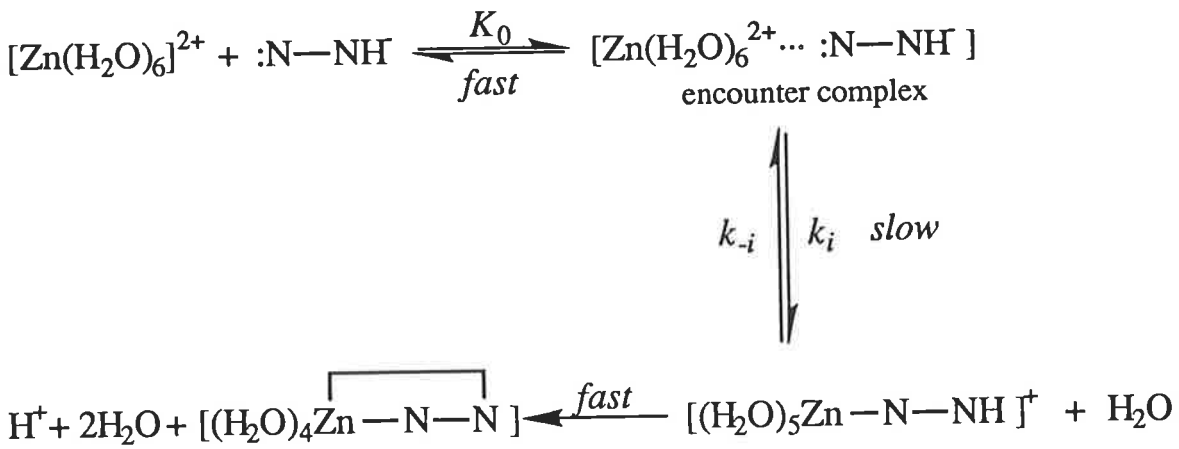

Figure 4.17 *A proposed mechanism for the formation of [Zn.MTS-QAA]. The HMTS-QAA$^-$ is represented by its coordinating quinolinium and amide nitrogen atoms and the only bound amide proton.*

Under the pseudo first order conditions of excess $[Zn^{2+}]$, k_{obs} is characterized by:

$$k_{obs} = \frac{k_i K_0 [Zn^{2+}]}{1 + K_0 [Zn^{2+}]} + k_{-i} \qquad (4.37)$$

where k_i is the complexation interchange rate constant;

K_0 is the stability complex of the encounter complex, and

k_{-i} is the interchange rate constant for the decomplexation reaction.

Non-linear, weighted least squares fitting[30,31] of the data in Table 4.5 to Equation 4.37 yielded $k_i = 149 \pm 15\ s^{-1}$, $K_0 = 85 \pm 13\ dm^3\ mol^{-1}$ and $k_{-i} = 7.5 \pm 0.7\ s^{-1}$. It can be seen that the derived k_{-i} value was much larger than the uncatalysed decomplexation rate constant, k_0, derived from the acid catalysed decomplexation of [Zn.MTS-QAA]. The extrapolated uncatalysed decomplexation rate constant of [Zn.MTS-QAA], k_0, obtained from the acid catalysed decomplexation of [Zn.MTS-QAA] (see Figure 4.11) was considered to be more accurate than the extrapolated k_{-i} value obtained from the formation of [Zn.MTS-QAA] (see Figure 4.16) as it was extrapolated from a linear variation of k_{obs}. Therefore, since k_0 was essentially zero, the data in Table 4.5 was refitted to Equation 4.37 with k_{-i} set to zero (Figure 4.18). This yielded $k_i = 96 \pm 9\ s^{-1}$ and $K_0 = 231 \pm 40\ dm^3\ mol^{-1}$. The errors given represent one standard deviation.

The derived K_0 value was much larger than any K_0 value quoted in the literature for Zn^{2+} encounter complexes.[43,47-49] In general, K_0 is not a measurable parameter but it has been regularly calculated by using the Fuoss equation[50]:

$$K_0 = \frac{4\pi N_A a^3}{3000} e^{-b}.\exp\left\{\frac{b\kappa a}{(1+\kappa a)}\right\} \qquad \textbf{(4.38)}$$

where $$b = \frac{z_M z_L e_0^2}{a \in k_B T}$$

$$\kappa^2 = \frac{8\pi N_A e_0^2}{1000 \in k_B T}.I$$

and where N_A is Avogadro's number;

a is the centre to centre distance between the solvated metal ion and the ligand at the point of closest approach (cm);

z_M, z_L are the formal charges on the reacting species;

e_0 is the electronic charge (esu);

$\in$ is the dielectric constant of the solvent;

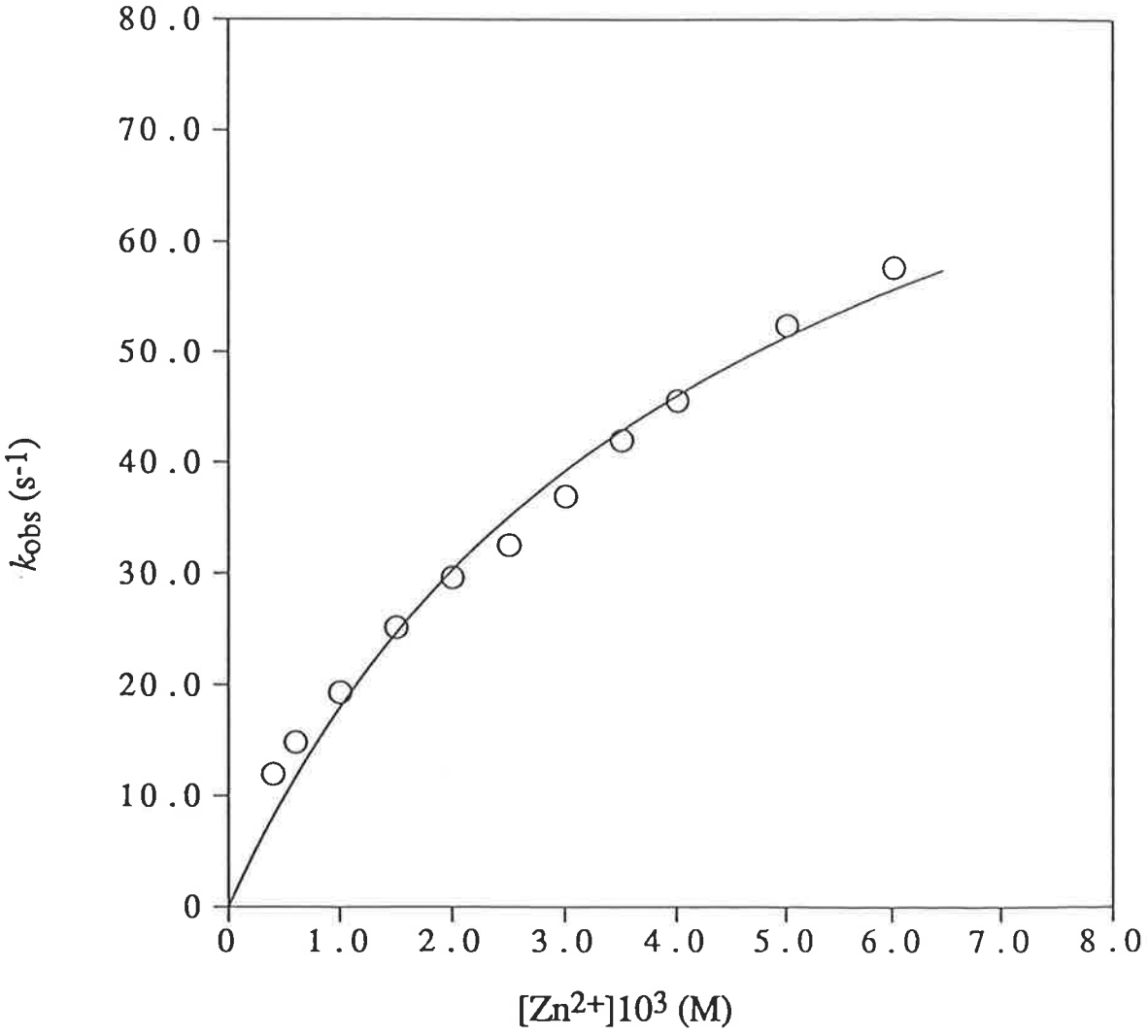

Figure 4.18 *Zn^{2+} concentration dependence of the observed pseudo first order rate constants, k_{obs}, for the formation of [Zn.MTS-QAA] in 50% ethanol/50% water at pH 6.6, 298.2 K and I = 0.10 ($NaClO_4$) when k_{-i} (intercept) = 0. The solid curve represents the non-linear least squares fit to Equation 4.37.*

k_B is Boltzmann's constant (ergs);

T is the absolute temperature (K);

κ is the Debye-Hückel ion atmosphere parameter, and

I is the ionic strength of the solution.

Fuoss derived this model equation on the basis of statistical arguments[50] and Eigen derived a similar equation on the basis of the theory of diffusion.[51] This equation should only be used to calculate K_0 values for ion-pair formation since he treats the metal ion and ligand as charged point spheres in a dielectric continuum. Application of the Fuoss equation to reactions between metal ions and neutral or unsymmetrical ligands is highly speculative. Nevertheless, using the Fuoss equation to calculate K_0 for the encounter complex formed between solvated Zn^{2+} and the unsymmetrical ligand HMTS-QAA$^-$ yielded $K_0 = 2.35$ dm^3 mol^{-1}. The dielectric constant of water ($\epsilon = 78.54$) and an estimated distance of closest approach of 6 Å were used in the calculation. Since the formation of [Zn.MTS-QAA] was studied in a 50% ethanol/50% water solvent mixture and since the electron donating strength of water ($D_N = 33.0$[44,45]) and ethanol ($D_N = 30.0$[45]) do not differ greatly, both ethanol and water molecules were expected to occupy the sites in the first coordination sphere of Zn^{2+}. Although ethanol and water are probably both present in the first coordination sphere of Zn^{2+} in this study, all kinetic comparisons are made with the lability of water as generally this is the most labile solvent bound to a metal ion.[34]

The second order formation rate constant, k_f, may be derived through:

$$k_f = K_0 k_i \qquad \textbf{(4.39)}$$

Using $K_0 = 231 \pm 40$ dm^3 mol^{-1} and $k_i = 96 \pm 9$ s^{-1} gave $k_f = (2.2 \pm 0.6) \times 10^4$ dm^3 mol^{-1} s^{-1}. This estimated value of k_f was much smaller than the k_f values quoted for Zn^{2+} complexation by other large bidentate nitrogen donor ligands in the literature (by a factor of 10^2).[42,43,52] The first order interchange rate constant, k_i, rather than the second order formation rate constant, k_f, should be compared to the first order water exchange rate constant, k_{ex}. k_i is directly related to k_{ex} through:

$$k_i = F k_{ex} \qquad \textbf{(4.40)}$$

where F is a statistical factor, usually less than one.[53,54] The F factor allows for the competition between solvent molecules in the second coordination sphere with the incoming HMTS-QAA$^-$ ligand for the developing vacancy in the first coordination sphere of Zn^{2+}. A value for the rate of water exchange on Zn^{2+} has not been directly determined yet. However, a limit of 3×10^7 s^{-1} $< k_{ex} < 6 \times 10^8$ s^{-1} has been estimated for the rate of water exchange on Zn^{2+} at 298.2 K from the study of a simple complexation reaction on Zn^{2+}.[43] Using this limit for k_{ex} and the derived value of k_i yielded a limit of 2×10^{-7} $< F < 4 \times 10^{-6}$ for F. These extremely low values of F imply that the ligand has a very low likelihood of moving from the second coordination sphere into the vacancy in the first coordination sphere of Zn^{2+} created by the dissociation of a water molecule. A small F value was anticipated because of the large nature of HMTS-QAA$^-$ and the steric hindrance problems which arise because of it. Even so, the estimated F values were much smaller than expected.

If formation of the first coordinate bond was the rate determining step, as shown in Figure 4.17, then k_i should be approximately equal to k_{ex} (within a factor of 10 has been considered adequate due to the uncertainty in F). Since $k_i \ll k_{ex}$, this cannot be the case here. The most likely explanation for the slow rate is that ring closure or formation of the second coordinate bond is the rate determining step. A mechanism illustrating this is shown in Figure 4.19.

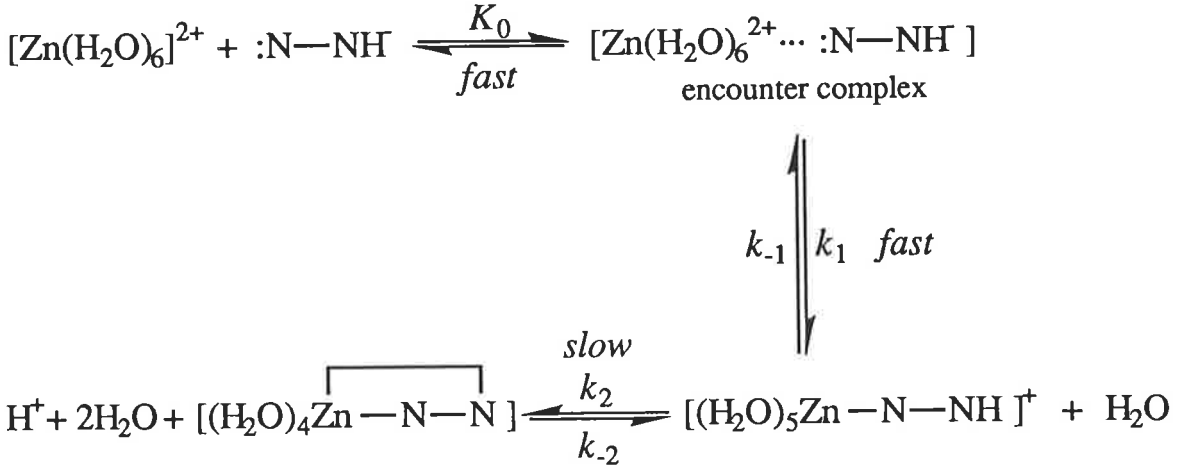

Figure 4.19 *The proposed mechanism for [Zn.MTS-QAA] formation.*

Steric hindrance upon formation of the second coordinate bond may be large enough to make ring closure rate determining. The presence of a proton on the amide nitrogen is unlikely to provide a significant amount of steric hindrance, whereas the -SO_2- group may. However, the amide proton must be

displaced upon the formation of the second coordinate bond. Furthermore, the electrostatic attraction between the solvated Zn^{2+} and HMTS-QAA$^-$ may be large enough to make the first coordination step faster than the second coordination step.

Upon taking $[(H_2O)_5Zn\text{-}N\text{-}NH]^+$ (see Figure 4.19) as a steady state intermediate, the observed pseudo first order rate constant, k_{obs}, is now characterized by:

$$k_{obs} = \frac{k_1 k_2}{k_{-1} + k_2}\left(\frac{K_0[Zn^{2+}]}{1 + K_0[Zn^{2+}]}\right) + \frac{k_{-1}k_{-2}}{k_{-1} + k_2}[H^+] \qquad \textbf{(4.41)}$$

If ring closure is rate determining, $k_2 \ll k_{-1}$, and therefore k_{obs} is characterized by:

$$k_{obs} = \frac{k_1 k_2 K_0[Zn^{2+}]}{k_{-1}(1 + K_0[Zn^{2+}])} + k_{-2}[H^+] \qquad \textbf{(4.42)}$$

By comparing Equation 4.41 to Equation 4.37 it can be seen that $k_1k_2/k_{-1} = 96 \pm 9$ s^{-1} and $K_0 = 231 \pm 40$ dm^3 mol^{-1} when $k_{-2}[H^+] = 0$.

References

1 R.J.P. Williams, *Endeavour, New Series*, **8**, 1984, 65.

2 C.J. Frederickson, *Int. Rev. Neurobiol.*, **31**, 1989, 145.

3 P.D. Zalewski, I.J. Forbes and C. Giannakis, *Biochem. Internat.*, **24**, 1991, 1093.

4 X. Xie and T.G. Smart, *Nature*, **349**, 1991, 521.

5 T.J.B. Simons, *J. Membrane Biol.*, **123**, 1991, 63.

6 R.Y. Tsien, T. Pozzan and T.J. Rink, *J. Cell Biol.*, **94**, 1982, 325.

7 M. Wahl, M.J. Lucherini and E. Gruenstein, *Cell Calcium*, **11**, 1990, 487.

8 R.G. Pearson, *J. Am. Chem. Soc.*, **85**, 1963, 3533.

9 R.G. Pearson, *Coord. Chem. Rev.*, **100**, 1990, 403.

10 D. Dakternieks, *Coord. Chem. Rev.*, **62**, 1985, 1.

11 D. Dakternieks, *Coord. Chem. Rev.*, **78**, 1987, 125.

12 M. Kodama and E. Kimura, *J. Chem. Soc., Dalton Trans.*, 1977, 2269.

13 D. Schacter, *J. Lab. Clin. Med.*, **54**, 1959, 763.

14 S. Watanabe, W. Frantz and D. Trottier, *Anal. Biochem.*, **5**, 1963, 345.

15 D. Mahanand and J.C. Houck, *Clin. Chem.*, **14**, 1968, 6.

16 G.L. Smith, R.A. Jenkins and J.F.Gough, *J. Histochem. Cytochem.*, **17**, 1969, 749.

17 C.J. Frederickson, E.J. Kasarskis, D. Ringo and R.E. Frederickson, *J. Neurosci. Methods*, **20**, 1987, 91.

18 D.D. Savage, C.Y. Montano and E.J. Kasarskis, *Brain Res.*, **496**, 1989, 257.

19 J.H. Billman and R. Chernin, *Anal. Chem.*, **34**, 1962, 408.

20 H. Nakamura, T. Yoshida, M. Todoko, K. Ueno and M. Takagi, *Bull. Chem. Soc. Jpn.*, **57**, 1984, 2839.

21 K.M. Mackay and R.A. Mackay, "Introduction to Modern Inorganic Chemistry", Intertext Books, London, 2nd Edn., 1973.

22 J.-M. Lehn and J.-P. Sauvage, *J. Am. Chem. Soc.*, **97**, 1975, 6700.

23 C. Haskard, Honours Dissertation, University of Adelaide, 1991.

24 H. Irving and R.J.P. Williams, *Nature (London)*, **162**, 1948, 746.

25 H. Irving and R.J.P. Williams, *J. Chem. Soc.*, 1953, 3182.

26 I. Mahadevan and E.R.T. Tiekink, Unpublished results.

27 G.D. Christian and J.E. O'Reilly, "Instrumental Analysis", Allyn and Bacon, Inc., Boston, 2nd Edn., 1986.

28 D.A. Skoog, "Principles of Instrumental Analysis", CBS Publishing, Philadelphia, 3rd Edn., 1985.

29 MACSPECIES is the Macintosh version of the species distribution program written by R.J. Motekaitis, Texas A & M University. The Macintosh version is by P.A. Duckworth, University of Adelaide.

30 T. Kurucsev, Unpublished material, University of Adelaide, 1990.

31 T. Kurucsev, *J. Chem. Educ.*, **55**, 1978, 128.

32 J.E. Erman and G.G. Hammes, *Rev. Sci. Instrum.*, **37**, 1966, 746.

33 C.H. Langford and H.B. Gray, "Ligand Substitution Processes", W.A. Benjamin, New York, 1966.

34 A. Merbach, *Pure Appl. Chem.*, **54**, 1982, 1479.

35 Y. Ducommun, K.E. Newman and A.E. Merbach, *Helv. Chim. Acta*, **62**, 1979, 2511.

36 F.K. Meyer, K.E. Newman and A.E. Merbach, *J. Am. Chem. Soc.*, **101**, 1979, 5588.

37 Y. Ducommun, K.E. Newman and A.E. Merbach, *Inorg. Chem.*, **19**, 1980, 3696.

38 Y. Ducommun, D. Zbinden and A.E. Merbach, *Helv. Chim. Acta*, **65**, 1982, 1385.

39 P.J. Nichols, Y. Ducommun and A.E. Merbach, *Inorg. Chem.*, **22**, 1983, 3993.

40 R. Doss and R. van Eldik, *Inorg. Chem.*, **21**, 1982, 4108.

41 R. Mohr and R. van Eldik, *Inorg. Chem.*, **24**, 1985, 3396.

42 Y. Ducommun, G. Laurenczy and A.E. Merbach, *Inorg. Chem.*, **27**, 1988, 1148.

43 G. Laurenczy, Y. Ducommun and A.E. Merbach, *Inorg. Chem.*, **28**, 1989, 3024.

44 R.H. Erlich, E. Roach and A.I. Popov, *J. Am. Chem. Soc.*, **92**, 1970, 4989.

45 W.J. DeWitte and A.I. Popov, *J. Solution Chem.*, **5**, 1976, 231.

46 J. Bidwell and J. Stuehr, *Inorg. Chem.*, **26**, 1987, 4029.

47 R.G. Wilkins, *Inorg. Chem.*, **3**, 1964, 520.

48 R.B. Rorabacher, *Inorg. Chem.*, **5**, 1966, 1891.

49 J.A. Miceli and J.E. Stuehr, *Inorg. Chem.*, **11**, 1972, 2763.

50 R.M. Fuoss, *J. Am. Chem. Soc.*, **92**, 1958, 5059.

51 M. Eigen, *Z. Phys. Chem. (Munich)*, **1**, 1954, 176.

52 R.H. Holyer, C.D. Hubbard, S.F.A. Kettle and R.G. Wilkins, *Inorg. Chem.*, **4**, 1965, 929.

53 J. Neely and R. Connick, *J. Am. Chem. Soc.*, **92**, 1970, 3477.

54 D. Saar, G. Macri and S. Petrucci, *J. Inorg. Nucl. Chem.*, **33**, 1971, 4227.

Chapter 5 : Experimental

5.1 : Cryptands and Lariat Ethers

5.1.1 : Origin and Purification of Materials

$RbClO_4$ and $CsClO_4$ were precipitated from solutions of their chlorides (BDH) by the addition of concentrated percloric acid (70% in water, Merck) and were recrystallized from water until chloride was absent. $KClO_4$ (BDH) was recrystallized from water. $TlClO_4$ was prepared from Tl_2CO_3 (Fluka) and $HClO_4$ by metathesis in water and recrystallized twice from water. $LiClO_4$, $NaClO_4$ (Fluka), $AgClO_4$ (Aldrich) and $AgNO_3$ (Johnson-Matthey) were used as received after drying. The metal perchlorates of Mg^{2+}, Ca^{2+}, Ba^{2+}, Sr^{2+}, Mn^{2+}, Co^{2+}, Ni^{2+}, Cu^{2+}, Zn^{2+}, Cd^{2+} and Pb^{2+} were prepared from their respective metal carbonates through reaction with the stoichiometric amount of perchloric acid and were recrystallized twice from water. $Hg(ClO_4)_2$[1] was received and used as a 0.1 mol dm^{-3} $HClO_4$ solution. All of the metal perchlorates except $AgClO_4$ and $Hg(ClO_4)_2$ were vacuum dried at 353-363 K for 48 hours and then stored over P_2O_5 (Merck) under dry nitrogen in a glove box. $AgClO_4$ was vacuum dried at room temperature for 48 hours and then stored over P_2O_5 under dry nitrogen in a glove box.

Tetraethylammonium perchlorate (NEt_4ClO_4) was prepared by acidification of tetraethylammonium hydroxide (NEt_4OH, 40% in water, Fluka) with a slight excess of perchloric acid. Crude NEt_4ClO_4 precipitated out of solution upon cooling. This was repeatedly recrystallized from hot water until free from acid (pH > 6). NEt_4ClO_4 was also prepared by the addition of concentrated aqueous tetraethylammonium bromide (NEt_4Br, BDH) to a 1.0 mol dm^{-3} solution of perchloric acid. The resulting NEt_4ClO_4 precipitate was repeatedly recrystallized from water until free from acid and bromide ion (tested with an aqueous $AgNO_3$ solution). Finally, the NEt_4ClO_4 was dried under vacuum at 335 K for 24 hours and stored over P_2O_5 under dry nitogen in a glove box. Tetrabutylammonium perchlorate (NBu_4ClO_4, Fluka) was used as received after drying under vacuum for 24 hours.

The diaza crown ethers 4,7,13-trioxa-1,10-diazacyclopentadecane, C21 (Kryptofix 21, Merck), and 4,7,13,16-tetraoxa-1,10-diazacyclooctadecane, C22 (Kryptofix 22, Merck), were used as received. Whereas, the cryptand

4,7,13,18-tetraoxa-1,10-diazabicyclo[8.5.5]eicosane, C211 (Kryptofix 211, Merck), was distilled under vacuum and stored under dry nitrogen.

Acetonitrile (Ajax), propylene carbonate (Aldrich), methanol (Ajax), N,N-dimethylformamide (BDH), trimethyl phosphate (BDH), triethyl phosphate (BDH) and tri-*n*-butyl phosphate (BDH) were purified and dried by literature methods.[2,3] Acetonitrile and methanol were then stored under nitrogen over Linde 3Å molecular sieves, whereas all the other solvents were stored under nitrogen over Linde 4Å molecular sieves. The water content of these solvents was below the Karl-Fischer detection level of approximately 50 ppm. Linde 3Å and 4Å molecular sieves (BDH) were activated by heating in a furnace for 8 hours at 673 K. Deionised water was ultrapurified with a MilliQ-Reagent system to produce water with a specific resistance of > 15 MΩ cm.

5.1.2 : Synthesis

5.1.2.1 : Preparation of C21C5

The cryptand 4,7,13-trioxa-1,10-diazabicyclo[8.5.5]eicosane, C21C5, was prepared as previously described in the literature.[4] A solution of C21 (2.0 g, 9.2 mmol) and triethylamine (2.5 g, 25.0 mmol, BDH) in dry benzene (100 cm^3, Ajax), and a solution of glutaryl dichloride (1.41 g, 8.34 mmol, Fluka) in dry benzene (100 cm^3) were added simultaneously to dry benzene (1200 cm^3) over 8 hours at room temperature with vigorous stirring under an atmosphere of dry nitrogen using Perfusor motor-driven syringes. The reaction solution was then filtered to remove the resultant solid triethylamine hydrochloride, and the benzene was removed under vacuum. The residue was then chromatographed on flash grade silica[5] (230-400 mesh, Merck, 4% methanol/96% dichloromethane, R_f = 0.30). Removal of the solvent and drying under high vacuum yielded the cryptand diamide as a white solid (2.2 g, 84%) of m.p. 388-390 K. The diamide was then reduced with borane-dimethyl sulfide[6] to the product C21C5 as follows. The diamide (1.3 g, 4.1 mmol) was dissolved in dry tetrahydrofuran (30 cm^3, BDH) and treated with boron trifluoride etherate (1.0 cm^3, 8.2 mmol, Fluka) at 325 K under dry nitrogen. The reaction mixture was heated to reflux and borane-dimethyl sulfide (1.2 cm^3, 10.9 mmol, 10% in dimethyl sulfide, Fluka) was added dropwise over 20 minutes with a syringe. Heating was continued for 3 hours, during which diethyl ether and dimethyl sulfide were distilled off as they formed. After the solution had cooled to room

temperature, the tetrahydrofuran was removed under vacuum and the white residue was refluxed in 6 mol dm^{-3} hydrochloric acid (25 cm^3, BDH) for 12 hours and then evaporated to dryness. The crude cryptand was obtained from the hydrochloride salt after ion exchanging an aqueous solution on Dowex 1-8x (OH^- form, 50-100 mesh). The basic eluent was then concentrated by removing some of the solvent under vacuum and extracted with chloroform (4 × 50 cm^3, Ajax). The chloroform was then removed from the combined extracts leaving an oily residue. Distillation under vacuum (378 K, 0.018 Torr) yielded $C21C_5$ (1.1 g, 92%) as a colourless viscous oil. ^1H NMR spectral analysis ($CDCl_3$, TMS = 0.00 ppm): δ1.35 (6H, m, aliphatic -CH_2-), 2.50 (12H, m, -NCH_2-) and 3.40 ppm (12H, m, -OCH_2-). ^{13}C NMR spectral analysis ($CDCl_3$, $CDCl_3$ = 77.00 ppm): δ71.30 (2C, -OCH_2-), 70.45 (2C, -OCH_2-), 69.96 (2C, -OCH_2-), 56.60 (2C, -NCH_2-), 56.12 (2C, aliphatic -NCH_2-), 54.42 (2C, -NCH_2-), 27.69 (2C, aliphatic -CH_2-) and 21.01 ppm (1C, aliphatic -CH_2-).

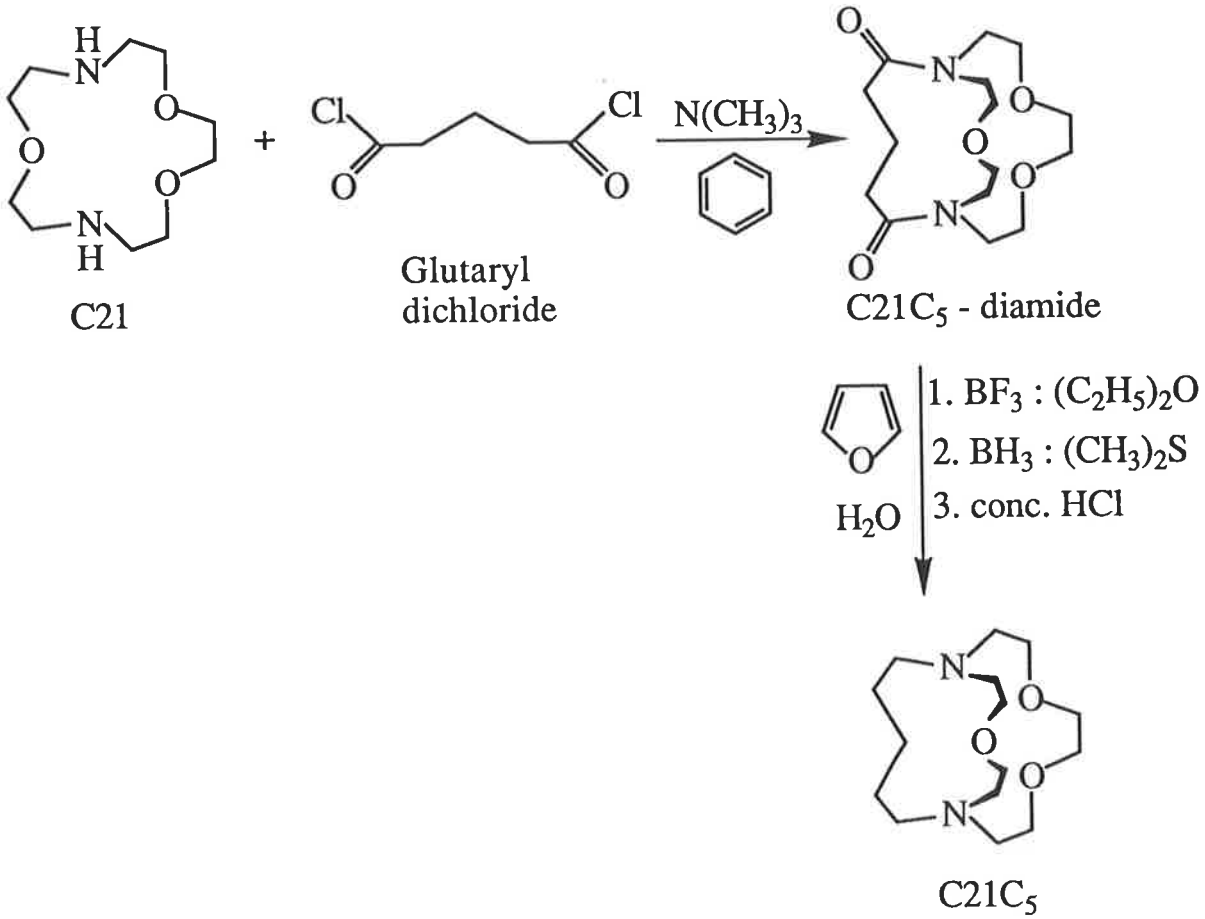

Figure 5.1 *Synthesis of C21C5.*

5.1.2.2 : Preparation of BHE-C22

The method employed in the synthesis of the bibracchial lariat ether 1,10-bis(2-hydroxyethyl)-4,7,13,16-tetraoxa-1,10-diazacyclooctadecane, BHE-C22, was a modification of the general method described by Kulstad and Malmsten.[7] Liquid ethylene oxide (2.0 cm^3, 40 mmol, Fluka) at 273 K was added to a stirred solution of C22 (2.0 g, 7.6 mmol) in dry methanol (50 cm^3) on an ice bath. The reaction mixture was stirred for 30 minutes at 273 K and then for 20 hours at room temperature, after which it was refluxed for 1 hour. After allowing the mixture to cool to room temperature, the solvent was removed under vacuum leaving an oil of crude BHE-C22. Distillation under vacuum (463 K, 0.05 Torr) yielded pure BHE-C22 (2.3 g, 86%) as a colourless oil. ^{13}C NMR spectral analysis ($CDCl_3$, $CDCl_3$ = 77.00 ppm): δ70.60 (4C, -OCH_2-), 69.79 (4C, -OCH_2-), 59.29 (2C, pendant arm -CH_2OH), 57.22 (2C, pendant arm -NCH_2-) and 54.99 ppm (4C, -NCH_2-).

5.1.2.3 : Preparation of BHE-C21

The only synthesis for 1,7-bis(2-hydroxyethyl)-4,10,13-trioxa-1,7-diazacyclopentadecane, BHE-C21, found in the literature was that described by Gramain and Frère.[8] However, it was decided to use a slightly modified version of the general method described by Kulstad and Malmsten[7] for BHE-C22. Liquid ethylene oxide (1.4 cm^3, 28 mmol) at 273 K was added to a stirred solution of C21 (1.0 g, 4.6 mmol) in dry methanol (50 cm^3) on an ice bath. The reaction mixture was stirred for 30 minutes at 273 K and then for 2 hours at room temperature, after which it was refluxed for 1 hour. After allowing the mixture to cool to room temperature, the solvent was removed under vacuum leaving an oil of crude BHE-C21. Distillation under vacuum (448 K, 0.02 Torr) yielded pure BHE-C22 (1.3 g, 92%) as a colourless oil. ^{13}C NMR spectral analysis ($CDCl_3$, $CDCl_3$ = 77.00 ppm): δ70.27 (2C, -OCH_2-), 69.70 (2C, -OCH_2-), 69.30 (2C, -OCH_2-), 59.49 (2C, pendant arm -CH_2OH), 58.48 (2C, pendant arm -NCH_2-), 55.81 (2C, -NCH_2-) and 55.33 ppm (2C, -NCH_2-).

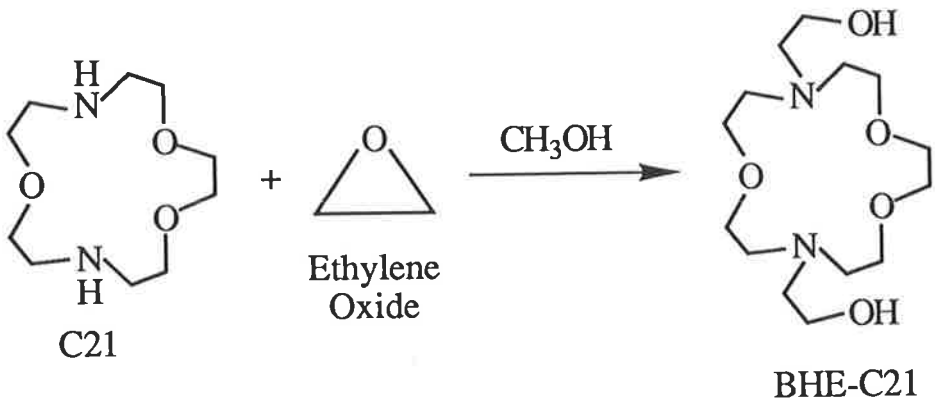

Figure 5.2 *Synthesis of BHE-C21.*

5.1.3 : Stability Constant Measurements

5.1.3.1 : Potentiometric Titrations

All solutions were prepared under a stream of dry nitrogen or under dry nitrogen in a glove box. Stability constants for $[Na.C211]^+$, $[Na.C21C_5]^+$, $[Na.BHE\text{-}C21]^+$ and $[Na.BHE\text{-}C22]^+$ in a variety of non-aqueous solvents were determined in duplicate by direct potentiometric titration of 20 cm^3 of 10^{-3} mol dm^{-3} $NaClO_4$ solutions with 10^{-2} mol dm^{-3} solutions (5 cm^3) of C211, $C21C_5$, BHE-C21 or BHE-C22, respectively. All solutions were 0.05 mol dm^{-3} in NEt_4ClO_4 except those made up in tri-*n*-butyl phosphate. Those solutions were 0.05 mol dm^{-3} in NBu_4ClO_4 due to the insufficient solubility of NEt_4ClO_4. The titrations were carried out under a stream of dry nitrogen in a thermostatted (298.2 ± 0.01 K) titration vessel using a Radiometer G502 Na^+ specific electrode and a Ag wire reference electrode in a 10^{-2} mol dm^{-3} $AgNO_3$ solution in a thermostatted reference vessel. $AgClO_4$ was used in all the tri-*n*-butyl phosphate titrations instead of $AgNO_3$ as the source of Ag^+ in the reference vessel due to the low solubility of $AgNO_3$ in tri-*n*-butyl phosphate. The thermostatted titration vessel was connected to the thermostatted reference vessel by a salt bridge containing 0.05 mol dm^{-3} supporting electrolyte solution (NEt_4ClO_4 or NBu_4ClO_4). Cell potentials were measured with an Orion Research SA 720 digital analyser. The stability constant of $[Li.BHE\text{-}C21]^+$ in acetonitrile was also determined by the method described for the Na^+ titrations, even though the Na^+ specific electrode is approximately 0.01 as sensitive to $[Li^+]$ as to $[Na^+]$. The only difference was that the $NaClO_4$ solution was replaced with a 10^{-3} mol dm^{-3} $LiClO_4$ solution. The Na^+ specific electrode was replaced by a Ag wire in all other titrations, but the equipment used was otherwise identical.

Stability constants for $[Ag.C211]^+$, $[Ag.C21C_5]^+$, $[Ag.BHE\text{-}C21]^+$ and $[Ag.BHE\text{-}C22]^+$ in a variety of non-aqueous solvents were determined by duplicated direct potentiometric titrations of 20 cm^3 of 10^{-3} mol dm^{-3} $AgNO_3$ solutions with 10^{-2} mol dm^{-3} C211, $C21C_5$, BHE-C21 or BHE-C22 solutions (5 cm^3), respectively. These data were employed in the derivation of the stability constants of $[M.C211]^+$, $[M.C21C_5]^+$, $[M.BHE\text{-}C21]^+$ and $[M.BHE\text{-}C22]^+$, where $M^+ = Li^+$, K^+, Rb^+, Cs^+ and Tl^+, in a variety of non-aqueous solvents from data obtained through duplicate competitive potentiometric titrations[9] of 20 cm^3 of 10^{-3} mol dm^{-3} $AgNO_3$ solutions with solutions 5.00×10^{-2} mol dm^{-3} in $MClO_4$ and 10^{-2} mol dm^{-3} in C211, $C21C_5$, BHE-C21 or BHE-C22, respectively. Due to the low solubility of $KClO_4$, $RbClO_4$ and $CsClO_4$, the stability constants of $[M.BHE\text{-}C21]^+$ and $[M.BHE\text{-}C22]^+$, where $M^+ = K^+$, Rb^+ and Cs^+, in N,N-dimethylformamide were determined from duplicate competitive potentiometric titrations in which the concentration of the titration solutions were halved. The concentration of all the titration solutions in the measurement of the stability constant for $[Li.C21C_5]^+$ in tri-*n*-butyl phosphate were also half the normal experimental concentrations quoted above. Furthermore, the concentration of the titration solutions in the measurement of the stability constants for $[Tl.C21C_5]^+$ in trimethyl phosphate and triethyl phosphate and $[Tl.C211]^+$ in tri-*n*-butyl phosphate were half, half and one tenth, respectively, the normal experimental concentrations quoted to accommodate the lower solubilities of these cryptates.

The Na^+ ion selective electrode response to $[Na^+]$ was calibrated before every Na^+ titration in each non-aqueous solvent. This was accomplished by titration of a known $NaClO_4$ concentration solution (usually 10^{-2} or 5.00×10^{-3} mol dm^{-3}) into a known volume of supporting electrolyte (20 cm^3 of 0.05 mol dm^{-3} NEt_4ClO_4 or NBu_4ClO_4). It was also calibrated in acetonitrile with a 10^{-2} mol dm^{-3} solution of $LiClO_4$ for the determination of the $[Li.BHE\text{-}C21]^+$ stability constant (see Figure 2.2). The Ag^+ ion selective electrode response to $[Ag^+]$ was similarly calibrated in every non-aqueous solvent by titration of a 10^{-2} or 5.00×10^{-3} mol dm^{-3} $AgNO_3$ or $AgClO_4$ solution into 20 cm^3 of 0.05 mol dm^{-3} NEt_4ClO_4 or NBu_4ClO_4. The response of the Na^+ and Ag^+ ion selective electrodes to change in $[Na^+]$ (and $[Li^+]$) and $[Ag^+]$, respectively, in acetonitrile, methanol, trimethyl phosphate, triethyl phosphate, tri-*n*-butyl phosphate and N,N-dimethylformamide was Nernstian.

5.1.3.2 : pH-Metric Titrations

The pH-metric titrations were carried out under an atmosphere of water saturated nitrogen in a water jacketed vessel maintained at 298.2 ± 0.01 K. A stream of water saturated nitrogen was bubbled through the titration solution to exclude atmospheric carbon dioxide which could contaminate the titration solution and cause systematic errors. The protonation constants of BHE-C21 and BHE-C22 were determined in triplicate by titration of 10 cm^3 aliquots of solutions containing 4×10^{-3} mol dm^{-3} $HClO_4$, 0.100 mol dm^{-3} NEt_4ClO_4 and 1.020×10^{-3} mol dm^{-3} BHE-C21 or 1.006×10^{-3} mol dm^{-3} BHE-C22, respectively, with standardized NEt_4OH (0.1037 mol dm^{-3}). The stability constants of $[M.BHE\text{-}C21]^{2+}$, where $M^{2+} = Mg^{2+}$, Ca^{2+}, Ba^{2+}, Sr^{2+}, Mn^{2+}, Co^{2+}, Ni^{2+}, Cu^{2+}, Zn^{2+}, Cd^{2+} Hg^{2+} and Pb^{2+}, and $[M.BHE\text{-}C22]^{2+}$, where $M^{2+} = Ba^{2+}$, Sr^{2+}, Mn^{2+}, Co^{2+}, Ni^{2+}, Zn^{2+} and Hg^{2+}, were determined by titrating similar solutions to which a *ca.* 0.1 mol dm^{-3} $M(ClO_4)_2$ solution was added using a Gilson Microman positive displacement pipette so as to give a metal to ligand ratio of 1:1 and 1:2. For each divalent metal ion, two titrations were performed at each of the two different metal to ligand ratios. The stock solutions of the divalent metal perchlorates were standardized in triplicate by conventional EDTA (BDH) complexiometric titration methods.[10,11] A drying tube containing "Carbosorb" soda lime (10-16 mesh, BDH) was attached to the bottle containing the standardized NEt_4OH to further prevent contamination of the titration by carbon dioxide. All solutions were in water.

The titrant, NEt_4OH, was introduced into the water jacketed titration vessel using a Metrohm E665 Dosimat autoburette equipped with a 5 cm^3 burette. An Orion Ross Sureflow 81-72BN combination electrode (containing 0.100 mol dm^{-3} NEt_4ClO_4 in water as the filling solution) connected to an Orion Research SA 720 pH meter was used to measure the potential. The pH meter and the autoburette were interfaced to a Laser XT/3-8086 IBM compatible personal computer which controlled the addition of titrant.[12] Either constant volume aliquots or successive additions of titrant which caused an approximate decrease of 4 mV in the potential were delivered to the titration vessel.

The pH electrode was calibrated regularly by titration of 10 cm^3 of 0.005 mol dm^{-3} $HClO_4$ with standardized NEt_4OH (1 cm^3) from the autoburette to

determine E_0 and pK_w. E_0 was obtained from fitting the resulting data to the Nernst equation:

$$E = E_0 + \frac{RT}{F}\ln[H^+] \qquad (5.1)$$

where E is the observed potential (Volts);

E_0 is the standard potential for the electrode (Volts);

R is the gas constant, 8.314 J K^{-1} mol^{-1};

T is the temperature (Kelvin);

F is Faraday's constant, 9.6487×10^4 Coulombs mol^{-1}, and

$[H^+]$ is the hydrogenion concentration.

By measuring the e.m.f. in millivolts rather than volts, converting to common logs (logarithm to base 10) and considering only the experimental temperature of 298.2 K, the Nernst equation becomes:

$$pH = \frac{E_0 - E}{59.15} \qquad (5.2)$$

where $pH = -\log[H^+]$.

An experimental value for pK_w was determined from:

$$pK_w = \frac{E_0 - E}{59.15} + pOH \qquad (5.3)$$

where $pK_w = pH + pOH$ and $pOH = -\log[OH^-]$. Under the conditions used in these studies, the average pK_w = 13.805 in water. Diffusion correction terms for 0.100 mol dm^{-3} NEt_4ClO_4 in water were used in calculating the calibration parameters, E_0 and pK_w. The protonation and stability constants were determined using the FORTRAN program MINIQUAD.[13]

5.1.4 : ^{7}Li and ^{23}Na Variable Temperature NMR Spectroscopy

Solutions of *ca.* 0.02 mol dm^{-3} $LiClO_4$, *ca.* 0.1 mol dm^{-3} $NaClO_4$ and $[M.C211]^+$, $[M.C21C_5]^+$, $[M.BHE\text{-}C21]^+$ and $[M.BHE\text{-}C22]^+$, where M^+ = Li^+ or Na^+, were prepared under a stream of dry nitrogen or under dry nitrogen in a glove box. Stock solutions of anhyrous $LiClO_4$ and $NaClO_4$

were prepared by weight in 10 cm^3 volumetric flasks and made up with the solvent of interest. Then C211, $C21C_5$, BHE-C21 or BHE-C22 was weighed into a 1 cm^3 or 2 cm^3 volumetric flask such that when the flask was made up to the mark with a stock anhydrous metal perchlorate solution it gave a solvated metal ion to coordinated metal ion ratio in the range 3:1 to 1:3. At least three solutions of different solvated metal ion to coordinated metal ion ratios and constant total M^+ concentration were prepared for each system. For the variable temperature ^7Li and ^{23}Na NMR studies, these solutions (about 0.8 cm^3) were degassed and sealed under vacuum in 5-mm NMR tubes (507-PP, Wilmad Glass Co.). These tubes were then coaxially mounted in 10-mm NMR tubes (513-PP, Wilmad Glass Co.) containing either D_2O (AAEC), d_6-acetone (Aldrich) or d_6-dimethyl sulfoxide (Aldrich) as the deuterium lock solvent depending upon the temperature under investigation.

The variable temperature ^7Li NMR spectra were run on a Brüker CXP-300 spectrometer operating at 116.64 MHz. For each solution, between 500-6000 transients were accumulated in a 8192 point data base over a 1199 Hz spectral width prior to Fourier transformation. The variable temperature ^{23}Na NMR spectra were run on a Brüker CXP-300 spectrometer operating at 79.39 MHz. Between 1000-6000 transients were accumulated in a 2048 point data base over a 8064.5 Hz spectral width for each solution prior to Fourier transformation. The solution temperatures were controlled to within ± 0.3 K using a Brüker B-VT 1000 temperature controller. The temperature unit was calibrated between 200-300 K by measuring the variation of the chemical shift difference for the ^1H resonances (CH_3 and OH) of methanol, and between 300-380 K by measuring the variation of the chemical shift difference for the ^1H resonances (CH_2 and OH) of ethylene glycol.[14-16] In all the variable temperature studies, spectra were collected at temperature intervals of *ca.* 3 K. The Fourier transformed spectra were transferred to a VAX 11-780 mainframe computer where they were subjected to complete lineshape analysis[17] using the program LINSHP[18] to obtain kinetic data.

5.2 : 2-Methyl-8-*p*-toluenesulfonamido-6-quinolyl-oxyacetic Acid (MTS-QAA)

5.2.1 : Origin and Purification of Materials

The ligand 2-methyl-8-*p*-toluenesulfonamido-6-quinolyloxyacetic acid (MTS-QAA),[19] NaOH (ConvoL, BDH) and sodium piperazine-N,N'-bis(2-ethane-sulfonate) buffer (NaPIPES, Calbiochem) were used as received. $NaClO_4$ (Fluka) was used as received after drying. The metal perchlorates of Co^{2+}, Ni^{2+}, Cu^{2+}, Zn^{2+}, Cd^{2+} and Mg^{2+} were prepared from their respective metal carbonates through reaction with the stoichiometric amount of perchloric acid (70% in water, Merck) and were recrystallized twice from water. All of the metal perchlorates were vacuum dried at 353-363 K for 48 hours and then store over P_2O_5 (Merck) under dry nitrogen in a glove box. Deionised water was ultrapurified with a MilliQ-Reagent system to produce water with a specific resistance of > 15 MΩ cm. Ethanol (Ajax) was purified and dried by the literature method.[2]

5.2.2 : pH-Metric Titrations

The pH-metric titrations were performed using a Metrohm E665 Dosimat autoburette equipped with a 5 cm^3 burette, an Orion Ross Sureflow 81-72BN combination electrode (containing 0.100 mol dm^{-3} $NaClO_4$ in water as the filling solution) and an Orion Research SA 720 pH meter. This set up is exactly the same as that described in section 5.1.3.2. The titration solutions were kept in a water jacketed vessel thermostatted to 298.2 ± 0.01 K. Bubbling a stream of solvent saturated nitrogen through the titration solutions maintained a carbon dioxide-free nitrogen atmosphere inside the titration vessel.

Protonation constants of MTS-QAA were determined by titration of a 10 cm^3 solution containing 4.943×10^{-3} mol dm^{-3} MTS-QAA, 0.01 mol dm^{-3} $HClO_4$ and 0.10 mol dm^{-3} $NaClO_4$ with standardized NaOH (0.1016 mol dm^{-3}). Stability constants of all the complexes formed between MTS-QAA and Co^{2+}, Ni^{2+}, Cu^{2+}, Zn^{2+}, Cd^{2+} and Mg^{2+} were determined by titrating similar solutions containing the appropriate metal perchlorate. A more detailed account of all the experimental concentrations used in the titrations of MTS-QAA in the presence of all the divalent metal ions is given below.

Zn^{2+} Titrations

A 10 cm^3 solution containing 3.353×10^{-3} mol dm^{-3} MTS-QAA, 0.01 mol dm^{-3} $HClO_4$ and 0.10 mol dm^{-3} $NaClO_4$ to which 0.22 cm^3 of a 0.1004 mol dm^{-3} $Zn(ClO_4)_2$ solution had been added was titrated with 0.1016 mol dm^{-3} NaOH. However, a 10 cm^3 solution containing 1.009×10^{-3} mol dm^{-3} MTS-QAA, 5×10^{-3} mol dm^{-3} $HClO_4$ and 0.10 mol dm^{-3} $NaClO_4$ to which 0.049 cm^3 of a 0.1004 mol dm^{-3} $Zn(ClO_4)_2$ solution had been added was titrated with 0.1016 mol dm^{-3} NaOH to obtain a more accurate value for the stability constant of $[Zn.MTS\text{-}QAA_2]^{2-}$.

Co^{2+} Titrations

A 10 cm^3 solution containing 9.501×10^{-4} mol dm^{-3} MTS-QAA, 5×10^{-3} mol dm^{-3} $HClO_4$ and 0.10 mol dm^{-3} $NaClO_4$ to which 0.045 cm^3 and 0.03 cm^3 of a 0.1023 mol dm^{-3} $Co(ClO_4)_2$ solution had been added was titrated with 0.1016 mol dm^{-3} NaOH.

Ni^{2+} Titrations

A 10 cm^3 solution containing 1.676×10^{-3} mol dm^{-3} MTS-QAA, 5×10^{-3} mol dm^{-3} $HClO_4$ and 0.10 mol dm^{-3} $NaClO_4$ to which 0.11 cm^3 of a 9.917 $\times 10^{-2}$ mol dm^{-3} $Ni(ClO_4)_2$ solution had been added was titrated with 0.1016 mol dm^{-3} NaOH.

Cu^{2+} Titrations

A 10 cm^3 solution containing 6.705×10^{-4} mol dm^{-3} MTS-QAA, 2×10^{-3} mol dm^{-3} $HClO_4$ and 0.10 mol dm^{-3} $NaClO_4$ to which 0.04 cm^3 of a 9.307 $\times 10^{-2}$ mol dm^{-3} $Cu(ClO_4)_2$ solution had been added was titrated with 0.1016 mol dm^{-3} NaOH.

Cd^{2+} Titrations

A 10 cm^3 solution containing 7.180×10^{-4} mol dm^{-3} MTS-QAA, 4×10^{-3} mol dm^{-3} $HClO_4$ and 0.10 mol dm^{-3} $NaClO_4$ to which 0.045 cm^3 of a 9.973 $\times 10^{-2}$ mol dm^{-3} $Cd(ClO_4)_2$ solution had been added was titrated with 0.1016 mol dm^{-3} NaOH.

Mg^{2+} Titrations

A 10 cm^3 solution containing 9.501×10^{-4} mol dm^{-3} MTS-QAA, 5×10^{-3} mol dm^{-3} $HClO_4$ and 0.10 mol dm^{-3} $NaClO_4$ to which 0.04 cm^3 of a 0.1002 mol dm^{-3} $Mg(ClO_4)_2$ solution had been added was titrated with 0.1016 mol dm^{-3} NaOH.

All solutions were in 50% ethanol/50% water and they all contained 0.10 mol dm^{-3} to maintain the ionic strength constant. Each protonation and stability constant was determined in triplicate. Stock *ca.* 0.1 mol dm^{-3} $M(ClO_4)_2$ solutions were prepared from the appropriate metal perchlorate salts and were standardized in triplicate by conventional EDTA complexiometric titration methods.[10,11] A Gilson Microman positive displacement pipette was used to add the metal perchlorate solutions to the ligand containing titration solutions. Furthermore, a drying tube containing "Carbosorb" soda lime was fitted to the bottle containing the standardized titrant (NaOH) to prevent and indicate (by colour change) the presence of carbon dioxide in the titration vessel.

The pH electrode was calibrated regularly by titrating 10 cm^3 solutions containing 0.005 mol dm^{-3} $HClO_4$ and 0.10 mol dm^{-3} $NaClO_4$ with standardized NaOH (1 cm^3, 0.1016 mol dm^{-3}) to determine E_0 and pK_w (see Equations 5.1 and 5.3). The protonation and stability constants were calculated with the MINIQUAD program.[13]

5.2.3 : Ultraviolet-Visible Spectroscopy

The ultraviolet-visible spectra of the free MTS-QAA, [Zn.MTS-QAA] and $[Zn.MTS\text{-}QAA_2]^{2-}$ were run in 1 cm quartz cells on a Hewlett Packard 8452A Diode Array Spectrophotometer. All solutions were in 50% ethanol/50% water, maintained at pH 6.6 and I = 0.10 with NaPIPES buffer and thermostatted to 298.2 ± 0.1 K. The solution for the free MTS-QAA contained 1.071×10^{-4} mol dm^{-3} MTS-QAA and 0.10 mol dm^{-3} NaPIPES. At pH 6.6, all of the ligand was in the monoprotonated form, $HMTS\text{-}QAA^-$. The solution for the [Zn.MTS-QAA] complex contained 1.007×10^{-4} mol dm^{-3} MTS-QAA, 2.007×10^{-3} mol dm^{-3} $Zn(ClO_4)_2$ and 0.10 mol dm^{-3} NaPIPES. An excess of Zn^{2+} was necessary to ensure the formation of predominantly [Zn.MTS-QAA]. Under these experimental conditions, 94% of the ligand was in the [Zn.MTS-QAA] form. Hence, the concentration of [Zn.MTS-QAA] in solution was 9.476×10^{-5} mol dm^{-3}. The solution for the

$[Zn.MTS\text{-}QAA_2]^{2-}$ complex contained 2.014×10^{-4} mol dm^{-3} MTS-QAA, 1.004×10^{-4} mol dm^{-3} $Zn(ClO_4)_2$ and 0.10 mol dm^{-3} NaPIPES. In this case, an excess of ligand was necessary to ensure the formation of predominantly $[Zn.MTS\text{-}QAA_2]^{2-}$. Under these experimental conditions, 91% of the total Zn^{2+} was in the $[Zn.MTS\text{-}QAA_2]^{2-}$ form. Hence, the concentration of $[Zn.MTS\text{-}QAA_2]^{2-}$ in solution was 9.126×10^{-5} mol dm^{-3}.

5.2.4 : Fluorescence Spectroscopy

All fluorescence spectra were run on a Perkin Elmer 3000 fluorescence spectrometer. An excitation wavelength of 350 nm was used to measure the emission spectra between 360 and 660 nm. Excitation and emission slit widths of 10 nm and a filter which passes light above 390 nm were employed. Solutions were contained in 1 cm quartz cuvets thermostatted to 298.2 ± 0.1 K. All solutions were in 50% ethanol/50% water and maintained at pH 6.6 and I = 0.10 with NaPIPES buffer. The total MTS-QAA concentration in each of the eleven solutions was kept kept constant at 2.518×10^{-6} mol dm^{-3} while the total Zn^{2+} concentration was increased from 0 to 1.254×10^{-4} mol dm^{-3}.

5.2.5 : Fluorescence Stopped-Flow Kinetics

Instrumentation

A stopped-flow fluorescence spectrometer similar to that described and illustrated by Erman and Hammes[20] was used in the kinetic studies of the Zn^{2+}-MTS-QAA systems. The two reaction solutions were initially loaded into two 10 cm^3 plastic reservoir syringes. Some of these solution were then transferred to two 5 cm^3 glass gas-tight driving syringes via manually operated three way Teflon stopcocks. The three way Teflon stopcocks allowed the driving syringes to be filled without having to remove them from the stopped-flow system. The driving syringes were housed inside a water jacketed metal compartment thermostatted to 298.2 ± 0.1 K. The formation or acid catalysed decomplexation reactions were commenced by manually pushing a piston connected to the driving syringes. Approximately 0.35 cm^3 of each of the reaction solutions was forced into a mixing chamber where the reaction took place. A metallic stop prevented more than the predetermined amount (0.35 cm^3) of solution from being injected into the mixing chamber. On the second manual push, the excess reaction or reacted mixture was forced into a 5 cm^3 glass stopping syringe located behind the mixing chamber via a three way Teflon stopcock. This three way Teflon

stopcock allowed the emptying of the stopping syringe without having to remove it from the stopped-flow system.

The light source was a constant voltage (≈ 10 V) Xenon lamp. A grating monochromator was used to select the excitation wavelength of 350 nm which was directed along the observation chamber. The changes in intensity of the filtered emitted fluorescence (≥ 70% transmission above 480 nm and ≤ 1% transmission below 450 nm) was followed by an eleven dynode photomultiplier. Data was acquired once the stopping syringe had triggered a microswitch and after a time delay of 100 ms. The output of the photomultiplier was displayed on a Telequipment S61 oscilloscope (as a function of time) and a more accurate reading was obtained from a Beckman Tech 300 digital mulimeter. Each stopped-flow kinetic trace was collected using a Datalab DL905 transient recorder. Eight to ten reaction traces were collected for each pair of solutions, prior to signal averaging and kinetic analysis using a Laser Turbo XT personal computer. Bisquare weighted least squares fitting of the averaged exponential signals to Equation 5.4 yielded the observed pseudo first order rate constants, k_{obs}.

$$A = C\exp(-k_{obs}t) \qquad \textbf{(5.4)}$$

where A is the amplitude (Volts);

C is a constant (Volts);

k_{obs} is the observed first order rate constant (s^{-1}), and

t is the time (s).

The k_{obs} values were then fitted to equations which best described the most likely reaction mechanism using the non-linear, weighted least squares program DATAFIT.[21,22]

Acid Catalysed Decomplexation Kinetics

The acid catalysed decomplexation kinetics of [Zn.MTS-QAA] in 50% ethanol/50% water and 75% ethanol/25% water at I = 0.10 ($NaClO_4$) were determined by mixing equal volumes of a solution containing 8.028×10^{-4} mol dm^{-3} $Zn(ClO_4)_2$, 4.029×10^{-5} mol dm^{-3} MTS-QAA and 0.10 mol dm^{-3} $NaClO_4$ with a series of nine $HClO_4$ solutions ranging in concentration from 0.020 mol dm^{-3} to 0.100 mol dm^{-3}, and recording the decay in fluorescence using the stopped-flow fluorimeter described above. In addition, the acid

solutions also contained varying concentrations of $NaClO_4$ (0.080 mol dm^{-3} to 0 mol dm^{-3}) to maintain the ionic strength at 0.10. A twenty times excess $[Zn^{2+}]$ was necessary in the complex solution to ensure the presence of only [Zn.MTS-QAA]. The acid catalysed decomplexation kinetics of $[Zn.MTS\text{-}QAA_2]^{2-}$ in 50% ethanol/50% water at I = 0.10 ($NaClO_4$) were determined by mixing equal volumes of a solution containing 2.007×10^{-5} mol dm^{-3} $Zn(ClO_4)_2$, 4.029×10^{-4} mol dm^{-3} MTS-QAA and 0.10 mol dm^{-3} $NaClO_4$ with the same series of nine $HClO_4$ solutions just mentioned above, and similarly recording the decay in fluorescence. In this case, a twenty times excess [MTS-QAA] was required in the complex solution to ensure the presence of only the $[Zn.MTS\text{-}QAA_2]^{2-}$ complex. Prior to each kinetic run, both of the reaction solutions were thermostatted to 298.2 ± 0.1 K. The concentrations quoted above were those prior to reacting the two reaction solutions in the mixing chamber of the stopped-flow fluorimeter. Furthermore, the $[HClO_4]$ was in excess to maintain pseudo first order conditions.

Formation Kinetics

The formation kinetics of [Zn.MTS-QAA] in 50% ethanol/50% water at pH = 6.6, 298.2 ± 0.1 K and I = 0.10 ($NaClO_4$) were determined by mixing equal volumes of a solution containing 4.029×10^{-5} mol dm^{-3} MTS-QAA, 1.00×10^{-3} mol dm^{-3} NaPIPES and 0.10 mol dm^{-3} $NaClO_4$ with a series of eleven $Zn(ClO_4)_2$ solutions of varying $[Zn^{2+}]$, and recording the increase in fluorescence using the stopped-flow fluorimeter described above. The Zn^{2+} solutions had a $[Zn^{2+}]$ range of 8.028×10^{-4} mol dm^{-3} to 1.204×10^{-2} mol dm^{-3} and they also each contained 1.00×10^{-3} mol dm^{-3} NaPIPES and 0.10 mol dm^{-3} $NaClO_4$. A twenty to three hundred times excess $[Zn^{2+}]$ was employed to ensure the formation of predominantly [Zn.MTS-QAA] (1-6% of the total ligand forms $[Zn.MTS\text{-}QAA_2]^{2-}$) and to maintain pseudo first order conditions. The concentration quoted for each species in each of the reaction solutions were those prior to reacting the two reaction solutions in the mixing chamber of the stopped-flow fluorimeter.

References

1 As provided by Dr. P.A. Duckworth, University of Adelaide, Australia.

2 D.D. Perrin, W.L.F. Armarego and D.R. Perrin, "Purification of Laboratory Chemicals", Pergamon, Oxford, U.K., 2nd Edn., 1980.

3 H. Yoshida, *J. Inorg. Nucl. Chem.*, **24**, 1962, 1257.

4 S.F. Lincoln, E. Horn, M.R. Snow, T.W. Hambley, I.M. Brereton and T.M. Spotswood, *J. Chem. Soc., Dalton Trans.*, 1986, 1075.

5 W.C. Still, M. Kahn and A. Mitra, *J. Org. Chem.*, **43**, 1978, 2923.

6 H.C. Brown, S. Narasimhan and Y.M. Choi, *Synthesis*, 1981, 996.

7 S. Kulstad and L.Å. Malmsten, *Acta Chem. Scand.*, **B33**, 1979, 469.

8 P. Gramain and Y. Frère, *Nouv. J. Chim.*, **3**, 1979, 53.

9 B.G. Cox, H. Schneider and J. Stroka, *J. Am. Chem. Soc.*, **100**, 1978, 4746.

10 A.I. Vogel, "Quantitative Inorganic Analysis", Longmans, Green and Co., London, 1955.

11 G. Schwarzenbach, H. Flaschka and H.M.N.H. Irving, "Complexiometric Titrations", Methuen, London, 2nd Edn., 1969.

12 P.A. Duckworth, University of Adelaide, private communication.

13 A. Sabatini, A. Vacca and P. Gans, *Talanta*, **21**, 1974, 53.

14 D.S. Raiford, C.L. Fisk and E.D. Becker, *Anal. Chem.*, **51**, 1979, 2050.

15 A.L. Van Geet, *Anal. Chem.*, **42**, 1970, 679.

16 A.L. Van Geet, *Anal. Chem.*, **40**, 1968, 2227.

17 S.F. Lincoln, *Prog. React. Kinetics*, **9**, 1977, 1.

18 FORTRAN-77 program for the VAX 11-780 mainframe computer, P. Clarke, 1987 (originally written by T.M. Spotswood, 1973)

19 As provided by Dr. I. Mahadevan, University of Adelaide, Australia.

20 J.E. Erman and G.G. Hammes, *Rev. Sci. Instrum.*, **37**, 1966, 746.

21 T. Kurucsev, Unpublished material, University of Adelaide, 1990.

22 T. Kurucsev, *J. Chem. Educ.*, **55**, 1978, 128.

Chapter 6 : NMR Data Analysis

6.1 : NMR Analysis of Two-Site Chemical Exchange

6.1.1 : ^{7}Li and ^{23}Na NMR Spectroscopy

NMR specroscopy is an excellent technique for studying the kinetics of chemical exchange processes. The chemical shifts of alkali metal nuclei are very sensitive to the immediate environment of an alkali metal ion in solution. Therefore, the ability of NMR spectroscopy to resolve and assign the separate signals due to alkali nuclei in different chemical environments makes it a very direct and powerful technique for alkali metal kinetic studies. Alkali metal NMR spectroscopy has also been widely used in kinetic studies because of the biological relevance of alkali metal ions such as Na^{+}, Li^{+} and K^{+}.

The ^{23}Na nucleus has a natural isotopic abundance of 100% and an intrinsic NMR sensitivity 9.3% that of the ^{1}H nucleus.[1,2] Similarly, the ^{7}Li nucleus has a natural isotopic abundance of 92.57% and an intrinsic NMR sensitivity 29.4% that of the ^{1}H nucleus. Both the ^{23}Na and ^{7}Li nuclei possess a nuclear spin of 3/2 which gives rise to quadrupolar charge distribution and hence the dominant relaxation mechanism for these nuclei is quadrupolar.[1,2] Despite the quadrupole moments, the natural linewidths of the ^{23}Na and ^{7}Li nuclei in solution are quite narrow, especially in the case of ^{7}Li where the natural linewidths are usually less than 1 Hz.[1,2,3] Thus, the chemical shifts of the two Lorentzian resonance lines corresponding to the complexed and uncomplexed alkali metal chemical environments can be measured with reasonable precision. The ^{23}Na chemical shifts exhibit a linear correlation with the solvent D_N, whereas the ^{7}Li chemical shifts show no correlation whatsoever.[1] These favourable ^{23}Na and ^{7}Li nuclei properties facilitate the application of variable temperature ^{23}Na and ^{7}Li NMR spectroscopy and complete lineshape analysis[4] to several Na^{+} and Li^{+} cryptates and bibracchial lariat ether complexes.

6.1.2 : Two-Site Chemical Exchange

The rates of alkali metal exchange, the activation parameters and the mechanism by which the alkali metal exchange occurs may be derived from the temperature variation of the NMR spectral lineshapes. The factors which determine the spectral lineshapes and the way chemical exchange can alter

those spectral lineshapes need to be understood to fully appreciate how lineshape analysis operates. It is now appropriate to describe the physical and mathematical concepts used in this study and in two-site chemical exchange.[4] Two-site chemical exchange is the exchange between two different magnetic environments.

In the absence of a magnetic field the nuclear spin states of a nucleus are degenerate in energy. When a magnetic field, $\mathbf{B_0}$, is applied to a nucleus along the z-axis the degeneracy of the nuclear spin states is lifted and the nuclear spins and their populations are assigned according to the Boltzmann distribution law. The highest nuclear spin state or energy level is that in which the nuclear spin is opposed to the direction of $\mathbf{B_0}$. Since $\mathbf{B_0}$ is fixed along the z-axis the individual nuclear magnetic moments will rotate about $\mathbf{B_0}$ in a cone of precession at an angular rate of ω_0, the Larmor frequency. A macroscopic magnetic moment, $\vec{\mathbf{M}}$, is generated along the z-axis such that $\vec{\mathbf{M}}=(0, 0, M_z)$ because only the z-component, M_z, contributes to $\vec{\mathbf{M}}$. The time required for M_z, the longitudinal component of $\vec{\mathbf{M}}$, to reach its thermal equilibrium value $M_{z\,eq}$ is characterized by a first order rate law and is called the longitudinal or spin-lattice relaxation time, T_1.

The introduction of another magnetic field $\mathbf{B_1}$ ($\mathbf{B_1} \ll \mathbf{B_0}$), rotating in the xy or transverse plane at an adjustable angular frequency ω, causes $\vec{\mathbf{M}}$ to tilt away from the z-axis and into the xy plane. Hence, the M_z component is diminished and magnetizations in the x and y directions are generated such that $\vec{\mathbf{M}}= (M_x, M_y, M_z)$. Also the individual nuclear magnetic moments will become bunched or phased in their precessional motion about the z-axis. The time required for the individual nuclear magnetic moments to dephase (or the time required for M_x and M_y to relax to zero) such that $\vec{\mathbf{M}}= (0, 0, M_z)$ again is designated the transverse or spin-spin relaxation time, T_2. The magnetic field $\mathbf{B_1}$ induces magnetic field components along the x and y axes such that the total magnetic field can be described by:

$$\vec{\mathbf{B}} = (B_1 \cos \omega t, -B_1 \sin \omega t, B_0) \qquad \textbf{(6.1)}$$

The Bloch equations[5] describe the time dependence of $\vec{\mathbf{M}}$ in the stationary (or laboratory) frame:

$$\frac{dM_x}{dt} = \gamma (M_y B_0 + M_z B_1 \sin \omega t) - \frac{M_x}{T_2} \quad \textbf{(6.2)}$$

$$\frac{dM_y}{dt} = \gamma (-M_x B_0 + M_z B_1 \cos \omega t) - \frac{M_y}{T_2} \quad \textbf{(6.3)}$$

$$\frac{dM_z}{dt} = -\gamma (M_x B_1 \sin \omega t + M_y B_1 \cos \omega t) - \frac{(M_z - M_{z\,eq})}{T_1} \quad \textbf{(6.4)}$$

where γ is the nuclear gyromagnetic ratio.

If the stationary set of Cartesian axes is replaced by a set of axes rotating at an angular frequency ω (frequency of $\mathbf{B_1}$ also) about the z'-axis (the rotating frame z-axis which is coincident with the z-axis of the stationary frame) such that $\mathbf{B_1}$ is stationary allows a more convenient form of the Bloch equations to be defined[4]:

$$\frac{dM_{xy}}{dt} = -\alpha M_{xy} - i \gamma B_1 M_z \quad \textbf{(6.5)}$$

$$\frac{dM_z}{dt} = \gamma \nu B_1 - \frac{(M_z - M_{z\,eq})}{T_1} \quad \textbf{(6.6)}$$

where $\alpha = \frac{1}{T_2} - i (\omega_0 - \omega)$;

M_{xy} is the transverse magnetization, and

ν is the component of $\vec{\mathbf{M}}$ which is 90° out of phase with $\mathbf{B_1}$ (ie. on the y'-axis).

From Equation 6.6 it can be seen that the variation of M_z is dependent on ν, which corresponds to the observed absorption mode of the NMR signal. The rarely used dispersion mode of the NMR signal is represented by υ (component of $\vec{\mathbf{M}}$ in phase with $\mathbf{B_1}$ and on the x'-axis) such that $M_{xy} = \upsilon + i\nu$, $\vec{\mathbf{M}} = (\upsilon, -\nu, M_z)$ and $\vec{\mathbf{B}} = (B_1, 0, B_0)$.

Under conditions of continuous wave slow passage NMR, ω is slowly swept through ω_0, such that dM_{xy}/dt and $dM_z/dt = 0$ and if B_1 is small such that $M_z \approx M_{z\,eq}$ always and M_{xy} is small, the absorption mode lineshape may be shown to be:

$$\nu = -M_{z\,eq} \frac{\gamma B_1 T_2}{1 + T_2^2 (\omega_0 - \omega)^2 + \gamma^2 B_1^2 T_1 T_2} \tag{6.7}$$

Since the magnitude of B_1 is generally small in continuous wave slow passage NMR, this results in $\gamma^2 B_1^2 T_1 T_2 \ll 1$ and negligible compared to the other denominator terms and hence the absorption mode lineshape acquires Lorentzian character:

$$\nu = -M_{z\,eq} \frac{\gamma B_1 T_2}{1 + T_2^2 (\omega_0 - \omega)^2} \tag{6.8}$$

The continuous wave slow passage NMR method is used in this discussion as it is a simpler model to envisage than the pulsed NMR method. However, later on it will be demonstrated that the ν mode lineshape attained from a pulsed Fourier transform experiment is similar to that obtained from a continuous wave slow passage experiment.

When a nucleus exchanges between two different magnetic sites A and B, the two Lorentzian resonances centred at frequencies ω_{0A} and ω_{0B} corresponding to sites A and B, respectively, will broaden and then coalesce to a single Lorentzian resonance. The mean site lifetimes are designated τ_A and τ_B for site A and B, respectively. The time that a nuclear spin spends in transit from site A to site B and vice versa is assumed to be so short that no nuclear spin precession or relaxation occurs in that time. This results in the nuclear spin from site A arriving at site B with its phase memory of site A intact. In turn this causes dephasing at site B and an increase in M_{xyB}, the transverse magnetization of site B, at a rate of $k_A M_{xyA} = \tau_A^{-1} M_{xyA}$, and a decrease in M_{xyA} at the same rate. Likewise transfer of a nuclear spin from site B to site A causes dephasing at site A, an increase in M_{xyA} at a rate of $k_B M_{xyB} = \tau_B^{-1} M_{xyB}$, and a decrease in M_{xyB} at the same rate. This can be illustrated by the following equations:

$$\frac{dM_{xyA}}{dt} = \frac{M_{xyB}}{\tau_B} - \frac{M_{xyA}}{\tau_A} \tag{6.9}$$

$$\frac{dM_{xyB}}{dt} = \frac{M_{xyA}}{\tau_A} - \frac{M_{xyB}}{\tau_B} \tag{6.10}$$

These chemical exchange induced dephasing effects must be incorporated into the Bloch equations for sites A and B in systems where two-site chemical exchange takes place.[6,7] This yields the following equations:

$$\frac{dM_{xyA}}{dt} = -\alpha_A M_{xyA} - i\gamma B_1 M_{z\,eq\,A} + \frac{M_{xyB}}{\tau_B} - \frac{M_{xyA}}{\tau_A} \qquad \textbf{(6.11)}$$

$$\frac{dM_{xyB}}{dt} = -\alpha_B M_{xyB} - i\gamma B_1 M_{z\,eq\,B} + \frac{M_{xyA}}{\tau_A} - \frac{M_{xyB}}{\tau_B} \qquad \textbf{(6.12)}$$

where $\alpha_A = \frac{1}{T_{2A}} - i(\omega_{0A} - \omega)$;

$\alpha_B = \frac{1}{T_{2B}} - i(\omega_{0B} - \omega)$;

T_{2n} is the transverse relaxation time, T_2, of site n in the absence of chemical exchange, and

ω_{0n} is the Larmor frequency of site n in the absence of chemical exchange.

Under steady state or continuous wave slow passage conditions, the M_z components do not deviate significantly from $M_{z\,eq}$, such that:

$$M_{zA} = M_{z\,eq\,A} = \chi_A M_{z\,eq} \qquad \textbf{(6.13)}$$

$$M_{zB} = M_{z\,eq\,B} = \chi_B M_{z\,eq} \qquad \textbf{(6.14)}$$

and $$\frac{dM_{xyA}}{dt} = \frac{dM_{xyB}}{dt} = 0 \qquad \textbf{(6.15)}$$

where χ_A and χ_B are the relative populations of sites A and B, respectively.

The total transverse magnetization, $M_{xy} = M_{xyA} + M_{xyB}$, may now be defined in terms of τ_A and τ_B[63,65]:

$$M_{xy} = \frac{-i\gamma B_1 M_{z\,eq}[\tau_A + \tau_B + \tau_A \tau_B (\alpha_A \chi_A + \alpha_B \chi_B)]}{(1 + \alpha_A \tau_A)(1 + \alpha_B \tau_B) - 1} \qquad \textbf{(6.16)}$$

The absorption mode (v) lineshape is proportional to the imaginary component of M_{xy}[4,9,10]:

$$v = \frac{-\gamma B_1 M_{z\,eq}\left\{ Y\left[1 + \tau\left(\frac{\chi_B}{T_{2A}} + \frac{\chi_A}{T_{2B}}\right)\right] + Q R \right\}}{Y^2 + R^2} \qquad \textbf{(6.17)}$$

where $\tau = \chi_B \tau_A = \chi_A \tau_B$;

$\Delta\omega = \omega_{0A} - \omega_{0B}$;

$$\delta\omega = \frac{1}{2}(|\omega_{0A} - \omega_{0B}|) - \omega;$$

$$Y = \tau\left[\frac{1}{T_{2A}\,T_{2B}} - \delta\omega^2 + \frac{\Delta\omega^2}{4}\right] + \frac{\chi_B}{T_{2B}} + \frac{\chi_A}{T_{2A}};$$

$$Q = \tau\left(\delta\omega - \frac{\Delta\omega}{2}(\chi_A - \chi_B)\right), \text{ and}$$

$$R = \delta\omega\left[1 + \tau\left(\frac{1}{T_{2A}} + \frac{1}{T_{2B}}\right)\right] + \frac{\Delta\omega}{2}\tau\left(\frac{1}{T_{2B}} - \frac{1}{T_{2A}}\right) + \frac{\Delta\omega}{2}(\chi_A - \chi_B)$$

The NMR lineshapes for exchanging chemical systems can be calculated from Equation 6.17. As the exchange rate is varied from "very slow" to "very fast" by temperature variation, the NMR lineshapes will vary. The appearance of the NMR lineshapes is dependent upon the exchange rate limiting conditions which will now be discussed. If exchange between the two different chemical environments is too slow to cause any significant broadening of the two Lorentzian singlets then the slow exchange condition exists. When exchange is so rapid that the coalesced singlet is simply the weighted average of the two singlets characterizing the two different chemical environments in the absence of exchange then the fast exchange condition is said to exist. The best kinetic results are obtained within the temperature range defined by these two limiting conditions, that is, where the singlets coalesce and the total lineshape is very sensitive to variation in τ_A and τ_B.

(i) Very Slow Exchange Limit

$$\tau_A^{-1}, \tau_B^{-1} \ll |\omega_{0A} - \omega_{0B}|, T_{2A}^{-1}, T_{2B}^{-1}$$

Under these limiting conditions Equation 6.17 approximates to:

$$\nu = \frac{-\gamma B_1 \chi_A M_{z\,eq} T_{2A}^{-1}}{T_{2A}^{-2} + (\omega_{0A} - \omega)^2} + \frac{-\gamma B_1 \chi_B M_{z\,eq} T_{2B}^{-1}}{T_{2B}^{-2} + (\omega_{0B} - \omega)^2} \qquad \textbf{(6.18)}$$

which contains no chemical exchange parameters and describes two distinct Lorentzian resonances centred at ω_{0A} and ω_{0B}.

(ii) Slow Exchange Limit

$$\tau_A^{-1}, \tau_B^{-1} \ll |\omega_{0A} - \omega_{0B}|;\ \tau_A^{-1} \approx T_{2A}^{-1};\ \tau_B^{-1} \approx T_{2B}^{-1}$$

In this limiting condition the rate of exchange is greater than in the previous condition and the absorption mode lineshape defined in Equation 6.17 now approximates to:

$$v = \frac{-\gamma B_1 \chi_A M_{z\,eq} (T_{2A}^{-1} + \tau_A^{-1})}{(T_{2A}^{-1} + \tau_A^{-1})^2 + (\omega_{0A} - \omega)^2} + \frac{-\gamma B_1 \chi_B M_{z\,eq} (T_{2B}^{-1} + \tau_B^{-1})}{(T_{2B}^{-1} + \tau_B^{-1})^2 + (\omega_{0B} - \omega)^2} \quad \textbf{(6.19)}$$

which also describes two Lorentzian resonances centred at ω_{0A} and ω_{0B}. However, due to exchange taking place, the resonances have become "exchange broadened". The linewidths of these Lorentzian resonances at half-height are:

$$W_{1/2A} = \frac{2}{T_{2Aobs}} = \frac{2}{T_{2A}} + \frac{2}{\tau_A} \quad \textbf{(6.20)}$$

and

$$W_{1/2B} = \frac{2}{T_{2Bobs}} = \frac{2}{T_{2B}} + \frac{2}{\tau_B} \quad \textbf{(6.21)}$$

(iii) Fast Exchange Limit

$$\tau_A^{-1}, \tau_B^{-1} > |\omega_{0A} - \omega_{0B}|$$

Now only a single Lorentzian resonance centred at $(\chi_A\omega_{0A} + \chi_B\omega_{0B})$ is observed as complete environmental averaging is experienced by the exchanging nuclear spins. The linewidth at half-height of the single resonance is:

$$W_{1/2} = \frac{2}{T_{2obs}} = \frac{2\,\chi_A}{T_{2A}} + \frac{2\,\chi_B}{T_{2B}} + 2\,\chi_A^2\,\chi_B^2\,(|\omega_{0A} - \omega_{0B}|)^2\,(\tau_A + \tau_B) \quad \textbf{(6.22)}$$

(iv) Very Fast Exchange Limit

$$\tau_A^{-1}, \tau_B^{-1} \gg |\omega_{0A} - \omega_{0B}|, T_{2A}^{-1}, T_{2B}^{-1}$$

Finally, under these limiting conditions a single, sharper Lorentzian resonance centred at $(\chi_A\omega_{0A} + \chi_B\omega_{0B})$ is observed. The absorption mode lineshape is defined as:

$$v = \frac{-\gamma B_1 M_{z\,eq} (\chi_A T_{2A}^{-1} + \chi_B T_{2B}^{-1})}{(\chi_A T_{2A}^{-1} + \chi_B T_{2B}^{-1})^2 + (\chi_A \omega_{0A} + \chi_B \omega_{0B} - \omega)^2} \quad \textbf{(6.23)}$$

which contains no chemical exchange information as the rate of exchange is so rapid that the exchanging nuclear spins experience the weighted average of

the two different chemical environments A and B. The linewidth at half-height of this observed resonance is:

$$W_{1/2} = \frac{2}{T_{2obs}} = \frac{2\chi_A}{T_{2A}} + \frac{2\chi_B}{T_{2B}} \qquad \textbf{(6.24)}$$

Pulsed NMR allows site lifetimes down to 10^{-6} s to be measured in chemically exchanging systems, whereas continuous wave slow passage NMR is limited to values $\geq 10^{-3}$ s.[4] Under pulsed NMR condition the magnetic field $\mathbf{B_0}$ is applied continuously along the z'-axis of the rotating frame and a short (1-50 μs), high energy pulse, $\mathbf{B_1}$, with a frequency close to the Larmor frequency ($\omega \approx \omega_0$) is applied along the x'-axis. The powerful $\mathbf{B_1}$ applies a torque to $\vec{\mathbf{M}}$ causing it to tilt away from its z'-axis allignment and towards the x'y' plane producing x and y components (transverse) of $\vec{\mathbf{M}}$. Instantly after the pulse, both T_1 and T_2 relaxation occursresulting in $\vec{\mathbf{M}}$ relaxing back to an allignment with the z'-axis. Transverse relaxation, T_2, causes the $M_{x'y'}$ component to decay exponentially to zero and produce a free induction decay (FID) signal which is observed in the x'y' plane. The FID or time domain spectrum is acquired and accumulated in the NMR spectrometers computer. By applying $B_1 = 0$ to the modified differential Bloch equations (6.5 and 6.6) an equation describing the FID is obtained[11]:

$$M_{xy} = C_1 e^{-\phi_+ t} + C_2 e^{-\phi_- t} \qquad \textbf{(6.25)}$$

where C_1 and C_2 are integration constants and

$$2\phi_{\pm} = (\alpha_A + \frac{1}{\tau_A} + \alpha_B + \frac{1}{\tau_B}) \pm [(\alpha_A + \frac{1}{\tau_A} - \alpha_B - \frac{1}{\tau_B})^2 + \frac{4}{\tau_A\tau_B}]^{1/2}$$

The Fourier transform (or frequency domain spectrum), S, of the FID is:

$$S = \int_0^{\infty} M_{z\,eq}\, e^{-i(\omega - \omega_1)t}\, .dt$$

$$= \frac{i\, M_{z\,eq}\, [\tau_A + \tau_B + \tau_A\tau_B(\alpha_A\chi_B + \alpha_B\chi_A)]}{(1 + \alpha_A\tau_A)(1 + \alpha_B\tau_B) - 1} \qquad \textbf{(6.26)}$$

where $$\alpha_A = \frac{1}{T_{2A}} + i(\omega_{0A} - \omega);$$

$$\alpha_B = \frac{1}{T_{2B}} + i(\omega_{0B} - \omega);$$

ω is the variable frequency, and

ω_1 is the fixed pulse carrier frequency.

The absorption mode lineshape is obtained from the imaginary part of Equation 6.26 and is the same as that obtained in a continuous wave slow passage experiment.

6.2 : Two-Site Lineshape Analysis

A series of ^{23}Na and ^{7}Li variable temperature NMR spectra were accumulated and Fourier transformed on a Brüker CXP-300 NMR spectrometer for Na^+ and Li^+ complex systems, respectively, whose rate of metal ion exchange falls within the NMR time scale. The temperature range spans the slow and fast exchange limits of the particular system being studied. The transformed spectra were then transferred to a Macintosh SE microcomputer using the data transfer program KERMIT.[12] The binary files were then converted into floating point decimal files using NMR Spec[13] on the Macintosh SE, and lastly transferred using standard methods to a VAX 11-780 mainframe computer where the lineshaping was performed using the non-interactive program LINSHP.[14]

The LINSHP program generates theoretical spectra corresponding to particular τ (= $1/k$) values. Examples of theoretical and experimental spectra are illustrated in the Results and Discussion section of this chapter (ie. Figures 3.2, 3.4, 3.9 and 3.11). Several input parameters are used by the LINSHP program to generate the theoretical spectra, and these include:

ν_c and ν_s - the frequency of the complexed and solvated cation resonance, respectively, of a coalescing pair of peaks in the absence of exchange (Hz);

$W_{1/2c}$ and $W_{1/2s}$ - the linewidth at half-height of the complexed and solvated cation resonance, respectively, in the absence of exchange (Hz);

χ_c and χ_s - the relative populations of the complexed and solvated cation sites, respectvely, and

R - is a parameter defined as $1/\tau_c\chi_s = 1/\tau_s\chi_c = k_d/\chi_s$

Once the range of R and the number of iterations to be made are defined along with the input parameters mentioned above, the LINSHP program iteratively determines the best R value in which the difference between the theoretical and experimental spectra is minimal.

Generally, the temperature dependent ^{23}Na and ^{7}Li linewidths and frequencies for the complexed and solvated cation resonances were obtained from an extrapolation of the low temperature values where no exchange induced modification had occured in order to minimise the introduction of systematic errors. Sometimes due to solvent melting point constraints it was

not possible to reach the temperatures where the very slow exchange limit existed. Here the linewidths and frequencies were obtained from separate solutions containing either totally solvated metal cation or totally complexed metal cation alone, for the same temperature range and total concentration as the solutions containing both species. Little or no variation in the relative populations was observed with variation in temperature in the lineshaped systems.

6.3 : Activation Parameter Determination

The decomplexation rate constant, k_d (= $1/\tau_c$), determined at every temperature by complete lineshape analysis, is directly related to the activation parameters and temperature through the Eyring equation[15,16]:

$$k_d = \frac{1}{\tau_c} = \frac{k_B T}{h} \exp\left(\frac{-\Delta G_d^{\ddagger}}{RT}\right) = \frac{k_B T}{h} \exp\left(\frac{-\Delta H_d^{\ddagger}}{RT} + \frac{\Delta S_d^{\ddagger}}{R}\right) \qquad \textbf{(6.27)}$$

where τ_c is the mean lifetime of the complex;

k_B is Boltzmann's constant;

T is the temperature (K);

h is Planck's constant;

$\Delta G_d^{\ddagger}$ is the decomplexation free energy of activation;

R is the gas constant;

$\Delta H_d^{\ddagger}$ is the decomplexation enthalpy of activation, and

$\Delta S_d^{\ddagger}$ is the decomplexation entropy of activation.

Equation 6.27 may be rearranged to the more convenient linear form:

$$\ln(T\tau_c) = \frac{\Delta H_d^{\ddagger}}{RT} + \left[\ln\left(\frac{h}{k_B}\right) - \frac{\Delta S_d^{\ddagger}}{R}\right] \qquad \textbf{(6.28)}$$

Plotting $\ln(T\tau_c)$ against $1/T$ produces a straight line of slope $\frac{\Delta H_d^{\ddagger}}{R}$ and an intercept of $\left[\ln\left(\frac{h}{k_B}\right) - \frac{\Delta S_d^{\ddagger}}{R}\right]$. Examples of these plots can be seen in Figures 3.3, 3.5 and 3.10. The values of k_d at 298.2 K and at the coalescence temperature for each system, $\Delta H_d^{\ddagger}$ and $\Delta S_d^{\ddagger}$ were determined using the non-linear, weighted least squares program DATAFIT[17,18] on the VAX 11-780 mainframe computer. DATAFIT minimises the residual differences in an n-dimensional sum of squares space between a calculated and an experimental surface (ie. k_d and T, respectively). The activation parameter errors quoted by DATAFIT are the standard deviations for each parameter in the sum of squares space.

References

1 A.I. Popov, *Pure Appl. Chem.*, **51**, 1979, 101.

2 A.I. Popov and J.-M. Lehn: in G.A. Melson (Ed.) : "Coordination Chemistry of Macrocyclic Compounds", Plenum Press, New York, 1979.

3 Y.M. Cahen, P.R. Handy, E.T. Roach and A.I. Popov, *J. Phys. Chem.*, **79**, 1975, 80.

4 S.F. Lincoln, *Prog. React. Kinetics*, **9**, 1977,1.

5 F. Bloch, *Phys. Rev.*, **70**, 1946, 460.

6 H.S. Gutowsky, D.M. McCall and C.P. Slichter, *J. Chem. Phys.*, **21**, 1953, 279.

7 H.M. McConnel, *J. Chem. Phys.*, **28**, 1958, 430.

8 H.S. Gutowsky and A. Saika, *J. Chem. Phys.*, **21**, 1953, 1688.

9 M.T. Rodgers and J.C. Woodbrey, *J. Phys. Chem.*, **66**, 1962, 540.

10 I.O. Sutherland, *Ann. Rep. NMR Spect.*, **4**, 1971, 71.

11 R.K. Gupta, T.P. Pitner and R. Wasylishen, *J. Mag. Res.*, **13**, 1974, 383.

12 Brüker, CXP-300 version available as Pascal code, W. Catchings, F. da Cruz, W. Schilit, M. Aebi and P. Placeway, Mac-kermit v0.98(69), 1989, Columbia University, Info-Kermit@cunixc.cc.columbia.edu.

13 J.R. Christie, NMR Spec v1.2, 1988.

14 FORTRAN-77 program for the VAX 11-780 mainframe computer, P. Clarke, 1987 (originally written by T.M. Spotswood, 1973).

15 W.F.K. Wynne-Jones and H. Eyring, *J. Chem. Phys.*, **3**, 1935, 492.

16 S. Gladstone, K.J. Laider and H. Eyring, "Theory of Rate Processes", McGraw-Hill, New York, 1941.

17 T. Kurucsev, Unpublished material, University of Adelaide, 1990.

18 T. Kurucsev, *J. Chem. Educ.*, **55**, 1978, 128.

Publications

Stephen F. Lincoln and Theo Rodopoulos, "Complexation of lithium(I), sodium(I), silver(I) and thallium(I) by 4,7,13,16-tetraoxa-1,10-diazabicyclo[8.5.5]eicosane and 4,7,13-trioxa-1,10-diazabicyclo[8.5.5]eicosane in trimethyl phosphate. A potentiometric titration and ^{7}Li and ^{23}Na nuclear magnetic resonance study", *Inorg. Chim. Acta*, **190**, 1991, 223-229.

Stephen F. Lincoln and Theo Rodopoulos, "Equilibrium and kinetic study of the complexation of lithium(I), sodium(I), silver(I) and thallium(I) by 4,7,13,16-tetraoxa-1,10-diazabicyclo[8.5.5]eicosane (C211) and 4,7,13-trioxa-1,10-diazabicyclo[8.5.5]eicosane ($C21C_5$) in trialkyl phosphate solvents", *Inorg. Chim. Acta*, **205**, 1993, 23-30.

Theo Rodopoulos, Pierre-André Pittet and Stephen F. Lincoln, "Complexation of monovalent metal ions by lariat ethers in non-aqueous solvents", *J. Chem. Soc., Dalton Trans.*, 1993, 1055-1060.

Theo Rodopoulos, Pierre-André Pittet, Indumathy Mahadevan, Stephen F. Lincoln, A. David Ward, Paul A. Duckworth, Ian J. Forbes and Peter D. Zalewski, "The complexation of zinc(II) by the fluorophore 2-methyl-8-*p*-toluenesulfonamido-6-quinolyloxyacetic acid in aqueous ethanol. An equilibrium and kinetic study", *J. Chem. Soc., Dalton Trans.*, submitted for publication.